



HAL
open science

Strategies in 3 and 5-axis abrasive water jet machining of titanium alloys

van Hung Bui

► **To cite this version:**

van Hung Bui. Strategies in 3 and 5-axis abrasive water jet machining of titanium alloys. Mechanics of materials [physics.class-ph]. Université Paul Sabatier - Toulouse III, 2019. English. NNT : 2019TOU30218 . tel-02936362

HAL Id: tel-02936362

<https://theses.hal.science/tel-02936362>

Submitted on 11 Sep 2020

HAL is a multi-disciplinary open access archive for the deposit and dissemination of scientific research documents, whether they are published or not. The documents may come from teaching and research institutions in France or abroad, or from public or private research centers.

L'archive ouverte pluridisciplinaire **HAL**, est destinée au dépôt et à la diffusion de documents scientifiques de niveau recherche, publiés ou non, émanant des établissements d'enseignement et de recherche français ou étrangers, des laboratoires publics ou privés.



THÈSE

En vue de l'obtention du DOCTORAT DE L'UNIVERSITÉ DE TOULOUSE

Délivré par l'Université Toulouse 3 - Paul Sabatier

Présentée et soutenue par
VAN HUNG BUI

Le 17 décembre 2019

**Strategies in 3 and 5-axis abrasive water jet machining of
titanium alloys**

Ecole doctorale : **MEGEP - Mécanique, Energétique, Génie civil, Procédés**

Spécialité : **Génie mécanique, mécanique des matériaux**

Unité de recherche :
ICA - Institut Clément Ader

Thèse dirigée par
Walter RUBIO et Patrick GILLES

Jury

Mme Claire LARTIGUE, Rapporteur
M. Raynald LAHEURTE, Rapporteur
M. Cyril BORDREUIL, Examinateur
M. Guillaume COHEN, Examinateur
M. Walter RUBIO, Directeur de thèse
M. Patrick GILLES, Co-directeur de thèse

ACKNOWLEDGEMENTS

Foremost, I would particularly like to thank my supervisor, Prof. Walter RUBIO, for leading and accompanying me to the end of this thesis.

I would like to express my most sincere gratitude to my co-supervisor, M. Patrick GILLES, and M. Guillaume COHEN who always guide and support me during the whole Ph.D. program. I arrived in France with many gaps, in terms of language, knowledge, and work experience which I have overcome during these three years, thanks to their patience and their expertise. I would also greatly appreciate their daily life support as good friends during my stay in a foreign country. Those years spent working together will be an unforgettable memory for me.

I would also like to sincerely thank the reporters of my thesis, Prof. Claire LARTIGUE, and M. Raynald LAHEURTE, who spent time to read, give me constructive comments and encourage me in fulfilling my writing. In addition, I would also like to thank the examiner, Prof. Cyril BORDREUIL for agreeing to participate in my thesis jury and contribute many useful remarks.

Furthermore, it is really a valuable opportunity for me to work in a professional research environment as ICA. I would like to acknowledge the SUMO research group and the members of its Executive Board in ICA. Thank you very much for the knowledge, experience, and advice that are very important and helpful in my doctoral dissertation study.

I would like to express my appreciation to the Ministry of Education and Training (MOET) of the Vietnamese government for funding my study in France.

I would like to express my thankfulness to my friends in Toulouse, who always encourage and stand by me in my difficult moments.

Last but not least, I would like to express my deepest gratitude to my dear family: my parents, my lovely wife, and my little daughter. Thank you very much! There is no word to express all my appreciation and gratefulness to you. Thanks for supporting me spiritually throughout writing this thesis and my life in general.

L'alliage de titane est généralement utilisé pour les pièces structurales aéronautiques ayant une taille importante et ainsi que des parois minces tout en devant résister à des efforts considérables. L'usinage de ces pièces est difficile avec les méthodes classiques telles que le fraisage, car les forces de coupe sont élevées et les parois minces peuvent être facilement déformées. L'usinage de l'alliage de titane (Ti6Al4V) par un procédé utilisant un jet d'eau abrasif (AWJ) peut potentiellement être utilisé pour remplacer les méthodes d'usinage conventionnelles. Cependant, la compréhension des différents aspects de ce procédé est insuffisante pour autoriser son industrialisation. Cette thèse présente un modèle de prévision de la profondeur usinée dans deux cas de direction du jet : un jet perpendiculaire à la surface de la pièce et un jet incliné. Dans un premier temps, la compréhension du processus d'enlèvement de matière et de la qualité de surface obtenue est étudiée à travers l'observation de l'influence des paramètres du processus. Dans un second temps, un modèle basé sur la distribution gaussienne des particules abrasives dans le jet d'eau est proposé pour caractériser un passage élémentaire et pour prédire le profil du fond de poche obtenu par une succession de passages élémentaires. Ensuite, une méthodologie d'usinage des coins de poche utilisant un contrôle adaptatif de la vitesse d'avance est présentée. Enfin un nouveau modèle du profil du fond de poche prenant en compte l'angle d'inclinaison du jet est présenté. Tout au long de ce travail de thèse, la validation expérimentale a montré un bon accord entre les valeurs mesurées et modélisées et a ainsi démontré la capacité du jet d'eau abrasif à usiner à une profondeur contrôlée.

Mots-clés: Usinage, Jet d'eau abrasif, Stratégie de fraisage, Alliage de titane, Ti6Al4V.

Titanium alloy is generally used for aeronautical structural parts having a large size and as thin walls while having to withstand considerable effort. Machining these parts is difficult with conventional methods such as milling, because the high cutting forces can easily deform the part. Machining of titanium alloy (Ti6Al4V) by an abrasive water jet (AWJ) process can potentially be used to replace conventional machining methods. However, the understanding of the different aspects of this process is insufficient to allow its industrialization. This thesis presents a model of prediction of the machined depth in two cases of direction of the jet: a jet perpendicular to the surface of the part and an inclined jet. At first, the understanding of the removal material process and the obtained surface quality is studied through the observation of the influence of the process parameters. In a second step, a model based on the Gaussian distribution of abrasive particles in the water jet is proposed to characterize an elementary pass and to predict the pocket bottom profile obtained by a succession of elementary passes. Then, a method to machine pocket corners using an adaptive control of the feed rate is presented. Finally, a new model of the pocket bottom profile taking into account the angle of inclination of the jet is presented. Throughout this thesis work, the experimental validation showed a good agreement between the measured and modeled values and thus demonstrated the ability of the abrasive water jet milling to machine to a controlled depth.

Keywords: Machining, Abrasive water jet, Milling strategy, Titanium alloy, Ti6Al4V.

TABLE OF CONTENTS

Chapter 1.....	1
1.1 Context.....	1
1.1.1 Evolution history and characteristics of abrasive water jet technology.....	1
1.1.2 Ecological machining with only sand and water.....	2
1.1.3 Flexible manufacturing processes with different materials.....	2
1.1.4 An appropriate process for machining of hard metals thin sheets.....	5
1.1.5 Parallel development in CFRP application.....	5
1.1.5.1 Challenges and ability of .AWJ in manufacturing CFRP.....	5
1.1.5.2 Application of abrasive water jet technology for machining CFRP.....	6
1.1.6 Drawbacks of Abrasive water jet machining.....	8
1.2 Review of abrasive water jet process.....	9
1.2.1 Technology of abrasive water jet machines.....	9
1.2.1.1 Pure water jet technology.....	9
1.2.1.2 Abrasive slurry jet technology.....	10
1.2.1.3 Abrasive water jet technology.....	11
1.2.2 Working system of abrasive water jet machine.....	12
1.2.2.1 The ultrahigh-pressure pump.....	13
1.2.2.2 Abrasive feed system.....	15
1.2.2.3 Water and air.....	15
1.2.2.4 Cutting head.....	15
1.2.2.5 Water orifice.....	16
1.2.2.6 Abrasive orifice.....	17
1.2.2.7 Mixing chamber and focusing tube.....	17

1.2.2.8	Abrasive particles	17
1.2.2.9	The position control system	18
1.2.3	Characteristic of the jet	18
1.2.4	Material removal mechanism (Micro – Macro machining).....	20
1.2.4.1	Removal material mechanisms in AWJ machining.....	20
1.2.4.2	Erosion mechanism of AWJ in cutting operation	23
1.2.5	Assessment of surface machined.....	24
1.2.5.1	Surface roughness and waviness.....	24
1.2.5.2	Surface morphology and grit embedment phenomenon	25
1.2.6	Process parameters in the abrasive cutting performance.....	26
1.2.6.1	The effect of water pressure.....	26
1.2.6.2	The effect of standoff distance (<i>SOD</i>)	29
1.2.6.3	The effect of abrasive mass flow rate.....	30
1.2.6.4	The effect of characteristics of abrasive particles.....	31
1.2.6.5	The effect of attack angle	33
1.2.7	Modeling of machining perpendicular to the workpiece surface	35
1.2.7.1	Abrasive water jet for-milling a single kerf (elementary pass)	35
1.2.7.2	The effect of process parameters on the generation of a single kerf.....	40
1.2.7.3	Abrasive water jet for pocket milling.....	45
1.2.8	Modeling of machining with a water jet inclination angle	53
1.2.8.1	Considering the effect of jet attack angle on the generation of elementary pass	53
1.2.8.2	Pockets machining.....	56
1.3	Conclusion.....	58
Chapter 2.	61

2.1	A new cutting depth model with rapid calibration in abrasive water jet machining of titanium alloy	61
2.1.1	Introduction.....	62
2.1.1.1	Bibliography.....	62
2.1.1.2	Conclusion on the literature	66
2.1.2	Model of the depth milled in pocket machining	66
2.1.2.1	Modelling elementary passes.....	66
2.1.2.2	Principle for summing of elementary passes.....	68
2.1.2.3	Taking the erosion mechanism into account	69
2.1.2.4	Simplification of the cutting depth model	70
2.1.2.5	Formation of the pocket bottom in relation to the sweep pitch.....	71
2.1.2.6	Method to set up the machined depth model	73
2.1.3	Application of the method.....	74
2.1.3.1	The different configurations tested	74
2.1.3.2	The experimental set-up	74
2.1.3.3	Results obtained for configuration N° 1.....	76
2.1.3.4	Identification of a rapid calibration procedure on configuration N° 1 .	78
2.1.3.5	Modelling with rapid calibration for configurations N° 2 to N° 6.....	79
2.1.3.6	Experimental validation of the models established by rapid calibration	83
2.1.4	Results and discussion.....	84
2.1.5	Conclusion	86
2.2	Adaptive speed control for waterjet milling in pocket corners	87
2.2.1	Literature review.....	88
2.2.2	Change of direction	90

2.2.2.1	Depth model for milled pockets	90
2.2.2.2	Direction change strategies	93
2.2.2.3	Change of direction at constant radius.....	94
2.2.2.4	Conclusion on change of direction at constant radius.....	99
2.2.2.5	Adaptive speed control during change of direction at constant radius	99
2.2.3	Experimental validation.....	100
2.2.3.1	Experimental validation of adaptive speed control.....	100
2.2.3.2	Results and discussion	102
2.2.4	Conclusion	104
Chapter 3.....		106
3.1	A modeling of elementary passes taking into account the inclination angle	106
3.1.1	Introduction.....	108
3.1.2	Model of elementary pass taking into account the firing angle.....	110
3.1.3	The experimental set-up.....	111
3.1.4	Results and discussion.....	114
3.1.4.1	Experimentation.....	114
3.1.4.2	Rapid calibration method	116
3.1.4.3	Taking into account the erosion phenomenon.....	118
3.1.5	Conclusions	120
3.2	Machining pocket with management of the tool inclination angle.....	121
3.2.1	Introduction.....	122
3.2.2	Proposed model with the inclination angle of the jet.....	126
3.2.3	Experimental set up.....	128
3.2.4	Validation of the proposed model.....	131

3.2.4.1	Assessment the proposed model for elementary pass.....	131
3.2.4.2	Assessment the proposed model for pocket	136
3.2.4.3	Influence of jet inclination angle on the geometrical characteristics of the milled pocket.....	139
3.2.5	Conclusion	146
Chapter 4.	148
4.1	General conclusions	148
4.2	Future work.....	150

LIST OF FIGURES

Fig. 1-1. Problem with closed edges of pocket milled [40]	8
Fig. 1-2. Schema of the cutting head of PWJ [40].....	10
Fig. 1-3. Schematic of high-pressure slurry jet (ASJ) [6].....	11
Fig. 1-4. A typical system of abrasive water jet machining technology	12
Fig. 1-5. Components of abrasive water jet machine (FLOW MACH 4 – ICA Lab).....	12
Fig. 1-6. Diagram of a booster pump(KTM water jet) [40].....	13
Fig. 1-7. The velocity profile of the particles which constituting the jet [40]	14
Fig. 1-8. Schema of the cutting head of AWJ machine.....	15
Fig. 1-9. Water orifice [40]	16
Fig. 1-10. Abrasive orifice	17
Fig. 1-11. FLOW MACH4C	18
Fig. 1-12. Structure of a water jet at high velocity [48].....	19
Fig. 1-13. Flow of water jet according to N. Zuckerman et al [53].....	19
Fig. 1-14. Impacting of a particle on the machined surface [54].....	21
Fig. 1-15. Erosion mode and two surface texture type in cutting ductile material [40] ...	24
Fig. 1-16. Machining parameters	26
Fig. 1-17. Effect of water pressure on depth of cut for different materials.....	27
Fig. 1-18. Effect of traverse speed on material removal rate and surface waviness	28
Fig. 1-19. Effect of standoff distance and traverse speed on dimensional characteristics of single kerf [57].....	30
Fig. 1-20. Evolution of the depth (mm) according to the abrasive flow rate (g / min) [40]	30
Fig. 1-21. Different shapes of particles under an investigation using Tesa Visio apparatus	33

Fig. 1-22. Definition of attack angle of abrasive water jet	33
Fig. 1-23. Direction of the jet during machining.....	34
Fig. 1-24. A single kerf machined by abrasive water jet [51]	36
Fig. 1-25. Characteristic of a kerf profile	37
Fig. 1-26. An experimental validation using Gaussian to model a single kerf in milling Titanium alloy	37
Fig. 1-27. Comparison theoretical models with the measured profile of single kerf [51]	38
Fig. 1-28. Relationship between the GD width parameters and the simple Gauss model [40]	39
Fig. 1-29. Profile of single kerf extracted from "Alicona" optical profilometer [40]	40
Fig. 1-30. Effect of <i>SOD</i> and <i>Vf</i> on a single kerf [40]	42
Fig. 1-31. Effect of water pressure on a single kerf with <i>SOD</i> = 100 mm [40]	43
Fig. 1-32. Effect of the size of abrasive particle on a single kerf with <i>SOD</i> = 100 mm [40]	44
Fig. 1-33. Single kerf and pocket machined [40]	46
Fig. 1-34. Using mask for milling pocket [40]	46
Fig. 1-35. Zigzag strategy [106]	47
Fig. 1-36. Milling a rectangular pocket without mask [102]	48
Fig. 1-37. Deflects appear due to change the direction of the jet [45]	49
Fig. 1-38. Two methods of replacing by circular arc trajectories	50
Fig. 1-39. Constant radius of Ti6Al4V specimen machined [40]	50
Fig. 1-40. Modeling profile of pocket machined.....	51
Fig. 1-41. The evolution of the pocket depth as a function of traverse speed [40]	52
Fig. 1-42. The influence of impact angle on erosion damage for several stainless steels [110].....	54
Fig. 1-43. The influence of water jet inclination angle on a formation of incision [46].....	55

Fig. 1-44. Schematic illustration of the jet plume structure in air before impingement onto the target surface: (a) normal impingement and (b) shallow angle impingement [47]...	55
Fig. 1-45. Wavy surface profile measured for two levels of desired depth of pockets at $\alpha = 45^\circ$ [111].....	56
Fig. 1-46. Milling experimental setup and cross-section of pocket milled [112].....	57
Fig. 1-47. Effect of the jet impact angle on characteristics of pocket milled [112].	57
Fig. 2-1. Modeling of the Gaussian curve [44].....	63
Fig. 2-2. Influence of operating parameters on elementary passes	64
Fig. 2-3. Offset passes and optimal abrasive flow rate	64
Fig. 2-4. Lateral offset and depths machined [45].....	65
Fig. 2-5. Profiles for elementary passes and abrasive size 220#	67
Fig. 2-6. Successive passes and pocket profile obtained by summing	68
Fig. 2-7. Direction of the jet after impact.....	70
Fig. 2-8. Influence of the sweep pitch on formation of the pocket bottom.....	72
Fig. 2-9. Method to set up the depth model.....	73
Fig. 2-10. Machine FLOW MACH4C.....	75
Fig. 2-11. Measurement device.....	76
Fig. 2-12. Mean profiles measured.....	76
Fig. 2-13. Measurement and modelling of elementary profiles	77
Fig. 2-14. Depths of pockets for configuration 1.....	77
Fig. 2-15. Pocket with a corrugated bottom machined with $P=100$ MPa, $SOD = 100$ mm, abrasive size 220 #, $Vf = 423$ mm/min, $B(423) = 1.420$ mm and $pitch = 1.71$ mm.	78
Fig. 2-16. Results obtained - Comparison of the depths calculated and measured	84
Fig. 2-17. Pocket with a slightly corrugated bottom machined with $P = 225$ MPa, $SOD = 100$ mm, abrasive size 220 #, $Vf = 1.035$ mm/min, $B(1035) = 0.993$ mm and $pitch = 1.02$ mm.....	85

Fig. 2-18. Changes in milling direction by 90° and corresponding defects [109]	89
Fig. 2-19. Changes of direction for triangular pockets [45]	89
Fig. 2-20. Distances on changes of direction	90
Fig. 2-21. Modelling the Gaussian profile	91
Fig. 2-22. Superposition of elementary passes.....	92
Fig. 2-23. Different changes of direction.....	93
Fig. 2-24. Changes of direction at constant radius	95
Fig. 2-25. Pitch and depth variations in constant radius strategy	98
Fig. 2-26. Relative depth variation for a constant radius strategy	99
Fig. 2-27. Correction of the pocket corner depth	100
Fig. 2-28. FLOW MACH4C machine.....	101
Fig. 2-29. Ti6Al4V milled.....	102
Fig. 2-30. Measuring a profile.....	102
Fig. 2-31. Modeled and measured profiles.....	104
Fig. 3-1. Profile of elementary pass and pocket	109
Fig. 3-2. Influence of jet inclination angles on elementary pass profiles	110
Fig. 3-3. Profile corresponding to the jet inclination angle at α	111
Fig. 3-4. Experimental setup specimens	112
Fig. 3-5. Measurement and extraction of elementary pass profile	113
Fig. 3-6. Modelled and measured profiles	114
Fig. 3-7. Width of cut for different inclination angles.....	116
Fig. 3-8. Depth of cut for different inclination angles	116
Fig. 3-9. Measured, calculated and corrected depth.....	117
Fig. 3-10. Measured, calculated and corrected width.....	118

Fig. 3-11. Comparison of elementary pass profiles for $SOD = 60$ mm, $Vf = 300$ mm/min	119
Fig. 3-12. Direction of the jet during machining	125
Fig. 3-13. Schematic of elementary pass profile corresponding to the jet inclination angle at α	128
Fig. 3-14. Experimental setup employed for AWJ machining of Ti6Al4V	129
Fig. 3-15. Measurement on Alicona	131
Fig. 3-16. The influence of the jet inclination angle on characteristics of the elementary pass.....	132
Fig. 3-17. The influence of the jet inclination angle on characteristics of the elementary pass.....	133
Fig. 3-18. The evolution of depth and width of elementary passes at various jet impingement angles.....	134
Fig. 3-19. Dependence of material removal mechanism on the jet inclination angle.....	135
Fig. 3-20. Influence of the jet inclination angle on characteristics of pockets milled ($SOD = 20$ (mm); $P = 1000$ (MPa); $Vf = 1000$ (mm/min), $Pitch = 0.7$ (mm)	137
Fig. 3-21. Influence of the jet inclination angle on characteristics of pockets milled ($SOD = 20$ (mm); $P = 1000$ (MPa); $Vf = 1000$ (mm/min), $Pitch = 1.1$ (mm)	138
Fig. 3-22. $He(\alpha)$ factor defined experimentally as a function of jet inclination angle. The dot line represents the best fit line to the data based on Eq. 3-12: a) $Pitch = 0.7$ (mm); b) $Pitch = 1.1$ (mm).....	139
Fig. 3-23. Explanation of different erosion rate from inclination angle of the jet	140
Fig. 3-24. Variation in the depth of pocket with two cases of the pitch.....	142
Fig. 3-25. Definition of the width of milled pocket	143
Fig. 3-26. Variation in the width of pocket with two pitch cases	144
Fig. 3-27. Definition of the slope of pocket wall.....	145
Fig. 3-28. Variation of slope of pocket wall depending on jet inclination angle	145

Fig. 3-29. Slope of pocket wall increased as repeating the trajectory over the same pocket milled at 50° 146

LIST OF TABLES

Table 1-1. Applications of AWJ machining in different industries.	3
Table 1-2. Applications of AWJ machining in composite materials.	6
Table 1-3. Summary table of the influence of process parameters [40]	45
Table 2-1. Configurations tested.....	74
Table 2-2. Rapid calibration on configuration 1.	78
Table 2-3. Rapid calibration for configurations 2 to 6.	80
Table 2-4. Errors for the various configurations tested.	85
Table 2-5. Distance in three areas.	97
Table 2-6. Distance in three areas considering $Pitch_{int} \ll R$	97
Table 2-7. Relative depth variation in the three areas.	98
Table 3-1. Constant operating parameters.	113
Table 3-2. $Ke(\alpha)$ coefficient.	118
Table 3-3. A given machine configuration.....	130
Table 3-4. Modeled and measured depth for milling pocket at different inclination angles.	143

GENERAL INTRODUCTION

The development of the material science has introduced a wide range kind of materials with especially properties such as harder (ceramics); heterogeneous structures (composites); heat sensitive (shape memory alloys); being higher strength at elevated temperatures (aerospace alloys). Machining such materials is not easy by conventional methods. It leads to a requirement of replacing familiar methods by new technologies from production researchers to solve such engineering difficulties.

In a particular domain, the aerospace industry, a necessity is to cut down component weight from galling materials such as Ti6Al4V. There exist some available processes to satisfy such material manufacturing, which are chemical milling and abrasive water jet machining. These two methods, with a vital advantage of imposing negligible forces, allow processing flexible structures of aerospace parts. Nevertheless, with the disposal of wasting acids into the environment, the chemical milling process is being surfed under threat because of the high costs of the required jobs for the acid treatment after machining. Meanwhile the abrasive water jet machining is considered promising as a versatile machining processes which can become a replacement for conventional methods for Ti6Al4V. Although abrasive water jet has received significant attention from researchers currently, most study results are applied for cutting. A few applications of abrasive water jet processes for controlled depth milling of Ti6Al4V are found in the literature, thus this field is still at new stage.

Some reports indicated a possibility of abrasive water jet (AWJ) technology to perform controlled depth milling of Ti6Al4V and can potentially apply to the aerospace industry. This domain regards to the characteristics of surface roughness, grit embedment and surface morphology as important parameters to evaluate the fatigue life of components machined by AWJ machining. However, the milling performance for a controlled depth requires a series experiment need to be conducted due to very complex process parameters while lacking a fully understand the machining process and cutting mechanism.

Therefore, in the initial stage, controlled depth milling and process modeling are being a fresh functionality to dig into due to the effects of process parameters is not clearly

understood. So, at the moment it is hard to obtain an expected milled depth on machining Ti6Al4V.

From the above reality, the contents of this Ph.D. work present a comprehensive study to develop a novel experimental methodology applying to abrasive water jet technology for hard metal milling applications, Ti6Al4V.

Managing the machining process parameters and manipulating the attack angle of the jet on the surface of a workpiece aims to jet does not cut through the workpiece while removing material. This methodology is able to machine at constant or variable depths by establishing machining configurations in which some process parameters are fixed by the machine technology. This thesis is composed of four chapters the first being introduction and the rest two dedicated to two cases corresponding to a perpendicular angle and an inclined angles of the jet.

Chapter 1 presents context of abrasive water jet technology and an historical brief of evolution of this technology. Along with a detailed study of the technology of abrasive water jet machines and its abilities to machine all materials, the effect of process parameters will be presented. This introduction part shows a very suitable process for machining of hard metals parts with thin thickness.

Chapter 2 is dedicated to the first case of abrasive water jet machining with a perpendicular attack angle of the jet to the workpiece surface. An experimental investigation is first undertaken to study the major milling performance in AWJ single pass milling on Ti6Al4V. Experimental analysis has been conducted to define a model in order to describe the single kerfs milled according to controllable parameters. Then this chapter exhibits a new model to compute the depth when milling pockets in aspect of open edges. Based on a given configuration including a given machine, specific pressure with a constant value of the firing distance of the jet, a new rapid calibration is introduced. It allows a saving of setup time to establish a model to predict the depth of cut on machining open pockets. Then, a proposed methodology is applied in milling the corner of pockets with an imposed corner radius. This new methodology permits to solve problems usually suffer in the course of machining pocket corners, especially the non-

uniform in depth. This method of generating the best strategy with a suitable traverse speed of the jet will be able to obtain a flat bottom on whole a pocket machined.

Chapter 3 presents the management of the jet firing angle that is a kinematic parameter. A new model of kerf profile taking into account the firing angle of the jet is introduced. The proposed model can be developed for the simulation of AWJM process and pave a way for milling flat bottom pockets and 3D complex shapes. To do that, further experiments are implemented to validate the effects of tool inclination angles on the formation of pockets milled in abrasive water jet machining.

Finally the general conclusion will summarize the main contributions of this study and will detail the possible developments to contribute to the implementation of industrial applications of 5-axis machining of free form parts with abrasive water jet milling.

1.1 Context

1.1.1 Evolution history and characteristics of abrasive water jet technology

The crucial point of the abrasive water jet machining technology is to make use a water at ultra-high pressure to mix abrasive particles, air, and water together to become the jet. A combination between input process parameters with suitable tool paths of machining strategies of the jet is considerable versatile and potential to cut any kind of material from soft materials (wood) to hard materials (metal alloys) along with the economic profit of saving material and time.

Historically, in the late years of 1950s decades, in the attempts of seeking a new solution to cut the wood, Norman Franz [1] discovered the fundamentals of the high-pressure water jet cutting by dropping heavy weights onto columns of water to force the fluid through a very fine orifice. The pressure powerful of water was enough to cut the wood and other materials. Some years later, in the 1970s, M. Hashish [2] was successful in conducting the first application of adding the garnet into the high-pressure water to extend the capability of the jet to cut any kinds of materials. Then, the water jet cutting process has been industrialized and commercialized in the market with a wide range of applications.

Following this way, researchers have focused on this field in order to investigate the process and improve its abilities. In his study [2], M. Hashish introduced the state of the art of the abrasive water jet cutting technology at very high pressure along with preliminary milling experiments on different materials such as aluminium, titanium, glass and graphite composites. Results confirmed that this non-conventional method is very versatile for cutting and it is one of the most energy methods and that has an outstanding potential to apply in milling application. Besides, other studies have shown the properties

and structure of the abrasive water jet, also the influence of parameters of the cutting process, and the modelling of cutting performance in brittle and ductile materials[3], [4].

The cutting technology with high water pressure is cataloged in three types: *(i)* pure water jet (PWJ), *(ii)* Abrasive water jet (AWJ) [5], *(iii)* abrasive slurry jet (ASJ) [6].

1.1.2 Ecological machining with only sand and water

When compared with other traditional and non-traditional machining processes, abrasive water jet technology shows it's environmentally friendly and ecological machining method. Materials supplying for process the operation in this technology are only water and abrasive particles.

Water can be collected directly from the wild through normal water supply systems. Before entering the machine, it is passed through some water purifiers to remove impurities or residues that can cause damages on high pressure pump.

Besides, using abrasive particles are also eco-friendly and it does not require a complex process to produce them. Abrasive particles are mostly from two resources: abrasive from natural origin and abrasive from a manufacturing operation (synthetic materials). The former that is available in large quantities in mines or sand-works and easily is gathered by crushing and sieving. The latter involves abrasive particles manufactured industrially.

1.1.3 Flexible manufacturing processes with different materials

Abrasive water jet cutting is an application broadly used in various industries: manufacturing industry, construction industry, coal mining industry, food production industry, electronic industry, and cleaning industry.

AWJ machining has been used to cut difficult-to-cut materials including ductile materials [7]–[10] and brittle materials [11]–[14]. These kinds of material could be machined by either conventional method (diamond saws) or other non-conventional methods such as plasma, lasers. However, heat – affected zone generated may produce undesirable changes in material characteristics and cannot meet the requirement of some features respected. Some specific applications [15] are presented (Table 1-1):

Table 1-1. Applications of AWJ machining in different industries.

Domain	Description of application
Aeronautics	Cutting process for materials such as titanium bodies for military aircrafts, engine components, aluminum body parts and interior cabin parts
Automotive	Parts such as interior trim (headliners, trunk liners, door panels), fiberglass components, and bumpers
Construction	Cutting and scarifying for reinforced concretes, sandblasting and cutting corroded rebar, drilling holes for bolting posts, repairing road and bridge, underground work and pile cutting
Oil and gas	Casing cutting for decommissioning of oil wells, rescue operations, platform cutting and repair, and pipe cutting
Coal mining	Being able to safely cut metal structures in the potentially explosive environment underground, digging coal with high productivity
Electronic industry	Cut out smaller circuit boards from a large piece of stock without damaging them and a very small kerf width. So there is no much waste of materials
Food industry	Food preparation, cutting some certain foods such as bread and the fat from meats

S. Paul et al. [16] presented the material removal mechanism of ductile materials with erosion models. The concept of generalized kerf shape is introduced into a qualitative model and the analytical model to predict the total depth since cutting aluminum and steel. Besides, cutting process for a total of six different metals i.e. Al 7075-T6, AISI 4340, molybdenum, Monel 400, ANSI 304 and Ti6Al4V is conducted by D. Arora et M. Ramulu [9]. They noted that the extent of deformation was found to depend on the strain hardening behavior of metals and the abrasive attack angle. A model for the depth of deformation and the depth of plastic deformation was found to be inversely proportional to the strength coefficient of metals. J. J. Rozario [17] proposed empirical models were built based on the experimental data in terms of different parameters i.e. depth of cut, kerf width and surface roughness and then using Taguchi's design of experiments and analysis of variance (ANOVA) to analyze the performance of AWJs in cutting 6063-T6 aluminum alloy.

G. Fowler et al. [18] have used a milling process on titanium alloy to observe grit embedment and surface morphology which is considered as important factors that affect to the service life of components manufactured. He has noted that with a high traverse speed and at low impingement angles or with low speed milling at jet impingement angles

up to 45° in the backward direction only, the grit embedment can be minimized. M. Hashish [7] demonstrate the feasibility of using AWJ process for controlled depth milling of gamma Titanium aluminide. It has been indicated-that it's possible to mil thin skins of about 0.5 mm with an accuracy of 0.025 mm with a jet angle of 15° firing angle. According to a study of M.C. Kong [10] applied AWJ to mill a function shape memory alloys (NiTi SMAs) considering water jet temperatures with and without abrasives particles. Results show that abrasive water jet is more efficient than plain water jet to control the milled depth.

B.H. Yan et al. [19], [20] applied AWJ technology for polishing SKD61 mold steel. SiC abrasive particles of various diameters were used with compound additives of pure water, water-solvent machining oil and water wax. The results showed that wax-coater particles not only produce a higher quality surface finish, but also save the polishing time. Application of AWJ is found further in turning process as presented by R. Manu et al.[21]. The experiment was conducted on 6063-T6 aluminum alloy cylindrical specimens in order to model the AWJ turning process considering material removal from the circumference of a rotating cylindrical specimen. The I. Finnie's model was used to evaluate the volume of material removed by impacting of particles taking into account the attack of the jet.

Regard to application of AWJ in brittle material. S. Paul et al [22] conducted cutting process on Polycrystalline ceramics and proposed the material removal mechanism with an analytical model developed to predict the total depth of cut. The model has been built using the hypothesis of the material removal mechanism that takes place in two zones on the machined surface i.e. micro-cutting and fracture in the first zone and plastic deformation and fracture in the second zones. This model also takes into account the size and shape of the abrasive particles. Experiments in AWJ cutting for Alumina ceramics is carried out by J. Wang [23] to study the effects of nozzle oscillation on the depth of cut with different combinations of process parameters. He showed that with nozzle oscillation at small angles and the cutting parameters being correctly selected the depth of cut can increase up to 82%.

A. Ghobeity et al. [24] implemented the drilling process for holes on glass and polymers with models to predict AJM erosion profiles when drilling holes with and

without masks. Besides, application of this technology for the grinding process is also found in studies of Z. W. Zhong et al [25] for glass and M.C. Kong [26] for Al₂O₃.

1.1.4 An appropriate process for machining of hard metals thin sheets

Aviation industry uses hard-to-machined materials. Furthermore, aviation parts are mostly thin parts with large size in dimensions. Manufacturing these parts requires to remove material selectively from their surfaces. Several processes are possible but they all present drawbacks:

- ✓ *Conventional milling.* Inherent problems are galling tendency, tool wear and deformation due to significant cutting forces and temperature gradient applied to the workpiece.
- ✓ *Electro discharge machining.* Material melting and re-solidification process cause in decreasing fatigue life of engineering components due to recast layer phenomenon [27].
- ✓ *Laser machining.* The high temperature during process leads to component distortion and fatigue life is reduced significantly [27].
- ✓ *Chemical machining:* in order to respect environmental safety, acids used must be treated before disposal. A significant cost is associated to this treatment. Furthermore, in order to remove material on selected areas, masks have to be prepared. Then these masks are installed before machining and must be removed afterwards.
- ✓ *Abrasive water jet machining:* the main disadvantage of this process is a low material removal rate (MRR) due to the use of improper cutting machines. In order to improve the MRR, it is first necessary to identify the elimination mechanisms corresponding to the considered material. Then, appropriate machining heads must be developed.

1.1.5 Parallel development in CFRP application

1.1.5.1 Challenges and ability of AWJ in manufacturing CFRP

Carbon Fiber Reinforced Plastic (CFRP) is getting apply widely (Table 1-2) in aerospace, marine, construction, military applications. These kind of composite materials show several outstanding advantages in characteristics: a very high strength-to- weight ratio / high modulus-to-weight ratio and corrosion resistance. To employ these composites, some machining operations such as milling, cutting, polishing, grinding, and drilling are usually required to meet demand of the final functional component [28]. Besides, machining processes are also necessary to repair composite components at where appear damaged.

However machining of the composite materials is truly hard to do because of inherent properties such as the anisotropic and non-homogeneous structure of composites, a high abrasiveness and a huge variation in their mechanical, thermal and physical properties. [28], [29]. On milling process operation of CFRPs, studies have reported the appearing of some types of deteriorations i.e. delamination, fiber pull-outs, matrix recession, inter-laminar cracks and thermal degradation, which will destroy mentioned outstanding characteristics of composite materials [30], [31].

From these limitations of the conventional methods on machining CFRPs, it has prompted scientists to find alternative non-conventional methods. Abrasive water jet process demonstrates good abilities to machine any kind of materials and also composites. [32], [33]. During the process operation, the jet creates minimal forces attacking to the target surface without heat treatment. Besides, this technology does not require any specific tooling or equipment.

1.1.5.2 Application of abrasive water jet technology for machining CFRP

The Table 1-2 shows different applications of AWJ for machining CFRP which are listed in the literature.

Table 1-2. Applications of AWJ machining in composite materials.

Material	Application	Description	Reference
Advanced engineering composite materials -AECMs (carbon fiber, glass fiber and	Milling	It is possible to mill a wide range of advanced engineering composite materials at high productive mask-less. Results show that fiber damage can be reduced by suitably controlling the energy of the jet with reasonable water jet process parameters and jet path	D.S. Srinivasu, D.A. Axinte - 2014 [34]

carbon-glass fiber).			strategy. The surface integrity milled can be improved by minimizing the damage and can effectively controlled by keep a uniform exposure time of the jet.	
Unidirectional graphite/epoxy composite material	Cutting		A comparison surround the surface characteristics after cutting by abrasive water jet and water jet is conducted on graphite/epoxy composite. It is drawn that abrasive water jet machining is more feasible machining process fort these kind of materials owing to material removal mechanisms and surperior quality surface generation.	M. Ramulu and D. Arola - 1992 [35]
Graphite/epoxy composites	Cutting		An investigation of the mechanism of delamination under AWJ machining on graphite/epoxy composites. It shows that at the initial cutting phase, the shock wave of the jet results in crack tips and then water penetration into crack tips is the main causes of delamination. A semi-analytical model to estimate the maximum delamination length is proposed.	J. Wang et al. - 2008 [36]
FRP & CFRP material	Cutting		The effect of process parameters on generation of kerf taper angle is observed on two types of composite materials graphite/epoxy and glass epoxy. Based on the energy conservation approach....	D.K. Shanmugama et al. - 2008 [37]
Carbon fibers reinforced plastic (CFRP)	Milling		Using AWJ for milling carbon fiber reinforced plastic (CFRP) composites, the influence of process parameters on material removal rate, surface quality and nature and size of defects are studied. Along with R_a , a newly criterion crater volume 'Cv' was proposed to evaluate the machined surface quality based on the quantification of the crater defects.	A. Hejjaji et al. [29], [38]
CFRP/	Drilling		CFRP/Ti6Al4V stacks were machined with abrasive water jet using different process parameters in order to evaluate the ability of AJW application for the drilling process. A positive taper angle is observed in Ti6Al4V while a negative is observed in CFRP in almost all cutting conditions. depending on the stack configuration, X-type or barrel-type kerf profile will be obtained	A. Alberdi et al. - [39]

1.1.6 Drawbacks of Abrasive water jet machining

Even if the abrasive water jet technology is a very useful machining process, especially in cutting processes, there exist some restrictions on this technology:

- A complex process with various input parameters makes many challenges to manage whole the process. The quality of machined products depends obviously on the characteristics of the jet, and on the induced workpiece erosion mode (cutting or deformation wear). Besides, to obtain a specified value of the cut depth, the accuracy is affected by a real time of performance (exposure time). This exposure time is the interaction real time between the jet and workpiece, and it becomes more complicated to manage it when the jet direction is changing following machining trajectories (Fig. 1-1).

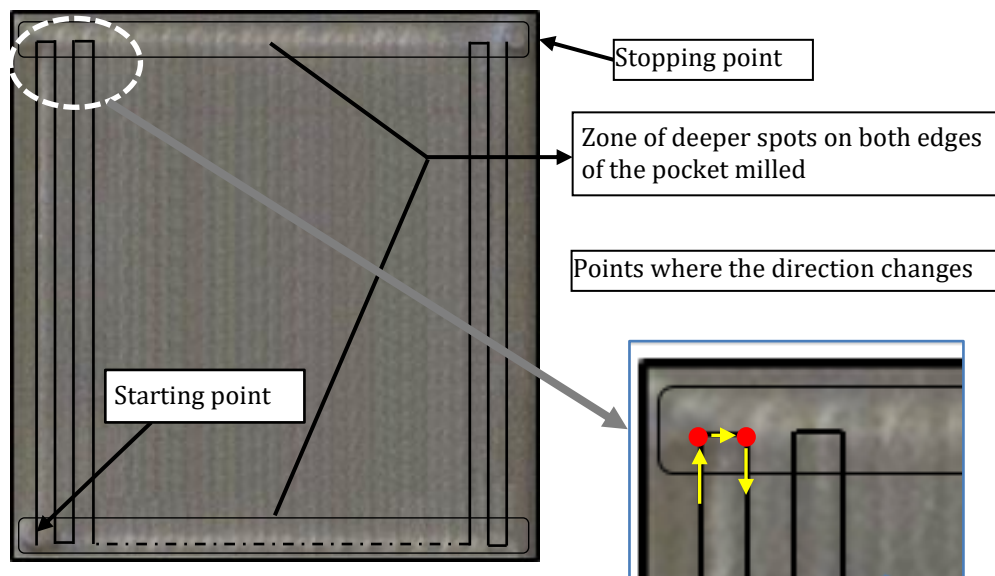


Fig. 1-1. Problem with closed edges of pocket milled [40]

- If the workpiece thickness is too high, the jet cannot cut through. It results in waviness pattern that occurs at the lower part of the cut surface due to jet deflection (Fig. 1-15).

- Abrasive particles lose energy when cutting along the thickness. It results in a kerf taper that has to be managed if particular wall geometry is required. (Fig. 1-46).

- Wear is due to the abrasive affecting the mixing chamber and the focusing tube. Or wear due to high water pressure affects the nozzle. The geometry of the jet is influenced by these wear and the quality of the machined surface is directly impacted

- During abrasive water jet milling, the jet does not pass through the workpiece and bounces off the surface. A cloud consisting of vapor and abrasive particles in suspension is thus produced. For industrialization of this process, hygiene and safety devices must be adopted.

- It has been noticed that there are generally problems associated with the use of this technique including the grit embedment on the machined surface, insufficient tolerance on the depth of cut; unsatisfying surface waviness and surface roughness of the milled areas[8].

1.2 Review of abrasive water jet process

1.2.1 Technology of abrasive water jet machines

Industrial applications of abrasive water jet technology are getting more popular than ever. The jet can be considered as a non-conventional machining tool to machine difficult-to-cut materials productively. These materials include hard metals, ceramics, marbles, and composites without creating the heat and affected zones during machining. In addition, the effects of cutting force on the workpiece are also neglect. As such outstanding advantages, abrasive water jet machining has been utilized to machine ductile and brittle materials.

1.2.1.1 Pure water jet technology

Pure abrasive water jet (Fig. 1-2) is identified by using a pure water to make a cutting operation. This type of cutting is limited to soft materials such as fabrics, PVC, plastics, ceramic fabrics, fiberglass, rubber, food and leather. This process is very fast and extremely efficient with low cutting force. A pure water is directed into a collimation tube through which the water is intensified to a high pressure. Then a nozzle with a small orifice made from sapphire, ruby or diamond is used to accelerate the water particles. Due to a friendly with the environment and healthy, the pure water jet has a lot applications in the food industry as well as in the medical field [5], [41]. For this application, the water pressure was varied between 20 and 120 MPa.

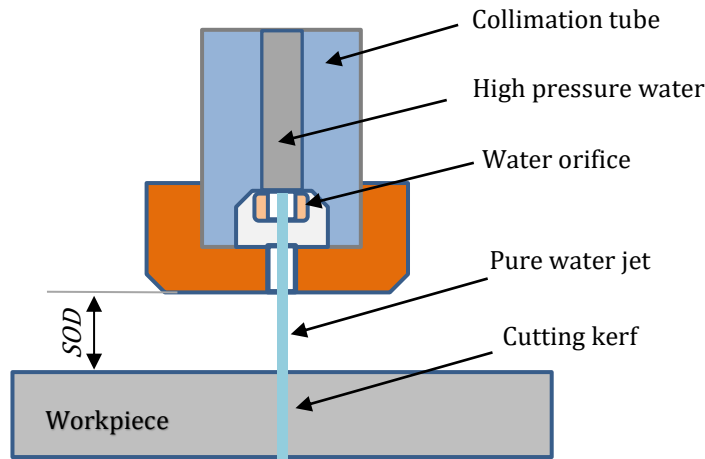


Fig. 1-2. Schema of the cutting head of PWJ [40]

1.2.1.2 Abrasive slurry jet technology

Abrasive Slurry Jet system (ASJ) is a water jet charged with abrasive. The abrasive and water are mixed already in a separate container and this mixture is pumped through the small orifice (Fig. 1-3). During performance, there is no entrained air to ensure that the characteristic of jet is homogeneous without a water droplet zone at small standoff distances.

At low pressure, the penetration rate of the jet on the target surface is not significant because of low kinetic energy of the jet. In this way, ASJ is seem to be feasible process to be benefit not only for cutting, but also for milling of multi-material [11], [42]. However, with high-pressure slurry, some problems related to the wear of the orifice and the focusing tube appears [43].

Nowadays, Abrasive slurry jets has been mainly developed for micro-machining because of some advantages over traditional micro-fabrication technologies. It is a very promising application in milling of micro-channels, especially in micro-fluidic devices and micro-electro-mechanical systems [6].

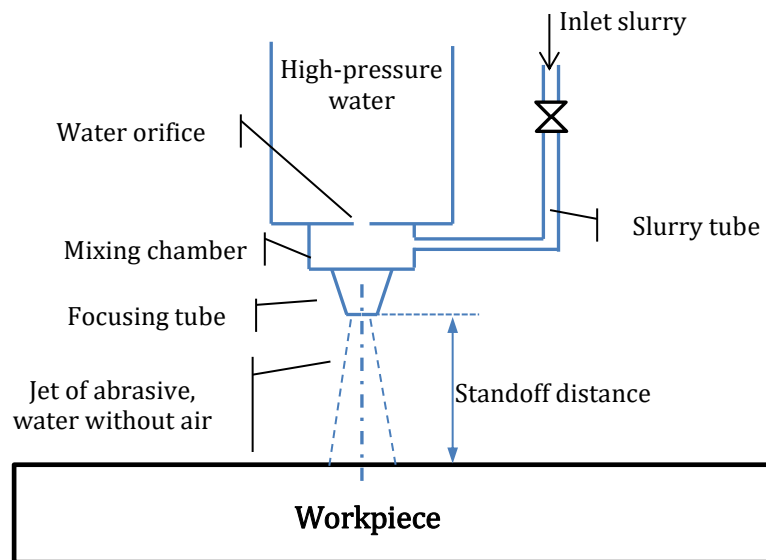


Fig. 1-3. Schematic of high-pressure slurry jet (ASJ) [6]

1.2.1.3 Abrasive water jet technology

The main idea of the abrasive water jet technology is to make use a water at ultra-high pressure to mix abrasive particles, air, and water together to become the unique jet. Using the intensifier technique, water is pumped to a very high pressure. Following through a small orifice of sapphire or diamond materials, high pressure water is converted to a very high velocity jet of water. Then, when it comes out of the orifice and go into a mixing chamber, abrasive particle (garnet, silicon carbide, alumina etc.) are added to the jet. The energy of the water will be gradually transferred to the particles within the mixing chamber as well as in the focusing tube. As a results, an abrasive water jet with high speed is generated. This jet will erode the target materials when it impacts.

Abrasive water jet technology is an advanced machining tool used to machine typically difficult to cut materials. In a typical system of abrasive water jet machine (Fig. 1-4), a hydraulically controlled high-pressure pump delivers the water to an accumulator that produces a uniform flow of high-pressure water and then high-pressure water moves to the cutting head.

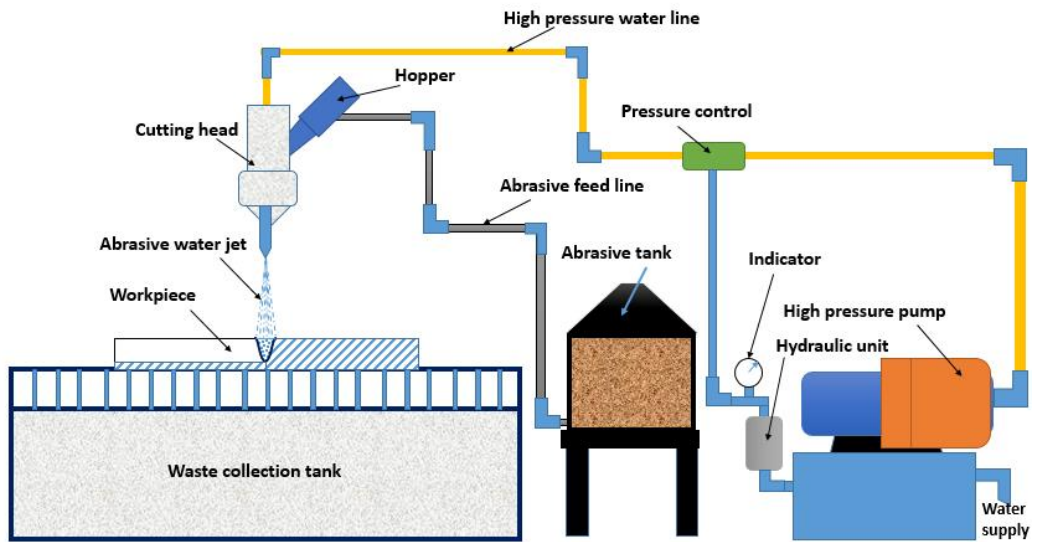


Fig. 1-4. A typical system of abrasive water jet machining technology

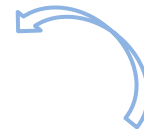
1.2.2 Working system of abrasive water jet machine

Fig. 1-5 is a typical illustration of a technology system of abrasive water jet machine. The system is comprised of three main groups: the ultrahigh-pressure pump, the machine, and the control system. In what follows, the attention will be concentrated in some main components in these groups.

✓ **The ultrahigh-pressure system:**
The pump, cutting head and plumbing



✓ **The machine:**
The X, Y, Z axes, cutting head wrist axes, and material support catcher



✓ **The control system:**
The programming software, operator interface, drive motors, and position and velocity feedback system



Fig. 1-5. Components of abrasive water jet machine (FLOW MACH 4 – ICA Lab)

1.2.2.1 The ultrahigh-pressure pump

Water is pressurized by a high-pressure pump and can reach about 400 MPa for piston pumps and 600 MPa in booster pumps (Fig. 1-6). Then, this piston allows the compression of water in rooms that play the role of water accumulator equipment.

A booster pump generates a very high pressure of water owing to a transmission pressure from a hydraulic (oil) circuit to a water circuit [40]. However, this kind of pumps operates at a low frequency of the order of 40 cycles per minute. For cutting, the low frequency of high-pressure pumps does not affect the cutting process. However, for water jet milling, any variation in pressure, or flow is not accepted to avoid a variation in the machined depth. For this reason, piston pumps are usually employed in AWJ machines.

As a pressurized water is passed through an orifice, a high-speed water jet is generated. The profile of abrasive water jet at the exit of the focusing tube is shown in Fig. 1-7 and it is described as a function of the distance travelled.

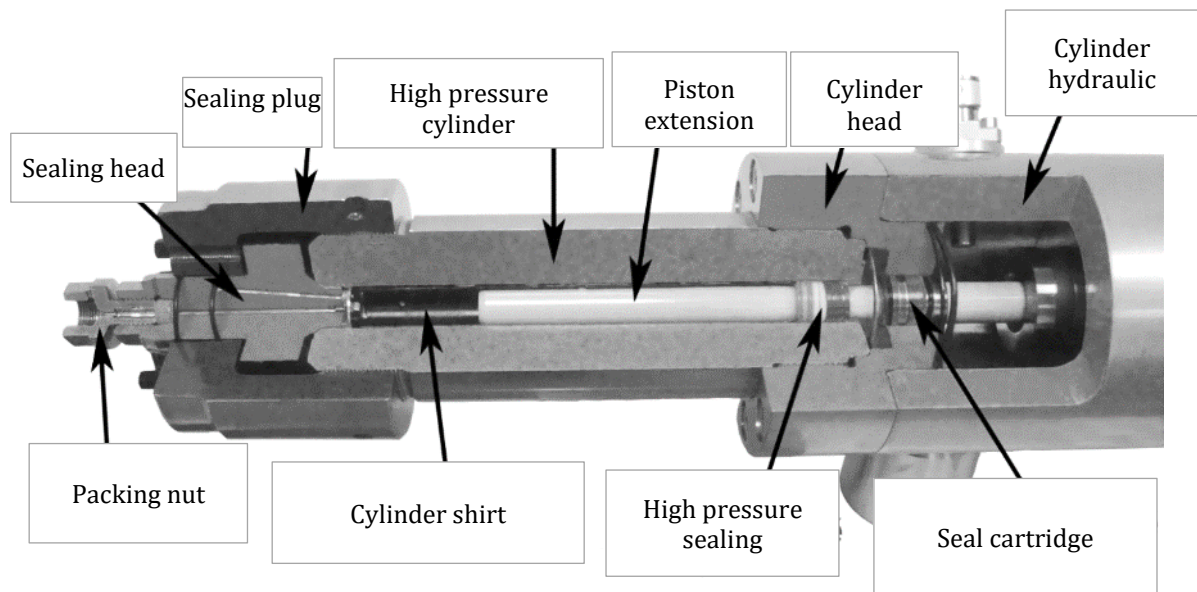


Fig. 1-6. Diagram of a booster pump(KTM water jet) [40]

In the study of A.W. Momber et al.[3], they has mentioned about using Bernoulli's Law and nozzle coefficient to define the velocity of the water jet (Eq. 1-1).

$$v_{water} = \eta \sqrt{\frac{2 * P_{water}}{\rho_{water}}} \quad \text{Eq. 1-1}$$

In this expression, v_{water} is the speed of water, P_{water} is the hydraulic pressure, ρ_{water} is the density of the water. The coefficient η denotes the nozzle efficiency that is defined by characterizing momentum losses because of wall friction, fluid-flow disturbances and compressibility of the water.

There are three phases of the velocity profile of the jet [40]:

- A consistent jet zone where the velocity where the velocity profile of the particles is almost uniform. This zone is usually used for cutting with a low standoff distances.
- A central zone (Zone A) where focused energy of the jet and the speeds is highest with small quantities of abrasive particles in this zone.
- A lateral zone (Zone B) contains a large number of abrasive particles and lower speeds.

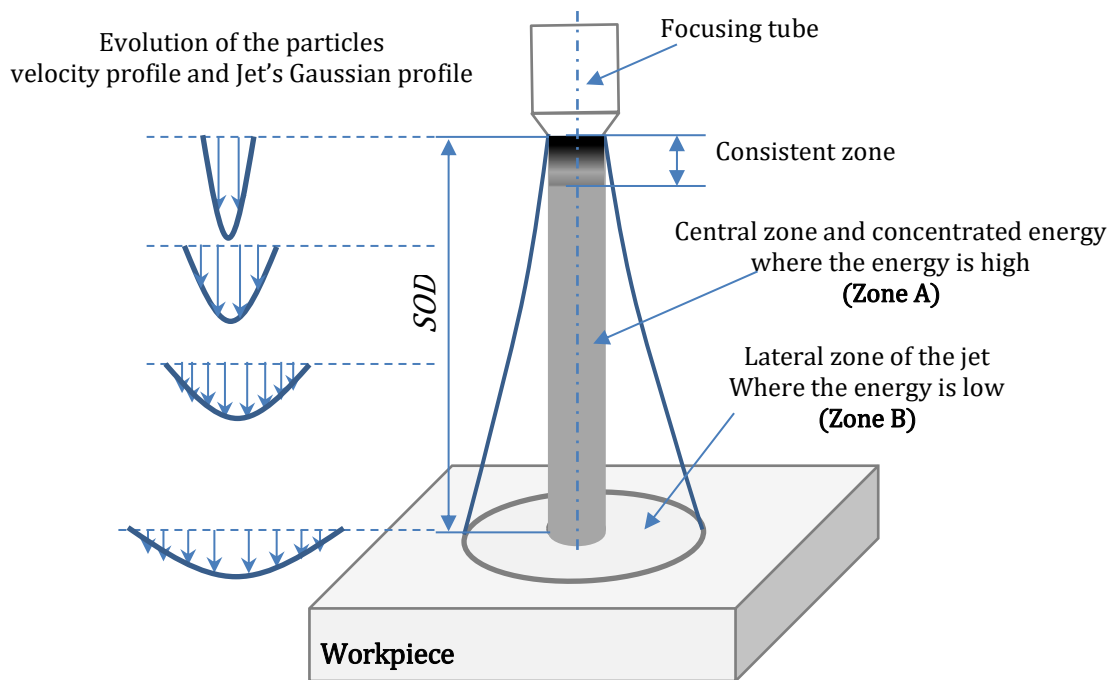


Fig. 1-7. The velocity profile of the particles which constituting the jet [40]

In literature [44]–[47], the velocity profiles were considered as the form of a bell. This bell profile will be widens and flattens as it moves away from tip of the focusing tube.

1.2.2.2 Abrasive feed system

The abrasive feed system consists of an abrasive hopper, an abrasive controllable valve, and a delivery pipes. The abrasive hopper plays as a container to store the abrasives. The abrasive controllable valve turns on/off the abrasive flow.

1.2.2.3 Water and air

The water used in this technology is pre-filtered network water (particles larger than $10\ \mu\text{m}$) before entering into the pump. It is then filtered twice at the inlet of the pump by two filters, one of $1\ \mu\text{m}$ and the other of $0.5\ \mu\text{m}$. This filtering system eliminates macros and micro-molecules that can block pumping and damage the pump[40].

Air which is drawn into the jet along with the abrasive particles and it takes more than 90% of the total volume of the tri-phase jet [40]. The air does not contribute to the removal material.

1.2.2.4 Cutting head

Fig. 1-8 show a cutting head of the abrasive water jet machine with its cross-section. The design of the cutting head allows the entrance of abrasive particles, then effectively mixing of abrasive particles and water in a mixing chamber.

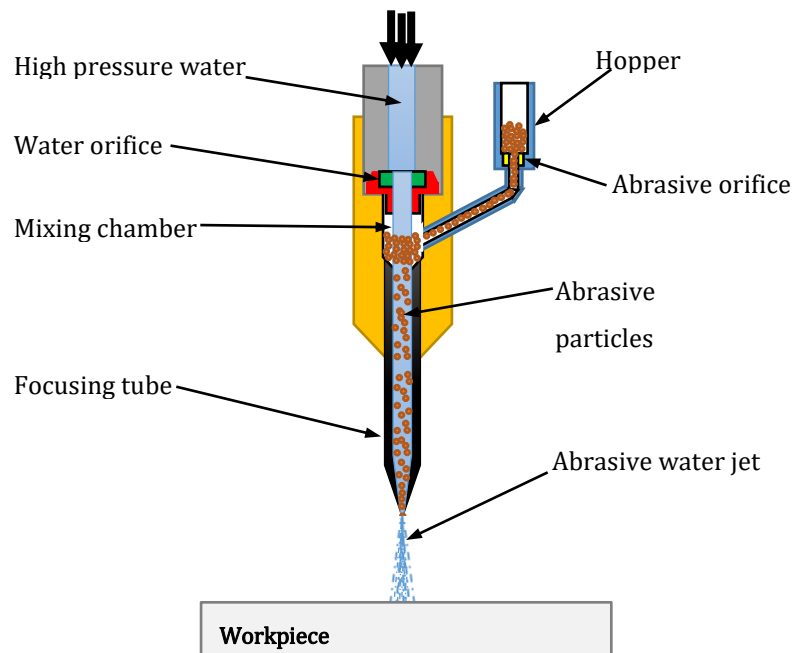


Fig. 1-8. Schema of the cutting head of AWJ machine

On working, the abrasive particles in the abrasive distributor located above the cutting head go into the mixing chamber due to itself gravity and the Venturi effect by the passage of the jet of water in the cutting head. At the end of working, as soon as stop supplying the abrasive, the inlet pipe is rapidly cleaned by the jet which contains only pure water at that moment.

Besides, thanks to a sapphire or diamond water orifice with a very small diameter from 0.1 to 0.4 mm, the energy of pressurized water is converted into kinematic energy which will be gradually transferred to the abrasive particles. Consequently, the stream of water, abrasive particles, and air are accelerated and directed to go to the focusing tube that allows concentrating the jet (Fig. 1-8). When the jet attacks a target surface, it will remove the material of the surface and form incisions. The geometry of the incision depends on, the one hand, properties of machined materials (ductile, brittle, or composite material) and, on the other, the combination of a set of process parameter in the operation.

1.2.2.5 Water orifice

Water orifice plays the role of a transformation of the pressure exerted on water particles to speed. It is made of a diamond, ruby or sapphire those materials of high wear resistant (Fig. 1-9). This structure facilitates the shape and consistency of the jet.

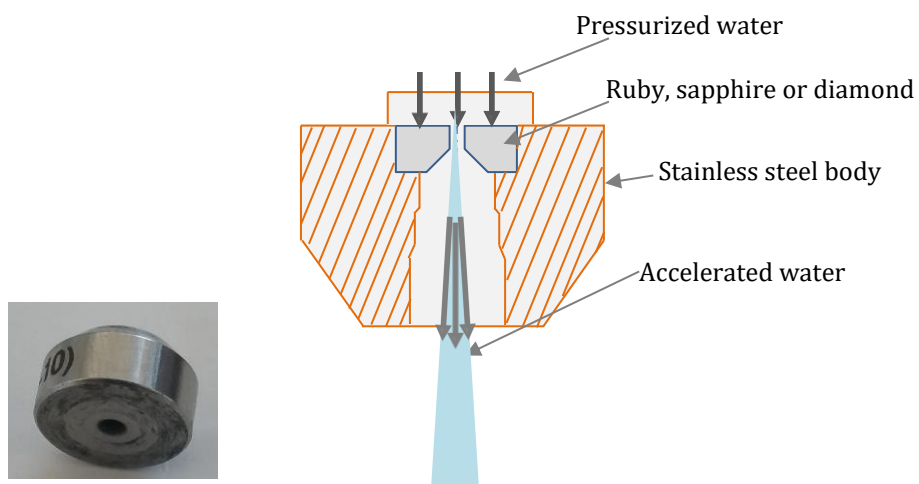


Fig. 1-9. Water orifice [40]

1.2.2.6 Abrasive orifice

Abrasive orifice (Fig. 1-10) defines the abrasive flow rate, abrasive particles pass through the abrasive orifice then go to the abrasive pipe and finally enter into the mixing chamber. For different types of abrasive particle, the variation of the abrasive flow is a function of the orifice diameter.

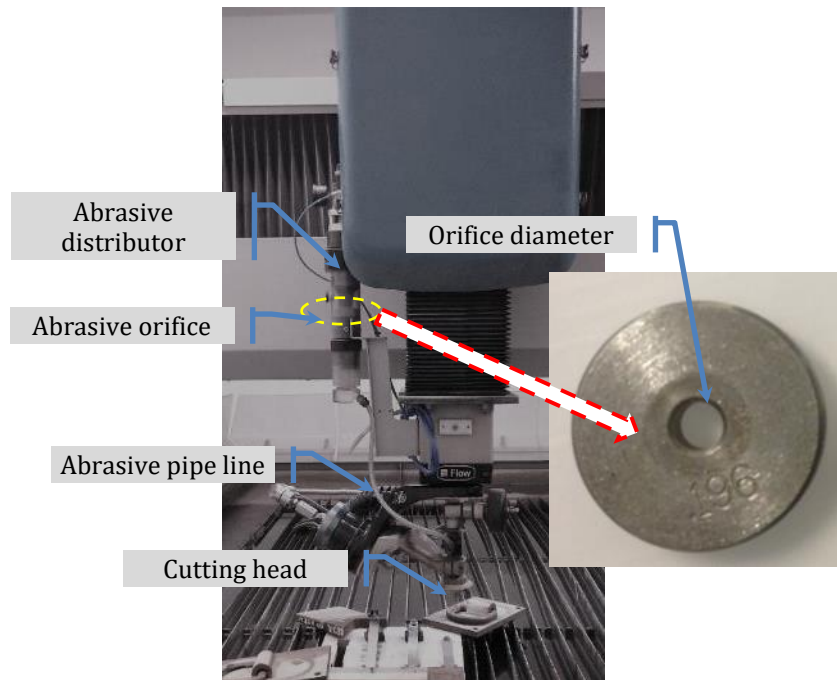


Fig. 1-10. Abrasive orifice

1.2.2.7 Mixing chamber and focusing tube

The focusing tube (Fig. 1-8) directs the jet to the cutting target and normally for AWJ cutting process, the focusing tube have a short entrance cone to facilitate abrasive grit entry. The length of the focusing tube affects particle velocity due to the frictional losses. Hence, an optimal structural design of tapered inlet, focusing tube diameter, and the length will limit erosion of the focusing tube [4].

1.2.2.8 Abrasive particles

Abrasives are mostly cataloged in two main families: abrasive from natural origin and abrasive coming from a manufacturing operation (synthetic materials). The former, a case of garnet, which is available in large quantities in mines or sand-works and easily

is gathered by crushing and sieving. The later involves abrasive particles manufactured industrially to meet specific demands.

1.2.2.9 The position control system

The position control system directs the cutting head follow to the programmed path. It consists in a 3axis or 5axis CNC machine.

For this study, it should be noted that all experiment is conducted on a FLOW MACH4C (Fig. 1-11) equipped with a PASER4 cutting head. The nozzle was of diameter 0.33 mm and the focus mechanism 1.02 mm in diameter and 101.6 mm in length. The pressure was generated using a Hyplex-Prime pump with a maximum of 400 MPa. Control of the NC machine was ensured by two software packages (Flowpath and Flowcut) provided by FLOW.

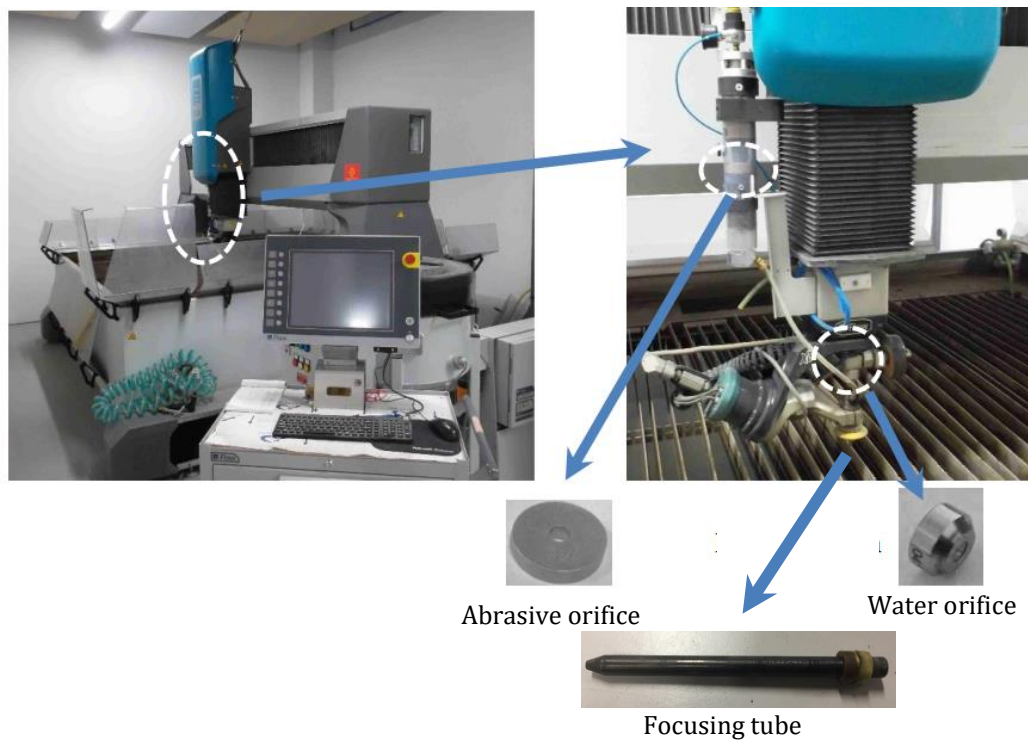


Fig. 1-11. FLOW MACH4C

1.2.3 Characteristic of the jet

K. Yanaida et al.[48] investigated a vast of experiments on geometrical structure of the jet (Fig. 1-12). The jet is divided into three zones along the axial direction consisting of the initial zone, the main zone and the final zone. They confirmed that the flow

properties are constant along the jet axis and the length of these zone depends on the diameter of the orifice, water pressure and jet velocity. M. Hashish et al. [49] investigated the high velocity cutting performance of the jet and showed a similar conclusion. In the transition zone (Fig. 1-12), the water velocity is a function of the jet radius and the radial profile of the water velocity has a typical bell shape.

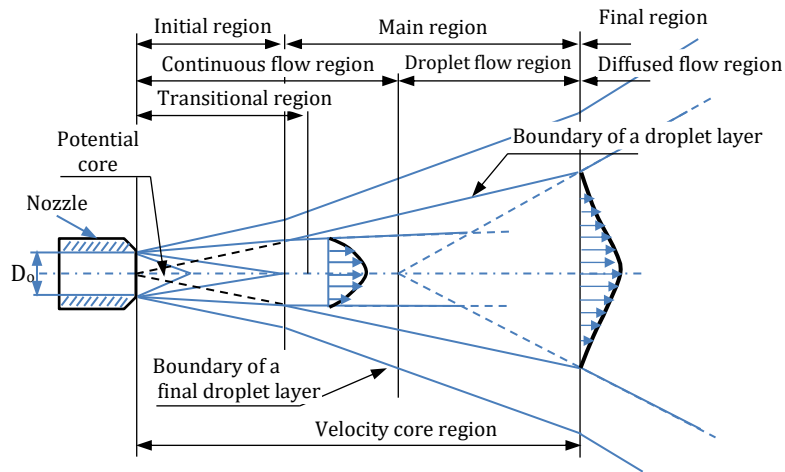


Fig. 1-12. Structure of a water jet at high velocity [48]

Several studies [5], [46], [50]–[52] showed that on working, particles flowing along the jet come and contact with material to be machined with a Gaussian distribution of particles (Fig. 1-7). Inside of the jet, there exists an inner zone A and an outer zone B (Fig. 1-7). Due to the friction interacting with the inner surface of the focusing tube, the velocity of particles in outer zone B is smaller than that in inner zone A. During machining, Impact mechanism plays the main role in removing material along the jet axis (Zone A) (Fig. 1-13).

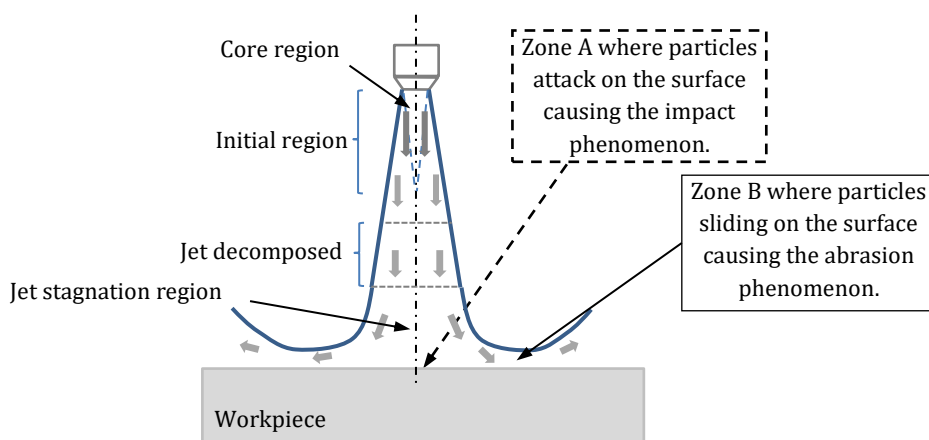


Fig. 1-13. Flow of water jet according to N. Zuckerman et al [53]

In addition, an erosion mechanism takes place, with particles on lateral zone of the jet (zone B). In other words, when machining, the action of the abrasive particles during process includes impact phenomenon and abrasion phenomenon (Fig. 1-13).

1.2.4 Material removal mechanism (Micro – Macro machining)

1.2.4.1 Removal material mechanisms in AWJ machining

In AWJ machining materials are divided into two main groups: ductile and brittle materials [42]. Removal mechanism of ductile materials is generated by a plastic deformation in which material is removed by the displacing or the cutting action. For a brittle material, the impact of the abrasive particles results in material removal owing to expand from initial cracks created out from the point of impact of the abrasive particles on the target [54].

In what follows, we will consider these two kinds of the material removal mechanism.

1.2.4.1.1 Erosion mechanism in ductile materials

The erosion mechanism of ductile materials in AWJ process is micro cutting. This action of material removal is considered similar to that of abrasive grains when grinding. Most of the material erosion models reported based on well-known models of I. Finnie [54], J. G. A. Bitter [55], [56], and M. Hashish [57].

The early model of erosion mechanism for the ductile material was introduced by I. Finnie [54]. The eroded volume is the consequence of the trajectory of the particle which interacting with the surface (Fig. 1-14). The interaction between the cutting face of the particle and the machined surface depends on the characteristic of particle, i.e. geometry, shape, hardness. Several hypotheses had been formulated to simplify the problem i.e. *(i)* there is only one cutting action producing material removal mechanism and this cutting action is harshly controlled by plastic deformation; *(ii)* there is no crack propagation of the particle during the impact ; *(iii)* the particle does not break up for impacting and move in a plane movement. Applying these hypotheses, I. Finnie has proposed two efficient expressions to predict the volume of material removed by abrasive water jet micro-machining.

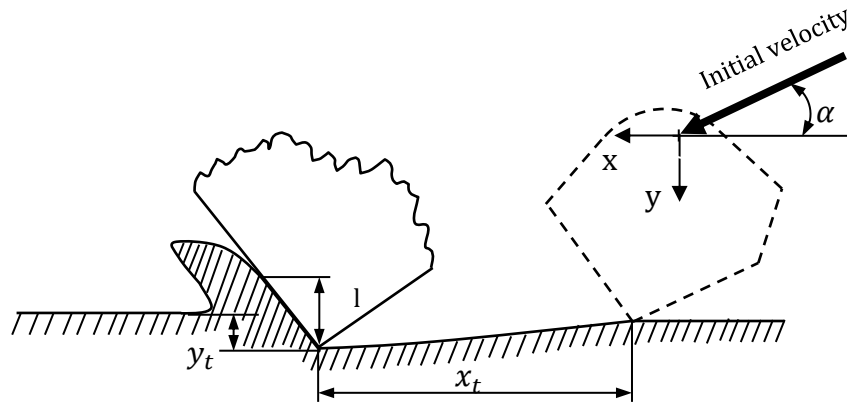


Fig. 1-14. Impacting of a particle on the machined surface [54].

However, the prediction models for material removal volume is just suitable for low impact angles and the impact angles around 90° were not considered. Besides, the phenomena of impact that may cause in a fragmentation of impacted surfaces was not taking into account. The models of I. Finnie had been improved in later studies.

Latterly, J. G. A. Bitter [55], [56] had evolved I. Finnie's model by taking into account another erosion behavior that is erosion due to deformation. As a collision of a particle on a target leading to erosion of material, there are two erosion mechanisms of the removed material. It is due to two different components of velocity vector. The tangential component of the velocity vector of a particle ($V_p \cos \alpha$) that causes in cutting or shearing erosion. The other is the normal component of the velocity vector ($V_p \sin \alpha$) in which material is removed by plastic deformation. The particle has been assumed that it is equivalent to a sphere and it only undergoes an elastic deformation. As soon as attacking a target material, if the maximum impact stress does not exceed the material elastic limit, the impact is elastic. Otherwise, that is the plastic deformation of the collided surfaces which results from the repetition of impacting. He developed two equation to calculate the material removal under each mechanism. Thus the model of J. G. A. Bitter is more comprehensive because there was a wide range of impact angles studied. For a given situation and to adapt his model, it is necessary to identify several parameters experimentally.

On impacting, if the vertical component of the particle velocity overtakes the limit speed, V_e , the material deformation is plastic and the horizontal component of velocity

produces a shear stress on a correspondent surface at the vertical section. In case of the stress in this section is greater than the shear stress of the material, the material will be removed. The action of the particle can then be separated into two stages. The first one is plastic deformation and the material is removed mainly due to this effect. This stage ends when the vertical component of the particle get to zero value. As a result of the repetition of the forces of the particle (rebounding), the particle goes out of the material.

Recently, M. Hashish's model [57] was performed in the case of cutting. Based on the I. Finnie's model, the cutting heights are defined by the impact of an abrasive water jet on a ductile metal material. The computation of the cutting depth considers, the physical and geometrical characteristics of the abrasive particle. M. Hashish presented the cutting process includes two modes, i.e. the cutting erosion mode and the deformation erosion mode. In the first mode, the material is removed by particle impact at angles, and in the second mode, the material is removed due to excessive plastic deformation by impacts at large angles. In his studies, M. Hashish presented three cases of the particle impact corresponding to three expressions of the removal material volume.

The two material removal mechanisms are the critical fundamental of the phenomenology of abrasive water jet. They are obtained by purely experimental analysis methodology during the process with different material removal mechanisms considered and characteristic of abrasive particles (geometry, velocity, and trajectory).

1.2.4.1.2 Material removal mechanism in brittle materials

The erosion of brittle material is a complex process [16], [24], [58], [59]. Although most studies are applied to specific cases of brittle materials, researchers agree that the brittle fracture behavior (cracking process) plays the main role in removing this type of material.

In his study, I. Finnie [54] stated that a simple approach is no longer accomplishable for brittle material. At the moment of the initial fracture being appeared, the rate of material removal depends on the inner propagation tendency, of the fracture and association with other fractures.

J. G. A. Bitter [55], [56] also introduced an expression to compute the material volume eroded by brittle fracture. D.B. Marshall et al [60] have investigated the formation of lateral crack in numerous brittle materials. Based on Vickers indentation, they proposed a lateral crack function of the subsurface on target material, which describes the relationship between the machined material and the indentation force to predict the length and depth of the cracks.

Slikkerveer et al. [61] studied the erosion rate in relation to roughness and strength of channels generated by AWJ machining in borosilicate glass. When impact on the material surface, each particle will remove a sphere cap of material. This sphere cap has a radius and eroded depth corresponding to that of the predicted lateral crack. In this study, the kinetic energy of particle is seen as an independent parameter and the erosion efficiency is represented by the amount of erosion per amount of kinetic energy. The surface roughness was studied and it decreases dramatically with energy because it is a function of kinetic power of the particle.

Recently, M. Papini et al.[62] have observed the influence of particle size, velocity, and impact angle on the roughness of single kerfs machined in borosilicate glass using abrasive jet micro-machining with an air. They made single impacts on the target using only one alumina particle. A plastic zone results from compressive stresses and forms the indentation zone. The formation of the initialization lateral crack begins at the bottom of the plastic area or the bottom of the indented zone. Then the lateral cracks will be propagated toward the surface and grow radially outward. When the lateral crack reaches the surface, a sphere cap is removed.

To summarize, when machining the brittle material by AWJ technology, the material is removed by the propagation and intersection of cracks ahead of and around the abrasive particle. The cutting process is a combination of brittle and ductile erosion mechanisms, but one or the other may dominate during the process.

1.2.4.2 Erosion mechanism of AWJ in cutting operation

Based on Bitter's theory [55], [56], M. Hashish [63] observed the formation process of a single kerf on a plexiglass material (Fig. 1-15), there are distinct zones in which the material will be removed by cutting or plastic deformation. There is a stable state of the

jet in which the material removal rate is equivalent to the speed of the jet. The jet has vertical trajectories up till the cutting depth reaches a depth of h_c (Fig. 1-15).

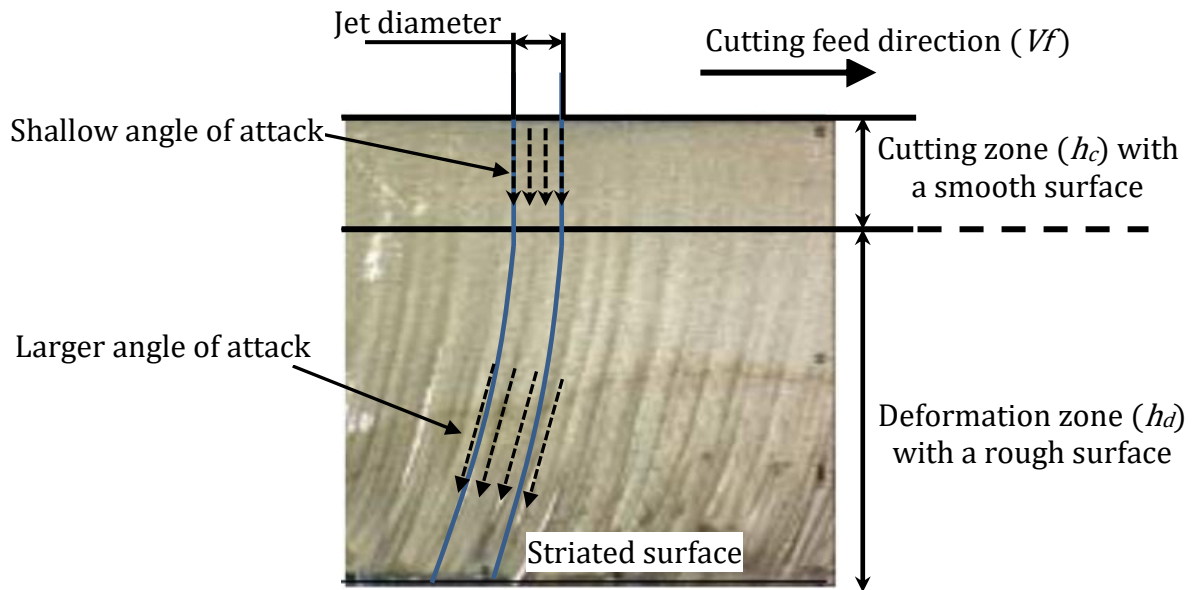


Fig. 1-15. Erosion mode and two surface texture type in cutting ductile material [40]

Then the removed material mass reduces due to the jet gradually loses energy. It leads to the abrasive particles are deviated from the vertical and the trajectories are gradually inclined. As the thickness of the workpiece is greater, the variation of the jet diameter is more important and the erosion occurs at large impact angles. Consequently, instabilities and streaks appear clearly on the cutting surface. When the depth of cut reaches its maximum (h_d), the material removal process is fully developed and dominated by erosion wear at large impact angles owing to jet upward deflection.

The work of M. Hashish is applied broadly in a lot of researches on the cutting process by abrasive water jet [5], [64]–[67].

1.2.5 Assessment of surface machined

1.2.5.1 Surface roughness and waviness

There are various investigations, [18], [32], [33], [65], [68]–[70] that have been carried out experimentally. They concluded that the surface roughness and waviness are influenced directly by abrasive flow rate, grit size, number of the scanning step, traverse

speed of the jet, cutting direction and the attack angle of the jet. For cutting process, along the depth of cut, the machined surface can be divided into two zones and characterized by two texture types (Fig. 1-15). The upper part of the depth of cut where the surface is smooth, the uniform surface texture may be reached due to in this zone, the abrasive particles attack the target surface at shallow impact angles. The critical surface roughness is employed to evaluate the surface quality in this zone. At the rest part of a cut depth corresponding to deformation zone, due to the deterioration of the water beam, the abrasive water jet which escapes from the workpiece with large angles of attacks constitutes large striations where the surface is characterized by waviness.

1.2.5.2 Surface morphology and grit embedment phenomenon

Surface morphology is important for the process of controlled depth milling in AWJM because the jet is not a solid tool. A rough surface can be due to some unwanted micro cracking and affect fatigue life.

According to G. Fowler et al. [70], the surface morphology in the milling process to control the depth of cut on Ti6Al4V is affected by the abrasive size, traverse speed, the jet impingement angle, and a number of passes. They showed that an increase in abrasive size results in higher roughness and waviness meanwhile a greater number of passes bring to a better surface roughness. The surface morphology is also influenced by the attack angle (Fig. 1-22) and the shape of the abrasive particles [4], [67], [70], [71]. Lower attack angles of abrasive particles produce a good quality of surface machined.

Grit embedment is the entrapment of abrasive particles in the machined surface. It occurs with a relatively low particle velocity [4], [18]. Besides, several studies investigated the effect of process parameters on the embedment of grit into surface milled [7], [18], [72]–[74]. Results of that studies showed that particle shape, particle hardness, characteristics of the target surface, and attack angles of abrasive particles is the main factors which affect the grit embedment.

Grit embedded cannot be eliminated from the machined surfaces it can cause reduction of surface roughness and waviness and the poor adhesion for coating [75]. Hence it is an unknown factor on the fatigue life [18].

1.2.6 Process parameters in the abrasive cutting performance

Material removal mechanism is very complex and depends mainly on the properties of workpiece material – ductile or brittle – as mentioned above. In AWJ machining, output parameters are contributed by numerous input parameters (Fig. 1-16).

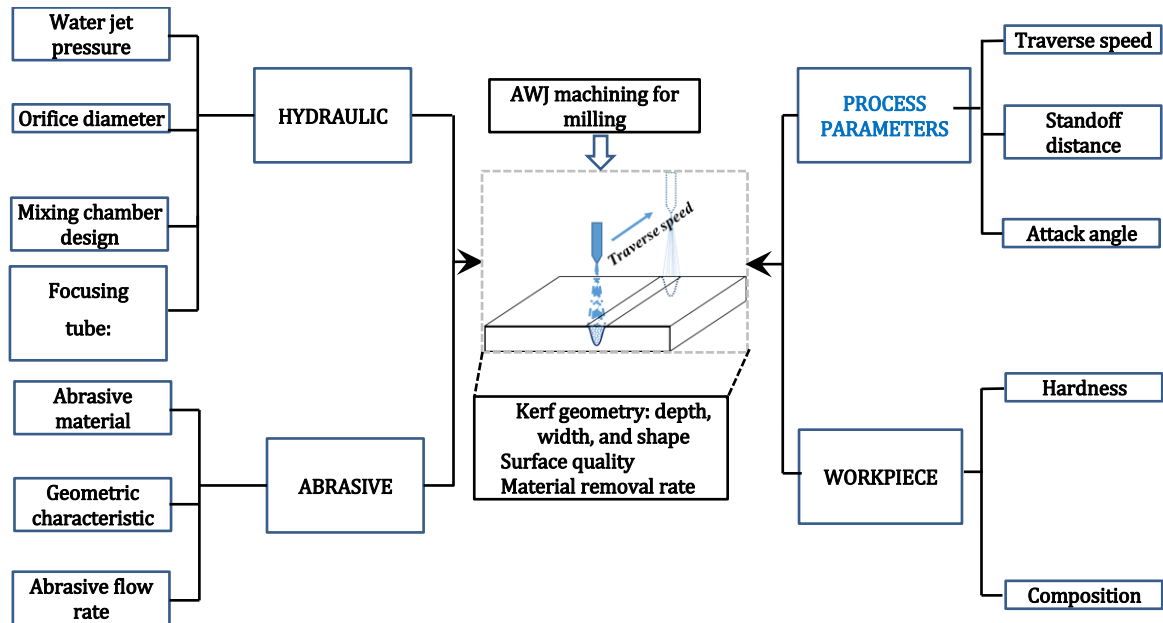


Fig. 1-16. Machining parameters

Process parameters are normally cataloged by four groups, namely hydraulic; abrasive; process parameters; workpieces [3]. Each factor in a group has an individual role during process operation. Consider an incision as an elementary machining pass on a part, a large number of investigations have been conducted on the effect of input parameters on material removal rate (MRR), kerf shape: depth and width of cut, taper angle etc.

Amongst a variety of associated parameters, effect of water pressure, abrasive flow rate, traverse speed, standoff distance, characteristic of abrasive particles, and the attack angle of the jet, will be considered.

1.2.6.1 The effect of water pressure

The pressure plays a role in the transfer of the energy from the water to the abrasive particles because erosion ability of jet is mainly dependent on the kinetic energy of particles. All the investigations shows that for each material, there is a threshold

pressure of the jet at which material removal phenomenon occurs and after this pressure value the material removal rate increases with the jet pressure [54], [57], [76]. Consequently, when pressure is higher, both the depth of cut and width of cut increase too [16], [77]. Fig. 1-17 [78] shows the relationship between the employed water pressure and depth of cut for ductile and brittle materials.

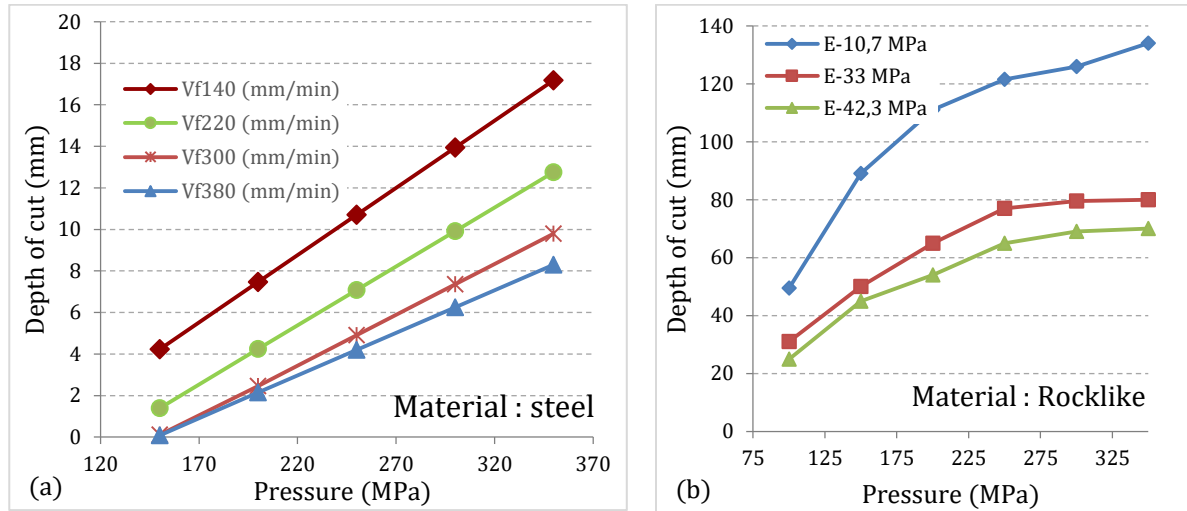


Fig. 1-17. Effect of water pressure on depth of cut for different materials
a) ductile material (Steel); b) brittle material (rocklike) [78]

For ductile materials, there is a linear relation between depth of cut and water pressure (Fig. 1-17a). However, for brittle materials, the relation is non-linear with a diminished value of cut depth. It means that the material removal rate will be less efficient at higher pressure levels (Fig. 1-17b).

As mentioned in some studies [77], [79], if the water pressure is raised up further, the jet can become poor in abrasives, abrasive grains can fragment and damping effects can appear at the bottom of the kerf. D. Arola et al. [33] considered the effect of water pressure on the surface quality on graphite/epoxy laminate part. They found that the effect of water pressure on surface roughness is insignificant in the upper portion of the kerf. However, in the below portion, the effect of pressure is considerable. An increase in pressure results in a decrease in surface roughness due to particle kinetic and particle fragmentation that increase. The effect of traverse speed V_f (mm/s)

Traverse speed is a very important factor that has effects on most response parameters of AWJ machining operation and it is easy to pilot. At low values of the traverse speed, the machining process is strongly sensitive to traverse speed changes. A

small variation in the feed rate results in significant changes of the removal material volume, especially in the depth of cut. It can be explained that the material removal process is depends on the real time of interaction between abrasive particles and target material. The material removal rate decreased significantly its value from low traverse speeds to high traverse speeds.

Z. Yong et al.[79] showed that damping processes due to an abrasive-water film at the bottom of the machined incision influence on the material removal volume. Hence, for very low traverse speed, abrasive particle density at the bottom is very high resulting in so much damping processes and there is so a constant value of depth of cut. Besides, for very high traverse rates that exceed over a critical traverse rate $v = v_{th}$, almost no material removal occurs because the number of attacking abrasive particles turns into very small.

M. Hashish has observed milling processes of aluminum alloy and found that in the range of traverse speeds from 0.5 to 5 m/s the material removal rate was approximately constant [57], [76]. G. Fowler et al. [8] have investigated the effect of traverse speed on material removal rate for the two type of abrasive particles (80# and 200#) in milling Ti6Al4V with a perpendicular jet to the machined surface. Results showed the MMR for both cases of this study is important at the lowest feed rate and fall down quickly when the traverse speed increases. The material removal rate is considered constant for higher speeds (Fig. 1-18a).

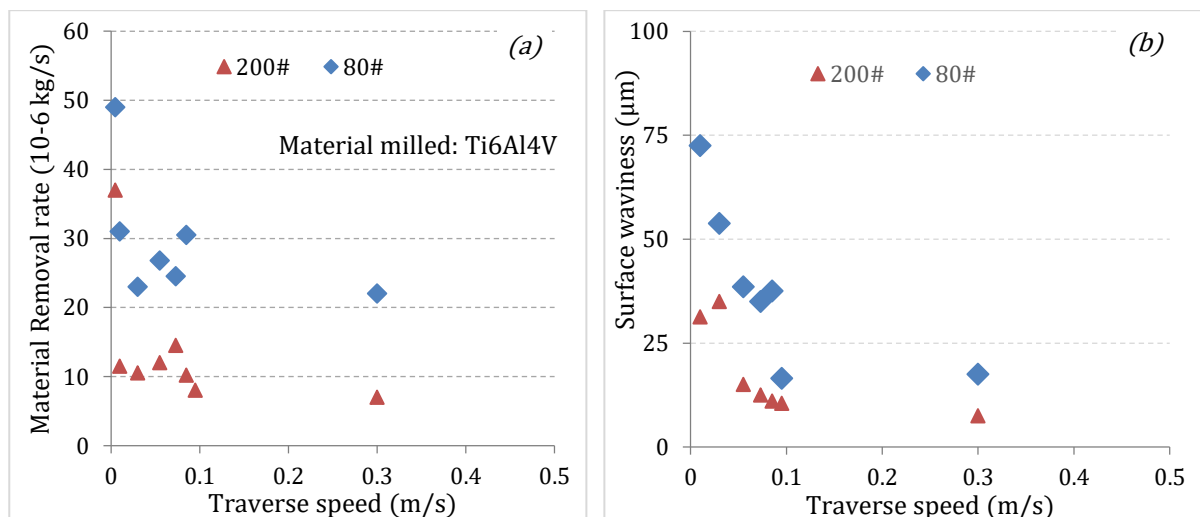


Fig. 1-18. Effect of traverse speed on material removal rate and surface waviness during AWJ milling of Ti6Al4V [8]

Besides, Fig. 1-18b shows the effect of jet traverse speed on the surface waviness of the kerf for the two particle sizes. There is the same trend of a reduction in surface waviness for both cases as traverse speed increases. It can be noted that with the larger size particle, the decreasing in surface waviness is more significant.

In the same trend, when traverse speed increases, the roughness of the machined surface will be going to a constant due to less overlap cutting action. K. MC. Ojmertz [80] has noted that low traverse speeds bring in the irregular surface morphology of the milled surface.

1.2.6.2 The effect of standoff distance (*SOD*)

Standoff distance is the distance between the tip of the nozzle and the workpiece (Fig. 1-7). The effect of standoff distance is the aim of various studies for different materials. They concluded that with an increase in the standoff distance the depth decreases linearly [7], [23], [33], [44], [49], [81], [82]. In terms of cut width, D. S. Srinivasu et al. [46] showed that the top kerf width is proportional to the standoff distance and after a specified value of standoff distance this tendency is not suitable anymore.

It should be noted that on the operating process if input parameters are kept at constant and considered as stability through the process, the kinetic energy of the jet escaping from the tip of the focusing tube is also constant. This means that the ability of the jet to remove material depends on the standoff distance, the attack angle and the traverse speed of the jet moving over the workpiece. When the standoff distance increases, the depth of cut decreases and the width of cut increases (Fig. 1-19) [4], [40], [57]. This can be explained as a result of the divergence of the water jet. At a higher standoff distance, the kinetic energy is reduced before impacting the target due to an interaction amongst abrasive particles and friction with the air. However, a higher standoff distance allows the jet to expand before impingement which results in increasing the width of cut. Hence it is interesting to conclude that at a specific value of traverse speed when the *SOD* increases, the depth decreases and the width increases with the same ratio and the area of cross-sections of the single kerf is constant (Fig. 1-19).

If the standoff distance increases so much, the divergence of the water jet becomes more important and leads to lower densities of abrasive particles in the outer

perimeter of the expanding. The tendency is not suitable anymore. Hence, the width of cut is grown down in the same way of the depth. For the cutting process, the standoff distance is normally used in a range from 2 to 3 mm such values the material removal rate is maximum and to avoid damage of the cutting head during moving on the workpiece.

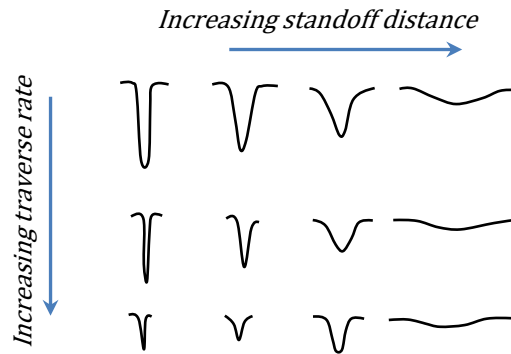


Fig. 1-19. Effect of standoff distance and traverse speed on dimensional characteristics of single kerf [57]

1.2.6.3 The effect of abrasive mass flow rate

Compare to the influence of water pressure and traverse speed, the effect of abrasive mass flow rate is not significant that is obviously observed in the literature [63], [77], [82]–[85]. The relationship between the depth of cut and the abrasive mass flow rate has a maximum value where the cutting energy of the jet is optimal. This is identified as an optimal abrasive flow rate (Fig. 1-20).

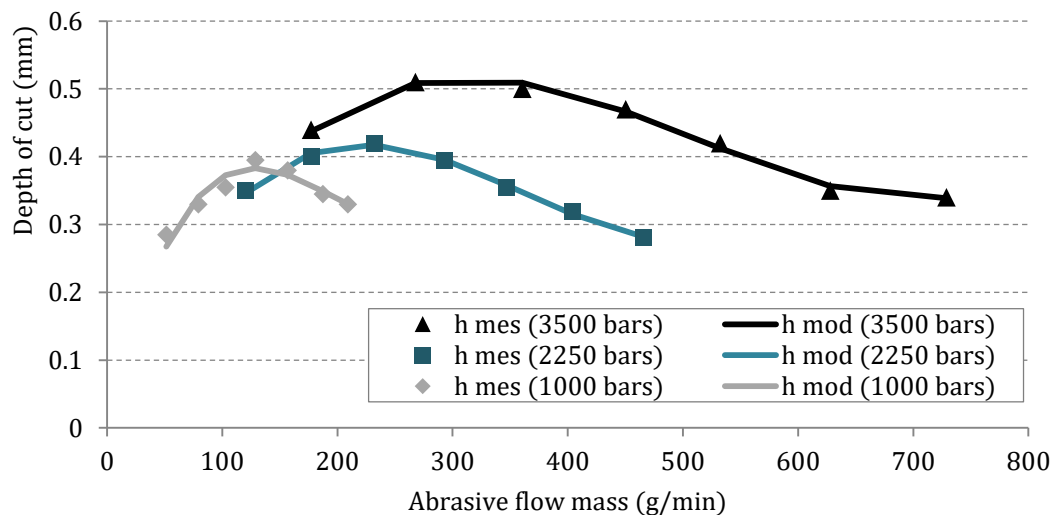


Fig. 1-20. Evolution of the depth (mm) according to the abrasive flow rate (g / min) [40]

This phenomenon is explained in some publications [44], [86], [87] in which author showed that when keeping the pressure, traverse speed and standoff distance as constant, the impact of the abrasive particles onto target material determines the ability of the abrasive water jet to penetrate the material. Both the speed of the abrasive particle and the frequency of the impingement are important since cutting is a cumulative process. While the velocity of particles specifies the impulsive loading and the potential energy transfer from the particles to the target, the frequency of impact determines the rate of energy transfer. Hence, an increase in the mass flow rate of the abrasive particles, a proportional increase in the depth of cut will emerge.

As the number of particles increases, the kinetic energy of the water must be distributed over more particles. Each particle then has a limited energy which reduces its ability to machine the material. Consequently, the concentrated force and erosion capability of the whole abrasive jet are fallen down significantly. Therefore, the depth of cut goes down after the mass flow rate increases to a specified value. This explanation is in agreement with the observations [63], [77].

In the same way, the abrasive mass flow rate has similar effects to the width of cut [88]. The single kerf will be a relatively wider width for both top and bottom when increasing the abrasive flow rate. In this case, the “kerf taper ratio” representing for the feature width to depth ratio will be approximating to 1. However, after a certain value of the mass flow rate that is called threshold value, both the depth and width cannot increase even if with a very high value of the abrasive mass flow rate.

Several studies on different materials [4], [44], [87] confirm that pressure is the main parameter that influences on the MRR and with a given pressure, the MRR has a maximum. There is, thus, an optimum abrasive flow rate for which the MRR is maximum. From this studied result, in later sections, the idea of optimal parameter selection for a given machining configuration in AWJM process will be discussed more detail.

1.2.6.4 The effect of characteristics of abrasive particles

When machining, the force is caused by the relationship between speed, weigh and kinetic energy of particles (Eq. 1-2). Depend on the material type, the surface is damaged by plastic deformation or fracture behavior.

$$E = \frac{1}{2} * m * v^2 \quad \text{Eq. 1-2}$$

In this equation, m (g) is the mass of the abrasive and v (m / s) the speed at the exit of the focusing tube and E is the kinetic energy.

The size of abrasive particles is a special number called “mesh”. Mesh number corresponds to the number of meshes per square inch of the grid that is used to sift abrasive particles considered. Common sizes are #80, #120, and #220. The abrasive size has significant effects on total kinetic energy, particles velocity, and the diffusion of the jet at the exit of the focusing tube. AH. Azimi et al. [89] have introduced the hypothesis of increasing particle velocity along with their size in case of using perfectly spherical sand particles. Then this hypothesis was asserted by experiments in which particles with bigger size and an identical density are easier to receive kinetic energy that transfers from water molecules. However, the focus of the abrasive water jet reduces as particle size grow up and smaller particles usually consume more energy because they are more sensitive to a turbulence of the jet [90].

Besides, some characteristics of abrasive particles such as the shape, hardness are important factors that also influence the removal operation of the material. In general, the shape of abrasive particles can be classified as shown in Fig. 1-21 using Tesa Visio apparatus. In this investigation, the abrasive used was garnet sand available (120 mesh) under the marketing name “Bengal Bay Garnet” originating from coasts of southern India in Bay of Bengal and supplied by “Opta Minerals”.

Most studies has confirmed that the greater the angularity of a particle, the greater the resulting material removal rate [4]. JE. Goodwin et al.[91] have made investigations by comparing the erosion between sand and industrial sand for machining. They noticed that the more abrasive particles have edges, the more efficient the machining is. According to this point, the role of the shape of the abrasive particles is therefore difficult to consider since the particles at the jet outlet no longer have their initial shape.

Particle’s hardness is classified according to their ability to scratch another surface body. A study of G. Fowler et al.[92] showed that the shape has less influence than the hardness. He presented that the rate of material removal is greater if the hardness of the

particles is higher. In contrast, the harder abrasive particles cause in faster wear for the focusing tube. S. Ferrendier [93] noted that the composition of the abrasive particle has an influence on the machining.

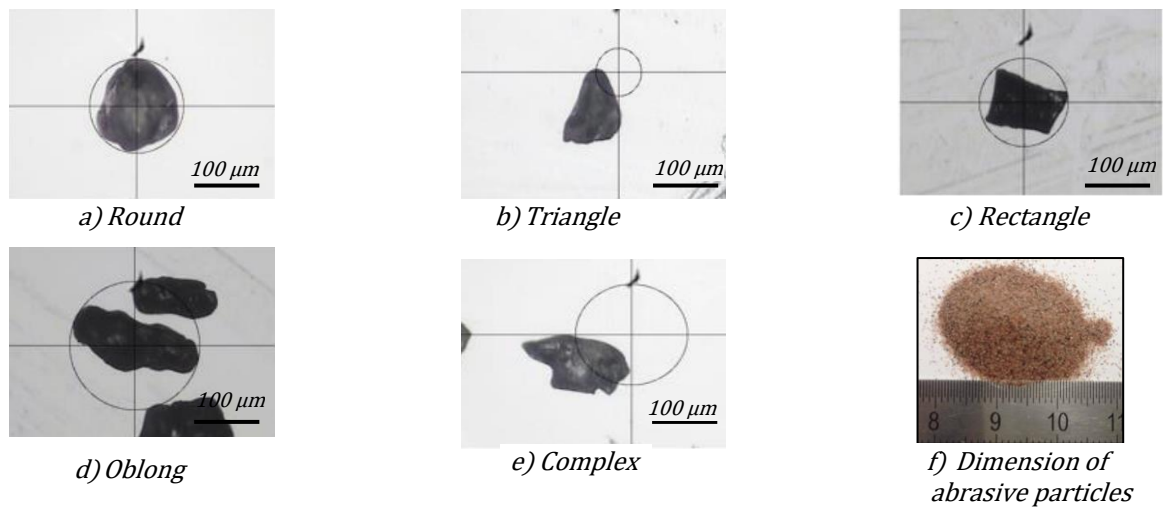


Fig. 1-21. Different shapes of particles under an investigation using Tesa Visio apparatus

1.2.6.5 The effect of attack angle

The attack angle is defined as the angle between the jet and the plane of the target material [71]. The inclination angle is defined between the projection of the jet axis onto the plane normal to the traverse speed and the surface. The impingement angle is defined between the projection of the jet axis onto the plane defined by the normal at the surface and the traverse speed and the surface. Fig. 1-22 illustrates these angles.

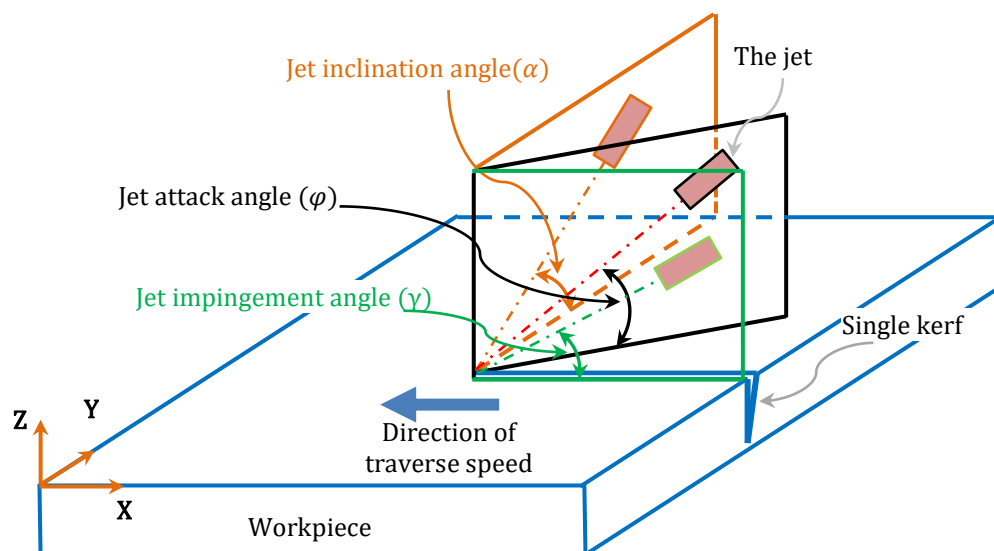


Fig. 1-22. Definition of attack angle of abrasive water jet

In most cases of AWJ machining, these three angles are 90 deg. It should be noted that if only one angle is mentioned, the other will be assumed to be 90 deg. The effect of the attack angle of the jet has been carried out [54], [71], [94], [95]. In the literature, these angles have different definitions. Thus, to be more convenient, it should be noted that the inclination angle is also called by tilt angle, firing angle (Fig. 1-23a) while the impingement angle is called impact angle or lead angle (Fig. 1-23b).

I. Finnie [54] reported an erosion study on various materials with different impact angles of abrasive particles. Results showed that there is a higher mass loss at low impact angles by abrasive particles ($\alpha = 20^\circ$) for ductile material and higher mass loss at high impact angles of the jet occurring on brittle material.

The effect of the impact angle of the jet to the material removal rate was also implemented by M. Hashish [71] on stainless steel 304. The effect on the kerf depth depends significantly on the impact angle. He suggested that there is a specific impact angle where the MRR can raise by a factor of 3 or 4 times in comparison with the material volume removed on machining at normal jet attack angles. He also observed the effect of milling direction on depth of cut of Plexiglas samples. Results showed that for backward milling (Fig. 1-23b), the process produced a shallower depth of cut than milling at 90° and forward milling produced the deepest depth of cut at 70° .

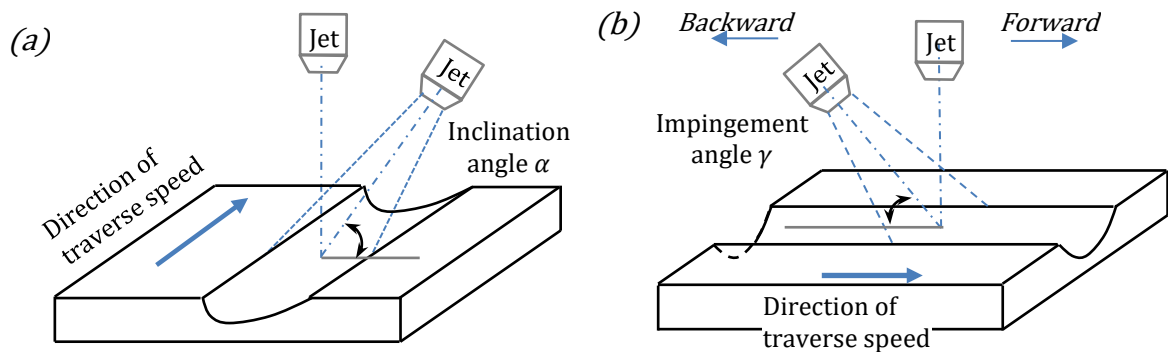


Fig. 1-23. Direction of the jet during machining

In a study on cutting of polymer matrix composites to investigate the influence of jet impact angle, Wang et al.[95] have similar conclusion on effect of the jet impact angle. He showed that the depth of cut increases as the jet impact angle increases from 50° upward and the peak value occurs at about 80° due to a different distribution of jet energy

at variations of the jet angle. J. Wang [67] presented the effect of the jet impact angle on the cutting performance in AWJ machining of alumina ceramics. He found that inclining the jet forward in the cutting plane is an effective procedure in improving the cutting and the optimum jet impact angle for cutting alumina ceramics is about 80° .

It has also been demonstrated that reduction in the jet impingement angle results in a reduction of surface roughness and waviness [71], [80]. G. Fowler et al. [70] conducted the AWJ milling process on titanium alloy and showed that at normal jet impingement, using high jet traverse speeds to minimize waviness but it results in an increase in surface roughness over that observed for milling at low impingement angles. It was explained by the effect of the suppression of secondary milling. He mentioned that roughness can be reduced by use a smaller abrasive particle and lower jet impingement.

In term of grit embedment phenomenon on machined surface, it is noted that at a high impact angle (90°), extensive grit embedment occurred whilst at low impact angles the grit embedment is less. It is interesting to note that there is the a similar tendency in AJW machining which can be seen in the literature [18], [71].

1.2.7 Modeling of machining perpendicular to the workpiece surface

Recently, significant attention has been paid in order to improve to perform the controlled depth machining by AWJ. M. Hashish [57], [76] conducted preliminary experiments on aluminum, titanium, glass, and he confirmed that there is a great potential on AWJ milling process. There is a necessary to come up with an analytical models to insure the machining performance. Studies are mainly based on semi-empirical or empirical methods and thanks to three methodologies which are the erosion mechanism in AWJ cutting [16], [63], [74], [96] , the energy conservation theory [84], [97] and the regression analysis technique [17], [33], [68].

1.2.7.1 Abrasive water jet for-milling a single kerf (elementary pass)

It appeared in the early 1990s and was intended for making closed pockets. In order to understand the pocket machining in AWJ machining the incisions, representing a single straight passage, must first be studied.

After exiting from the tip of the focusing tube, the velocity profile of the mixed jet is described as a Gaussian profile (Fig. 1-13a) [44], [46], [78]. The jet is used as a milling tool generating a bell's profile related to the fluid behaviour of the jet (Fig. 1-24).

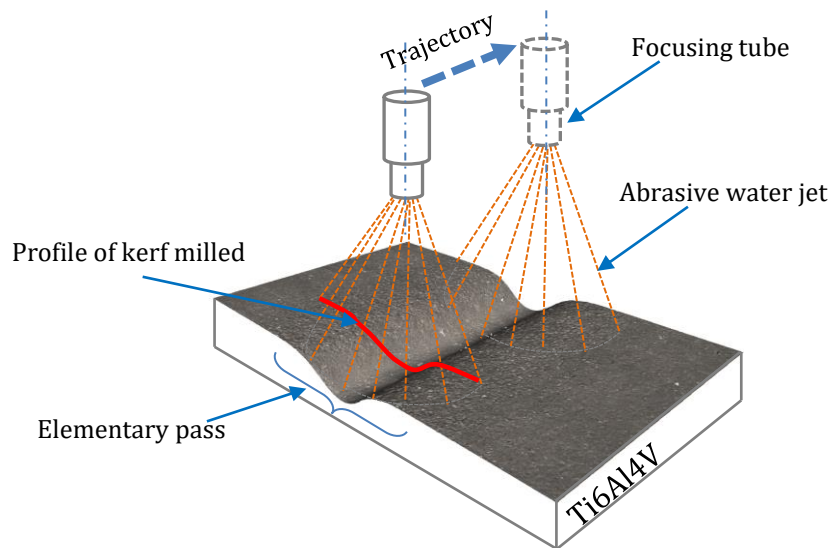


Fig. 1-24. A single kerf machined by abrasive water jet [51]

B. Freist et al. [98] used a cosine function to fit the kerf geometry of channel milled on ceramic. And using a similar approach, A. Laurinat et al. [99] have introduced an analytical model to predict the depth of cut in ductile materials. D. S. Srinivasu and D.A. Axinte [47] have proposed an analytical model for top width of jet footprint in AWJ milling on SiC ceramics material at various jet impingement angles. He showed the physical phenomena for generation of the single kerf, especially the top width considering the influence of jet traverse speed, the jet plume divergence, and the standoff distance. The proposed indicated a good efficiency to predict the trend of top kerf width variation. However, the prediction deviation slightly increases at lower jet impingements. J. Billingham et al [100] presented a mathematical model of abrasive water jet footprints for arbitrarily moving jets from moving of single and multiple overlapped footprints with low errors. In his study M.C. Kong [100] established a predict model for the depth of cut of abrasive water jet footprint in arbitrarily moving cases of the jet using statistical and empirical approaches. These approaches usually requires numerous experiments.

In his works, A. Alberdi et al. [44], [45] used a Gaussian bell function to modelled the kerf profile of a straight channel since milling by AWJ machine. This kerf profile is

characterized by the maximum depth (h_{max}), maximum width (b), and the width at the half of the maximum depth ($b_{0.5}$) (Fig. 1-25).

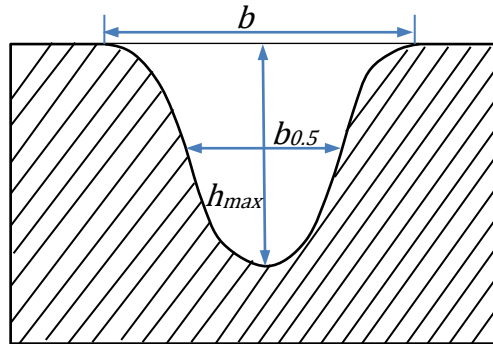


Fig. 1-25. Characteristic of a kerf profile

According to the Gaussian model, the profile of an incision machined by AWJM, is described using only two coefficients (Eq. 1-3) [44].

$$y(x) = a * e^{\frac{-(x-x_0)^2}{b^2}} \quad \text{Eq. 1-3}$$

With: “a, b”, the maximum depth and width factor of the single kerf respectively; “ x_0 ”, the position of the single kerf on the X-axis. Fig. 1-26 is a specific example of modeling a single kerf using Gaussian function and this experiment is implemented for Ti6Al4V in abrasive water jet machine.

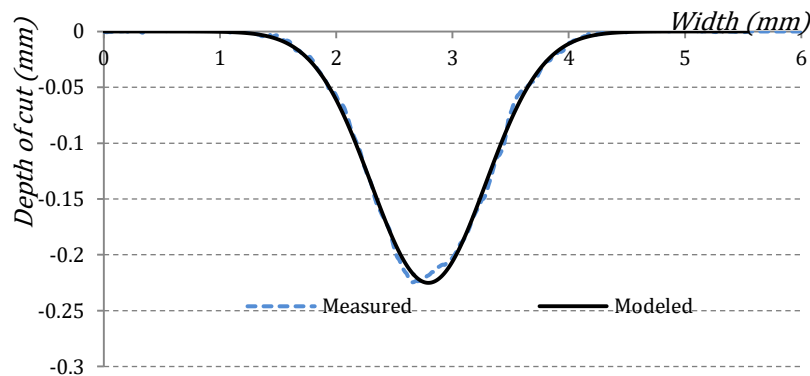


Fig. 1-26. An experimental validation using Gaussian to model a single kerf in milling Titanium alloy

T. Sultan [40] has conducted experiments in case of single kerfs on Ti6Al4V. He compared Gaussian model with. Lorentz model, Pearson model, and Gauss decomposed (GD) model (Fig. 1-27).

$$Y(x) = \frac{a}{2} * e^{-\left(\frac{x-x_0}{b_1}\right)^2} + \frac{a}{2} * e^{-\left(\frac{x-x_0}{b_2}\right)^2} \quad \text{Eq. 1-4}$$

With a = maximum depth; x_0 = adjusting distance on x -axis; b_1, b_2 = width parameters relative to each distribution of the jet.

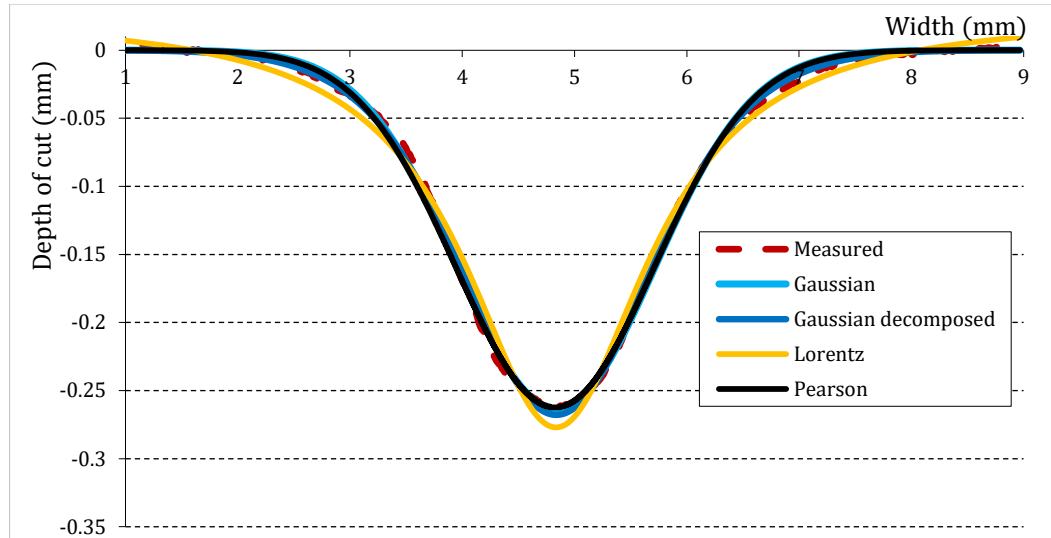


Fig. 1-27. Comparison theoretical models with the measured profile of single kerf [51]

Experiment results demonstrated that Gauss decomposed (GD) model-can improve modelling of elementary passes (Eq. 1-4). These results are in accordance with the study of M. Zaki [50]. The profile obtained by a single jet path in AWJ machine is not only a Gaussian profile but a sum of two Gaussian profiles corresponding to two physical phenomena. The proposed Gauss Decomposed (GD) model (Eq. 1-4) incorporates three variables i.e. “ a ” representing for the depth, “ b_1 ” and “ b_2 ” representing for the width factor. A comparison of the two models (Fig. 1-28) on single kerf made on titanium shows that the coefficient b of the Gauss initial model represents the mean of the two coefficients b_1 and b_2 of the decomposed Gaussian model.

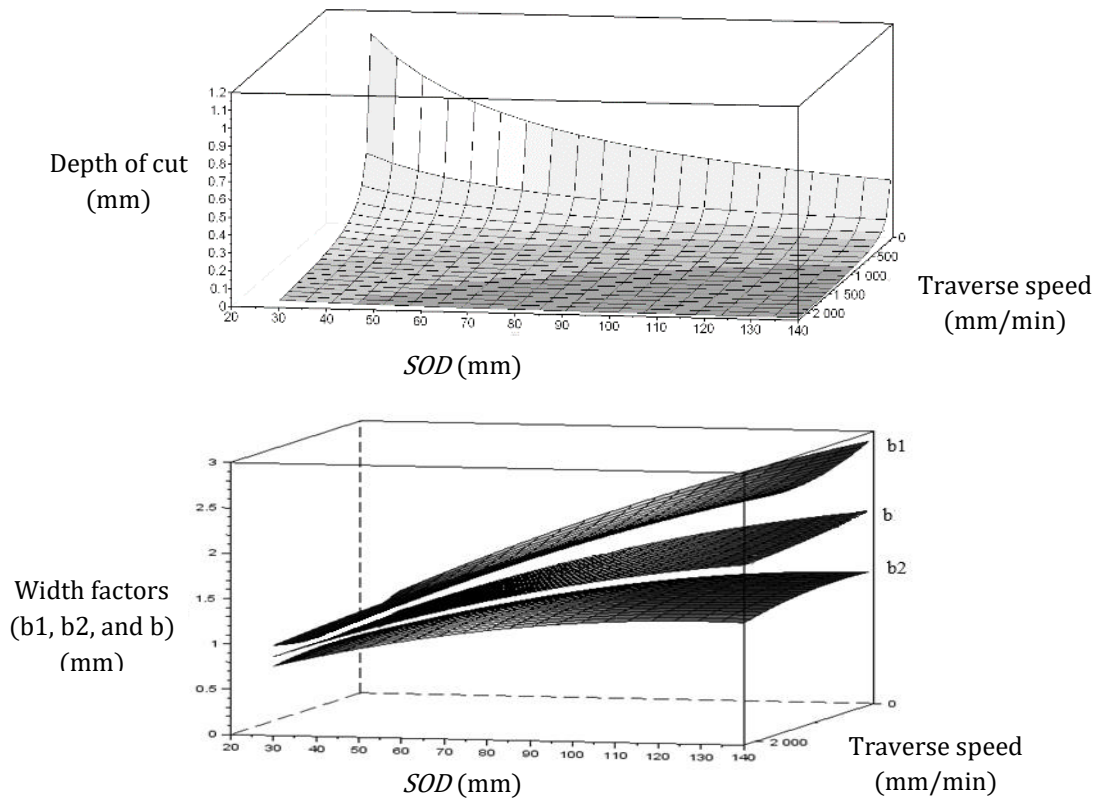


Fig. 1-28. Relationship between the GD width parameters and the simple Gauss model [40]

To model single kerfs, T. Sultan [42] conducted a lot of experiment by varying different process parameters such as water pressure, standoff distance, traverse speed, abrasive particles, abrasive flow mass (abrasive orifice). Coefficients in Eq. 1-4 was modeled by Eq. 1-5-Eq. 1-7.

$$a = a_0 * Vf^{a1} * SOD^{a2} * Gr^{a3} * P^{a4} \quad \text{Eq. 1-5}$$

$$b1 = b10 * Vf^{b11} * SOD^{b12} * Gr^{b13} * P^{b14} \quad \text{Eq. 1-6}$$

$$b2 = b20 * Vf^{b21} * SOD^{b22} * Gr^{b23} * P^{b24} \quad \text{Eq. 1-7}$$

The disadvantage of this modeling is that it requires a lot of experiments to represent the influence of all the parameters.

From these obstacles, it is mandatory to understand deeper the phenomenon of abrasive water jet. T. Sultan [42] shown that in case of small *SOD* the Gauss decomposed model tend to a normal Gaussian model [51] (Fig. 1-28).

1.2.7.2 The effect of process parameters on the generation of a single kerf

Apply Gaussian model for milling a single kerf, we have conducted sets of test for predicting the geometrical parameters of the single kerf as well as the area removed inside the incision (area milled) and the MRR.

All the experiments is carried out on titanium alloy Ti6Al4V and then the profile of these single kerf machined is extracted by using an "Alicona" optical profilometer for surface measurement (Fig. 1-29). This equipment uses the technology of the focal length variation for each pixel. Autofocus function is able to record the coordinate of the center and achieve a precision of the order of 10 nanometers theoretically. Manipulation is made on specimens over a measurement length of 2 mm wide corresponding to 1000 lines. The selected number of lines makes it possible to average the measurements on the area observed. On the acquisition thus obtained, the Alicona software retrieves the coordinates of 6000 points and thus draws the curve of the measured profile (Fig. 1-29). This measurement method is both accurate and acceptable in terms of measurement time.

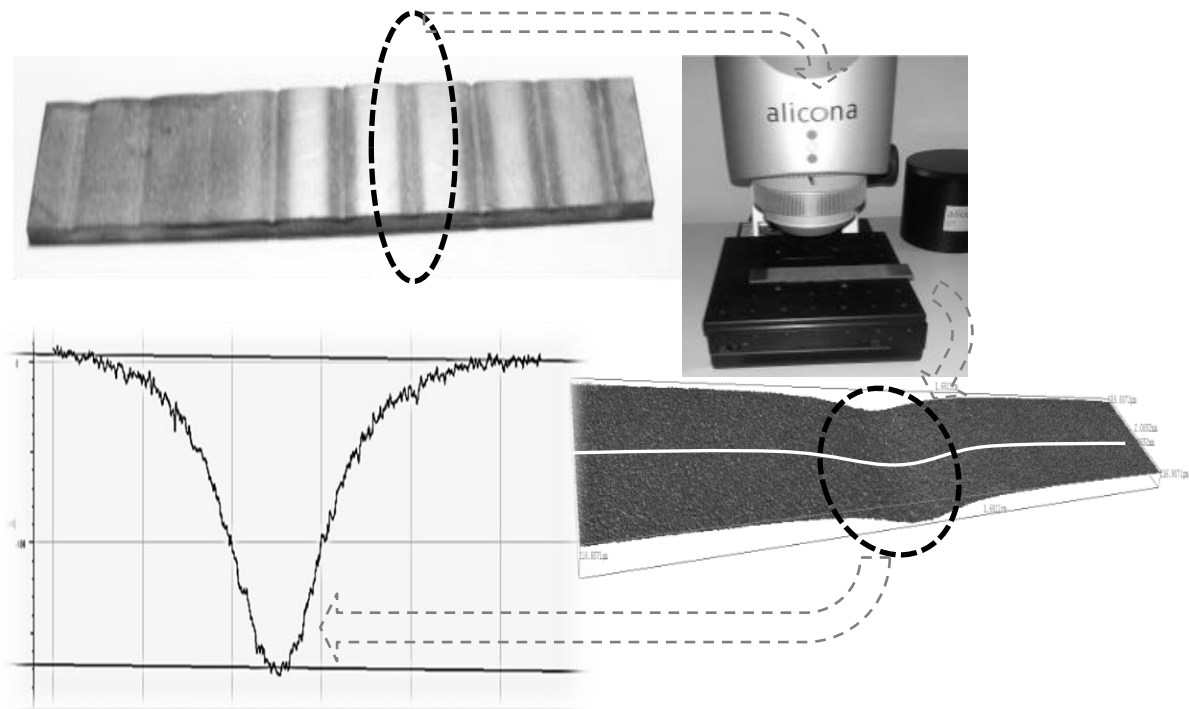


Fig. 1-29. Profile of single kerf extracted from "Alicona" optical profilometer [40]

Using the least squares method, the variation between the geometrical parameters (Eq. 1-5, Eq. 1-6, and Eq. 1-7) measured (resulting from the values of the Gaussian model)

and the modeled geometrical parameters were calculated. The result of small variations shows that the models of the geometric parameters of the incision are in good correlation with the measured values resulting from the Gaussian model. Besides, the area of the cross-section of a single kerf can be obtained by calculating the integral of the Gaussian model expression (Eq. 1-8 and Eq. 1-9) [40].

$$S = \int_{-\infty}^{+\infty} a \left(e^{-\left(\frac{x}{b1}\right)^2} + e^{-\left(\frac{x}{b2}\right)^2} \right) dx = \sqrt{\pi} * a * (b1 + b2)/2 \quad \text{Eq. 1-8}$$

$$S_{mes} = \sqrt{\pi} * a_{mes} * bm_{mes} \quad \text{Eq. 1-9}$$

$$S_{mod} = \sqrt{\pi} * a_{mod} * bm_{mod}$$

Moreover, the material removal rate can then computed by multiplying the internal surface of the area of the incision by the traverse speed (Eq. 1-10 and Eq. 1-11).

$$MRR_{mes} = S_{mes} * Vf = \sqrt{\pi} * a_{mes} * bm_{mes} * Vf \quad \text{Eq. 1-10}$$

$$MRR_{mod} = \sqrt{\pi} * a_{mod} * bm_{mod} * Vf \quad \text{Eq. 1-11}$$

Where: MRR_{mes}, MRR_{mod} – the material removal rate measured and modelled; a_{mes}, a_{mod} – maximum depth of cut measured and modelled; bm_{mes}, bm_{mod} – width factors measured and modelled.

Consider a single kerf generated by abrasive water jet milling process (Fig. 1-24), the effect of input parameters to the output parameters can be discussed as follows:

1.2.7.2.1 The effect of SOD and Vf

The effect of the main process parameters is described in Fig. 1-30 [40]. The depth and width of the single kerf decrease as the traverse speed (Vf) increases. But the depth decreases more significant than the width when Vf increases (Fig. 1-30(a) and (b)). In addition, this trend is reversed according to the variation of the standoff distance (SOD). As SOD increases, the depth decreases, but this change is less than that of the width.

Fig. 1-30(c) shows the area milled of the incision as a function of the traverse speed (V_f). The area decreases significantly as traverse speed increase due to the exposure time of interaction between the jet and the target decrease. Besides, the material removal rate which depends on the area machined per a time unit and describes in Eq. 1-10 and Eq. 1-11 also follows this evolution. Indeed when traverse speed increases, MRR will be reduced (Fig. 1-30(d)). However, the values of the area machined decreases sharply as traverse speed increases while the material removal rate reduce slowly.

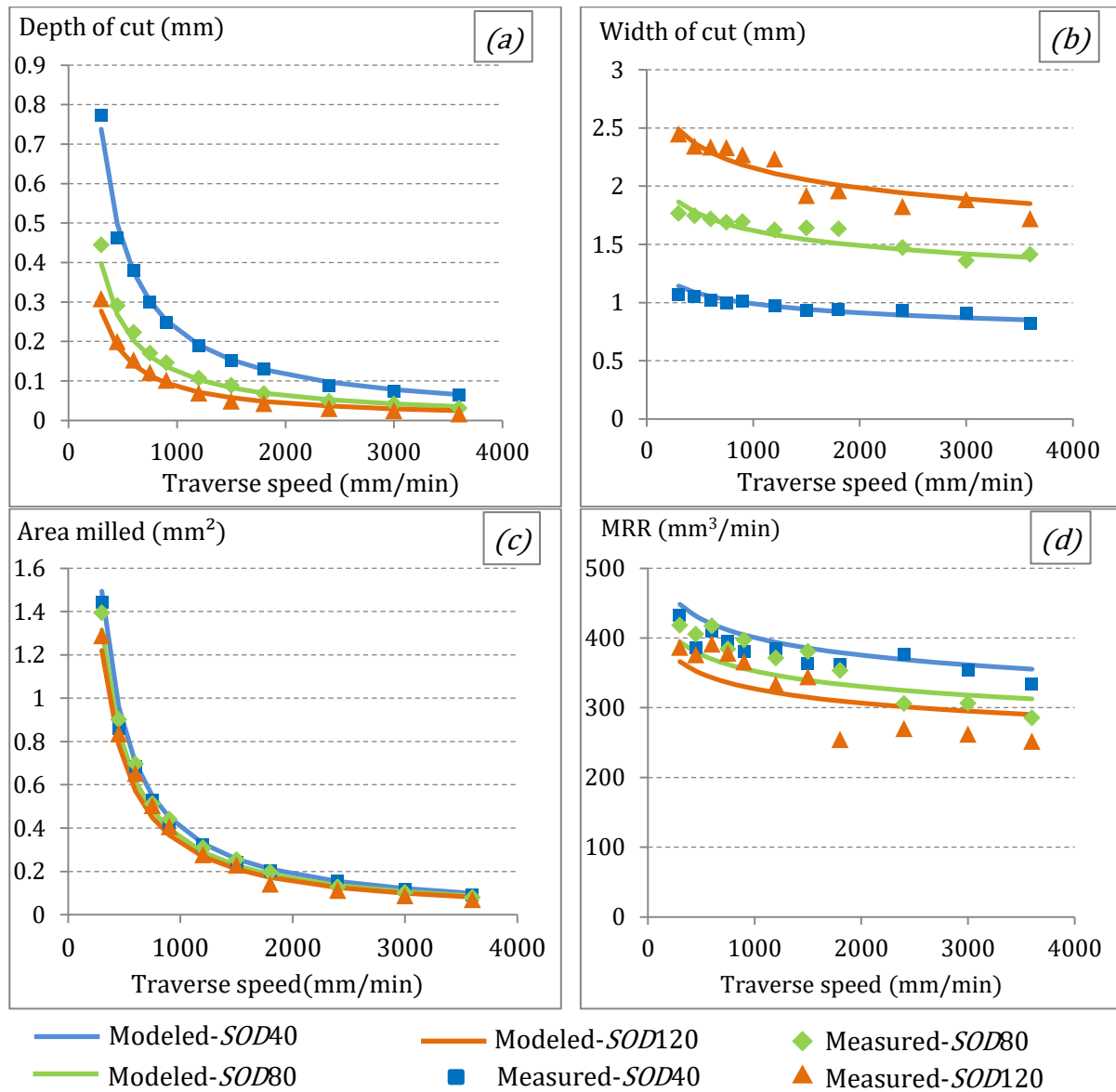


Fig. 1-30. Effect of SOD and V_f on a single kerf [40]

The average error between the measured and modelled value of area milled (mm²) and those of the material removal rate (MRR) (mm³/min) is quite similar, about 9.4%. This little difference has confirmed that the normal Gaussian is stability and allows

enough reliability for modelling single kerf. Moreover, this difference may come from a lateral plastic deformation phenomenon that occurs on the edges of the incisions (§1.2.3) and it becomes more important for high values of SOD and V_f . The MRR is influenced by traverse speed much more than the effect of SOD . Thus, in order to achieve a high yield, it requires to use low traverse speeds.

1.2.7.2.2 The effect of pressure (P)

The influence of pressure is showed in (Fig. 1-31), with the increases of the impact energy, the material removal rate increases. Indeed, water pressure has a much stronger influence on the depth of cut than the width, this influence is more clearly at the lower traverse speeds (Fig. 1-31a, b).

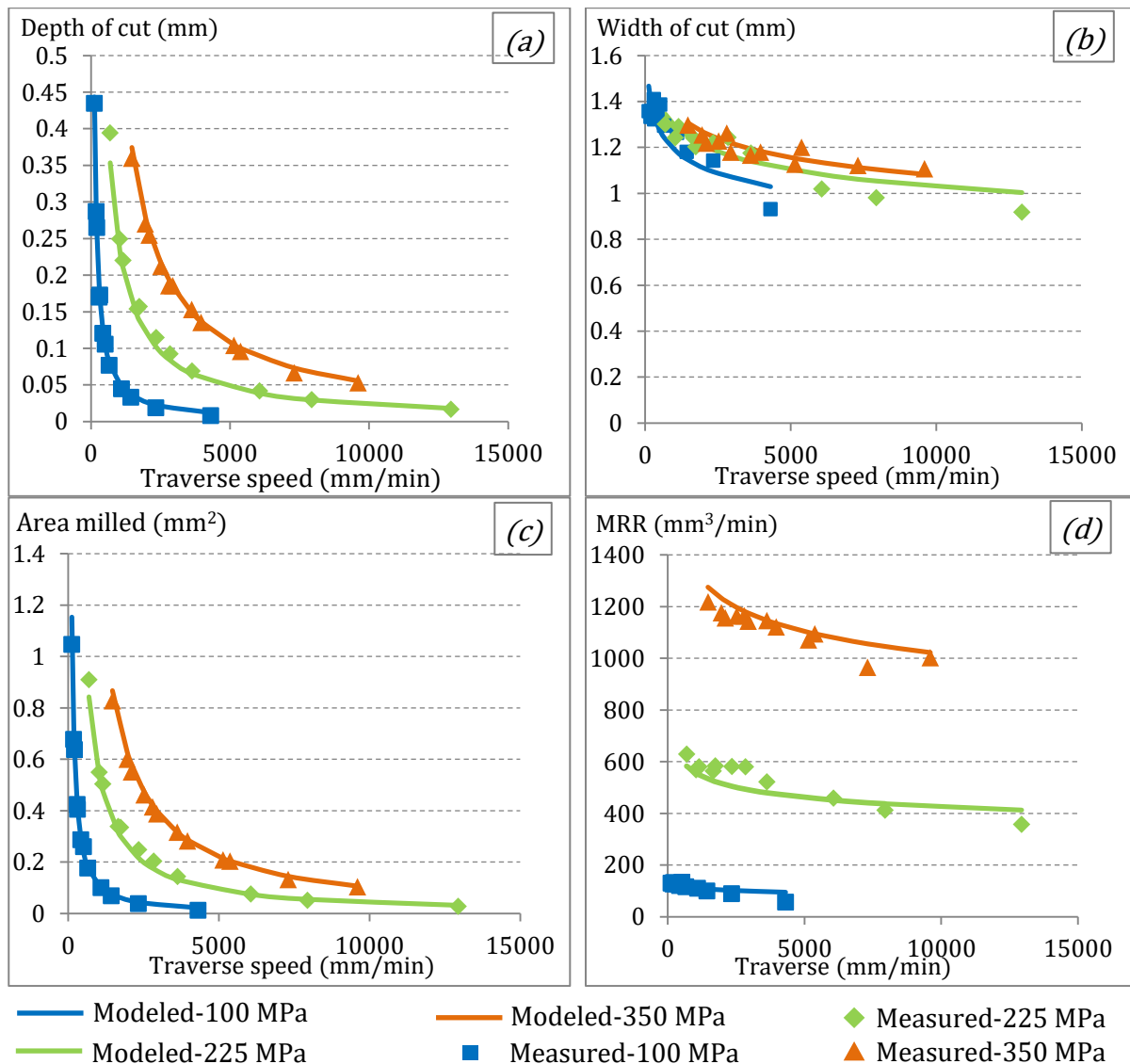


Fig. 1-31. Effect of water pressure on a single kerf with $SOD = 100$ mm [40]

The MRR is strongly influenced by pressure (Fig. 1-31d). This is understood by the remarkable influence of the pressure on the depth of the incision, which is directly proportional to the area milled of the incision.

1.2.7.2.3 The effect of the abrasive particle size

The abrasive size has strong effect to the milled area and the MRR (Fig. 1-32). It remains to a lesser extent with respect to the pressure but remains more influential than the firing distance. For a fixed traverse speed, the gain in the MRR decrease 40% when the size of particle increases from 120 mesh to 220 mesh.

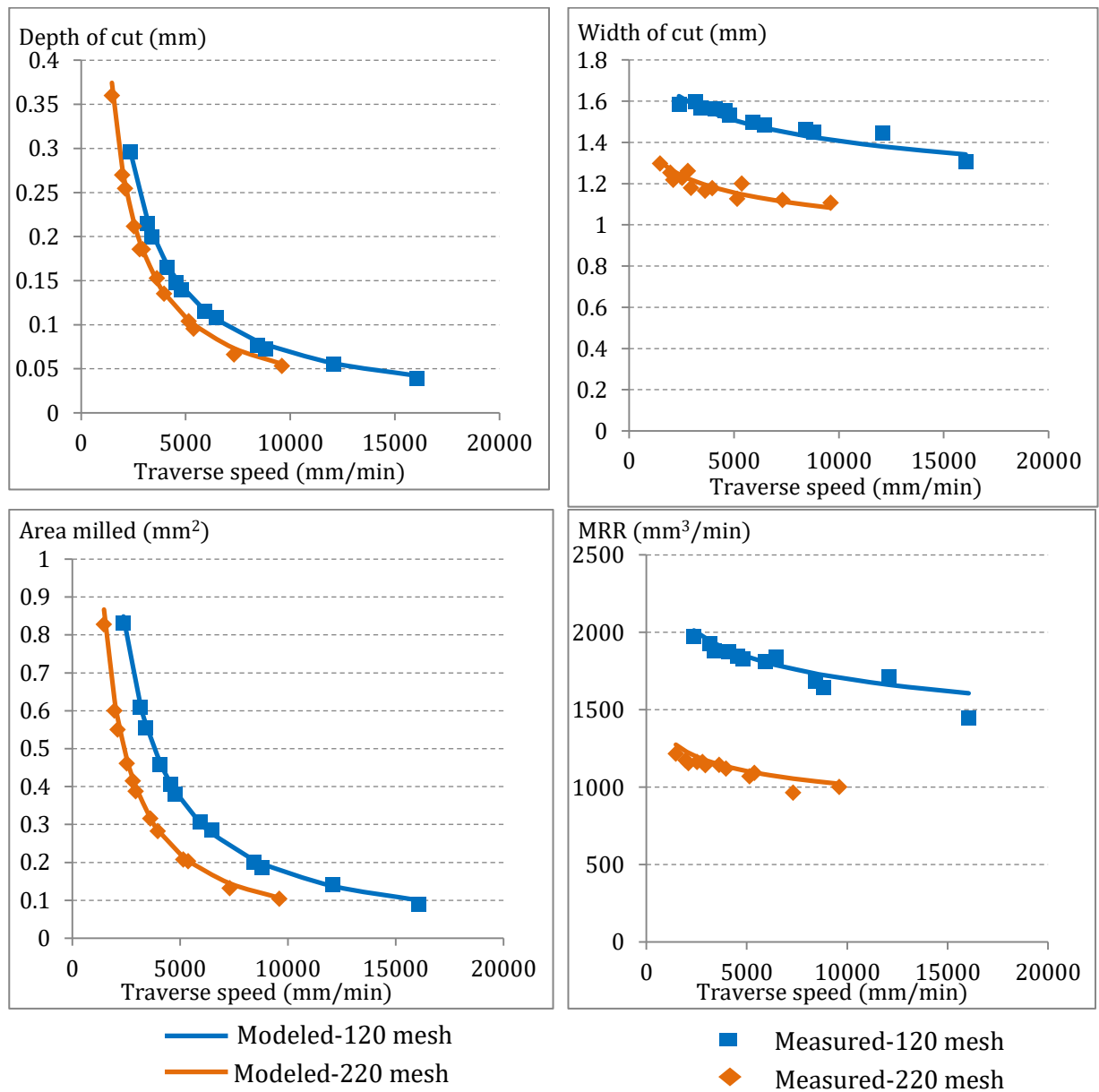


Fig. 1-32. Effect of the size of abrasive particle on a single kerf with $SOD = 100$ mm [40]

Regard to the influence of abrasive size on the surface roughness and waviness, G. Fowler [70] reported that an increase in particle size results in a reduction in surface waviness and surface roughness (Fig. 1-18b). For all traverse speeds, the surface waviness with the larger abrasive particle is greater than that with the smaller abrasive particle. In addition, the roughness of single kerf milled with particle size (120#) is lesser than that of single kerf milled with particle size (80#).

Table 1-3 summaries the influence of the process parameters on the subsequent response parameters that observed from AWJ machining for controlled depth of Ti6Al4V.

Table 1-3. Summary table of the influence of process parameters [40]

	depth (mm)	Width (mm)	Area milled (mm ²)	MRR (mm ³ /min)	Waviness	Roughness
<i>Vf</i> (mm/min) (↑)	↘↘↘	↘	↘↘↘	↘	X	X
<i>SOD</i> (mm) (↑)	↘	↗↗↗	↘	↘	X	X
Pressure(MPa) (↑)	↗↗↗	↗↗	↗↗↗	↗↗↗	X	X
Particle size (↑)	↘	↘↘	↘	↘↘	X	X

1.2.7.3 Abrasive water jet for pocket milling

In order to achieve a constant depth of penetration, the exposure time must be constant. Indeed, the more the exposure time increases, the deeper the impression on the part is deep. In the same way, to achieve a pocket with constant depth, the crossing of the jet paths must be avoided.

Study of the feasibility of AWJ milling process for controlled-depth was conducted with different approaches such as optimizing process parameters [101], using the mask to protect the surface to be machined [76] , and choosing suitable strategies to generate toolpath [102]. G. Fowler [26] and F. Cenac [13] demonstrated that abrasive water jet process can generate pocket by using a succession of single kerfs that shifted by an offset distance (Fig. 1-33).

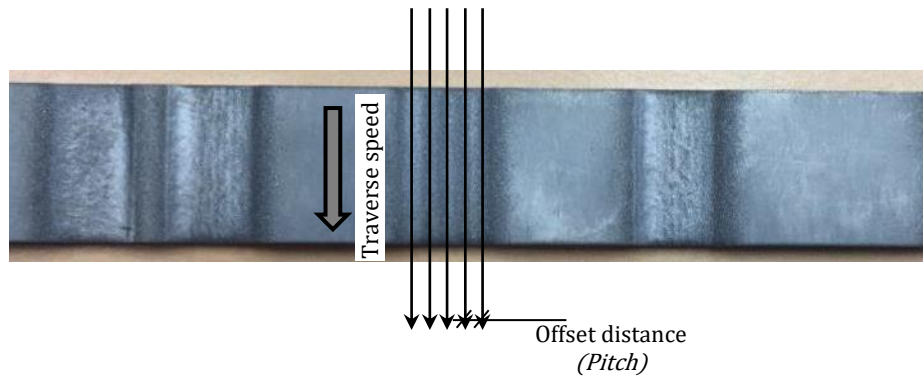


Fig. 1-33. Single kerf and pocket machined [40]

1.2.7.3.1 Using the mask

M. Hashish [69] presents the use of protective mask in the closed machining of pocket (Fig. 1-34). The masks used in AWJ are protective plates made of a material whose hardness or thickness is such that the jet of abrasive water does not cross them. He also pointed that the hardness of this mask must be equal or harder material to be machined with thickness being at the least the depth of the designed pocket.

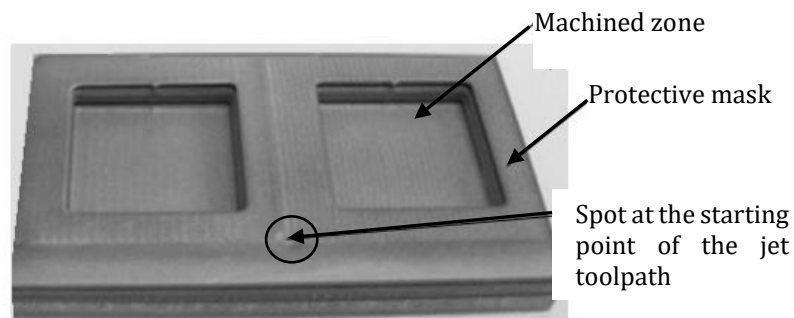


Fig. 1-34. Using mask for milling pocket [40]

In addition, the use of a mask makes it possible to avoid spots [103] which are over-depths due to starting or stopping the jet (Fig. 1-34). The use of a mask thus makes it possible to perform this start on the mask and to join the zone to be machined when the jet is stabilized. The second advantage of using a mask is to focus the machining on a specific area.

However, in the case of machining hard metals it is both difficult and expensive to use a mask because its implementation will involve a material at least as hard as that of the part. In addition, the use of a mask assumes its establishment and removal which

increases the production time [80]. It is therefore very interesting to find solutions to avoid it.

1.2.7.3.2 Milling pocket without mask

To produce a closed pocket without using mask, there are different approaches to reach controlled depth milling. M. Hashish et al. [76] proposed methods of using rapid Cartesian motion on turntable or rotary device. K. M. C. Ojmertz et al. [104] presented an approach based on a specific amount of abrasive in the mixing chamber to make a first removal of material. Then a large milled surface is generated by superposition of adding adjacent cavities. However, this method involves numerous start/stop of the abrasive water jet and generates spots.

Besides, several studies presented the control of the tool path in order to obtain a specified depth pocket. G. Escobar Palafox et al. [105] applied the one-way strategy on the Inconel 718. This strategy is rarely used since the jet must be restarted after each passage and outside the pocket to be machined. S. Paul et al. [106] employed the zigzag strategy to observe the variation of the depth machined on steel (Fig. 1-35). The results showed ability to smooth the depth irregularities that appear during on one-way scan. Moreover, T. Nguyen et al [107] applied this strategy for machining of variable depth pockets using control of the tool inclination angle. This technique has also been used on triangular pockets by A. Alberdi et al. [45]. They compared the influence of a transverse and longitudinal scan on the machined surface.

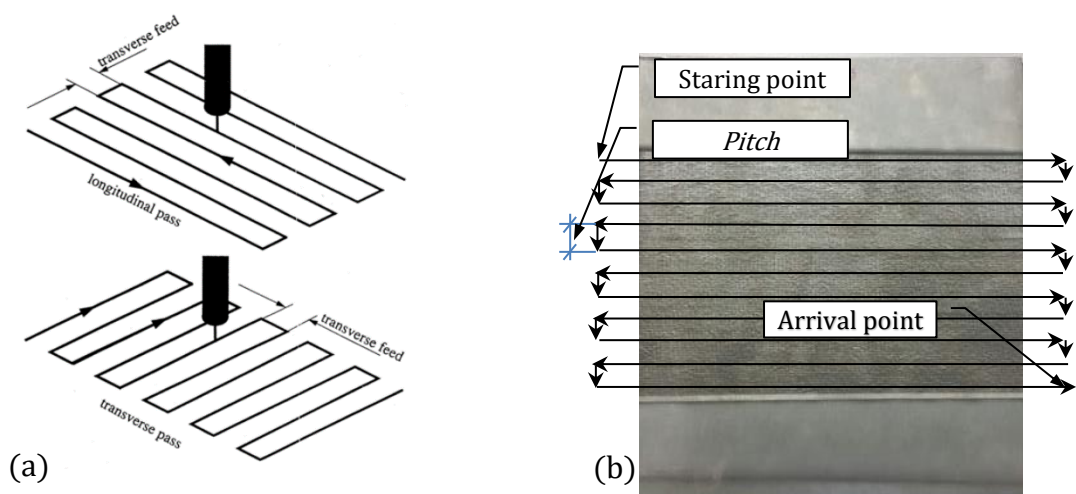


Fig. 1-35. Zigzag strategy [106]

The spiral machining strategy is also a very interesting solution for machining pockets. Like zigzag strategy, this solution involves starting and cutting the jet during machining. Moreover, its trajectory follows the succession of passes from the borders to the center of the pocket or vice versa. A. Alberdi [45] and J. Folkes [108] have presented applications of the spiral machining to reduce the irregularities on edges when milling rectangular and circular pockets.

M.C. Kong [102] introduced a new approach relying on choice of suitable strategies to perform maskless plain water jet milling in case of Ti-based superalloys. The depth of cut can be obtained by dividing machining into several machined layers (Fig. 1-36). The proposed trajectory leads to minimize the variation in jet dwell time by keeping a continuous relative movement and by ensuring the equal volume of eroded material in a series of layers. Hence it ensures, on the one hand, a constant exposure time for each machined zone and, on the other hand, that the tool path covers the entire surface to be machined.

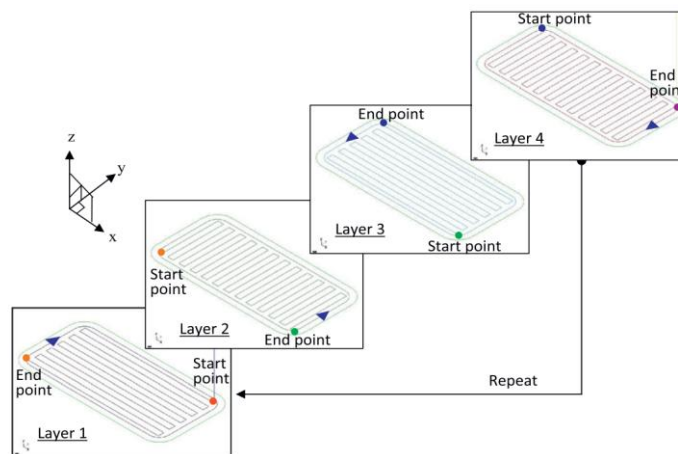


Fig. 1-36. Milling a rectangular pocket without mask [102]

1.2.7.3.3 Change of the direction during machining

AWJ milling was first introduced by M. Hashish in 1987 and then it was received vast attention of other scientists such as G. Fowler et al.[8], [18], [92]; A. Alberdi et al.[45]; S. Paul et al.[106]; U. Goutham et al.[109]. During a change of direction following two consecutive straight lines, the machine has to decelerate down to zero speed and accelerate to reach again the initial feed rate imposed. This results in too deep areas (Fig. 1-37) due to greater exposure time.

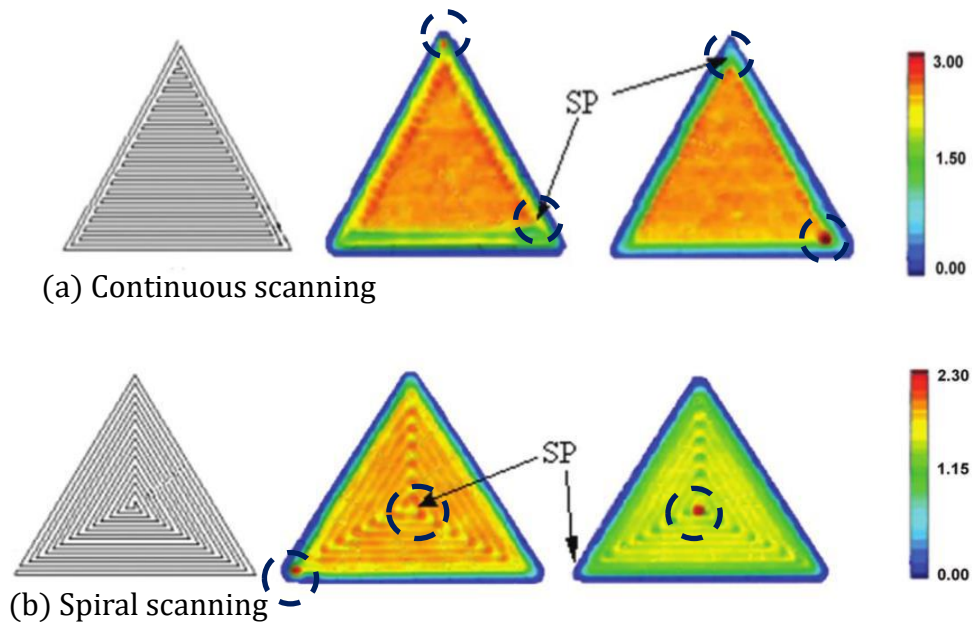


Fig. 1-37. Deflects appear due to change the direction of the jet [45]

In order to remedy this phenomenon, T. Sultan [40] has demonstrated that a rectangular pocket can be obtained by replacing the right angles by arcs of circles. Therefore, straight tool paths can be replaced by circular arc trajectories to keep a constant feed with the equal exposure time of the jet on the target (Fig. 1-38). There are two types for this solution: (i) using concentric arcs (Fig. 1-38a) and (ii) using equal arcs (Fig. 1-38b). But in case of pocket machining it involves to manage corner radii in order to respect the specified pocket radius associated to the kinematic of AWJ machine. Indeed, by selecting arcs with the same center at the corners of the path (Fig. 1-38a), a constant pitch (Fig. 1-35) will be obtained throughout the machining process. However, the smallest radius (corresponding to the smallest arc) must not be less than the value r_{mini} which satisfies the maximum acceleration delivered by the machine (Eq. 1-12). This limits the choice of parameters allowing machining at high feed speeds.

$$r = Vf^2/\omega \quad \text{Eq. 1-12}$$

With ω the acceleration of the cutting head (m / s^2), Vf the traverse speed (m / s) and r (m) the radius of the arc traversed by the cutting head.

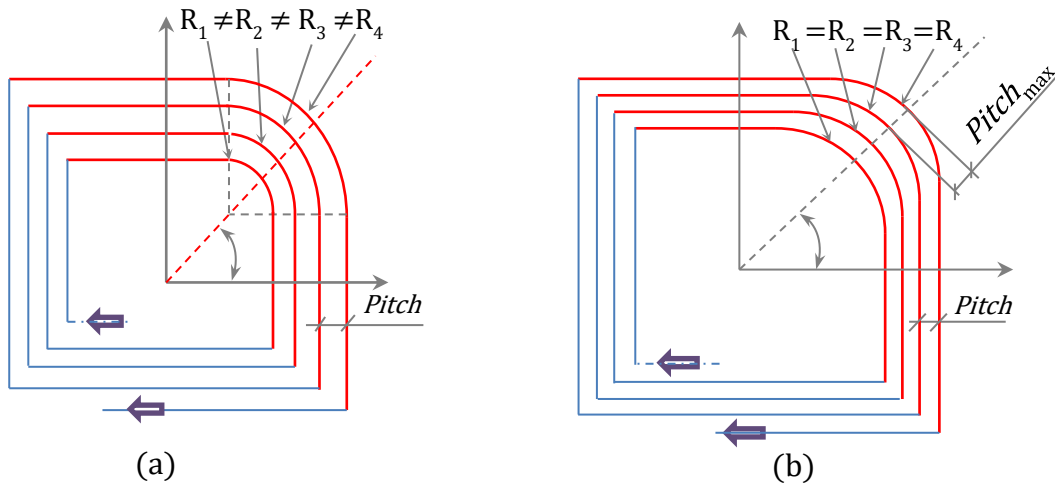


Fig. 1-38. Two methods of replacing by circular arc trajectories

In second case with equal arcs (Fig. 1-38b), by this way, it makes possible to choose a single radius for the entire path which obeys the maximum acceleration requirements of the machine. Nevertheless, a new problem is presented in this case, the distance between two adjacent kerfs, the pitch, is no longer constant throughout the machining process. It is constant between the straight parallel toolpaths and increases as it approaches the corner of the pocket. In the middle of the arcs, the offset reaches a maximum value equal to the $\sqrt{2} \times \text{pitch}$.

It has been observed that this solution can cause in streaks and speed bumps (Fig. 1-39) in the corners of the pockets.

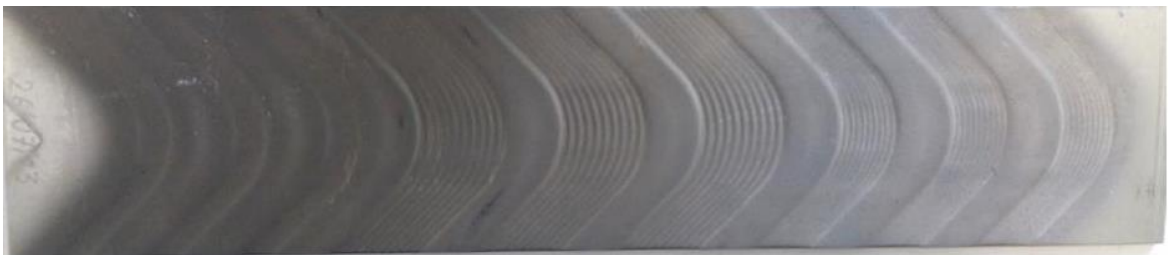


Fig. 1-39. Constant radius of Ti6Al4V specimen machined [40]

It is noticeable that there is no method was employed to manage the traverse speed at these corner in order to obtain a given tolerance of whole depth of pocket milled which is respected.

1.2.7.3.4 The formation of the open pocket in AWJ Machining

A constant depth pocket can be made by the succession of several single kerfs using a constant step over, namely “Pitch” [40] given in Fig. 1-33. The material removal mechanism which occurs during the performance of the pocket is thus associated with that which appear in the generation of an incision.

Based on the study results of T. Sultan [40], it is possible to obtain an equation to model the pocket milled (Eq. 1-13).

$$Y(x) = \sum_{i=1}^n \frac{a_0 * V_f^{a_1} * SOD^{a_2}}{2} * \left(e^{-\left(\frac{x-i*pitch}{b_{10}*V_f^{b_{11}}*SOD^{b_{12}}}\right)^2} + e^{-\left(\frac{x-i*pitch}{b_{20}*V_f^{b_{21}}*SOD^{b_{22}}}\right)^2} \right) \quad \text{Eq. 1-13}$$

With "i" the index that defines the number of the incision for a pocket machined in "n" incisions.

To illustrate the summation principle graphically, Fig. 1-40 shows a modeled incision, the successive passages, the profile of the corresponding pocket obtained by summation and the measured pocket that has actually been made. The pocket shown was obtained with a feed speed of 445 mm / min, a SOD of 90 mm and a pressure of 100 PMa and is the result of the summation of 10 incisions with a pitch of 1.6 mm.

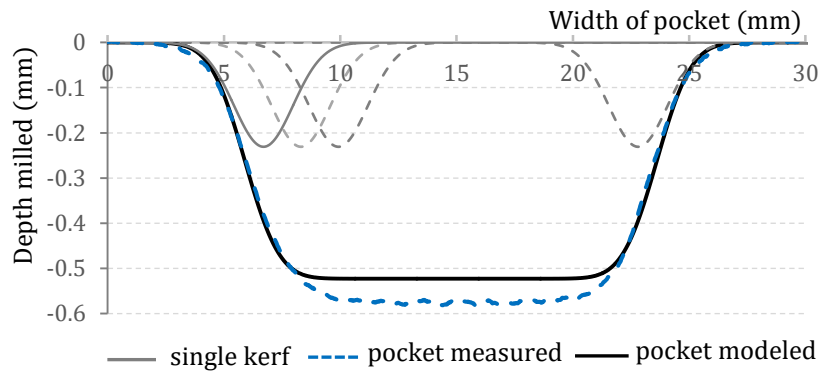


Fig. 1-40. Modeling profile of pocket machined

It has been confirmed that the depth of pocket can be calculated for a given pitch since factors of the single kerf (Eq. 1-13) is solved by the least square method. In addition, the variation of the depth of pocket is a function of the traverse speed (Fig. 1-41) with different values of standoff distances. The evolution of the pocket depth follows the same

trend as the depth of the single kerf (Fig. 1-30) and it can be noted that the traverse speed (V_f) is much more influential on depth than SOD .

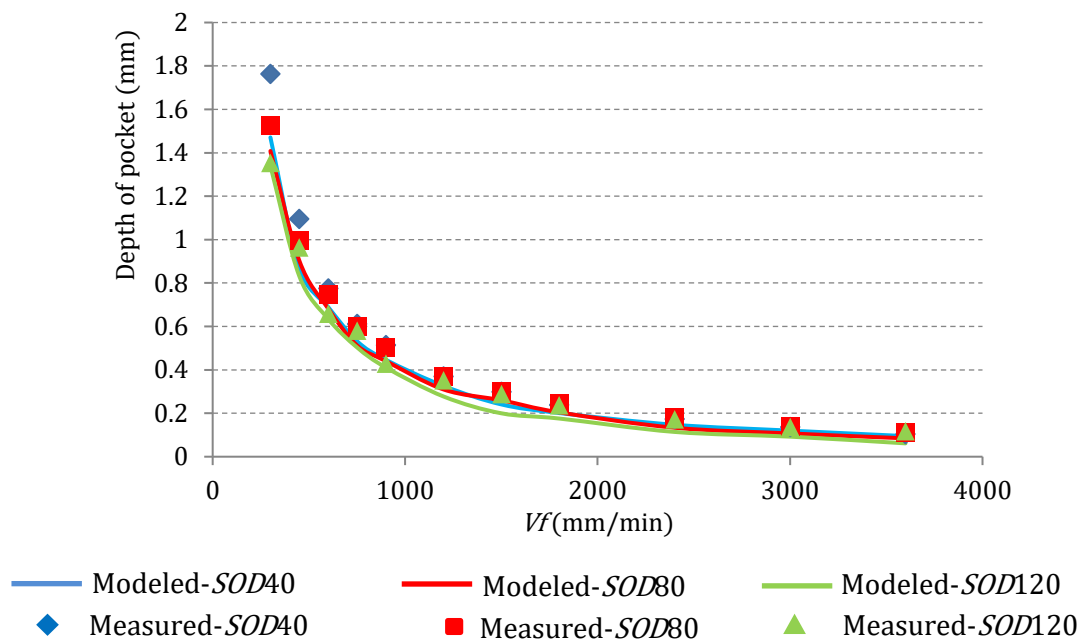


Fig. 1-41. The evolution of the pocket depth as a function of traverse speed [40]

The deviation between the pocket depths resulting from the summation of the incisions (Fig. 1-40) and those of the measured pockets depends on several parameters: the traverse speed, the standoff distance, the pressure, the abrasive size, and pitch.

In order to observe the evolution of this deviation, T. Sultan has conducted a number experiments and the deviation was made as a function of the machine input parameters mentioned. But the analysis of the evolution of this gap has proved difficult because the trends were fairly random.

Abrasive water jet performance depends on a large number of process parameters. Research on the influence of all input process parameters on the characteristics of the single kerf as well as pocket milled by AWJ at the same time is impossible because of the complexity of the material removal mechanism. Thus it requires to regroup the influence of input parameter and find out a global parameter to control during process.

From this idea, these machining parameters can be separated into two categories:

- The setting parameters does not allow to modify during machining,

- Control parameters can be controlled through the NC program.

The setting parameters consist of the pressure, the type of abrasive and the abrasive flow rate. As presented in § 1.2.6.3, for a given abrasive type and size, the pressure is associated to an optimal abrasive flow rate (Fig. 1-20) to maximize the MRR (§ 1.2.6.3). The setting parameters thus define the machine configuration. The control parameters are the *SOD*, the feed rate *Vf*. It should be noted that both standoff distance and traverse speed have the influence on the dimensional characteristics of single kerf milled. According to Fig. 1-28, *Vf* has a greater influence on the kerf depth of cut but *SOD* has greater impact on the kerf width. Thus to achieve a desired value of depth of cut on milling single kerf, using *Vf* as a controllable parameter is easier than *SOD*. On the other hand, in order to facilitate to control the water jet for pocket milling with a flat bottom, standoff distance should be fixed during machining and can be considered as a setting parameter. From these reasons, it is necessary to confirm that *Vf* is the only one parameter during the machining process.

Considering the normal Gaussian model and the traverse speed *Vf* as the only one parameter when a machine configuration is chosen, the Gaussian model used to characterize an elementary pass profile is defined by equation (Eq. 1-3).

1.2.8 Modeling of machining with a water jet inclination angle

1.2.8.1 Considering the effect of jet attack angle on the generation of elementary pass

Y.I. Oka et al. [110] presented a predictive equation for estimating erosion damage caused by solid particle impact (Eq. 1-14).

$$E(\alpha) = g(\alpha) E_{90} \quad \text{Eq. 1-14}$$

In this equation, $E(\alpha)$ and E_{90} denote a unit of material volume removed per mass of particles (mm^3 / kg). This model can be utilized under any impact conditions and for any type of material. The impact angle dependence of erosion damage was defined for several material as aluminum, copper, carbon steel and stainless steel. He concluded the erosion rate could be expressed in a semi-empirical form (Eq. 1-15).

$$g(\alpha) = (\sin(\alpha))^{n_1} \{1 + H_v[1 - \sin(\alpha)]\}^{n_2} \quad \text{Eq. 1-15}$$

Where the constants n_1 and n_2 are found experimentally and depend on the particle hardness and other impact conditions, and H_v (GPa) is the initial target hardness. It is reported that the first term represents the contribution due to repeated plastic deformation, which depends on the impact energy, transferred normal to the surface, while the second term expresses the cutting action, which depends on the energy transferred parallel to the surface. Fig. 1-42 shows the impact angle dependence of erosion damage $E(\alpha)$ at an impact velocity of 104 m / s by SiO₂-1 particles of 326 μm , for several types of stainless steels

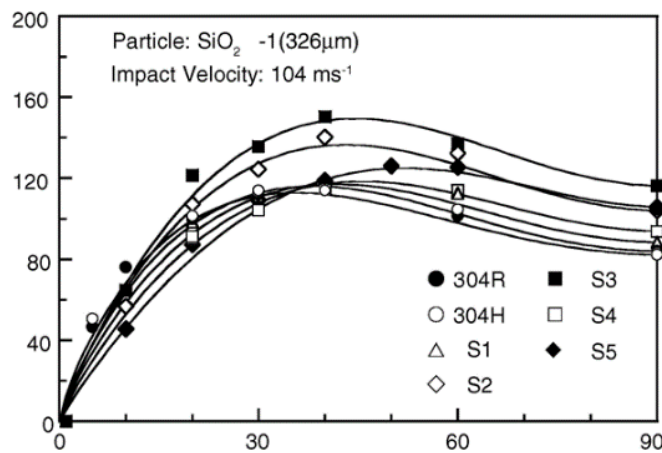


Fig. 1-42. The influence of impact angle on erosion damage for several stainless steels [110]

D.A. Axinte et al. [46] presented the influence of the impingement angle and traverse speed (Fig. 1-43) on kerf geometry and its dimensional characteristics for silicon carbide ceramics. He has concluded that the free jet plume diverges gradually and the diameter of the jet increases steadily with the increase in distance from the tip of the focusing tube to the target to be machined. Hence, the impact angle, the diameter of focusing tube, and SOD has a direct influence on the width of cut. In this study, he reported that the jet footprint is transformed gradually from a circular shape to an elliptical one when the jet impingement angle decreases (Fig. 1-43b). The variation of top width values may be described as a function of the decrease in α .

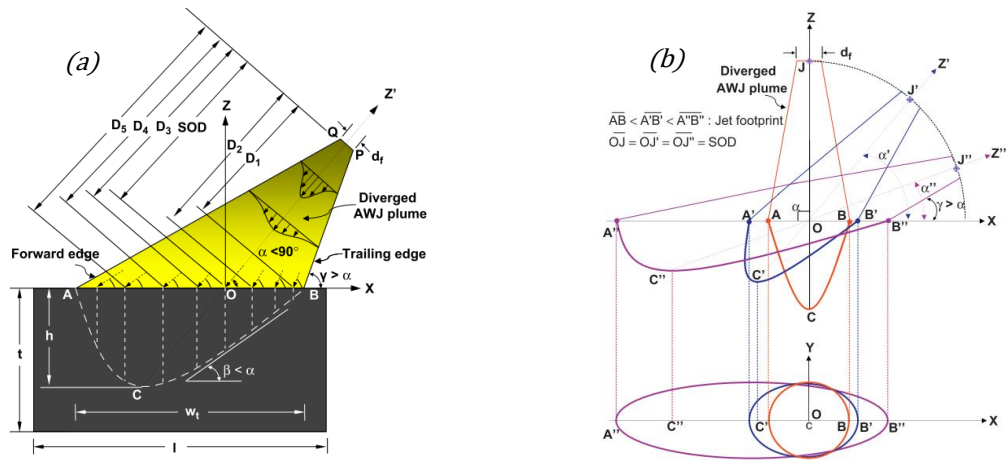


Fig. 1-43. The influence of water jet inclination angle on a formation of incision [46]

D.A. Axinte et al. [47] observed the effect of the diameter of the focusing, the jet plume divergence in air, the standoff distance, and jet impingement angle to the characteristics of profile of single kerf milled (Fig. 1-44).

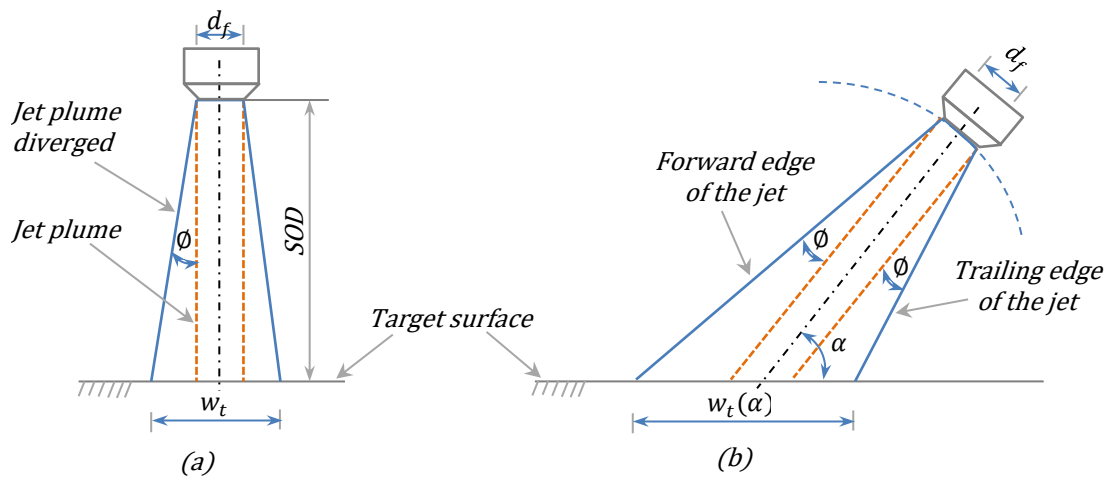


Fig. 1-44. Schematic illustration of the jet plume structure in air before impingement onto the target surface: (a) normal impingement and (b) shallow angle impingement [47]

An analytical model (Eq. 1-16) for top width of jet footprint in abrasive water jet milling on SiC ceramics is introduced and the influence of jet feed rate was included.

$$w_t(\alpha) = \left[SOD + \frac{d_f}{2 \tan(\alpha)} \right] \frac{\sin(\phi_v)}{\sin(\alpha - \phi_v)} + \frac{d_f}{\sin \alpha} + \left[SOD - \frac{d_f}{2 \tan(\alpha)} \right] \frac{\sin(\phi_v)}{\sin(\alpha + \phi_v)} \quad \text{Eq. 1-16}$$

Where, SOD standoff distance; d_f - the diameter of the focusing tube; ϕ_v - effective jet plume divergence that represents for the phenomenon of the difference between the real

top width and theoretical top width. This phenomenon is due to the effectiveness of the jet plume divergence in eroding the target surface as a function of traverse speed (Vf).

1.2.8.2 Pockets machining

N. Tamannaee et al. [111] have investigated the abrasive slurry jet process on a talc-filled thermoplastic olefin (TPO) (60% PP, 25% EP rubber and 15% talc) and found that the material erosion rate is a function of the impact angle and the talc filler content. A maximum erosion rate of a ductile erosion response is indicated at 45° of the jet attack angle. In this study, experiments were performed to investigate the ability for increasing and control the side-wall slope of pocket milled (Fig. 1-45). Results showed that a repetition of single kerf over the same channel by directing the jet inclination angle can produce a slope of 82° at a depth of $224 \mu\text{m}$. However, it proved to be impossible to continue with this solution to obtain a flat bottom of the pocket milled. Fig. 1-45 shows a planar area ending in a relatively steep right sidewall with a moving of the jet from left to right. It was noted that when the abrasive jet flowed across the ridges of the previous single kerfs, the slurry was diverted into these channels and the waviness emerges significantly.

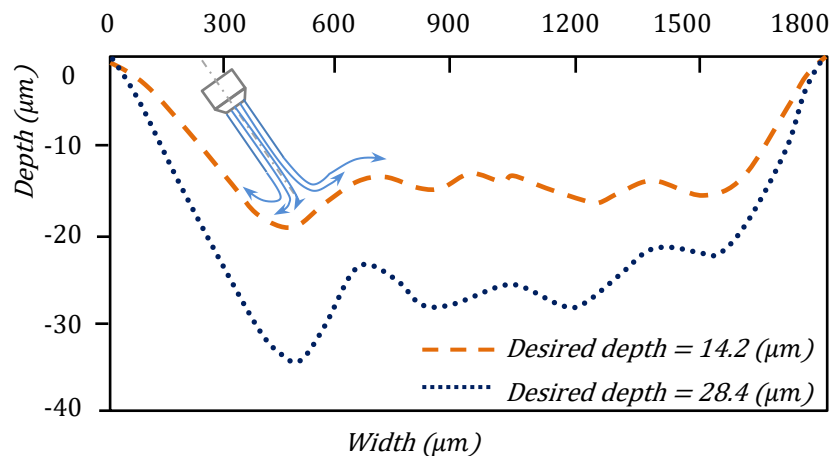


Fig. 1-45. Wavy surface profile measured for two levels of desired depth of pockets at $\alpha = 45^\circ$ [111].

Besides, T. Nguyen et al. [112] have presented an investigation of generation mechanisms of channels milled by AWJ on amorphous glass material. In this study, the effect of the jet inclination angle on the characteristic of pocket of material was also mentioned.

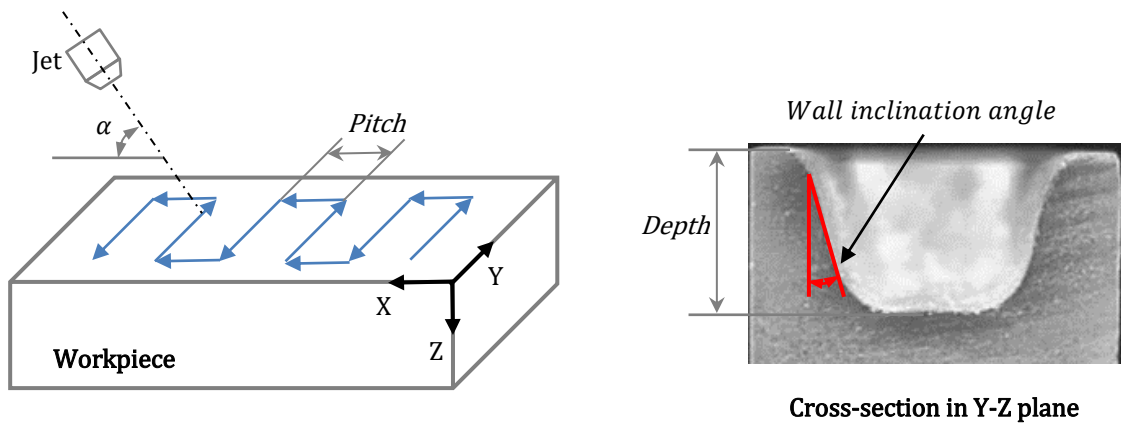


Fig. 1-46. Milling experimental setup and cross-section of pocket milled [112].

Indeed, an increase in the impact angle from 45° to 75° results in a slight increase in the depth of cut and the material remove rate (Fig. 1-47a, b). It was explained that when the jet inclination angle increases component of jet energy normal to the surface target and permit a steeper transient cutting surface.

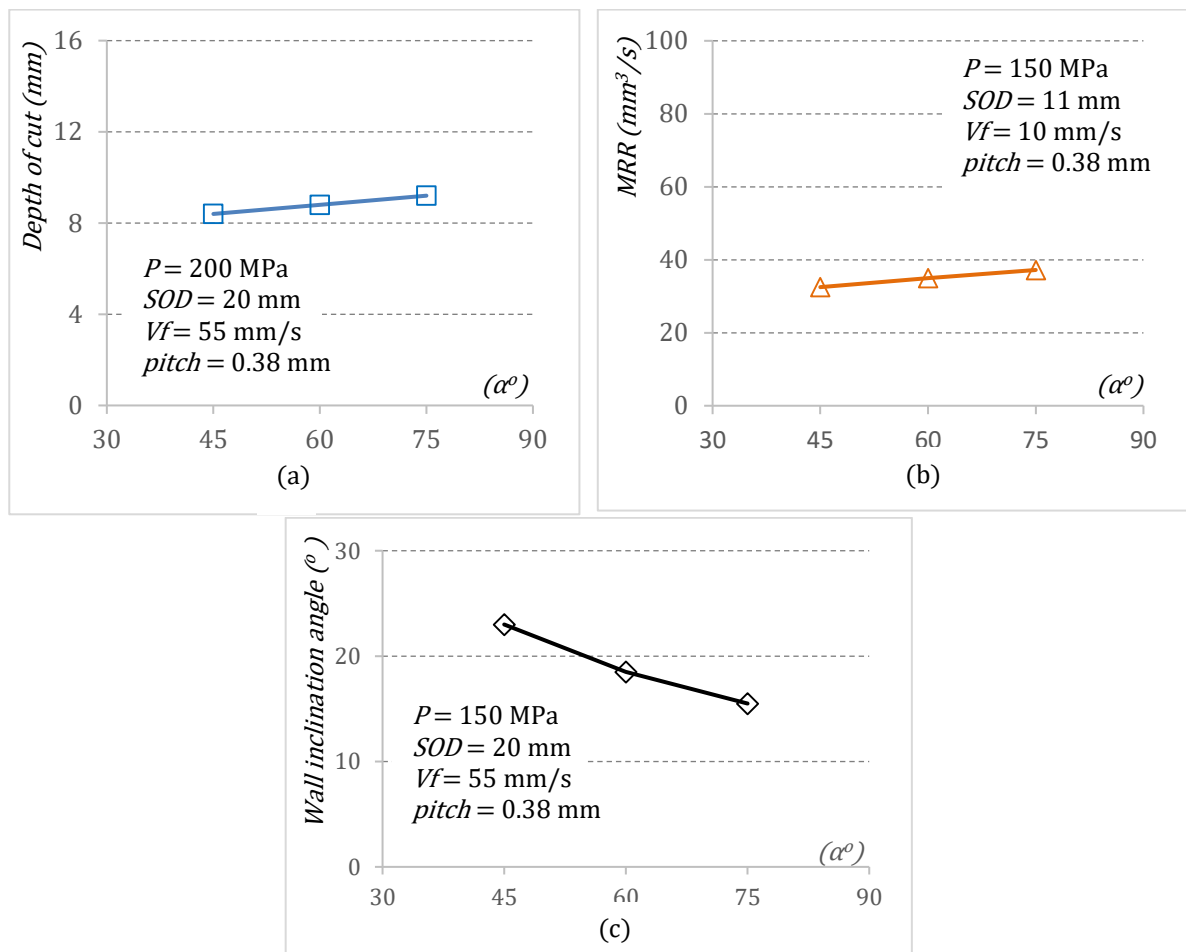


Fig. 1-47. Effect of the jet impact angle on characteristics of pocket milled [112].

In addition, the wall inclination angle decreases as the jet impact angle increase (Fig. 1-47c) due to increases the component of jet energy normal to the workpiece surface, which facilitates the removal of the brittle material and increases the concentration of material removal action in the vertical direction to generate less inclined walls. A similar results is also found in the other study of T. Nguyen [107].

1.3 Conclusion

The state of the art study on different types of the water jet technology (a non-conventional method) i.e. pure water jet; abrasive slurry jet; and abrasive water jet have pointed out that this technology is flexible manufacturing processes with different materials. Applying this technology on machining different kinds of materials (plastic, composites, ductile metals, brittle metals...) has been received the attention of a lot of researchers. They have demonstrated that AWJ has several advantages over other techniques of machining studied (conventional methods and other non-conventional method). Without impact force on the workpiece surface which being neglect and creating the heat-affected zones during machining, AWJ machining is a most suitable process for machining of hard metals thin sheets, particularly aviation parts which are mostly thin parts with large size in dimensions. Manufacturing these parts requires to remove material selectively from their surfaces.

Research on applications of AWJ machining have presented a vast results for hard material but most results focus on cutting process. During operating process, the material is removed by two main erosion mechanisms, which are cutting and plastic deformation. Depending on the properties of material to be machined (ductile or brittle material), either cutting or plastic deformation will dominate. Removing material is governed by various process parameters which significantly influence on the milling depth, material removal rate, surface roughness, and waviness. In order to improve the ability of the AWJ machining in milling application for hard materials, several studies have indicated that the jet traverse speed plays a significant role in controlling the desired kerf geometrical characteristics. Besides, it is noted that a flat surface is obtained when the abrasive water jet is carried out an arbitrary path which covers all desired surface.

In efforts of development applicable potential of the jet to mill titanium alloy (Ti6Al4V), T. Sultan has demonstrated a reasonable utility of Gaussian profile to model elementary pass which milled by AWJ machine in case of the jet perpendicular to the workpiece surface. His results show clearly the agreement with several results found in publications. In addition, He also reported that a flat bottom of the open pocket can be obtained by using the summation principle of superposition of the jet which is characterised by a pitch parameter.

Although research on this technology has gained numerous achievement, applying it for mill a closed pocket and especially, 3D parts with complex shapes of hard materials is still at the infancy stage. Indeed, from the bibliography there exist the following lacks that need to dig deeper into:

- ✓ The modeling approach is adopted for controlling the depth milled. However, in general, these methodologies take into account all the input parameters, which leads to complex models associated with a large number of experiments. Thus it is necessary to develop a new model with high-efficiency, flexible, and the least experiments required. It can support for the ambition of controlled depth milling by abrasive water jet for any kind of material, in this case, milling on TiAl4V6.
- ✓ Regarding milling a closed pocket, irregularities at the depth of cut are observed when the jet change the direction during the process, in particular at the corner of pocket milled. This phenomenon is related to the inherent problem of machine kinematic in case of acceleration/deceleration of the jet which affects the exposure time of the jet on the target surface. It results in the bottom of the pocket is not flatness one over whole depth milled. But there is no solution yet presented to remedy it.
- ✓ In aspect of machining with inclination angle of the jet on the surface, this parameter is mainly taken into account of study MRR and effect on machined surface quality (grit embedment, roughness and waviness surface). It should be noted that there is no model to predict elementary pass as well as pocket milling with the jet inclined. Moreover, the material removal mechanism with an inclination angle of the jet needs to be considered to develop fully the application potential of this technology. In another aspect, the jet inclination angle is a critical

factor to manage the slope of closed pockets as well as arbitrary surface shapes as mentioned in the literature but almost no noticeable results were found.

In following chapters, the content of each chapter is presented as the format of an article. Indeed,

➤ Chapter 2 consist of two articles which studied on AWJ machining perpendicular to the workpiece surface:

- Bui VH, Gilles P, Sultan T, et al (2017) A new cutting depth model with rapid calibration in abrasive water jet machining of titanium alloy. International Journal of Advanced Manufacturing Technology 93:1499–1512. <https://doi.org/10.1007/s00170-017-0581-x>.
- Bui VH, Gilles P, Sultan T, et al (2019) Adaptive speed control for waterjet milling in pocket corners. International Journal of Advanced Manufacturing Technology. <https://doi.org/10.1007/s00170-019-03546-z>.

➤ Chapter 3 consist of two articles which studied on AWJ machining with a water jet inclination angle:

- Bui VH, Gilles P, Cohen G, Rubio W (2018) A modeling of elementary passes taking into account the firing angle in abrasive water jet machining of titanium alloy. In: AIP Conference Proceedings.
- Machining pocket with management of the tool inclination angle (unpublished).

MACHINING WITH THE JET PERPENDICULAR TO WORKPIECE SURFACE

2.1 A new cutting depth model with rapid calibration in abrasive water jet machining of titanium alloy

(This section is presented as the format of an article and it has been published in International Journal of Advanced Manufacturing Technology- DOI: 10.1007/s00170-017-0581-x)

Abstract: Titanium alloys are widely used in the aeronautical and engineering fields as they show an excellent trade-off between the mass and mechanical properties, but as hard materials, they are difficult to machine using cutting tools. The abrasive water jet affords a good solution to produce titanium parts, especially slim ones. To do so there is a need to adopt a modelling approach for the depth milled. However, a general methodology that takes into account all the parameters leads to complex models based on a large number of experiments. The present article proposes a depth of cut model combined with a rapid calibration method. The case addressed is that of open rectangular pockets on a Ti6Al4V titanium alloy. The approach introduces the machine configuration notion considering that a given machine, pressure level and abrasive impose the abrasive flow rate needed in order to obtain an optimal material removal rate. For a chosen configuration, calibration of the model is performed from a series of elementary passes and just three pocket machining passes. The method is rapid and effective as the accuracy of the models obtained over a number of configurations was to within the order of 5%.

Key words: Machining, Abrasive water jet, Titanium, Cutting depth model.

2.1.1 Introduction

2.1.1.1 Bibliography

Titanium alloy are widely used because they are lightweight, resistant and have a good resistant to corrosion. Thanks to these properties, they are used in various industrial sectors and in particular the aeronautic sector. The considered parts are structural parts and the grade of titanium is Ti6Al4V. This grade is mainly composed of titanium, aluminium (6%), vanadium (4%) and other constituents such as carbon (0.08%), iron (0.25%), iron (0.25%), oxygen (0.13%), nitrogen (0.05%) and hydrogen (0.012%). The main properties of this alloy are high tensile strength (860 MPa), a high yield strength (800 MPa) and an elongation of more than 10%.

These aeronautical structural parts have to withstand considerable forces while being large in size with thin walls. Machining the latter is difficult using conventional methods such as milling because the cutting forces are high and the thin walls can be easily deformed. In order to avoid these difficulties and to guarantee the quality of these parts, other machining processes have been studied. Among them, chemical machining and abrasive water jet machining are the most developed, but chemical machining has major disadvantages because it uses acids that are dangerous for the environment.

Blind machining using an abrasive water jet is a method that affords a number of advantages. Firstly, the constituents leading to the removal of material are simply water and abrasive. In addition, the structure of the machines and tools is simple and a very fine water jet can generate only low levels of force. The latter feature makes it possible to limit the deformation of parts during machining. Finally, the abrasive water jet allows matter to be removed on all types of materials. For these reasons, this process has been widely studied for the machining of slim parts made of hard materials like titanium alloys and a number of studies present the parameters influencing machining quality and performance [8], [109]. The kerf left by a single pass of the jet was studied and its shape can be modelled using a Gaussian curve [44], [46], [113]. When the Gaussian curve is centred on the y axis, the corresponding equation (Eq. 2-1) is characterised by a depth H and a width B .

$$y(x) = H \times e^{\left(-\frac{x^2}{B^2}\right)} \quad \text{Eq. 2-1}$$

In their article, A. Alberdi et al. [44] characterise a profile obtained experimentally using measurement of the maximum depth h_{max} and the width at mid-height $b_{0.5}$ (Fig. 2-1).

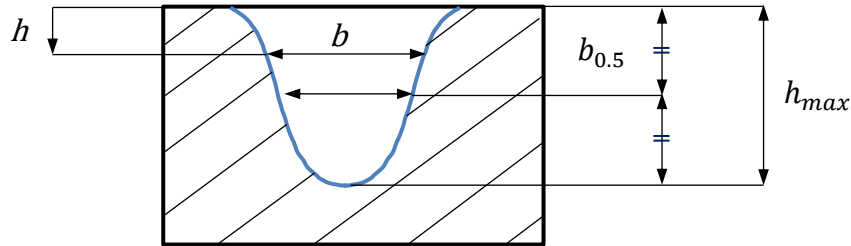


Fig. 2-1. Modeling of the Gaussian curve [44]

From these two single measurements, the shape of the Gaussian curve is defined by the authors using equations (Eq. 2-2) and (Eq. 2-3):

$$h = h_{max} \times e^{\left(-\frac{b^2}{2c^2}\right)} \quad \text{Eq. 2-2}$$

$$c = \frac{b_{0.5}}{2 \times \sqrt{2 \times \ln(2)}} \quad \text{Eq. 2-3}$$

Equation (Eq. 2-2) allows the depth h corresponding to a width b to be calculated using the maximum depth h_{max} and a parameter c . The latter is calculated (Eq. 2-3) from the width $b_{0.5}$ measured at mid-height. According to this model, the width corresponding to a height $h = 0$ is infinite and the studied height therefore has to be limited [44]. The considered operating parameters are the feed rate V_f , the standoff distance SOD and the abrasive mass flow rate. Their influence on the maximum depth h_{max} , the width $b_{0.5}$ and the material removal rate (MRR) were studied experimentally on elementary passes (Fig. 2-2).

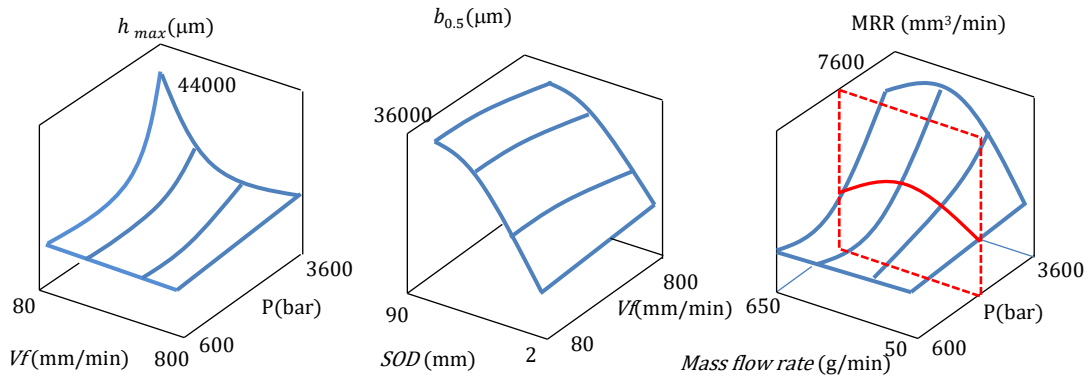


Fig. 2-2. Influence of operating parameters on elementary passes

The graphs (Fig. 2-2) show that:

- The depth of an elementary pass depends mainly on the pressure and the feed rate,
- The width of an elementary pass depends mainly on the *SOD* but also the feed rate,
- The MRR is in relation to the pressure and flow of abrasive.
- Machining of pockets by the repetition of offset passes (Fig. 2-3a) then becomes possible [45]. A number of studies covering various materials confirm that, in this case too, the pressure is the main parameter influencing the MRR [87] and Fig. 2-2 shows that, for a given pressure, the MRR presents a maximum [86]. There is thus an optimal abrasive flow for which the MRR is maximal (Fig. 2-3b).

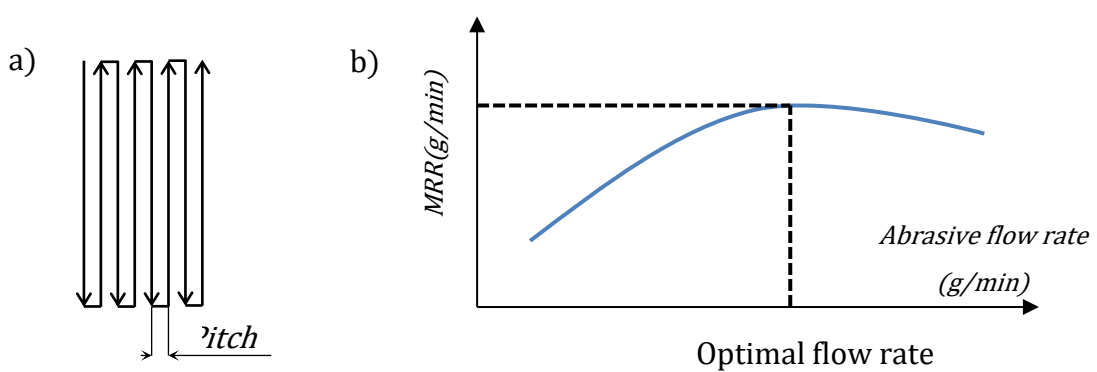


Fig. 2-3. Offset passes and optimal abrasive flow rate

The curve (Fig. 2-3b) shows that below the optimal abrasive flow rate, there is a share of the kinetic energy in the water that is not used to propel the abrasive. Similarly,

beyond the optimal abrasive flow, a part of the abrasive remains unable to receive the kinetic energy needed to produce a removal of material. The optimal abrasive flow is thus set once the type of abrasive has been chosen and the pressure set. Other parameters can influence the MRR. This concerns the tilt angle of the jet in relation to the surface [107] or the number of machining passes superimposed. It has been observed that the MRR is smaller during a second pass due to the residual stresses induced during the first pass and the shape onto which the jet impacts [72]. In the present study, only a jet perpendicular to the surface and machining in a single pass are considered.

It is possible to model an elementary pass and predict the profile of a pocket bottom by superimposing several elementary passes [111]. Some works propose to model the removal of material using an abrasive water jet by finite elements [114] on a single pass of the jet and simulate successive passes [111], [115]. In order to take machining parameters into account directly, depth models using a potential function are proposed [45]. They show the influence of the offset pitch on the depth milled (Fig. 2-4) in relation to a magnitude N expressing the overlapping of elementary passes. $N=0$ means that the passes do not overlap, $N=2$ means that there are two passes over a width b_0 and $N=4$ that there are four passes.

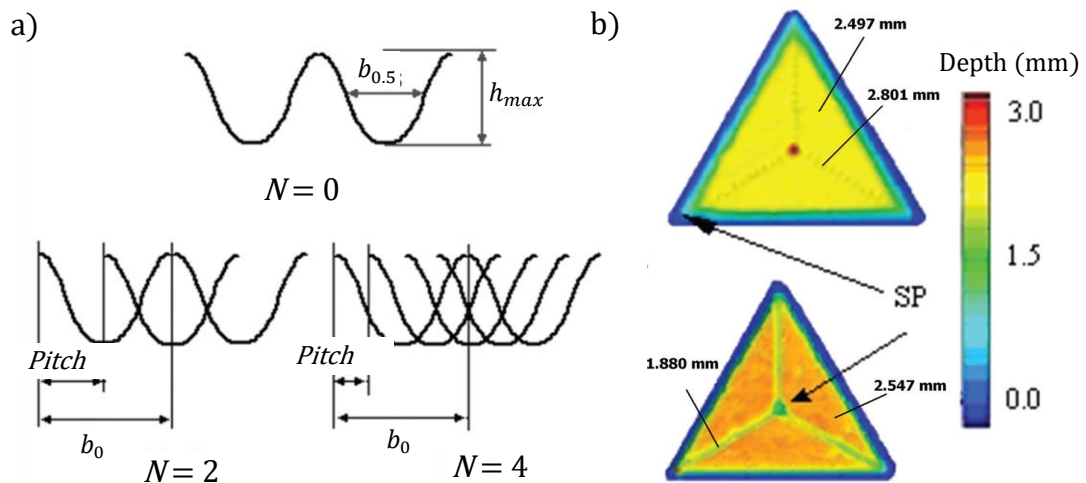


Fig. 2-4. Lateral offset and depths machined [45]

Various sweep strategies can be adopted: one-way [105] (although this limits productivity), zigzag or spiral [45], [109].

2.1.1.2 Conclusion on the literature

Abrasive water jet machining depends on a large number of parameters. Among them, a distinction can be made between machine setting parameters and control parameters.

The setting parameters are those that cannot be modified during machining. This involves the pressure, the type of abrasive and the abrasive flow rate. The pressure controls the MRR [44], [87]. When this pressure is set for a given type of abrasive, there will be an optimal abrasive flow (Fig. 2-3b) enabling the kinetic energy of the water to be used most effectively. The setting parameters thus define the optimal configuration of the machine for the machining considered.

The control parameters are those that can be controlled using the NC program. These parameters are the *SOD*, the feed rate *Vf* and the pitch offset. For a given configuration, these parameters will be those to be varied in the machining program. It should be noted that the *SOD* determines the width of the elementary passes [44] and that to obtain a pocket with constant depth, it should not vary during machining. This parameter can then be considered to be equivalent to a setting parameter.

In what follows, a configuration is defined for a given material, a given pressure, a defined type and flow of abrasive and a constant *SOD*. The control parameters will then be the feed rate and the offset pitch.

2.1.2 Model of the depth milled in pocket machining

2.1.2.1 Modelling elementary passes

Considering the model of a Gaussian curve (Eq. 2-1) and the feed rate *Vf* as the only one parameter when a configuration is considered, the chosen model used to characterise an elementary pass profile is defined by equation (Eq. 2-4):

$$y(x) = H(Vf) \cdot e^{\left(-\frac{x^2}{B(Vf)^2}\right)} \quad \text{Eq. 2-4}$$

Each elementary pass is characterised by its maximum depth $H(Vf)$ and a width factor $B(Vf)$. It has been shown that for a given configuration (§2.1.1.2), the width and

depth parameters only depend on the feed rate (Fig. 2-2). This influence will be taken into account using models (Eq. 2-5 and Eq. 2-6):

$$H(Vf) = H_0 \times Vf^{Hv} \quad \text{Eq. 2-5}$$

$$B(Vf) = B_0 \times Vf^{Bv} \quad \text{Eq. 2-6}$$

In these expressions H_0 , Hv , B_0 , and Bv are coefficients that are determined experimentally. To do so, it is necessary to perform elementary passes varying the feed rate and noting the profile of each pass in a plane perpendicular to the direction of feed movement. The values (H , B) for each elementary pass are then calculated using the least squares method. It should be noted that not all elementary passes can be used as when the feed rate is high, the depth obtained will be reduced and the roughness (Fig. 2-5a) will lead to a substantial error in modelling (Fig. 2-5a).

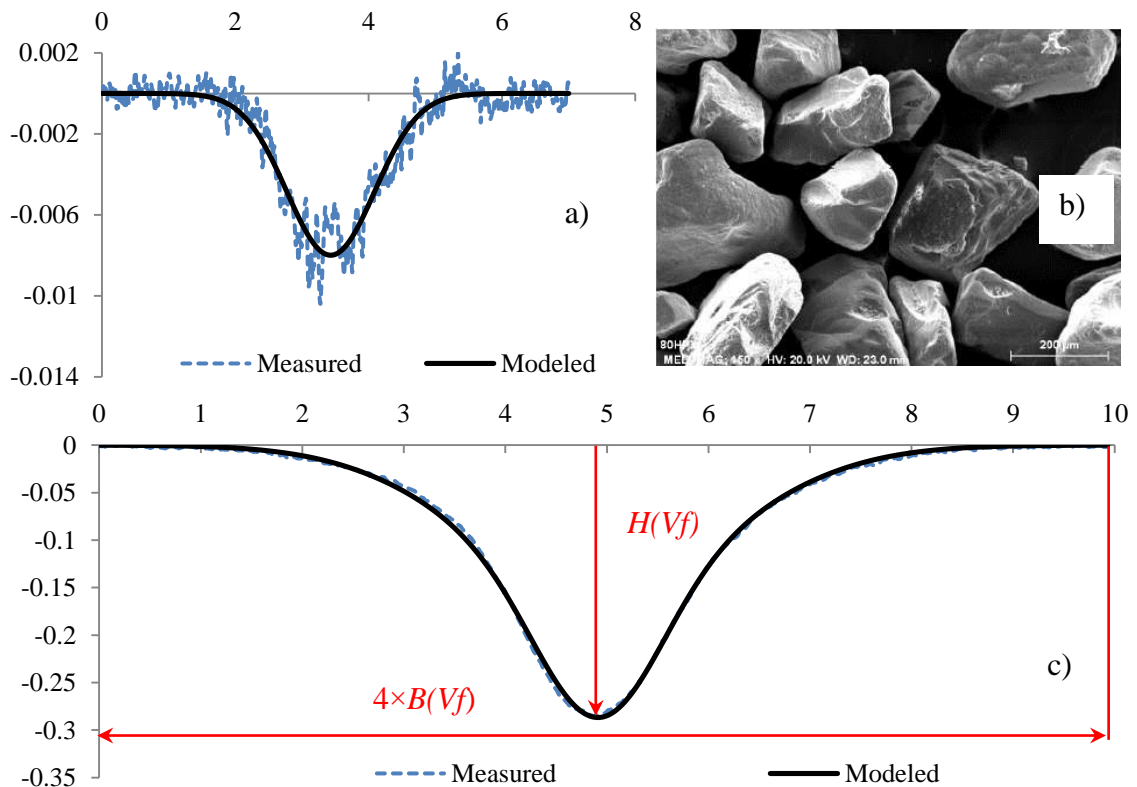


Fig. 2-5. Profiles for elementary passes and abrasive size 220#

In order to perform effective modelling, there is a need to consider the dimensions of the grains of abrasive (Fig. 2-5b) and only retain passes with a depth greater than the

mean of the maximum dimensions observed on 20 grains of abrasive. These measurements can be conducted using the profile projector or again with a simple micrometer. When the profile has considerable depth as compared with the roughness (Fig. 2-5c), modelling will be effective. The curves of the profiles measured and modelled then clearly show the depth $H(Vf)$ of the elementary pass obtained and it is to be noted that the interval $[-2 \times B(Vf); 2 \times B(Vf)]$ contains all the points that have a depth greater than a hundredth of the maximum depth (Fig. 2-5c). It can therefore be considered that that interval contains the totality of the elementary pass.

2.1.2.2 Principle for summing of elementary passes

The machining considered is performed in a single pass making elementary passes modelled by equation (Eq. 2-4) offset by the *pitch*. The pocket profile obtained (Fig. 2-6) will thus be the sum of elementary passes.

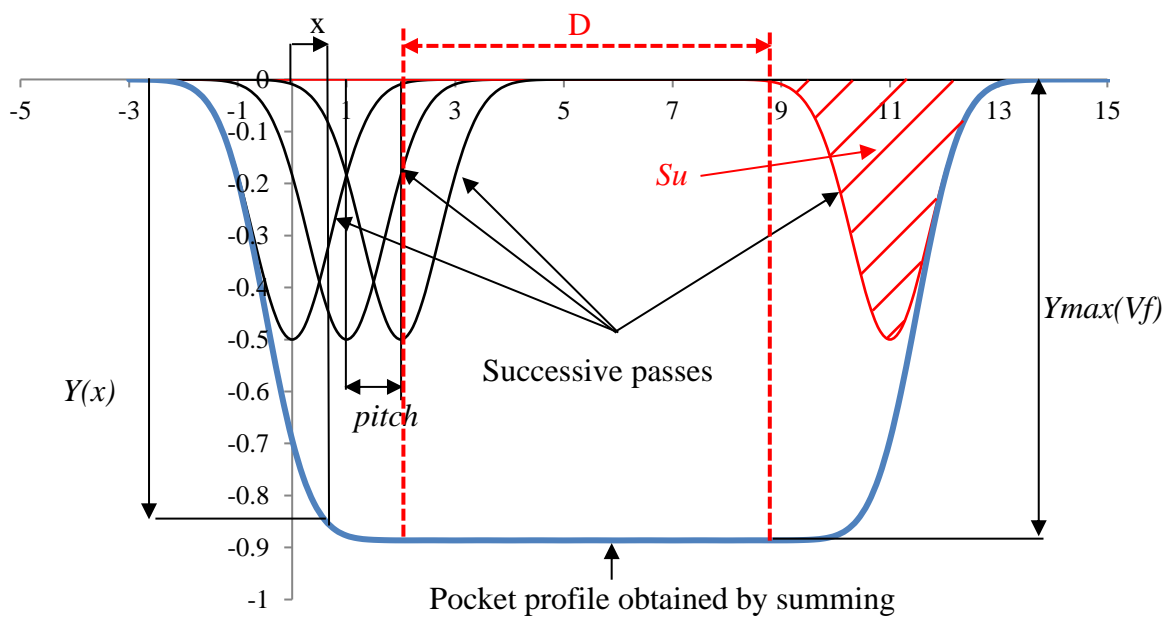


Fig. 2-6. Successive passes and pocket profile obtained by summing

The pocket bottom profile is thus calculated as the sum of the elementary profiles offset by the pitch (Eq. 2-7).

$$Y(x) = \sum_{i=0}^n \left[H(Vf) \cdot e^{\left(-\frac{(x-i \cdot \text{pitch})^2}{B(Vf)^2} \right)} \right] \quad \text{Eq. 2-7}$$

In this expression, the *pitch* is the offset pitch. The magnitudes $H(Vf)$ and $B(Vf)$ are respectively the maximum depth and the width parameter of a kerf left by a single pass and are modelled by equations Eq. 2-5 and Eq. 2-6. This expression allows a first value of the depth Y_{max} of the pocket to be calculated (Fig. 2-6).

2.1.2.3 Taking the erosion mechanism into account

A number of studies describe the action of a grain of abrasive on a given material in order to define the mechanisms for removal of material. The global objective of these studies is to understand the action of a grain of abrasive, to model it and generalise it to simulate removal of material by the water jet as a whole. The mechanisms for removal of material can be observed on various applications [73], [106] but the main ones are cutting and fatigue related to abrasion, the brittle fracture and fusion associated with the impact of grains of abrasive on the surface. The main models for removal of material associated with these mechanisms [54], [55], [57] consider the following hypotheses:

- Removal of material is due to the cutting action associated with a plastic deformation,
- On impact of a particle, no propagation of cracks appears ahead of the particle,
- A particle does not fragment on impact and is driven by a plane movement.

This last hypothesis is important as it highlights the fact that a particle will exert an action on the matter during the path it follows after impact on the surface. During this displacement it will erode the surface that has been machined until its kinetic energy becomes attenuated and the erosion effect cancels out. As a result, there exists a difference between a single elementary pass and a succession of elementary passes. In the first case, the jet impacts a plane surface (Fig. 2-7a) and escapes remaining concentrated on the kerf it is in the process of hollowing out while in the second case, the front of material tends to orient the escape of the jet on the machined surface (Fig. 2-7b) generating removal of additional material.

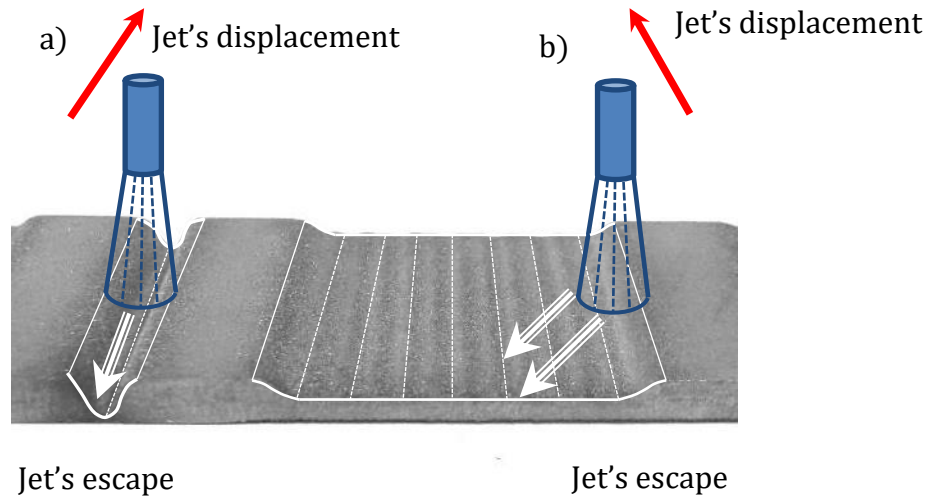


Fig. 2-7. Direction of the jet after impact

Preliminary experiments show that the depth measured is always greater than the depth calculated using equation (Eq. 2-7) due to the additional abrasion mechanism that appears during machining of the pocket. Now, the direction of the jet's escape depends mainly on the jet's width, meaning that of an elementary pass, and the sweep pitch. It will be detailed in the following paragraphs that the sweep pitch must always be smaller than the width parameter B of the jet to guarantee an overlap and thus obtain a flat bottom. For a given configuration defined in §2.1.1.2, the direction of the jet's escape will remain relatively constant as also the abrasion phenomenon. It is thus possible, for a given configuration, to define a coefficient of erosion He in order to take into account the erosion due to the escape of the jet (Eq. 2-8).

$$Y(x) = He \cdot \sum_{i=0}^n \left[H(Vf) \cdot e^{\left(-\frac{(x-i \cdot pitch)^2}{B(Vf)^2} \right)} \right] \quad \text{Eq. 2-8}$$

2.1.2.4 Simplification of the cutting depth model

The maximum depth will be constant as soon as a flat bottom appears (Fig. 2-6). The principle of summing is equivalent to stating that on a section of pocket of length D containing n elementary passes:

- the sum of the areas of elementary passes,
- the area of the machined pocket section,

are equal. The area S_u (Fig. 2-6) characterising the material removed by an elementary pass made at speed Vf is (Eq. 2-9):

$$S_u = \int_{-\infty}^{+\infty} H(Vf) \cdot e^{\left(\frac{-x^2}{B(Vf)^2}\right)} = \sqrt{\pi} \times H(Vf) \times B(Vf) \quad \text{Eq. 2-9}$$

The area A_{pe} of the pocket section of length D and depth $Y_{max}(Vf)$ (Fig. 2-6) containing n elementary passes is described in (Eq. 2-10):

$$A_{pe} = Y_{max}(Vf) \times D = n \times \sqrt{\pi} \times H(Vf) \times B(Vf) \quad \text{Eq. 2-10}$$

The distance D is equal to the number of elementary passes n multiplied by the pitch (Eq. 2-11):

$$D = n \times \text{pitch} \quad \text{Eq. 2-11}$$

The equality of areas calculated (Eq. 2-10) considering the relation (Eq. 2-11) as well as consideration for the erosion factor He thus allows the maximum depth in relation to the feed rate and the pitch to be calculated (Eq. 2-12):

$$Y_{max}(Vf) = He \cdot \frac{\sqrt{\pi} \cdot H(Vf) \cdot B(Vf)}{\text{pitch}} \quad \text{Eq. 2-12}$$

2.1.2.5 Formation of the pocket bottom in relation to the sweep pitch

When the sweep pitch is great as compared with the width $B(Vf)$ of the elementary pass considered, there will be no overlap and the pocket bottom will not be formed (Fig. 2-8a). When the pitch diminishes, an overlap appears and a corrugated pocket bottom will emerge (Fig. 2-8b). When the sweep pitch is of the order of the parameter $B(Vf)$, a flat pocket bottom will appear (Fig. 2-8c). Finally, when the sweep pitch becomes low as compared with the width of the elementary pass, the overlap will become significant and repeated erosion will cause degradation of the surface condition (Fig. 2-8d).

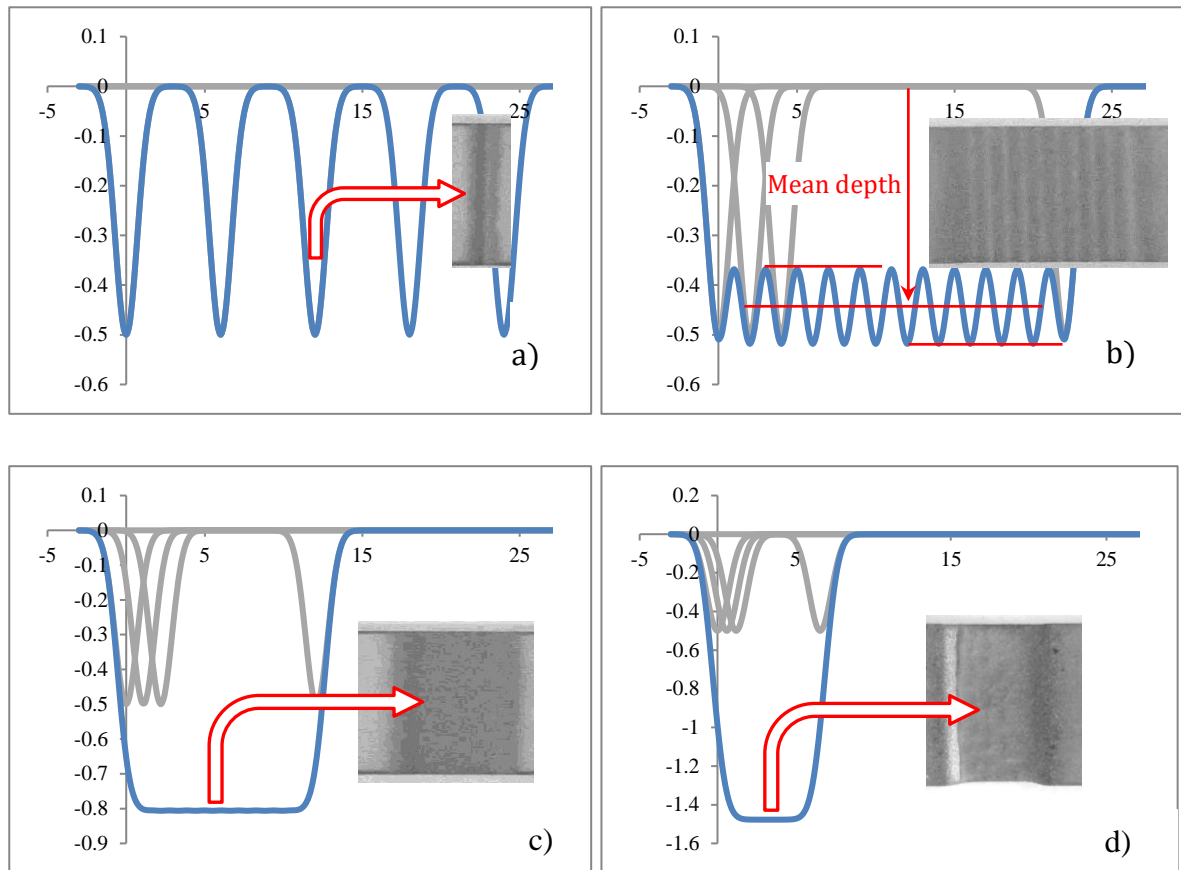


Fig. 2-8. Influence of the sweep pitch on formation of the pocket bottom

To guarantee a flat pocket bottom and a surface condition that is not degraded, it is therefore necessary for the pitch to be such that it ensures a correct overlap without however leading to a repeated erosion that will degrade the surface. For these reasons, the pitch to be used to produce a pocket must be defined from the factor $B(Vf)$ of the elementary pass used (Eq. 2-13):

$$0.7 \times B(Vf) \leq Pitch \leq 1 \times B(Vf) \quad \text{Eq. 2-13}$$

When a pocket is machined using a pitch greater than $B(Vf)$ an undulated bottom will appear and the model (Eq. 2-12) will not apply exactly. Nevertheless, the corrugated bottom shows a regular oscillation and the depth model allows for an extremely good prediction of the mean depth machined (Fig. 2-8b).

2.1.2.6 Method to set up the machined depth model

The method presented (Fig. 2-9) relies on the given configuration, that is a given material, pressure, stand-off distance, type of abrasive, and flow of abrasive. It allows the coefficients for the various models to be defined from experiments (Fig. 2-9).

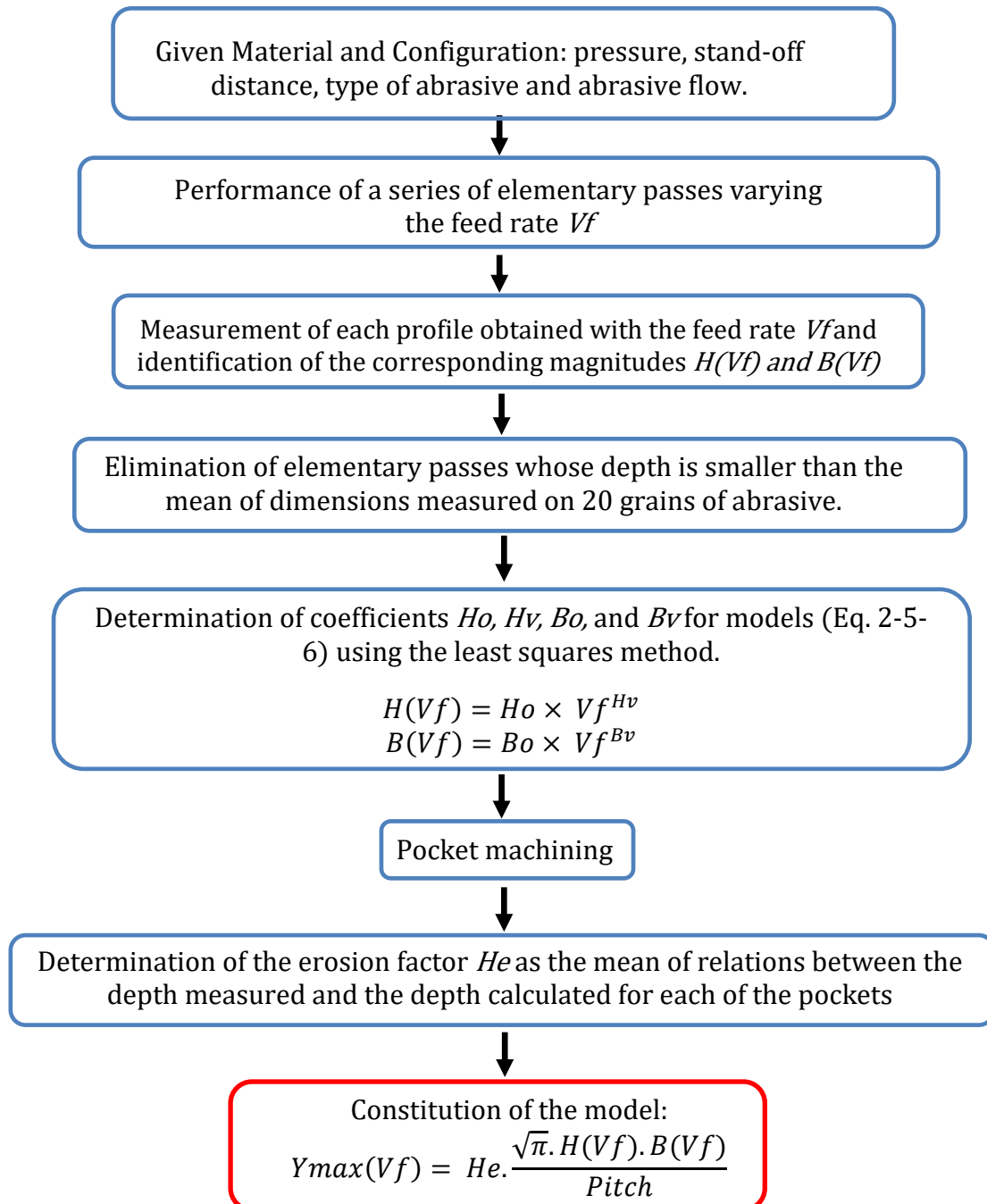


Fig. 2-9. Method to set up the depth model

2.1.3 Application of the method

2.1.3.1 The different configurations tested

A number of configurations were defined using three pressure levels, two *SOD* levels and two types of abrasive. The combinations are shown in the following table (Table 2-1):

Table 2-1. Configurations tested.

Configuration N°	Stand-off distance SOD (mm)	Pressure (bars)	Size of the abrasive (#)
1	100	1000	220
2	100	2250	220
3	100	3500	220
4	40	3500	220
5	100	3500	120
6	40	3500	120

Configurations 1, 2 and 3 were intended to determine the influence of pressure on the model. Configurations 3 and 4 were used to identify the influence of the *SOD*. Comparisons between configurations 3 and 5 as well as 4 and 6 allow the influence of the abrasive to be characterised. As stated previously, an optimal flow of abrasive corresponds to a given abrasive conditioned by the pressure (Fig. 2-2). Preliminary tests conducted on elementary passes for the material studied Ti6Al4V allowed optimal flows to be defined for each configuration. The optimal flow of abrasive was 128 g/min for configuration 1, 222 g/min for configuration 2, 313 g/min for configurations 3 and 4 and 408 g/min for configurations 5 and 6.

2.1.3.2 The experimental set-up

The machine used was a FLOW MACH4C (Fig. 2-10) equipped with a PASER4 cutting head. The nozzle was of diameter 0.33 mm and the focus mechanism 1.02 mm in diameter and 101.6 mm in length. The pressure was generated using a Hyplex-Prime pump with a maximum of 4000 MPa. Control of the NC machine was ensured by two software packages (Flowpath and Flowcut) provided by FLOW. Two abrasives of different

brands and sizes were tested: Barton HPX 220# and Opta Minerals120#. The flow of abrasive was set using a pierced washer whose diameter conditions the flow.

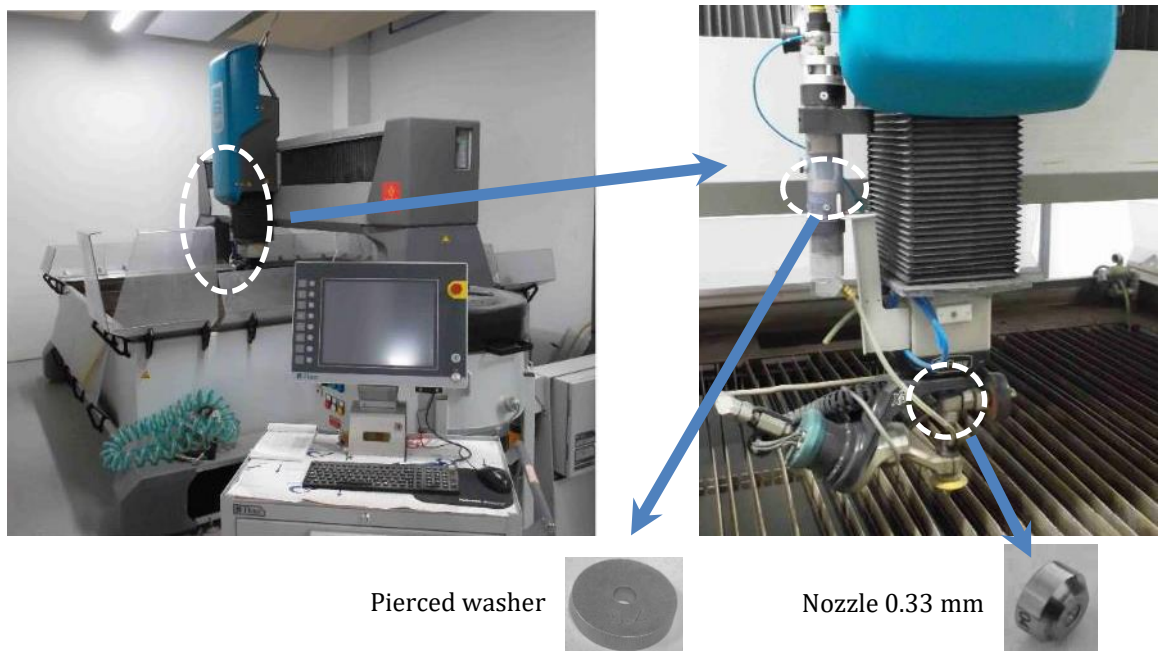


Fig. 2-10. Machine FLOW MACH4C

The material machined was Ti6Al4V titanium alloy. The coupons machined were 4 mm thick and the pockets were rectangular, 15 mm wide and about 15 mm long (Fig. 2-11). This last dimension is adjusted to obtain a sufficient number of elementary passes to guarantee that a regular bottom be obtained. Measurement of the profiles of the elementary passes and pocket bottoms was performed using an ALICONA IF optical profilometer (Fig. 2-11). This device allows a surface to be acquired and 1000 curves, distributed regularly over 2 mm, are calculated by making the intersection between the surface and the 1000 planes perpendicular to the feed movement.

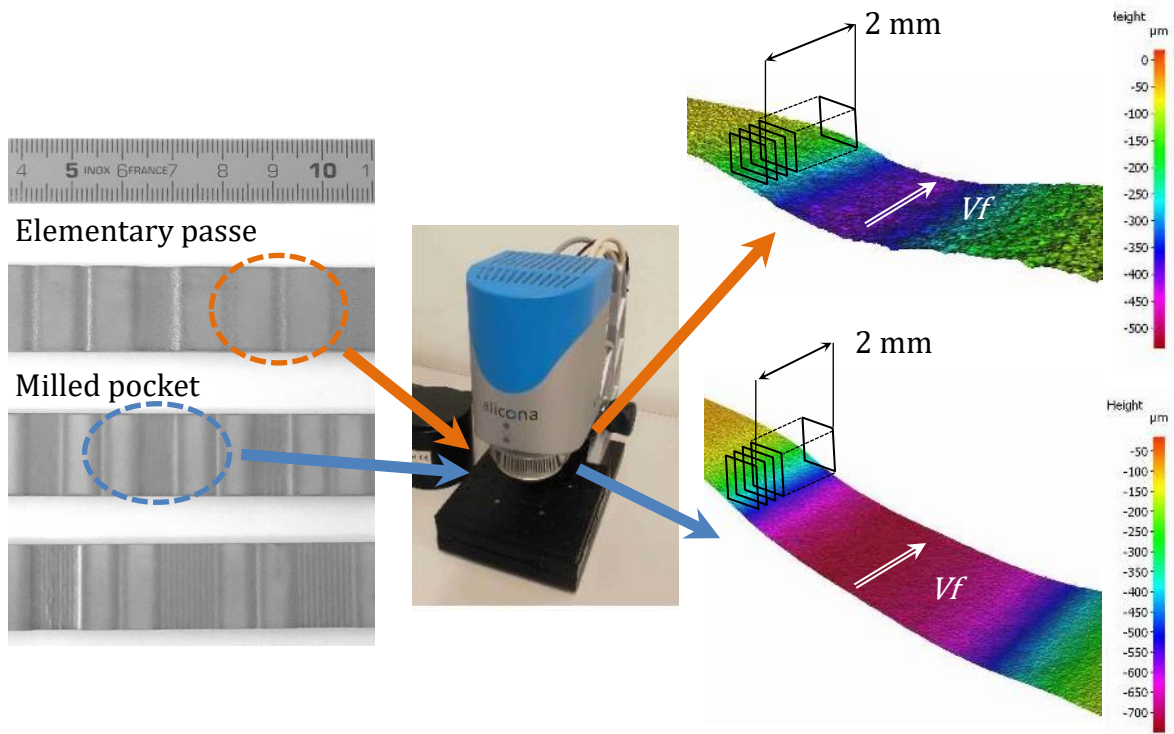


Fig. 2-11. Measurement device

The profiles considered in this study (Fig. 2-12) are mean profiles calculated over those 1000 curves.

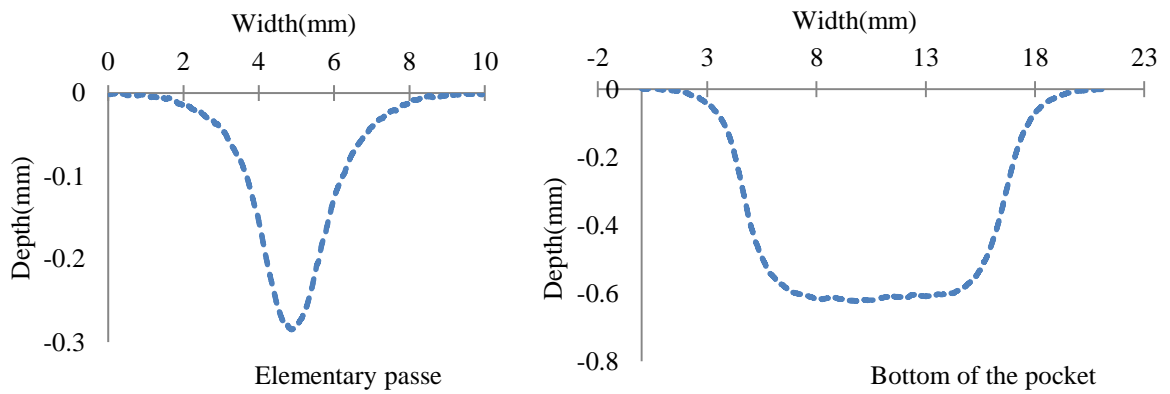


Fig. 2-12. Mean profiles measured

2.1.3.3 Results obtained for configuration N° 1

The first configuration was observed making 12 elementary passes with feed rates of between 125 mm/min and 4300 mm/min. Depths $H(Vf)$ and width factors $B(Vf)$ are shown (Fig. 2-13).

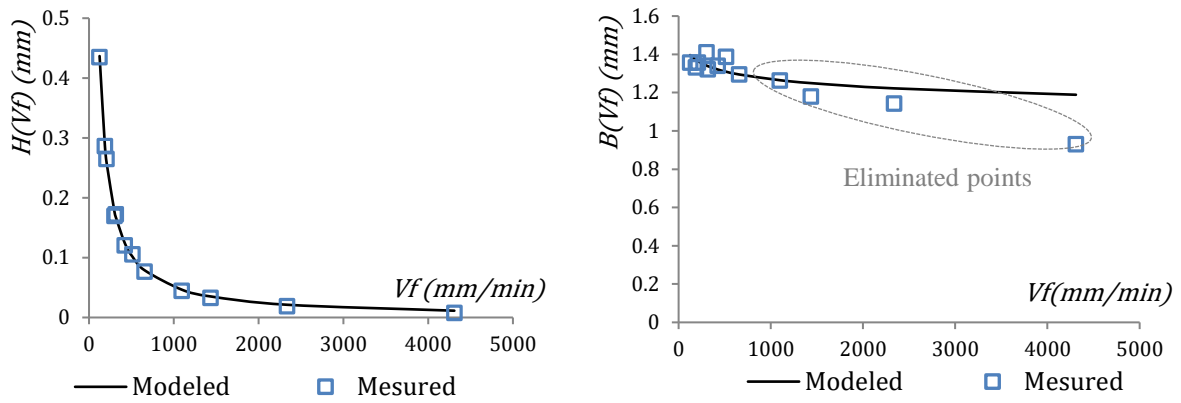


Fig. 2-13. Measurement and modelling of elementary profiles

The abrasive used had a grain size of 220# and the mean size measured on 20 grains was 0.053 mm. The models obtained (Fig. 2-13) by equations (Eq. 2-5 and Eq. 2-6) did not consider the four last points of each graph for which the depth was less than 0.053 mm. The coefficients calculated (Eq. 2-5 and Eq. 2-6) were $H_0 = 62.333$; $H_v = -1.028$; $B_0 = 1.429$; $B_v = -0.001$. The mean accuracy obtained over all the points by the depth model $H(Vf)$ was 7.2% and that obtained on the width parameter model $B(Vf)$ was 7.6%. Modelling of the elementary passes is thus effective. A series of 12 pockets was then machined aiming at 4 depth levels: 0.60; 0.35; 0.15 and 0.05 mm. For each depth level, two pockets were calculated by equation (Eq. 2-7) using $Pitch = 0.7 \times B(Vf)$ and $Pitch = 1 \times B(Vf)$ so as to obtain the depths aimed at and a flat bottom (Eq. 2-13) and a third pocket was calculated setting $pitch = 1.2 \times B(Vf)$ in order to verify the appearance of a corrugated bottom. In this latter case, it is the mean depth (Fig. 2-8b) that is estimated by the equation (Eq. 2-7). The depths calculated and measured for the twelve pockets are shown (Fig. 2-14).

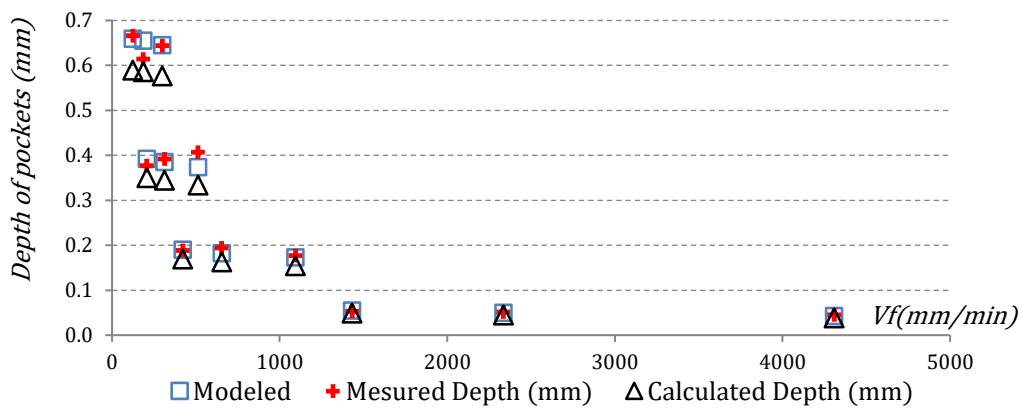


Fig. 2-14. Depths of pockets for configuration 1

The erosion coefficient He was calculated in accordance with the approach presented (Fig. 2-9). Its value of 1.096 allowed the depth model to be completed (Eq. 2-12). The depths modelled are shown (Fig. 2-14). The model set up has a mean error of 3.6% and a maximum error of 8% and is thus effective. Also, for a targeted depth level, the pocket machined using $pitch = 1.2 \times B(Vf)$ does indeed produce a corrugated bottom (Fig. 14) whose profile corresponds to the modelled pocket profile (Eq. 2-8).

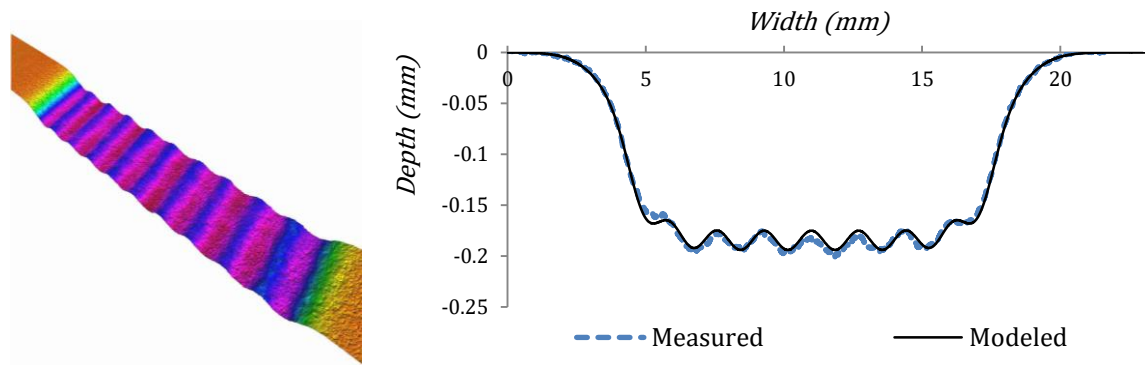


Fig. 2-15. Pocket with a corrugated bottom machined with $P=100$ MPa, $SOD= 100$ mm, abrasive size 220 #, $Vf= 423$ mm/min, $B(423) = 1.420$ mm and $pitch = 1.71$ mm.

2.1.3.4 Identification of a rapid calibration procedure on configuration N° 1

The performance of elementary passes while varying the feed rate is fairly rapid and only takes a few minutes. However, production of pockets is much longer and may take several hours. An investigation was conducted to determine whether a good estimation of the coefficient He was possible only producing a limited number of pockets. To this purpose, the points corresponding to the lowest and the highest feed rate used to establish models $H(Vf)$ and $B(Vf)$ (Eq. 2-5 and Eq. 2-6) were retained as well as a third value situated between the first two (Table 2-2).

Table 2-2. Rapid calibration on configuration 1.

N°	Vf (mm/min)	$H(Vf)$ (mm)	Calculated Y_{max} (mm) by (Eq. 2-7)	Mesured Y_{max} (mm)	Mesured depth/Calculated depth	Modeled Y_{max} mm) by (Eq. 2-12)	Precision
1	125	0.575	0.589	0.666	1.160	0.653	2.0%
2	187	0.580	0.586	0.614		0.659	7.3%
3	208	0.349	0.351	0.377		0.396	5.2%

4	301	0.582	0.577	0.644		0.662	2.7%
5	314	0.348	0.344	0.392	1.107	0.396	1.0%
6	423	0.174	0.170	0.189		0.197	4.6%
7	514	0.344	0.334	0.407		0.391	3.9%
8	655	0.169	0.163	0.194	1.144	0.193	0.6%
9	1095	0.164	0.154	0.177		0.186	5.1%
10	1433	0.051	0.049	0.053		0.060	12.1%
11	2336	0.049	0.045	0.052		0.055	7.5%
12	4309	0.043	0.038	0.045		0.049	7.6%

$$He = 1.137$$

The extreme values are those of line N° 1 and N° 8, while line N° 5 was chosen as an intermediate value. The erosion factor He is determined as being the mean of the relations between the depth measured and the depth measured calculated for lines N° 1, 5 and 8. This factor $He = 1.137$ then allows the model to be finalised and calibration from just these three pockets allows a mean accuracy of 5% to be obtained, which is only just greater than that of 3.4% obtained considering all the pockets. The rapid calibration method thus applies extremely well to modelling of the depth of the pockets and it should be noted that even if that calibration relies on the results obtained up to line N° 8, it allows for a good prediction for the depths obtained on lines N° 9, 10, 11 and 12 since the mean of deviations on these lines is 8.1%. The model thus extrapolates beyond the domain that was used to define it.

Calibration is possible using just two pockets. In the case presented (Table 2-2) a calibration relying on lines N° 1 and N° 8 leads to an accuracy of the depth model of 5.8%, a calibration relying on lines N° 1 and N° 5 has an accuracy of 4.8% and a calibration relying on lines N° 5 and N° 8 has an accuracy of 4.4%. It is thus possible to limit calibration just machining two pockets, or even only one, but in such cases the approach fails to benefit from a mean effect and may lead to impaired precision.

2.1.3.5 Modelling with rapid calibration for configurations N° 2 to N° 6

Having been set up on configuration N°1, the rapid calibration method was used on configurations N° 2 to N° 6 that involve setting parameter changes for the pressure, *SOD* and flow and type of abrasive. As for handling of configuration N° 1, a series of 12 elementary passes was performed and the shallower passes were eliminated to establish models of $H(Vf)$ and $B(Vf)$. Following this, three pockets were produced to define the erosion coefficient He . To do so, the size of the grains of abrasive considered were 0.053 mm for the abrasive of size 220 # and 0.092 mm for the abrasive of size 120 #. The results are presented in Table 2-3 and the shaded columns concern the values used to determine the erosion coefficient He .

Table 2-3. Rapid calibration for configurations 2 to 6.

	Configuration N°2 <i>P=225 MPa, SOD = 100 mm, abrasive size 220 #</i>											
<i>Vf</i> (mm/min)	691	1035	1150	1666	1742	2343	2846	3629	6066	7941	12941	23872
Coefficients for (Eq. 2-5) and (Eq. 2-6) <i>Ho = 407.337 ; Hv = -1.061 ; Bo = 1.947 ; Bv = -0.061</i>												
<i>Pitch</i> (mm)	1.834			0.727				1.112				
Calculated depth (mm) by (Eq. 2-7)	0.497			0.467				0.127				
Measured depth (mm)	0.560			0.521				0.152				
<i>He</i> = 1.145	1.126			1.115				1.195				

	Configuration N°3 <i>P=350 PMa, SOD = 100 mm, abrasive 220 #</i>											
<i>Vf</i> (mm/min)	1470	1958	2099	2522	2803	2946	3623	3963	5145	5375	7305	9602
Coefficients for (Eq. 2-5) and (Eq. 2-6)												

<i>Ho = 469.310 ; Hv = -0.983 ; Bo = 2.350; Bv = -0.083</i>												
<i>Pitch</i> (mm)	1.834					1.763						0.961
Calculated depth (mm) by (Eq. 2-7)	0.447					0.222						0.115
Measured depth (mm)	0.474					0.232						0.127
<i>He</i> = 1.068	1.060					1.046						1.099

<i>Configuration N°4</i> <i>P=350 MPa, SOD = 40 mm, abrasive 220 #</i>												
<i>Vf</i> (mm/min)	2816	3750	4020	4831	5368	5642	6939	7590	9853	10294	13991	18390
Coefficients for (Eq. 2-5) and (Eq. 2-6) <i>Ho = 1644.825 ; Hv = -1.048 ; Bo = 1.151; Bv = -0.072</i>												
<i>Pitch</i> (mm)	1.195					1.148						0.626
Calculated depth (mm) by (Eq. 2-7)	0.384					0.184						0.090
Measured depth (mm)	0.425					0.205						0.110
<i>He</i> = 1.147	1.107					1.113						1.221

<i>Configuration N°5</i> <i>P=350 MPa, SOD = 100mm, abrasive size 120 #</i>												
<i>Vf</i> (mm/min)	2371	3164	3394	4085	4558	4794	5919	6459	8428	8814	12083	16048

Coefficients for (Eq. 2-5) and (Eq. 2-6)												
$H_o = 931.979$; $H_v = -1.037$; $B_o = 2.787$; $B_v = -0.071$												
Pitch (mm)	1.834			1.037				1.300				
Calculated depth (mm) by (Eq. 2-7)	0.454			0.441				0.212				
Measured depth (mm)	0.492			0.483				0.232				
$He = 1.088$	1.077			1.094				1.092				

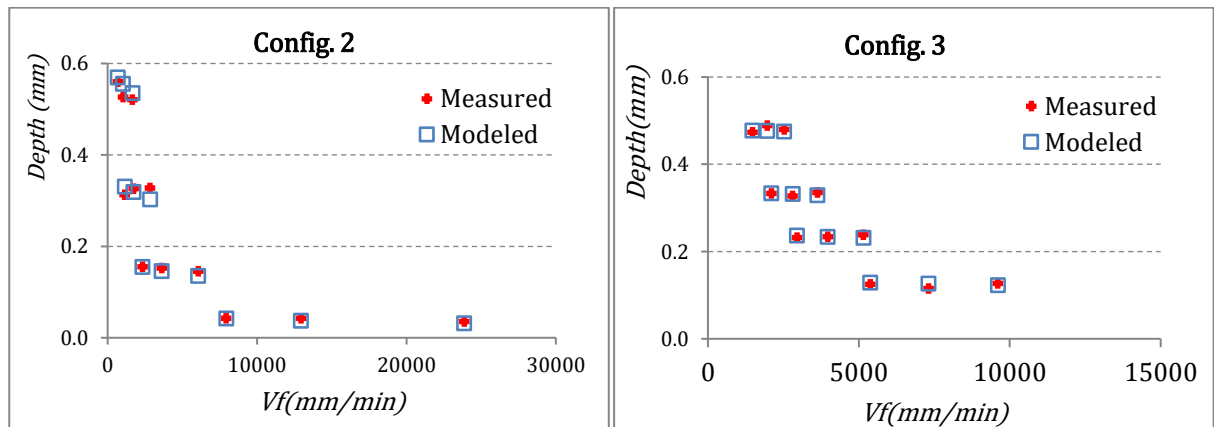
Configuration N°6												
$P = 350 \text{ MPa}$, $SOD = 40 \text{ mm}$, abrasive size 120 #												
V_f (mm/min)	4542	6060	6500	7824	8730	9183	11336	12371	16142	16881	23142	30736
Coefficients for (Eq. 2-5) and (Eq. 2-6)												
$H_o = 2005.306$; $H_v = -1.037$; $B_o = 1.912$; $B_v = -0.112$												
Pitch (mm)	1.195			0.676				0.847				
Calculated depth (mm) by (Eq. 2-7)	0.357			0.338				0.159				
Measured depth (mm)	0.385			0.319				0.187				
$He = 1.066$	1.078			0.944				1.176				

The various coefficients calculated and presented (Table 2-3) show specific features:

- The values of coefficients Hv for the depth model of an elementary pass (Eq. 2-5) vary between -1.061 and -0.983. The depth of an elementary pass can thus be considered as inversely proportional to the feed rate Vf .
- The value of the coefficient Bv for the width model of an elementary pass (Eq. 2-6) varies between -0.112 and -0.010, which confirms that the width of an elementary pass is quasi-independent of the feed rate Vf .
- The coefficient of erosion He varies very little since it remains between 1.066 and 1.147. The ratio between the sweep pitch and the width of an elementary pass (Eq. 2-13) gives a constant orientation to the jet's escape and thus produces identical additional erosion on the various machined pockets.

2.1.3.6 Experimental validation of the models established by rapid calibration

Identification (Table 2-3) of the parameters for depth (Eq. 2-5) and width (Eq. 2-6) models of the elementary passes as well as the coefficient of erosion He allows the depth machined for configurations 2 to 6 (Table 2-1) to be predicted using equation (Eq. 2-12). As for configuration 1, for each configuration 2 to 6, four depth levels were considered, eight pockets calculated to obtain a flat bottom and four to verify the appearance of a corrugated bottom. The corresponding machining tasks were performed and the results obtained are presented (Fig. 2-16).



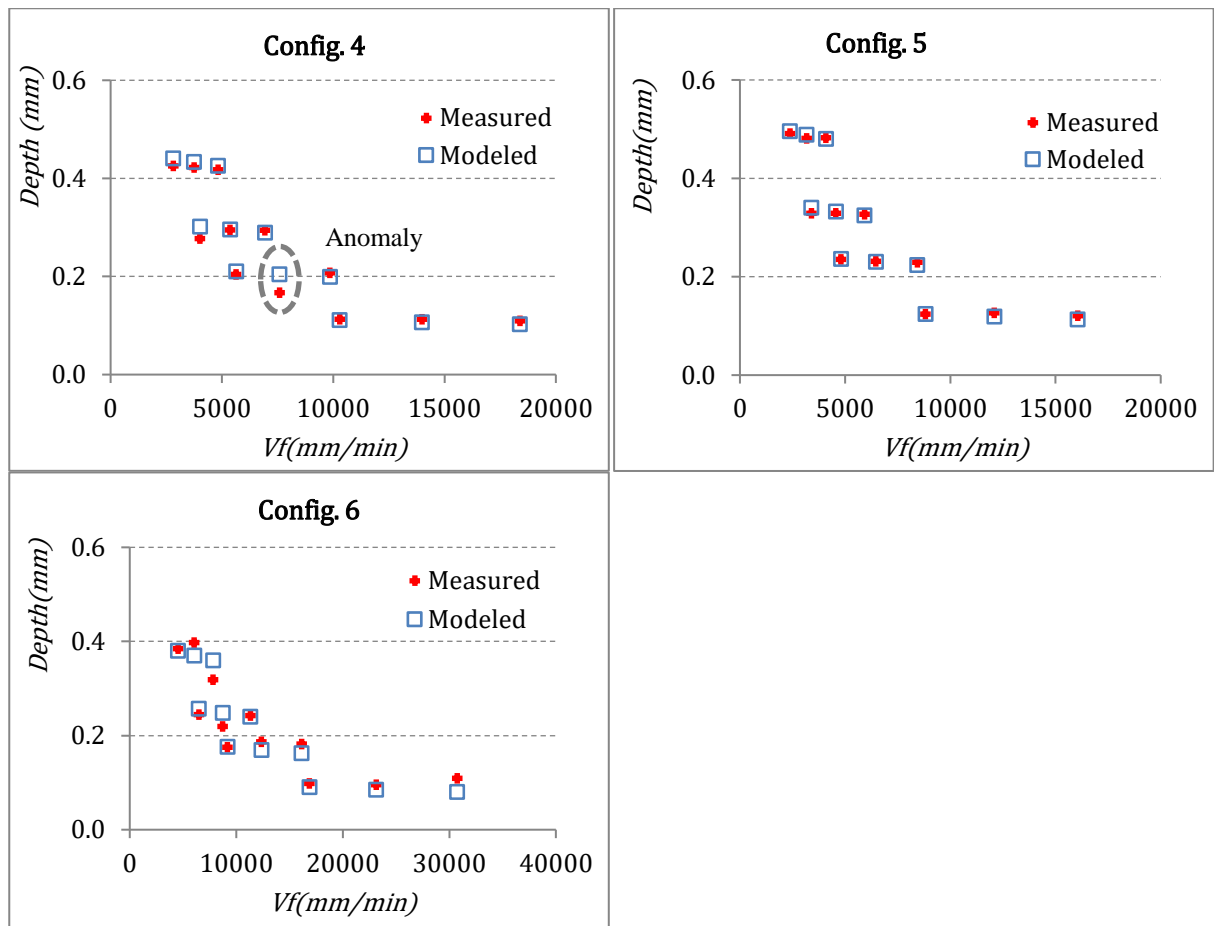


Fig. 2-16. Results obtained - Comparison of the depths calculated and measured

2.1.4 Results and discussion

The results presented show an extremely good correlation between the depths obtained using the model and the depths measured. For the various configurations, the mean for errors obtained between the calculated results and the measured results (Table 2-4) is of the order of 5%. The error calculated for each machined pocket remains close to that mean since the maximum error calculated for each configuration remains less than 13% except for configuration N° 4 for which a maximum error of 22.6% resulting from an anomaly is observed. This value is only present once and is identified on the graph (Fig. 2-16). For that pocket, the depth machined is considerably shallower than that calculated and derives from clogging of the abrasive supply system. If this value is ignored, the maximum error for the configuration 4 will be 8.9%. The method adopted applies uniformly over the various configurations tested and over the feed rate ranges used. The

mean and maximum errors also show that this method is effective since it combines rapid and simplified calibration with a very high level of accuracy.

Table 2-4. Errors for the various configurations tested.

Configuration N°	Max error (%)	Mean error (%)
1	12.1%	5.0%
2	12.4%	5.2%
3	9.7%	2.4%
4	22.6%	5.1%
5	5.8%	2.4%
6	5.8%	1.9%

For each configuration, the four pockets with corrugated bottoms are effectively obtained but a corrugated bottom also appears for $Pitch = 1 \times B(Vf)$ for the greatest depths when the pressure exceeds 100 MPa (Fig. 2-17).

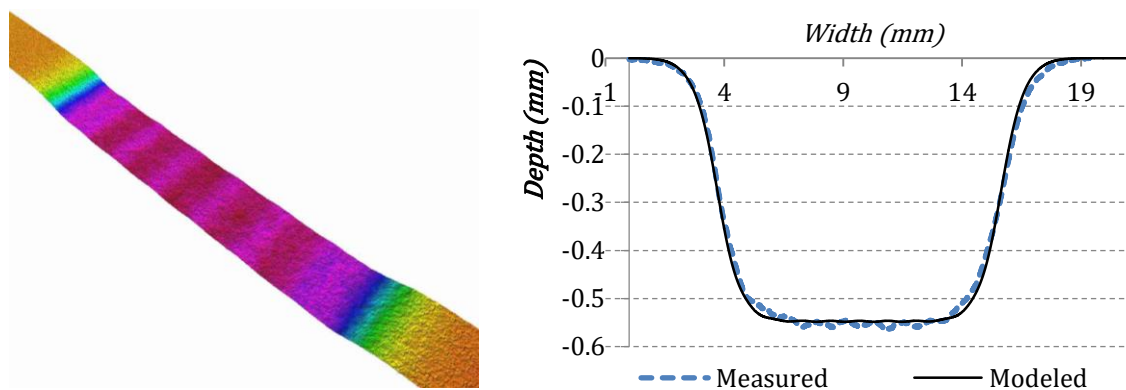


Fig. 2-17. Pocket with a slightly corrugated bottom machined with $P = 225$ MPa, $SOD = 100$ mm, abrasive size 220 #, $Vf = 1.035$ mm/min, $B(1035) = 0.993$ mm and $pitch = 1.02$ mm.

The ratio between the width factor $B(Vf)$ and the sweep pitch (Eq. 2-13) thus seems to be slightly influenced by the pressure. For configurations 2 to 6, the corrugated bottom appears only once abnormally for $Pitch = 1 \times B(Vf)$ when the greatest depth is achieved. A pitch of between $0.6 \times B(Vf)$ and $0.9 \times B(Vf)$ would thus be more appropriate.

2.1.5 Conclusion

The study presents a model for pocket depth in blind machining using an abrasive water jet in a context where a machine, a pressure and an abrasive are given. The material considered was a titanium alloy (Ti6Al4V). In order to achieve productive machining, the optimal abrasive flow rate, i.e. that corresponding to the greatest MRR, is considered. This machine, material, pressure, abrasive and optimal abrasive flow rate combination plus the stand-off distance defines the machining configuration concept. For a configuration thus defined, the feed rate influences the width and depth of an elementary pass and the depth of the pockets will only depend on the feed rate and the sweep pitch.

The width and depth of a series of elementary passes were modelled. These two parameters allow a simple pocket depth model to be defined that takes into account the erosion specific to the milling of pockets. So as to proceed with rapid implementation of the model, a rapid calibration method is proposed that allow accuracy to be maintained. The entire approach is validated experimentally since the models developed varying the pressure, stand-off distance and type of abrasive are accurate to within 5%. Furthermore, the study details the mechanisms for formation of pocket bottoms and shows that there exists an interval of the sweep pitch over the width of an elementary pass ratio within which the pocket bottom can be considered to be flat and with a satisfactory surface condition. To round off this approach, a further study will be proposed in order to establish a connection between the geometry of an elementary pass, the shape of the pocket bottom generated by that elementary pass and a given sweep pitch, as well as characterisation of the surface condition taking the erosion mechanism into account.

2.2 Adaptive speed control for waterjet milling in pocket corners

(This section is presented as the format of an article and it has been published in International Journal of Advanced Manufacturing Technology- DOI: 10.1007/s00170-019-03546-z)

Abstract: Milling thin titanium alloy workpieces using conventional manufacturing processes is a delicate operation. During machining the cutting forces can deform the part while resulting compressive stresses could actually enhance its mechanical properties. Nevertheless, when parts are both large in size and thin, deformation generated by machining will be incompatible with the geometrical specifications. From this perspective, abrasive water jet milling offers a suitable alternative solution. Numerous works present the results relating to the depths milled, the surface characteristics and machining strategies when milling pockets. Such studies show that the change of direction when milling closed pockets generates defects arising from the distribution of the jet's energy over the milled surface or the kinematics of the machine. When a pocket corner radius is imposed, changes of direction are made following circular arcs with a radius lower than the specified one. In the present paper, an analysis of the width milled during successive circular trajectories is presented and a predictive model for the depth is adopted. This model is then used to propose a milling method that allows both the imposed radius and tolerance on the pocket depth to be respected.

Keywords: Machining, abrasive waterjet, milling strategy, titanium alloy, Ti6Al4V.

2.2.1 Literature review

Titanium alloys have excellent mechanical properties and one of the most commonly used is the Ti6Al4V alloy. This grade is mainly composed of titanium, aluminium (6%), vanadium (4%), and other constituents such as carbon (0.08%), iron (0.25%), oxygen (0.13%), nitrogen (0.05%) and hydrogen (0.012%). The main properties of this alloy are high tensile strength (860 MPa), high yield strength (800 MPa) and an elongation of more than 10%. It is therefore difficult to machine using conventional turning and milling methods due to its high strength and galling tendency. During such machining, the cutting forces can become high and cause deformations in the workpiece or significant excess heating. In both cases, the finished workpiece's geometry will show deviations outside specifications. This situation is exacerbated when the workpieces are part of an aerostructure that must be resistant, of large dimensions and lightweight. Achievement of these last two properties often requires the use of thin walls that are difficult to machine as they are extremely deformable and sensitive to vibrations.

Other material removal solutions have been studied to overcome the difficulty of milling such parts. Among them, abrasive waterjet milling is a highly interesting alternative solution as it uses natural components (water and abrasive) and only generates low cutting forces. It thus limits deformation of the workpiece and resolves some production waste recycling issues. This process has thus been widely studied to machine open or closed pockets [45], [105], [106]. In the case of closed pockets, the various strategies necessarily generate changes of direction during machining. In their study, Goutham et al.[109] consider rectangular pockets and changes of direction at 90°. This study shows that the changes of direction lead locally to defects in the pocket depth (Fig. 2-18). When the jet slows down and then stops to change feed direction, the workpiece's exposure time increases and the depth machined increases.

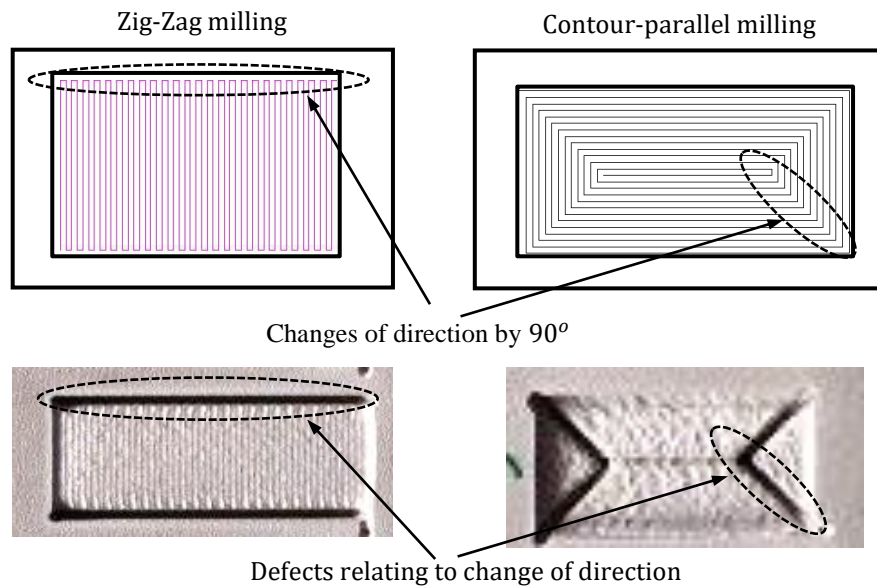


Fig. 2-18. Changes in milling direction by 90° and corresponding defects [109]

In their works, A. Alberdi et al. [45] presented the milling of triangular pockets (Fig. 2-19) based on two strategies using changes of different directions by 90°. One pocket produced in parallel contours was machined moving, in one instance, from the interior to the exterior and in the other instance moving from the exterior to the interior. All the pockets showed irregularities on the bottom depth (Fig. 2-19). These irregularities appeared in the zones where changes of direction were made.

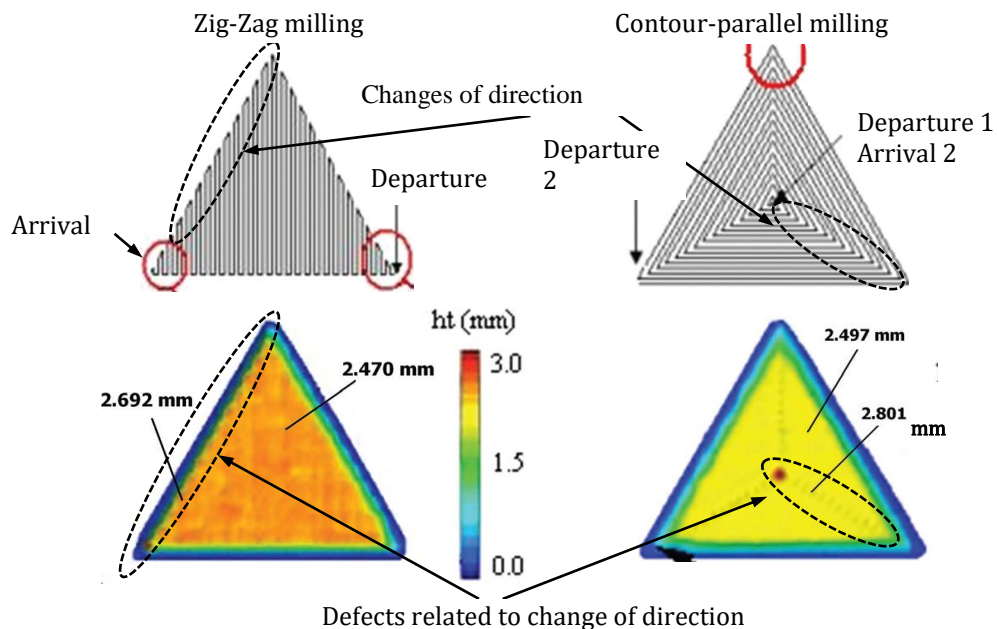


Fig. 2-19. Changes of direction for triangular pockets [45]

In the same study, an analysis of the defects generated on change of direction is presented and it is stated that the variation in the distance between two adjacent trajectories is the origin of the observed defect. When the trajectories are parallel, the distance between the point situated under the jet and the point closest to the already milled surface is constant. This distance is greater when there is a change of direction (Fig. 2-20) and this generates a difference in depth. The variation in distance between two successive passes is thus one of the causes of the variation in depth milled.

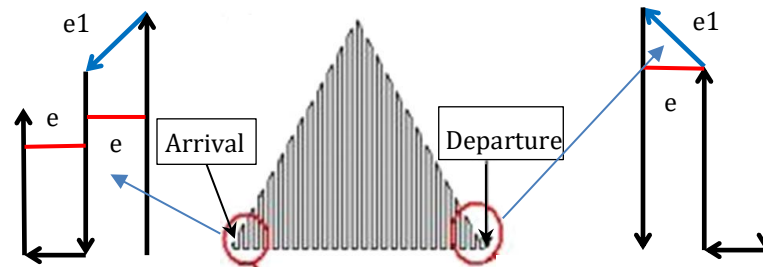


Fig. 2-20. Distances on changes of direction

2.2.2 Change of direction

2.2.2.1 Depth model for milled pockets

To predict the depth of the milled pockets, modelling of their shape is required. Different approaches have been used to determine the influence of machining parameters on the milled surface. These approaches are based on experiments [8], [44]–[46], [105], [106], [109], on an advanced computational method [113], on design of experiment [87], on analysis of the material removal mechanism [107], on analysis of the surface roughness [72] or on a CFD method [115]. It is also possible to consider an elementary profile [111], [114]–[116] to model it [114], [115] and calculate the equation for a pocket bottom profile by considering an offset between each pass [87], [116].

The setting parameters are not modifiable during milling: they are pressure (P), a grade of abrasive particle, the abrasive flow rate (ma), and the standoff distance (SOD). The control parameters are those that can be controlled by the NC program during machining. Considering an elementary pass, the only controlled parameter is the traverse speed (Vf).

Amongst proposed models, the model based on an exponential function is effective in modelling an elementary pass. This elementary pass is generated by moving the jet in a straight line over a machined surface of the workpiece (Fig. 2-21-a). Several studies on metallic materials [44], [45], [116][1, 7, 15] have confirmed that the profile of an elementary pass can be represented using the Gaussian profile (Eq. 2-14).

$$y(x) = -H \times e\left(\frac{-x^2}{B^2}\right) \quad \text{Eq. 2-14}$$

This Gaussian profile (Fig. 2-21-b) is characterised by the maximum depth H and the width factor B [116]. They are established using a power function (Eq. 2-15). The width of the profile is estimated by the interval of $[-2xB; 2xB]$ and contains all the points of the profile curve where $y(x) \leq -0.01xH$. This consideration excludes cases of particle impacting without removing material.

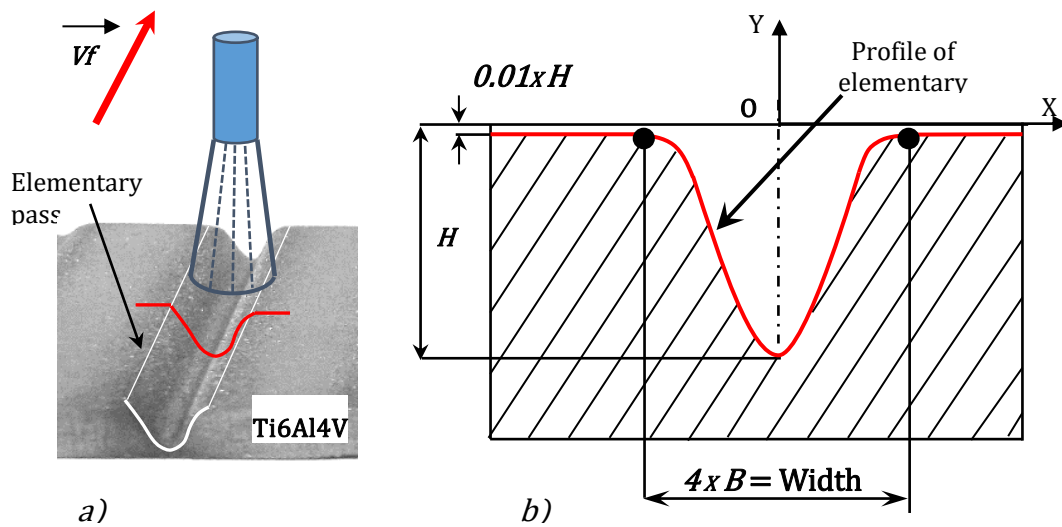


Fig. 2-21. Modelling the Gaussian profile

$$H(Vf) = H_0 \times Vf^{Hv} \quad \text{and} \quad B(Vf) = B_0 \times Vf^{Bv} \quad \text{Eq. 2-15}$$

In this expression, H_0 , Hv , B_0 , and Bv are experimental coefficients calculated by the least squares method. Traverse speed Vf is expressed in millimetres per minute and $H(Vf)$ and $B(Vf)$ are obtained in millimetres.

As an elementary profile is characterised by the equation (Eq. 2-14), it is possible to determine the cross-section profile of an open pocket bottom as being the sum of n

elementary passes (Fig. 2-22) with an offset distance named *Pitch*. According to Eq. 2-14, Eq. 2-16 expresses the superposition of n offset elementary passes for a given *Pitch*:

$$Y(x) = He \cdot \sum_{i=0}^n \left[H(Vf) \cdot e^{\left(\frac{(x-i \cdot Pitch)^2}{B(Vf)^2} \right)} \right] \quad \text{Eq. 2-16}$$

In this equation, the coefficient He allows an additional erosion that appears when a succession of elementary passes is performed to be taken into account. This erosion arises from the action produced by a given pass on the surface generated by the previous passes. Indeed, the main material removal mechanism [54], [56], [57] identified suggests that a particle does not fragment on impact and that it is driven by a plane movement. Hence, it generates an additional erosion (a second effect of impacting particles) on the surface that has already been milled.

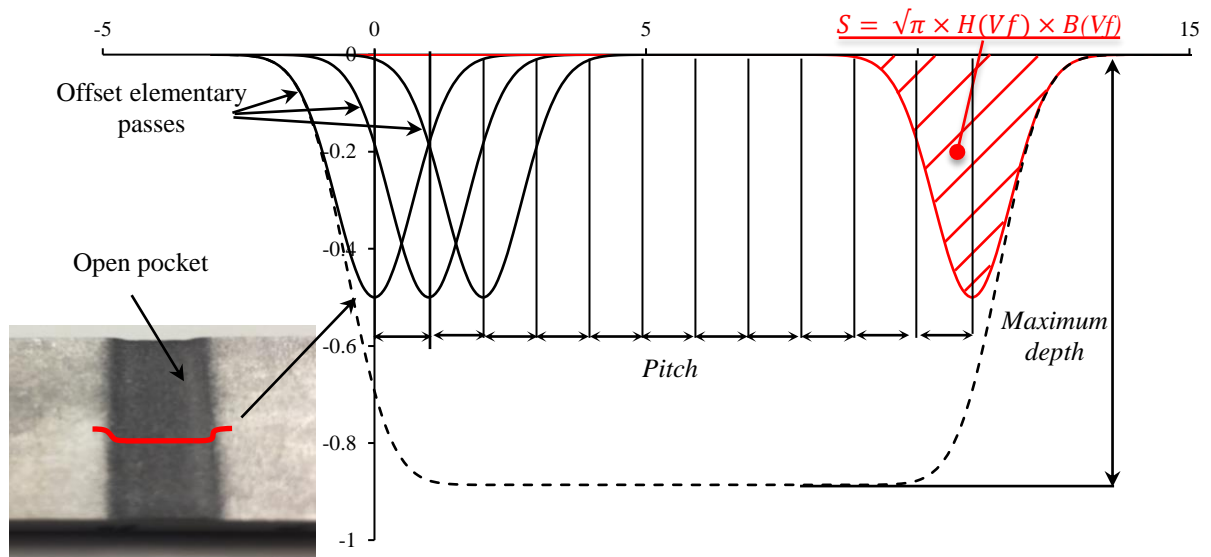


Fig. 2-22. Superposition of elementary passes

Once the maximum depth has been reached, it can be specified according to Eq. 2-17 [116].

$$\text{Maximum depth} = He \frac{\sqrt{\pi} \cdot H(Vf) \cdot B(Vf)}{\text{Pitch}} \quad \text{Eq. 2-17}$$

It should be noted that it is possible to modify the jet's impact angle by tilting the cutting head. In their work, Hlavac et al.[117] use the tilting angle in order to reduce the

product shape distortion in water jet cutting. In this study, only an impact angle of 90° will be considered while a variable angle will be studied in a forthcoming work.

2.2.2.2 Direction change strategies

The issue studied in the present paper concerns milling of closed pockets for which changes of direction by 90° are needed. On a change of direction without circular arc (Fig. 2-23a), the machine has to decelerate (Fig. 2-23-c) down to zero speed, change direction and accelerate to again reach the specified traverse speed. During the deceleration and acceleration phase, the jet remains longer on the same location than during a continuous trajectory at constant speed. A greater depth thus inevitably emerges (Fig. 2-23-a). To avoid this problem, the direction can be changed using circular arc trajectories (Fig. 2-23-b).

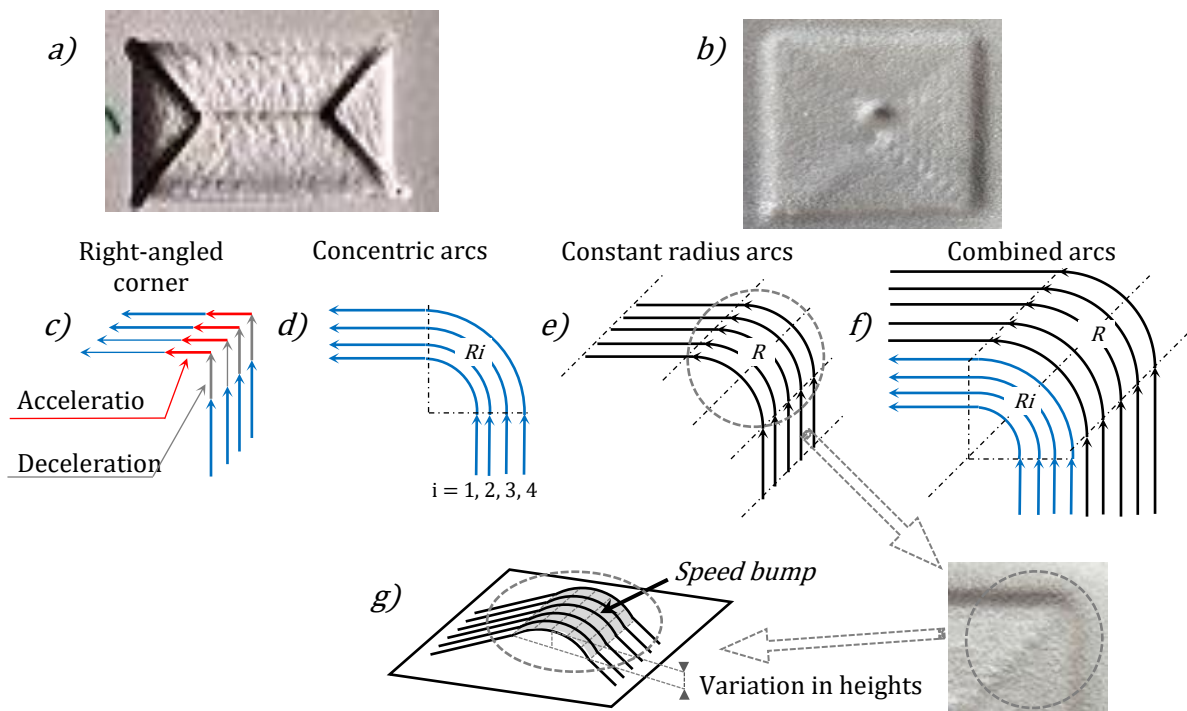


Fig. 2-23. Different changes of direction

Several solutions are possible to change direction using circular arc trajectories:

- Concentric arcs (Fig. 2-23d) allow the distance between two consecutive passes to be retained. The quantity of energy of the jet will then be distributed over the same milled surface quantity and the depth will remain constant. However, the

pocket corner radius will depend on the number of passes needed to produce the pocket and cannot therefore respect a specification.

- Constant radius arcs (Fig. 2-23e) allow a set radius to be maintained. The distance between two consecutive arcs will not be constant and the energy distribution of the jet over a surface quantity will depend on the jet's position. This surface quantity will be maximal when the jet is in the middle of the circular arc. The depth machined will thus be reduced in the pocket corner that will then show a bump (Fig. 2-23g). Failing correction, this pocket corner will resemble a speed bump.
- A combination of the previous solutions (Fig. 2-23f) allows the pocket corner radius to be controlled. This solution uses the small radius needed in the centre of the pocket and limits its value on the outer radius specified R once it has been reached. If no correction is applied, the pockets obtained will have a constant depth as long as the radii remain concentric but will show speed bumps when the radius remains constant.

2.2.2.3 Change of direction at constant radius

2.2.2.3.1 Identification of three distinct areas

When the arcs have a constant radius, the distance between two consecutive passes will vary according to the point considered on the trajectory. This distance is calculated as the length of the perpendicular to the mid-line between two passes. Geometrically, evolution of the distance has a mathematical relationship with initial pitch, $Pitch_{init}$. In the present work, the initial pitch $Pitch_{init}$ will be quite small in relation to the radius R of the pocket corner ($Pitch_{init} \ll R$).

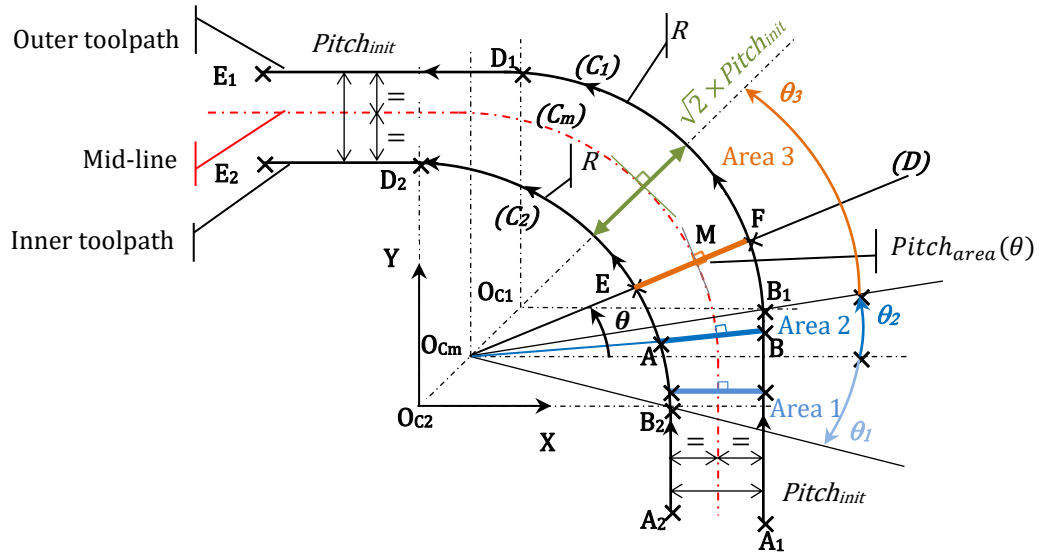


Fig. 2-24. Changes of direction at constant radius

Fig. 2-24 illustrates the change in distance of two adjacent toolpaths, i.e. outer toolpath (A_1, B_1, D_1, E_1) and inner toolpath (A_2, B_2, D_2, E_2) at a corner of a milled pocket with constant radius R . Three areas need to be defined for an angle smaller than 45° and a different calculation has to be performed of the distance for each of them:

- **Area 1:** the inner path is a circular arc, the mid-line and the outer path are line segments. This area corresponds to an angle sector θ_1 . Angles in this sector are negative.
- **Area 2:** the inner path and the mid-line are circular arcs, the outer path is a straight line. This area corresponds to an angle sector θ_2 .
- **Area 3:** the inner path, the mid-line and the outer path are circular arcs. This area is limited at an angle of 45° on the corner with the angle sector θ_3 .

For the rest of the trajectory, the calculation is performed similarly using the symmetry.

2.2.2.3.2 Evaluation of the distance in three different areas

Considering the origin (O_{c2}, X, Y), the equation of the circle corresponding to the inner toolpath (C_2) can be written (Eq. 2-18):

$$(C_2): x^2 + y^2 = R^2 \quad \text{Eq. 2-18}$$

Considering the same origin (O_{C2}, X, Y), the equation of the circle corresponding to the outer toolpath (C_1) and the equation of the circle corresponding to the mid-line (C_m) can be written (Eq. 2-19):

$$(C_1): (x - x_{o1})^2 + (y - y_{o1})^2 = R^2 \quad \text{Eq. 2-19}$$

$$(C_m): (x - x_{om})^2 + (y - y_{om})^2 = R^2$$

From Fig. 2-24, the coordinates of centre points O_{C1} and O_{Cm} belonging to (C_1) and respectively to (C_m) can be expressed (Eq. 2-20):

$$(O_{C1}): x_{o1} = y_{o1} = Pitch_{init} \quad \text{Eq. 2-20}$$

$$(O_{Cm}): x_{om} = y_{om} = \frac{Pitch_{init}}{2}$$

In addition, the vertical line ($A_1 B_1$) is established (Eq. 2-21):

$$(A_1 B_1): x = R + Pitch_{init} \quad \text{Eq. 2-21}$$

The normal to the circular arc (C_m) at each point M is defined by the straight line (D) passing through the point $O_{Cm} (x_{om}, y_{om})$ and its equation can be written according to θ (Eq. 2-22):

$$(D): y = \tan(\theta) \times \left(x - \frac{Pitch_{init}}{2} \right) + \frac{Pitch_{init}}{2} \quad \text{for } 0 \leq \theta \leq \frac{\pi}{4} \quad \text{Eq. 2-22}$$

Using equations (Eq. 2-18) to (Eq. 2-22), the distances $Pitch_{area}(\theta)$, for the three areas 1, 2 and 3 can be evaluated. Results are shown in Table 2-5. The detailed calculation can be found in Appendix.

Table 2-5. Distance in three areas.

	Angle (θ)	$Pitch_{area}(\theta)$
Area 1	$\theta \in \left[\text{atan}\left(\frac{-Pitch_{init}/2}{R - Pitch_{init}/2}\right); 0 \right]$	$R + Pitch_{init} - \sqrt{R^2 - [(R - Pitch_{init}/2)\tan\theta + Pitch_{init}/2]^2}$
Area 2	$\theta \in \left] 0; \text{atan}\left(\frac{Pitch_{init}/2}{R + Pitch_{init}/2}\right) \right]$	$\frac{R + Pitch_{init}/2}{\cos\theta} + \frac{\sqrt{2}}{2} Pitch_{init} \cos\left(\frac{\pi}{4} - \theta\right) - \frac{1}{2} \sqrt{4R^2 - 2Pitch_{init}^2 \sin^2\left(\frac{\pi}{4} - \theta\right)}$
Area 3	$\theta \in \left] \text{atan}\left(\frac{Pitch_{init}/2}{R + Pitch_{init}/2}\right); \frac{\pi}{4} \right]$	$\sqrt{2} Pitch_{init} \cdot \cos\left(\frac{\pi}{4} - \theta\right)$

These expressions can be simplified when the initial pitch is very small compared with the corner radius ($Pitch_{init} \ll R$). Corresponding results are presented in Table 2-6.

Table 2-6. Distance in three areas considering $Pitch_{init} \ll R$.

	Angle (θ)	$Pitch_{area}(\theta)$
Area 1	$\theta \cong 0$	$\cong Pitch_{init}$
Area 2	$\theta \in \left] 0; \text{atan}\left(\frac{Pitch_{init}/2}{R + Pitch_{init}/2}\right) \right]$	$\cong \frac{Pitch_{init}}{2} \left(1 + \sqrt{2} \cos\left(\frac{\pi}{4} - \theta\right) \right)$
Area 3	$\theta \in \left] \text{atan}\left(\frac{Pitch_{init}/2}{R + Pitch_{init}/2}\right); \frac{\pi}{4} \right]$	$= \sqrt{2} Pitch_{init} \cdot \cos\left(\frac{\pi}{4} - \theta\right)$

From Table 2-6, it can be established that when the initial pitch is very small compared with the corner radius ($Pitch_{init} \ll R$), the distance between two consecutive passes does not depend on the magnitude of the corner radius R . A computation of the distance along the middle line using the symmetry in relation to the middle of the corner is performed. A representation is given (Fig. 2-25a) for different values of the initial pitch and shows that these distances mainly depend on the initial pitch value. Introducing $Pitch_{area}(\theta)$ in (Eq. 2-17), it can be defined $Depth(\theta)$ in relation with angle θ (Eq. 2-23). Since the reference origin is on the upper surface, the $Depth(\theta)$ is defined negative.

$$Depth(\theta) = -He \frac{\sqrt{\pi} \cdot H(Vf) \cdot B(Vf)}{Pitch_{area}(\theta)} \quad \text{Eq. 2-23}$$

From (Eq. 2-23), for different values of $Pitch_{init}$, $Depth(\theta)$ was plotted on Fig. 2-25b using $H(Vf) = 0.154$ mm, $B(Vf) = 1.577$ mm et $Ke = 1.1$. These values are derived from the coefficients determined by the rapid calibration procedure (see section 2.1).

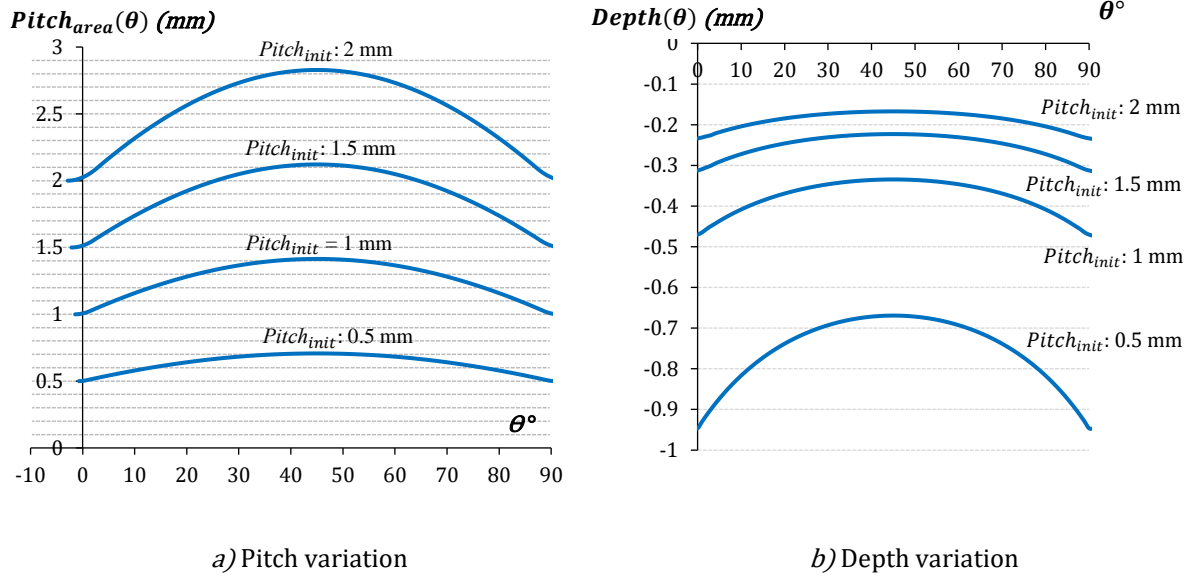


Fig. 2-25. Pitch and depth variations in constant radius strategy

Let's study the relative variation in depth. Let $Depth_{init}$ the depth obtained with a pitch equal to $Pitch_{init}$ (Eq. 2-24).

$$Depth_{init} = -He \frac{\sqrt{\pi} \cdot H(Vf) \cdot B(Vf)}{Pitch_{init}} \quad \text{Eq. 2-24}$$

The relative variation in depth is defined by:

$$\Delta Depth(\theta) = \frac{Depth(\theta) - Depth_{init}}{Depth_{init}} = \frac{Pitch_{init}}{Pitch_{area}(\theta)} - 1 \quad \text{Eq. 2-25}$$

By reporting in (Eq. 2-25), (Eq. 2-23) and (Eq. 2-24), we obtain, according to the values of $Pitch_{area}(\theta)$ of Table 2-6, equations of the relative depth variation. Corresponding results are presented in Table 2-7.

Table 2-7. Relative depth variation in the three areas.

	Angle (θ)	$\Delta Depth(\theta)$
Area 1	$\theta \cong 0$	$\cong 0$
Area 2	$\theta \in \left] 0; \text{atan}\left(\frac{Pitch_{init}/2}{R + Pitch_{init}/2}\right) \right]$	$\cong \frac{2}{1 + \sqrt{2}\cos\left(\frac{\pi}{4} - \theta\right)} - 1$
Area 3	$\theta \in \left] \text{atan}\left(\frac{Pitch_{init}/2}{R + Pitch_{init}/2}\right); \frac{\pi}{4} \right]$	$\frac{1}{\sqrt{2}\cos\left(\frac{\pi}{4} - \theta\right)} - 1$

These expressions show that the relative depth variation is independent of $Pitch_{init}$. A single and unique curve (Fig. 2-26) can thus be plotted to represent the relative depth variation in relation to angle θ .

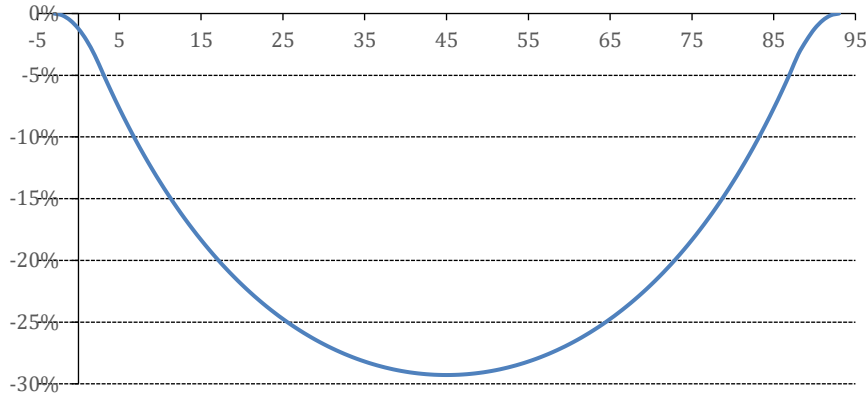


Fig. 2-26. Relative depth variation for a constant radius strategy

2.2.2.4 Conclusion on change of direction at constant radius

The geometric study of the distance between two consecutive passes with the constant radius R and the use of the simplified model for depth (Eq. 2-24) allow the following results to be established:

- (i) *The distance between two adjacent toolpaths does not depend on that radius (R), but depends on the initial pitch ($Pitch_{init}$).*
- (ii) *The relative depth variation is only dependant of angle θ (Table 2-7 and Fig. 2-26).*
- (iii) *The milled depth in a pocket corner can be predicted with a given constant radius by using the initial depth defined by (Eq. 2-24) and $Pitch_{area}(\theta)$.*

2.2.2.5 Adaptive speed control during change of direction at constant radius

Let Vf_{init} be the traverse speed to obtain a depth $Depth_{init}$ from a pitch $Pitch_{init}$ (Eq. 2-24). In the circular area, traverse speed is modified to have a constant depth. This leads to:

$$Depth(\theta) = Depth_{init} \tag{Eq. 2-26}$$

By reporting (Eq. 2-15), (Eq. 2-23) and (Eq. 2-24) in (Eq. 2-26), traverse speed modified $Vf(\theta)$ is defined by:

$$Vf(\theta) = Vf_{init} \left(\frac{Pitch_{area}(\theta)}{Pitch_{init}} \right)^{\left(\frac{1}{Hv+Bv} \right)} \quad \text{Eq. 2-27}$$

Consider now a pocket whose initial depth is $Depth_{init}$ and a tolerance $\pm T_{Depth}$ (Fig. 2-27-a). On milling of the pocket corner, the depth diminishes and its variation reaches the upper limit $Depth_{init} + T_{Depth}$ for an angular value θ_0 . The initial speed is then modified considering a corrected depth $Depth(\theta_0)$ calculated by equation (Eq. 2-28).

$$Depth(\theta_0) = Depth_{init} - T_{Depth} \quad \text{Eq. 2-28}$$

Using (Eq. 2-23), the modified traverse speed is:

$$Vf(\theta_0) = \left(\frac{(T_{Depth} - Depth_{init}) Pitch_{area}(\theta_0)}{Ke\sqrt{\pi}BoHo} \right)^{\left(\frac{1}{Hv+Bv} \right)} \quad \text{Eq. 2-29}$$

When the tolerance is lower (Fig. 2-27-b), the approach must be iterative and several changes in speed are required. The representation in Fig. 2-27 assumes instantaneous speed changes.

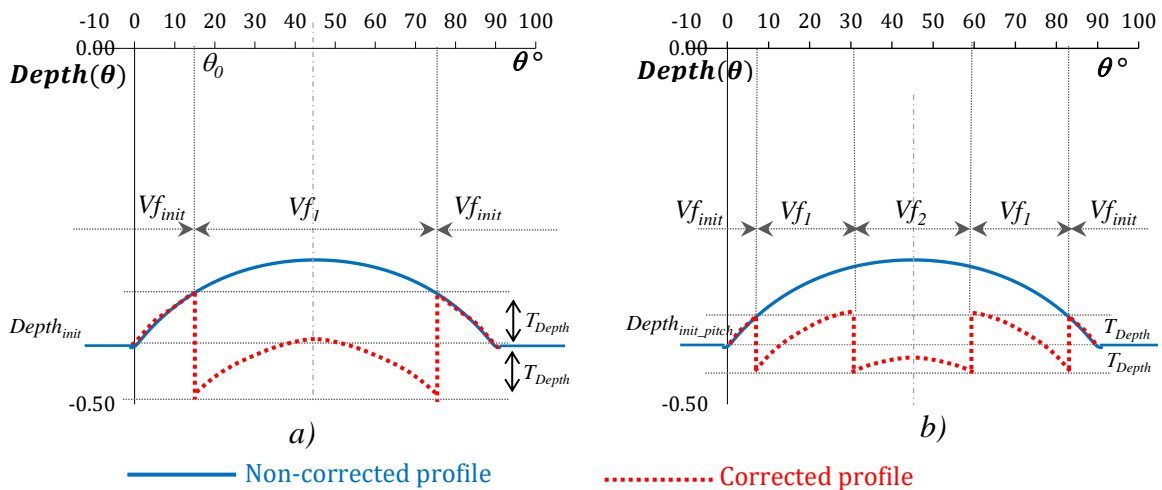


Fig. 2-27. Correction of the pocket corner depth

2.2.3 Experimental validation

2.2.3.1 Experimental validation of adaptive speed control

The machine configuration is defined by: a Flow MACH4-C machine (Fig. 2-28), a nominal pressure of 100 MPa and an abrasive with grain size 120 mesh and flow 0.34 kg/min. The cutting head is equipped with a nozzle diameter 0.3302 mm and a focusing tube of diameter 1.016 mm and 101.6 mm in length.

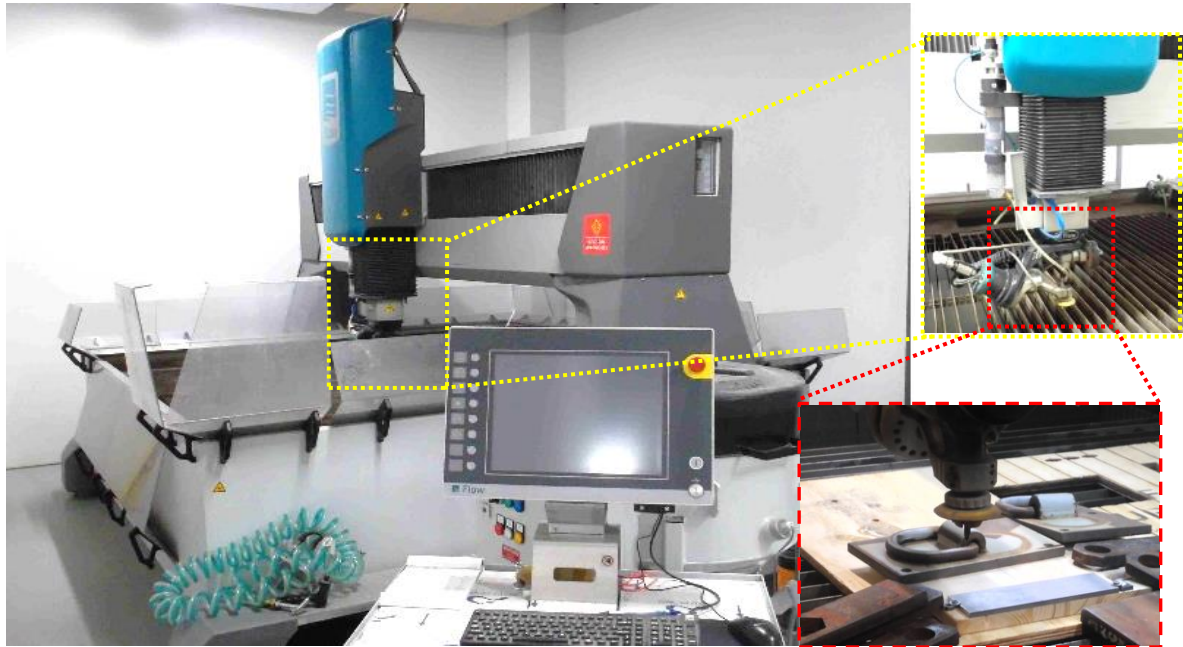


Fig. 2-28. FLOW MACH4C machine

The material is Ti6Al4V titanium alloy as previously described. The rapid calibration procedure described in article [116] was applied. Coefficients $H_o = 69.255$, $H_v = -0.935$, $B_o = 1.662$, $B_v = -0.008$ and $H_e = 1.1$ were determined. Based on a pitch equal to $0.6B(Vf)$ as recommended in [116], the traverse speed is 688.3 mm/min to obtain a pocket depth of 0.5 mm (Eq. 2-17).

Five different milling operations were conducted (Fig. 2-29):

- Milling with concentric radii (R varying from 0.05 to 20 mm) to check obtaining a flat bottom when the distance between successive trajectories remained constant.
- Milling with constant radius $R = 20$ mm to show the speed bump.
- Three milling operations with speed correction for radii $R = 25$ mm, $R = 20$ mm and $R = 15$ mm to validate the method. For these three cases, a tolerance of ± 0.05 mm was considered and four adaptations of the speed were needed to respect that (Fig. 2-29).

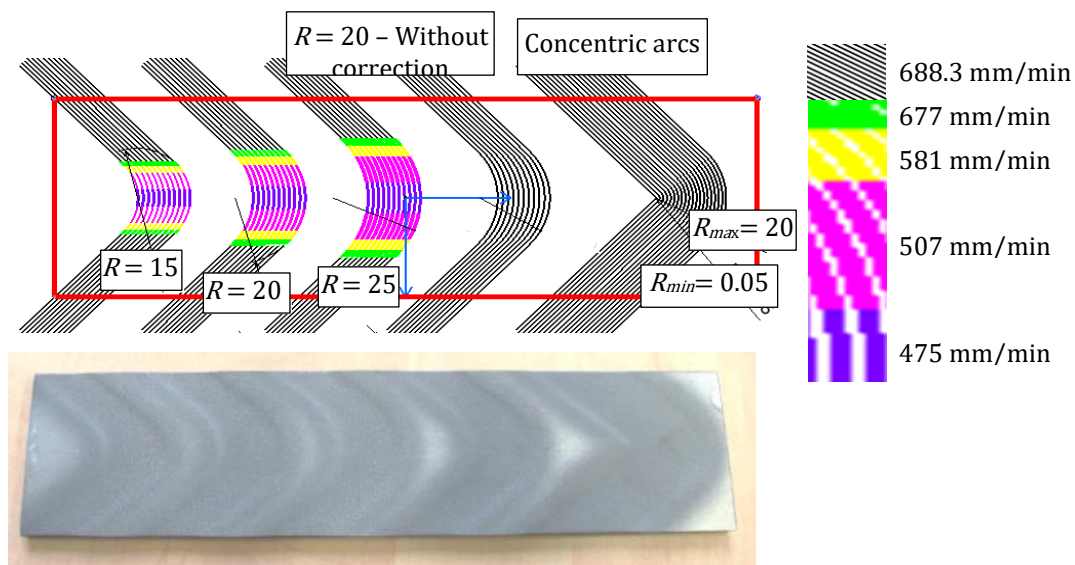


Fig. 2-29. Ti6Al4V milled

Measurements of the profiles milled were conducted using an Alicona IF profilometer (Fig. 2-30). This autofocus instrument allows a square zone with 25 mm sides to be mapped taking the coordinates of pixels some micrometres square to within an accuracy of a few micrometres. Precise mappings of the zones measured can be constructed (Fig. 2-31) by making several acquisitions. To measure a profile, two straight lines are plotted on the surface measured (Fig. 2-30) and the intersection of their projection over the measured surface is then constructed. This intersection constitutes the profile measured and its plot can be generated considering the Y and Z coordinates.

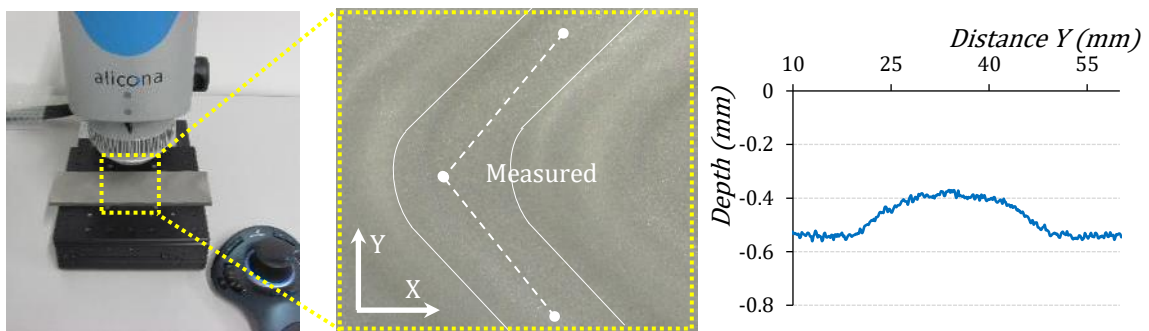
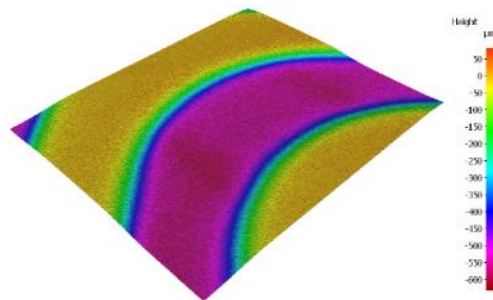
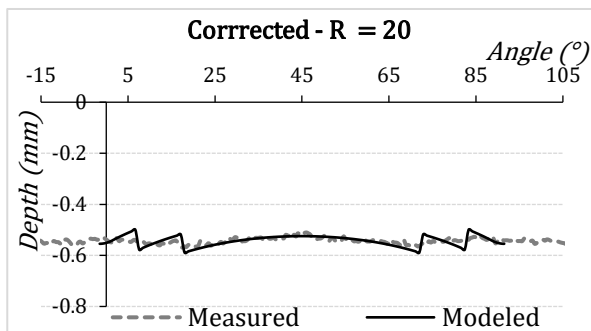
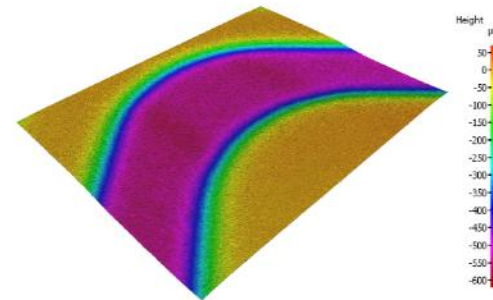
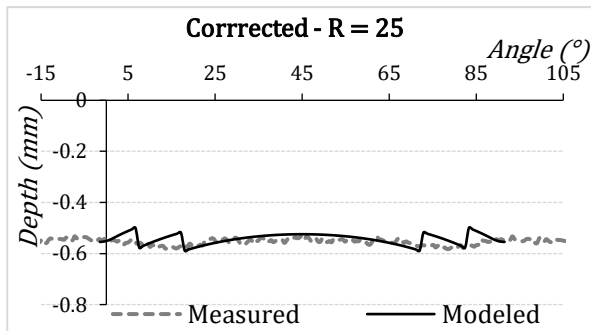
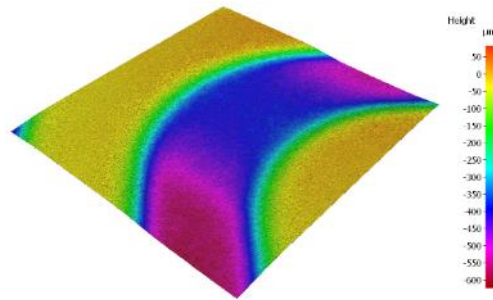
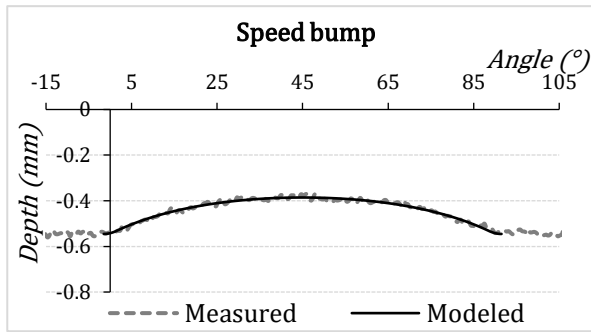
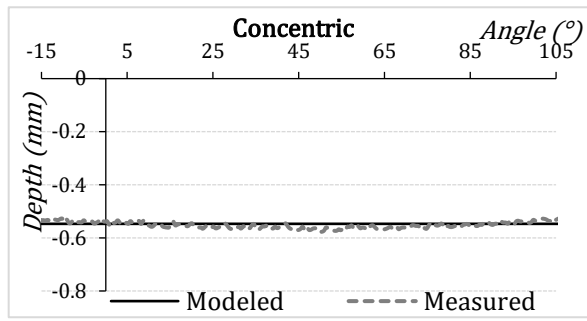


Fig. 2-30. Measuring a profile

2.2.3.2 Results and discussion

The results are shown in Fig. 2-31. A recalibration was made in the Y direction (Fig. 2-30) to compare the profiles measured whose abscissa is in (mm) and the theoretical profiles whose abscissa is in ($^{\circ}$).



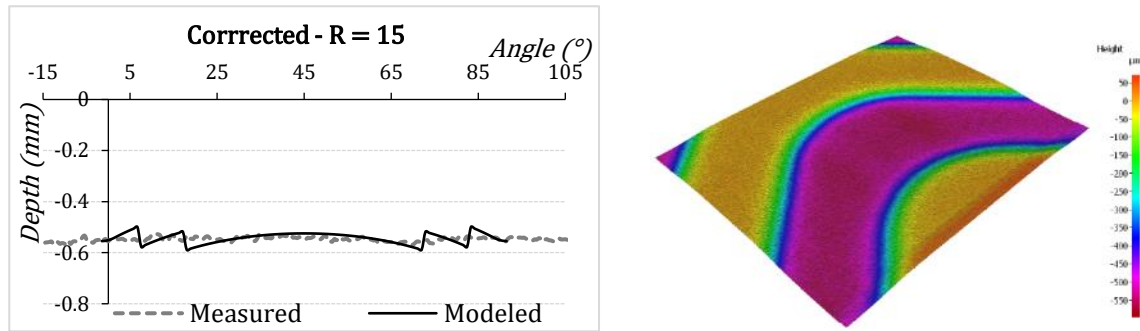


Fig. 2-31. Modeled and measured profiles

The maximum obtained depth was 0.57 mm (Fig. 2-31). This is slightly greater than the target depth of 0.5 mm and is the result of a pressure of 110 MPa during the tests instead of the programmed pressure of 100 MPa. The variation comes from the machine that is a cutting machine not provided with a pressure control loop for which the manufacturer chose to increase that parameter to ensure cutting. The modelled profiles were therefore adjusted considering an erosion coefficient He of 1.22 instead of 1.1 (Eq. 2-17). The profiles measured were extremely close to the modelled profiles. This shows, firstly, that the prediction of the initial speed bump defect is accurate and, secondly that the correction method proposed is effective. The results confirm that the radius R does not influence the defect and that the latter is only related to the pitch. The profiles show that the changes in speed are barely perceptible on the milled surface. The $SOD = 100$ mm forms a spot of approximately 7 mm in diameter. Therefore each point of the surface is milled at least 0.61 s, regardless of the changes in traverse speed. Smoothing effect is thus produced on the surface.

2.2.4 Conclusion

The study presented highlights the issue of changes of direction during abrasive water jet milling of pocket corners. It shows that right-angled changes of direction are not suited to the process as they require a passage through a zero rate that generates an excess depth. It is also shown that concentric arcs alone are not possible since the outer radius is then determined by the scanning pitch and the number of previous passes. This radius cannot then respect a given specification. The paper emphasises the need to mill pocket corners using a constant radius. In this case, a speed bump type defect will appear on the pocket corner bottom. This defect is related to a variable distance between two

consecutive toolpaths. This variation in distance leads to a variation in the distribution of the jet's energy that itself leads to a variation in the milled depth. The geometric study of the distance between two passes shows that this variation in distance is not related to the circular arc radius and depends only on the scanning pitch considered. The study defines a rational curve to model the variation in depth whatever the pocket corner radius and pitch considered. An adaptive method for speed correction combined with a tolerance on the depth is also adopted. Finally, experimental validation is presented to show the relevance of the geometric approach allowing the initial defect to be predicted. The performance of adaptive control is also validated by tests. The results show that the entire study is coherent and a forthcoming paper will develop a comprehensive milling strategy to mill rectangular pockets consistent with a tolerance on the milled depth.

MACHINING WITH THE JET

INCLINATION ANGLE

3.1 A modeling of elementary passes taking into account the inclination angle

*(This section is presented as the format of an article and it has been published in AIP Conference Proceedings - DOI: 10.1063/1.5034945)
PROCEEDINGS OF THE 21ST INTERNATIONAL ESAFORM CONFERENCE ON MATERIAL FORMING: ESAFORM 2018, Apr 2018, Palermo, Italy.*

Abstract: The use of titanium alloys in the aeronautical and high technology domains is widespread. The high strength and the low mass are two outstanding characteristics of titanium alloys which permit to produce parts for these domains. As other hard materials, it is challenging to generate 3D surfaces (e.g. pockets) when using conventional cutting methods. The development of Abrasive Water Jet Machining (AWJM) technology shows the capability to cut any kind of materials and it seems to be a good solution for such titanium materials with low specific force, low deformation of parts and low thermal shocks. Applying this technology for generating 3D surfaces requires to adopt a modelling approach. However, a general methodology results in complex models due to a lot of parameters of the machining process and based on numerous experiments. This study introduces an extended geometry model of an elementary pass when changing the inclination angle during machining Ti6Al4V titanium alloy with a given machine configuration. Several experiments are conducted to observe the influence of major kinematic operating parameters, i.e. jet inclination angle (α) (defined into the plane perpendicular to the feed direction) and traverse speed (V_f). The material exposure time and the erosion capability of abrasives particles are affected directly by a variation of the traverse speed (V_f) and inclination angle (α). These variations lead to different erosion rates along the kerf profile characterized by the depth and width of cut. A comparison

demonstrated an efficiency of the proposed model for depth and width of elementary passes. Based on knowledge of the influence of both inclination angle and traverse speed on the elementary pass shape, the proposed model allows to develop the simulation of AWJM process and paves a way for milling flat bottom pockets and 3D complex shapes.

Keywords: Abrasive water jet machining (AWJM), Titanium Alloy, Alloy cutting depth model.

3.1.1 Introduction

Titanium alloys (especially a grade of Ti6Al4V) are very attractive owing to a combination of desirable mechanical properties such as lightweight, excellent fatigue performance and a high resistance to the aggressive environment. So there are various industrial domains using this material, especially aeronautics. However, other properties of this material, high strength, low thermal conductivity and chemical reactivity with cutting tool materials, make it really difficult for machining process using conventional approaches. Aeronautical structural parts are large in size with thin walls. Therefore, machining this kind of material usually suffers problems like dramatical reduction of the tool life and deformation of parts due to high cutting forces. Several methods have been developed to avoid these difficulties and to meet the quality standards of these parts. Abrasive water jet, electroerosion and laser applications produce good results.

Among non-conventional machining methods, AWJM is a promising technique used to mill these titanium alloys by its outstanding characteristics. A simple combination of water and abrasive particles generates a low level of cutting forces and permits a limitation of the part deformation during machining [116]. This method has demonstrated several advantages in comparison with the conventional machining techniques [118]. An elementary pass will be symmetrical for a jet angle (α) of 90° , i.e. perpendicular to a flat surface (Fig. 3-1a). Its shape can be described using Gaussian curve [44], [51], [116] and is characterized by a depth H , a width factor B and taper angle β (slope of the kerf). Repetition of several elementary passes (Fig. 3-1b) generates a pocket using an offset distance called *Pitch* [45], [116]. Process parameters affect the elementary passes profile. Hence, the profile geometry and the quality of the pocket bottom can then be directly linked to process parameters. The profile of an elementary pass was characterized using the maximal depth and the width at mid-height [44]. Bui et al. [116] proposed a model of the elementary pass profile using a rapid calibration method. In their approach, a given machine configuration is defined by a given machine, a fixed water jet pressure level and defined abrasive particles. They cannot be changed during the process. For a given machine configuration, an optimal abrasive rate can be obtained. Parameters that can be controlled using the NC program are the standoff distance *SOD*, the traverse speed (V_f) and the *pitch* offset.

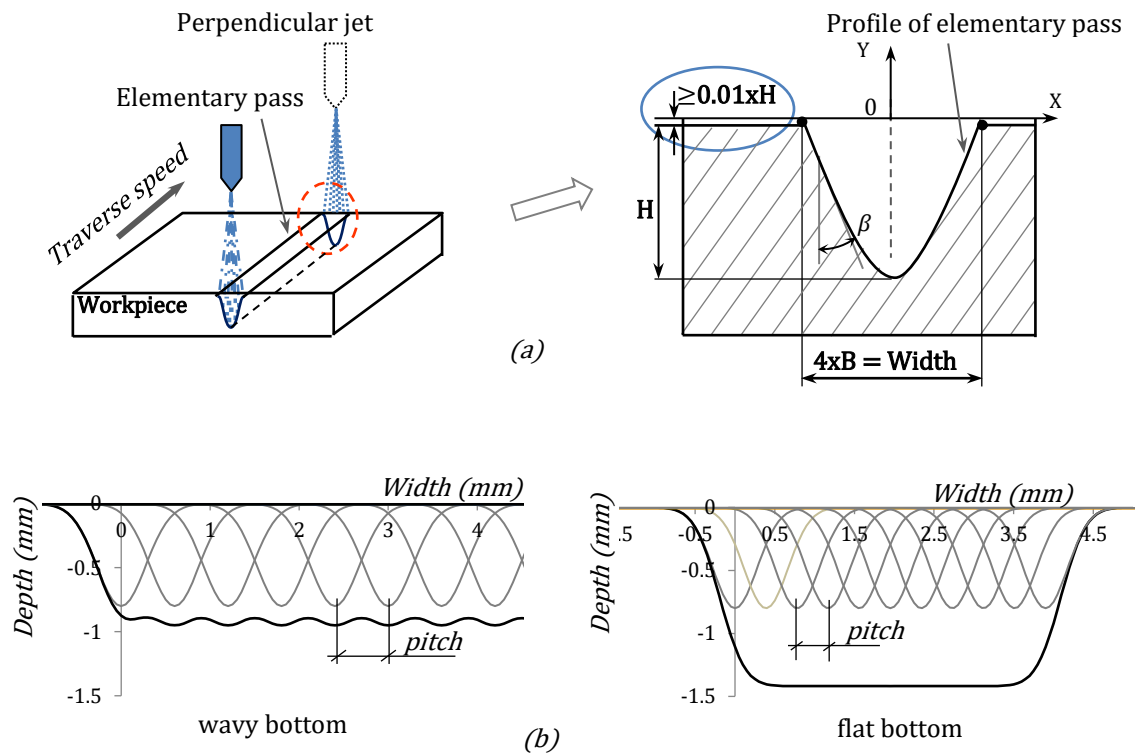


Fig. 3-1. Profile of elementary pass and pocket

To machine an open rectangular pocket with a flat bottom, standoff distance SOD must be a constant and that the width factor must be combined with the $Pitch$ offset [116]. Besides, when machining a complex shape by multi-axis machining, the jet is piloted according to the local geometry of the final complex shape and the control of the jet orientation is then fundamental [46]. Characteristics of kerf profile, depth H , slope β of the side walls, and width ($4xB$) measured in the plane perpendicular to the traverse speed direction, depend not only on SOD and Vf but are also influenced by the jet angle [46], [47]. Hence it is important to develop a model for the kerf profile prediction of elementary passes taking into account the influence of the jet inclination angle (α), the standoff distance SOD and the traverse speed (Vf).

In this paper, this model is defined and is calibrated according to a given machine configuration previously defined and a jet inclination angle (α) of 90° . Experimental results proved efficiency when applying the model to characterize elementary passes for different jet inclination angles.

3.1.2 Model of elementary pass taking into account the firing angle

Bui et al. [116] established a model (Eq. 3-1) based on Gaussian distribution and a rapid calibration method. In this equation, the traverse speed is the only parameter.

$$y(x) = H(Vf) \times e^{-\left(\frac{x^2}{B(Vf)^2}\right)} \quad \text{Eq. 3-1}$$

Srinivasu et al. [46] have shown that when the jet impingement angle decreases from α_1 (90°) to α_2 ($< 90^\circ$), the footprint width increases (Fig. 3-2). The geometry of the top width of the elementary pass will be transformed from a circle to an ellipse. Moreover, the depth of cut decreases and the profile becomes asymmetric (Fig. 3-2).

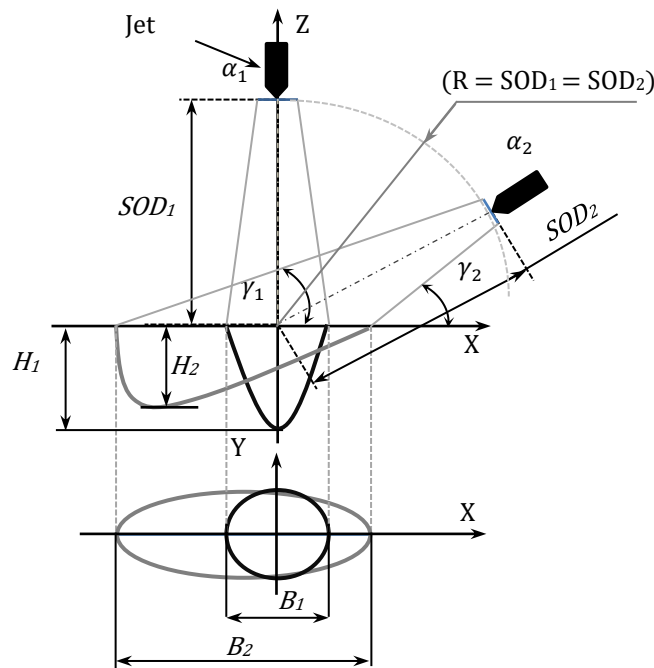


Fig. 3-2. Influence of jet inclination angles on elementary pass profiles

The proposed model (Eq. 3-2) takes into account the influence of the inclination angle (α) and Fig. 3-13 shows the corresponding profile.

$$y(x) = H(Vf) \cdot e^{-\left(\frac{x^2}{B(Vf)^2}\right)} + \tan\left(\frac{\pi}{2} - \alpha\right) \times x \quad \text{Eq. 3-2}$$

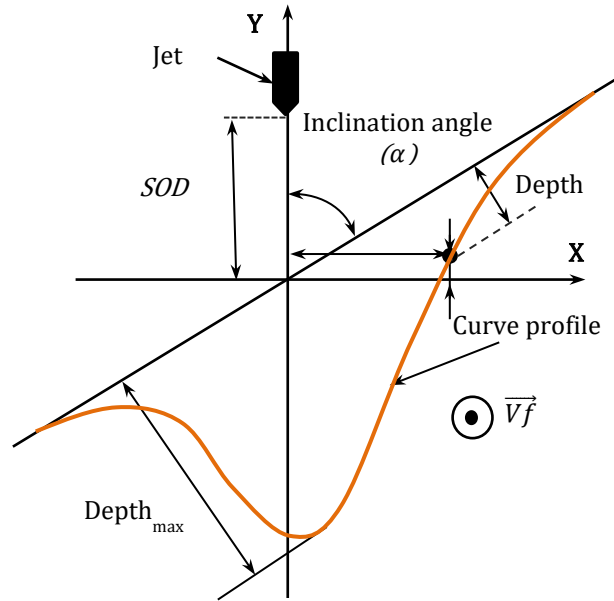


Fig. 3-3. Profile corresponding to the jet inclination angle at α

For a considered traverse speed (Vf), the maximum depth $H(Vf)$ and the width factor $B(Vf)$ of the corresponding elementary pass are computed by Eq. 3-3 and Eq. 3-4:

$$H(Vf) = H_0 \times Vf^{Hv} \quad \text{Eq. 3-3}$$

$$B(Vf) = B_0 \times Vf^{Bv} \quad \text{Eq. 3-4}$$

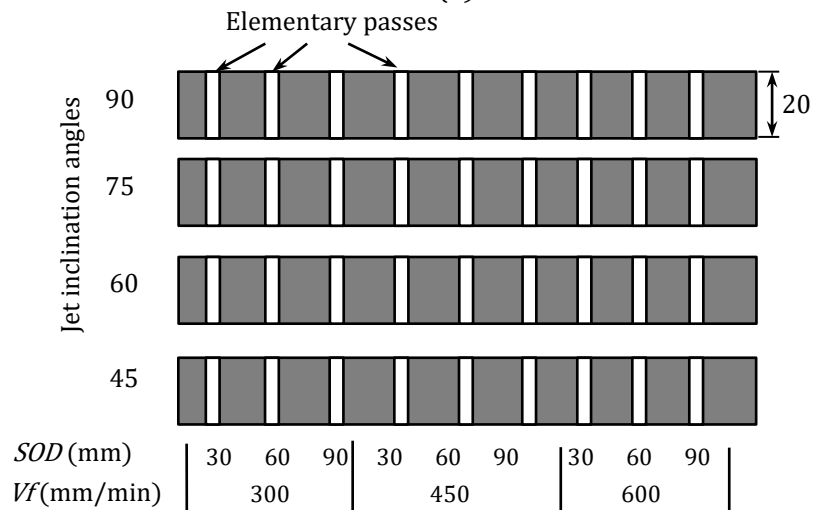
In these equations, H_0 and B_0 are coefficients while Hv and Bv are exponents. They are calculated by the least square method according to experiments using different traverse speeds [116].

3.1.3 The experimental set-up

Experimental trials are implemented in a FLOW MACH4C machine equipped with a PASER4 cutting head with a nozzle diameter of 0.33 mm, a focusing tube diameter of 1.016 mm and 101.6 mm length (Fig. 3-4a). An Hyplex-Prime pump generates a maximum pressure of 400 MPa. Two software packages, Flowpath and Flowcut, permit to manage the NC controller. The abrasive type is Opta Minerals 120# and an abrasive flow rate is set by a pierced washer whose diameter conditions the flow.



(a)



(b)

Fig. 3-4. Experimental setup specimens

Titanium alloy material with a grade of Ti6AL4V is employed throughout the experimental assays. This grade has a high tensile strength (860 MPa), a high yield strength (800 MPa) and an elongation of more than 10%. Titanium alloys specimens with a sectional dimension of 20 mm x 6 mm and variable length according to a magnitude of the inclination angle are shown in Fig. 3-4b. The experimental plan considers the following points:

- Three configurations are defined using three *SOD* levels 30, 60 and 90 mm. For each configuration, three values of traverse speed (*Vf*), 300, 450 and 600 mm/min, are used. This selection is intended to determine the influence of the *SOD* on the new model (Eq. 3-2) and its characteristics. The *Ho*, *Hv*, *Bo* and *Bv* coefficients are

calculated for each configuration using the least squares method. At the jet inclination angle of 90° , these coefficients are considered as *global factors* that can be applied to the new model at different inclination angles of the jet.

- In order to study the influence of the jet inclination angle (α), experiments are carried out by varying (α) in the range of $45^\circ - 90^\circ$ by steps of 15° . Workpieces are inclined at an angle corresponding to the inclination angle (α) and the cutting head is perpendicular to the machine table (Fig. 3-4a). For each value of the inclination angle (α), the three levels of traverse speed (300, 450, and 600 mm/min) are used. To ensure that all cutting trials are performed under the same conditions, Workpieces are organized and assembled (Fig. 3-4b). The constant operating parameters are shown in Table 3-1.

Table 3-1. Constant operating parameters.

Pressure (MPa)	100	Diameter of focusing nozzle (mm)	1.016
Washer diameter (mm)	6	Abrasive size (mesh)	120
Orifice diameter (mm)	0.3302		

An ALICONA IF optical profilometer (Fig. 3-5) is used to measure and extract profiles. This equipment enables to measure 1000 curves, distributed regularly over 2 mm, using an intersection between the measured surface and 1000 planes perpendicular to the direction of traverse speed.

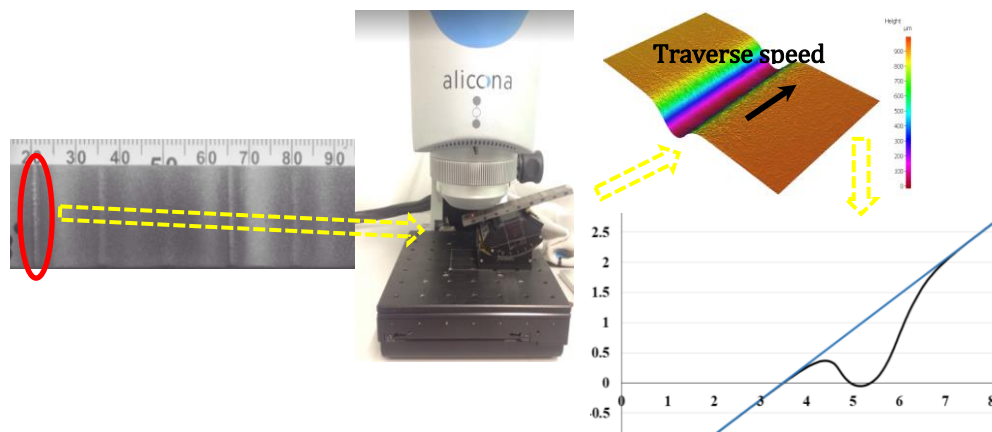


Fig. 3-5. Measurement and extraction of elementary pass profile

3.1.4 Results and discussion

3.1.4.1 Experimentation

Profiles of elementary passes (Fig. 3-6) are analyzed and the influence of kinematic parameters (α and V_f) on kerf profiles are characterized. Curves show a good efficiency of the model (Eq. 3-2). The depth is defined in Fig. 3-13 and the width is defined as the distance between the two points whose depth reaches 0.01 mm of the maximum depth (Fig. 3-1a). Fig. 3-6c shows the influence of the firing angle for $SOD = 60$ mm, $V_f = 300$ mm/min. When the jet inclination angle is different than 90° the kerf profile becomes asymmetric.

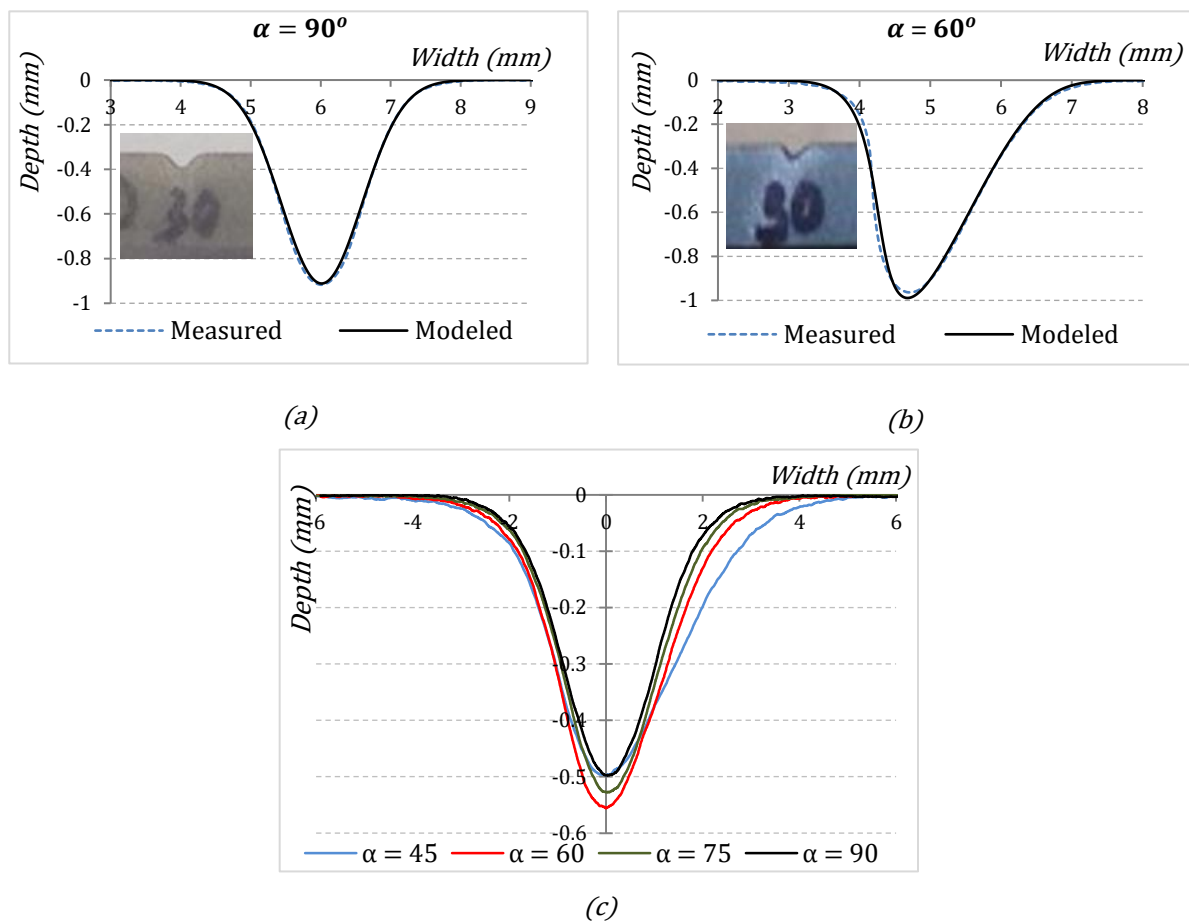


Fig. 3-6. Modelled and measured profiles

For each elementary pass (36 single kerfs), a set of values of the depth H , the width factor B and the inclination angle (α) are calculated with the least square method. The actual values of the inclination angle are calculated and in all cases, a maximum deviation of 0.25° is observed. Fig. 3-7 shows that when the inclination angle (α) decreases, the

width increases. This is due to [46] (i) the variation of different axial distances between the nozzle and the workpiece and (ii) the variation on 'effective' impact angle of abrasive particles at target regions (Fig. 3-2). However, as investigated from Fig. 3-8, when changing the inclination angle, the depth of cut varies in small interval. Maximum width is observed at $\alpha = 45^\circ$ (Fig. 3-7) and maximum depth is obtained at $\alpha = 60^\circ$ (Fig. 3-8). A slightly different observation of cut depths from previously reports at normal angle can be explained, on the one hand by the effective impact angle of abrasive particles, different than 90° , when the jet axis is perpendicular to the surface and on the other hand with hardness of workpiece materials [111]. Fig. 3-7 and Fig. 3-8 show the influence of the jet inclination angle on the depth and top width of elementary passes for three standoff levels and three traverse speed levels. With an increase in the *SOD*, the maximum value of cut depths will rapidly decrease but the top width of cut raises gradually because of the divergence of the jet plume [47]. Similarly, at high traverse speed, the cut depth decreases due to the smaller exposure time of the target. Conversely, the traverse speed has a small influence on the top width and it confirms that the *SOD* is the main factor that affects the top width. This last point confirms previous works [44].

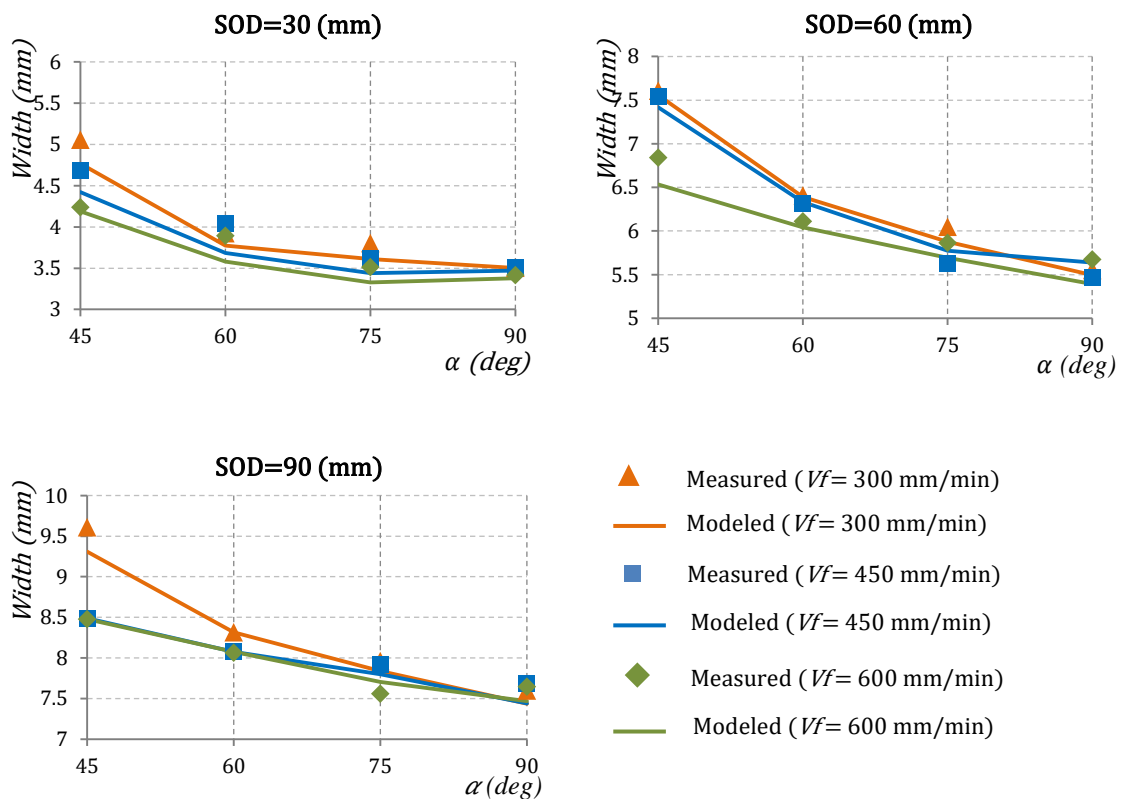


Fig. 3-7. Width of cut for different inclination angles

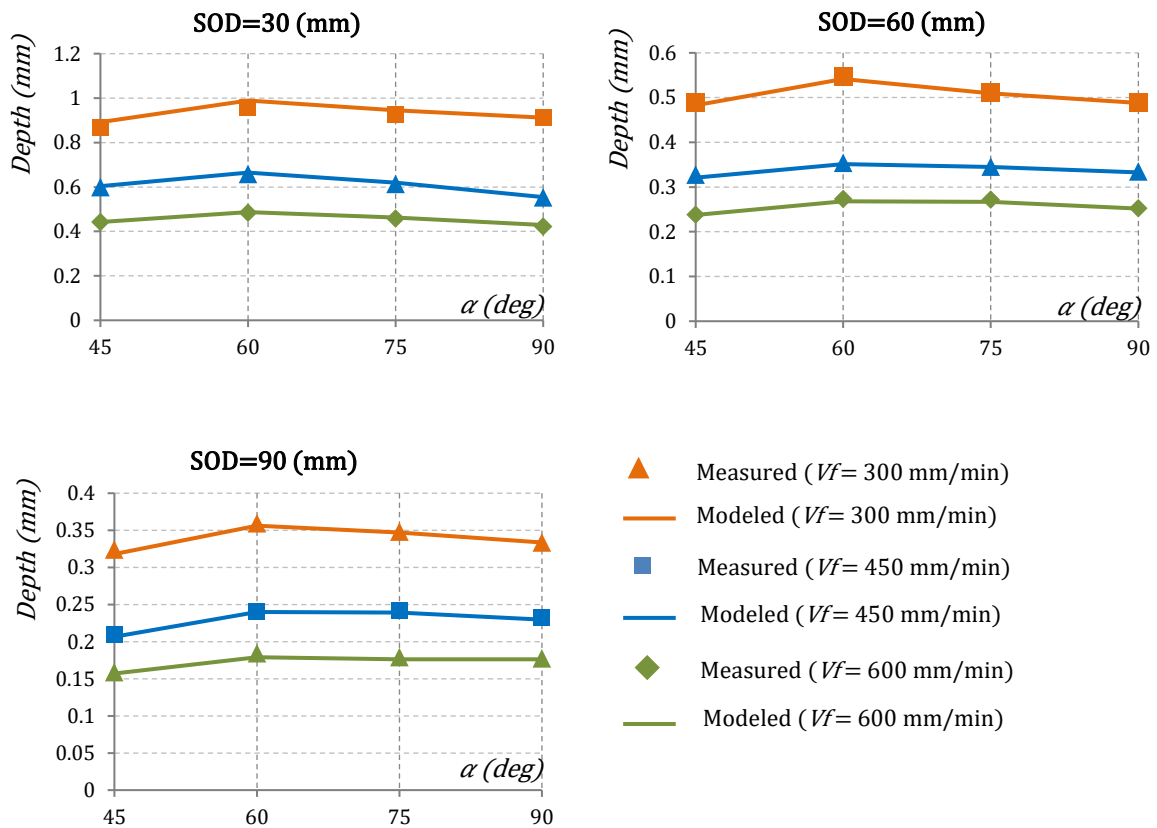


Fig. 3-8. Depth of cut for different inclination angles

3.1.4.2 Rapid calibration method

A rapid calibration method is applied to the jet inclination angle $\alpha = 90^\circ$ [116]. This rapid calibration method consists in a series of elementary passes performed with three values of standoff distance ($SOD=30, 60, 90$ mm). For each value of the SOD, three elementary passes are made using three levels of traverse speeds (Vf) (300, 450, 600 mm/min) and the corresponding H_o , H_v , B_o , and B_v (Eq. 3-3 and Eq. 3-4) are computed. Then models of $H(Vf)$ and $B(Vf)$ are established and called global models. These models are used to predict elementary pass profiles for different inclination angles, $\alpha = 75^\circ, 60^\circ, 45^\circ$ using Eq. 3-2. A series of elementary passes is performed to verify the influence of the inclination angle (α). Results are presented for measured and calculated configurations as shown in Fig. 3-9 and Fig. 3-10.

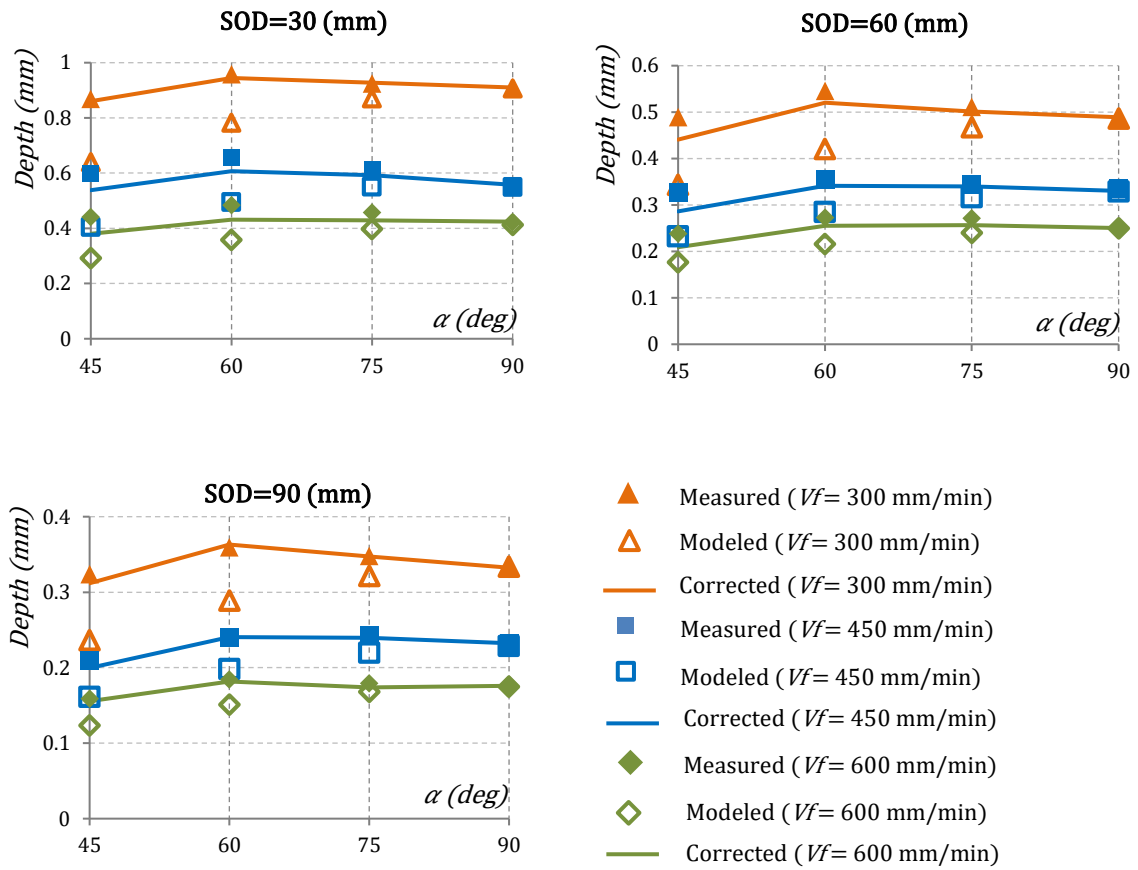
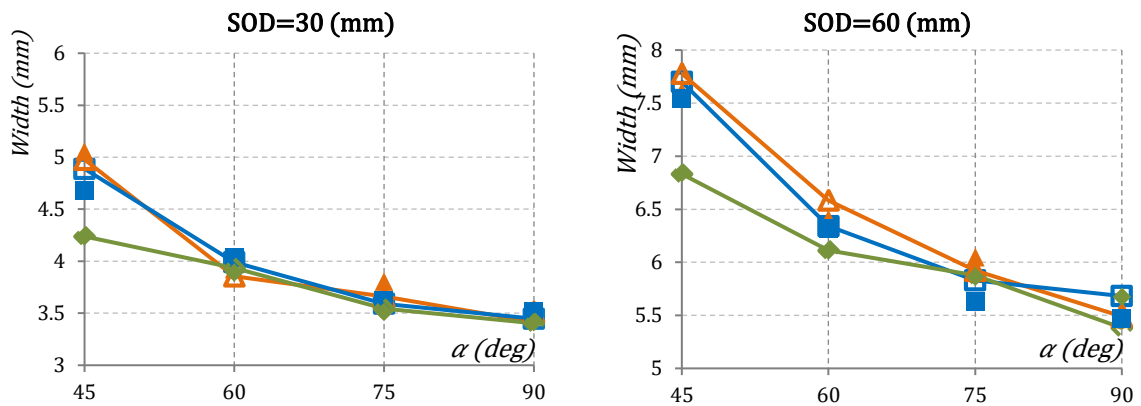


Fig. 3-9. Measured, calculated and corrected depth



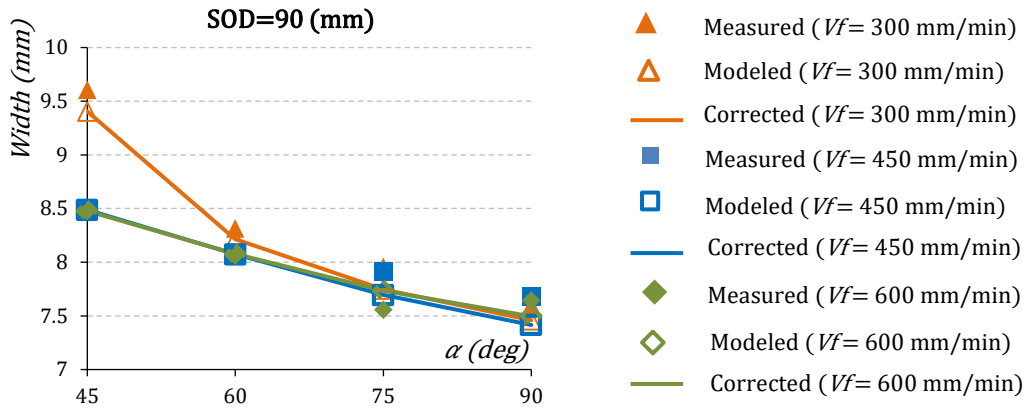


Fig. 3-10. Measured, calculated and corrected width

3.1.4.3 Taking into account the erosion phenomenon

Fig. 3-9 and Fig. 3-10 are showing big differences between measured and calculated depths, especially for the smallest angles. Depending on the magnitude of α , the removal of the material is caused by impact phenomenon or erosion phenomenon. Both exist simultaneously during machining. At the normal angle of the jet, the main mechanism of material removal is impact and it will be gradually replaced by erosion mechanism when the inclination angle decreases. To take into account the change of removal material mechanisms, an erosion factor (Ke) depending on the jet inclination angle is introduced (Eq. 3-5).

$$y(x) = Ke(\alpha) \times H(Vf) \times e^{-\left(\frac{x^2}{B(Vf)^2}\right)} + \tan\left(\frac{\pi}{2} - \alpha\right) \times x \quad \text{Eq. 3-5}$$

The $Ke(\alpha)$ coefficient (Table 3-2) is identified as an average value calculated for all trials performed with the same jet inclination angle. For a given inclination angle, the corresponding values of the $Ke(\alpha)$ coefficient (Table 3-2) obtained with different SOD are close and the average values are also close.

Table 3-2. $Ke(\alpha)$ coefficient.

	$SOD=30$ (mm)	$SOD=60$ (mm)	$SOD=90$ (mm)	Average value
90	1.0	1.0	1.0	1.0

75	1.073	1.070	1.068	1.07
60	1.212	1.204	1.224	1.213
45	1.325	1.232	1.272	1.276

Values of the corrected depth and the corrected width are shown in Fig. 3-9 and Fig. 3-10. Differences between measured and corrected values are quite small, 5%. As can be seen from Fig. 3-11, the model is able to predict shape characteristics of kerf profiles with fine precision. It should be noticed that the correction made on the width of cut is tiny and that modelled and corrected values are close.

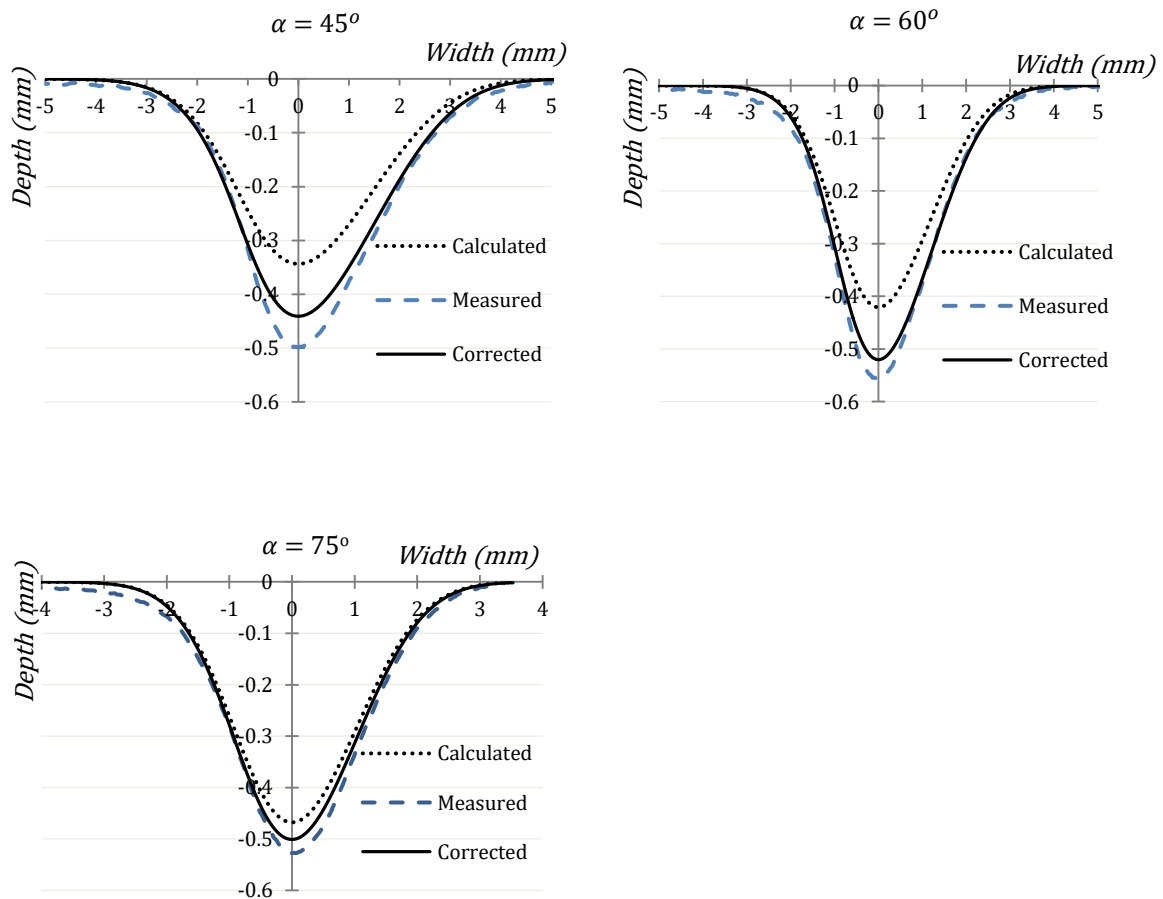


Fig. 3-11. Comparison of elementary pass profiles for $SOD = 60$ mm, $V_f = 300$ mm/min

The K_e coefficient only depends on the inclination angle and it can be determined experimentally and modeled using a linear function (Eq. 3-6):

$$Ke(\alpha) = 1.5771 - 0.0065 \times (\alpha)$$

Eq. 3-6

The correlation coefficient is $R^2 = 0.976$. It shows a good relationship between the inclination angle and erosion coefficient.

3.1.5 Conclusions

This work presents a geometrical model of elementary passes taking into account the jet inclination angle in AWJM. This model characterizes the profile of elementary passes by the depth and the width. For a given configuration, the profile of elementary passes will be changed when the inclination angle varies.

Using the rapid calibration method and considering an erosion rate $Ke(\alpha)$, the model permits to describe profiles of elementary passes and is validated experimentally with good accuracy.

This model will be useful to predict geometrical characteristics for milling flat bottom pockets and 3D complex shapes. A further work will be proposed in order to establish a relationship between inclination angles, the pitch offset, the material removal mechanism and the shape and surface quality of elementary passes.

3.2 Machining pocket with management of the tool inclination angle

(This section is presented as the format of an article and it will be submitted to a journal in the near future)

Abstract: Titanium alloy is broadly used for highly engineered parts, i.e. applications in aerospace due to its high tensile strength relative to its density, high corrosion resistance, fatigue resistance, high crack resistance, and ability to withstand moderately high temperatures without creeping. However, machining this kind of material using conventional methods is a truly laborious operation, especially in generating large and thin parts with complex shape like pockets. In this context, machining of such titanium alloys by abrasive water jet (AWJ) is a new machining area and at infancy state. This promising method could replace conventional methods considering its capability to cut any kind of material with low specific cutting force and without heat-affected zone. The main obstacle needs to be addressed for the benefit of AWJ is to control uncertainty on depth, surface waviness, and surface roughness according to the geometrical product specification.

This current work proposes a geometrical model of the pockets milled profile taking into account the influence of the jet inclination angles. Several experiments were implemented to observe the influence of the jet inclination angle, one of the kinematic process parameters, on the profile of the open pocket milled and its dimensional characteristics. The experimental results demonstrate the efficiency of the proposed model to predict of the geometrical characteristics of milled pockets.

Insight the influence of this key kinematic process parameter on the generation of pockets and their dimensional characteristics, this work paves a good fundamental for developing strategies for controlled 3D AWJ machining of complex shapes.

Keywords: Abrasive water jet machining (AWJM), Titanium Alloy, cutting depth model, multiaxis machining.

3.2.1 Introduction

Titanium alloys have many outstanding mechanical properties such as excellent combination of high specific strength (strength-to-weight ratio), fracture resistant characteristics, and their exceptional resistance to corrosion [119]. They are widely used for highly engineered parts with multi-application including marine, military, industrial, medical, and architectural. There is a high proportion of titanium alloy (about 14%) in total material mass used in most recent aircraft. Amongst different kinds of titanium alloys, Ti6Al4V represents an alloy containing aluminium (Al) of 6wt% and Vanadium (V) of 4wt%. This combination leads Ti6Al4V is designed for a good balance of characteristics which including strength, ductility, fracture toughness, high-temperature strength, creep characteristics, weldability, workability, and thermal processability (higher strength is easily obtained by heat treatment). Hence, this alloy is employed especially for airframes and engine parts. For instance, in airframes, it is used for general structural material (cockpit window frame, wing box), and fastener (bolts, seat rails). In engines, it is used for fan blades, fan case, and positions where temperature is relatively low. The relevant standard of this alloy for utility is the yield strength of annealed material is 800 MPa or higher, tensile strength is 860 MPa or higher, and elongation is 10% or higher at room temperature.

Machining this kind of materials using conventional turning and milling methods is actually a challenge due to its high strength and galling tendency. The first study attempts on the machining of titanium alloys was found from the 1950s, researchers has been focused on the improvement of efficient fabrication solutions for surface integrity and longer tool life [119]. On these machining operations, strong cutting forces combined with high strength generates a great cutting stress that localized at tool-workpiece contact that induced deformations in machined part or leads to a high temperature increasing. Due to the adverse thermal properties of titanium alloys, the machining-created thermal energy cannot be effectively dissipated and causes heat-affected zones. Consequently, the cutting tool is rapidly worn and on the other hands, the finished workpiece's geometry will show deviations outside specifications.

In this context, abrasive water jet (AWJ) machining is considered as a promising non-conventional technology enabling processing any material regardless to its

properties. An AWJ machining systems employ a high-pressure water jet forced through a small orifice (0.1-0.3 mm). This orifice allows to entrain and accelerate abrasive particles to a significant high velocity. When the high-velocity jet plume impacts a workpiece, the material is removed by the erosive mechanism. Owing to the erosion by fine abrasive particles, mechanical loads impacting on the target is negligible [120]. Hence, this process does not generate heat-affected zones [83]. From these outstanding advantages, it has been demonstrated that AWJ machining is a promising and versatile process, which can express its entire potential in different application domains. AWJ technology has been fully developed for through cutting. However, when the jet plume is used as a milling tool to govern machined workpiece geometry, outcomes from the literature is at a green stage with many challenges, especially to control accuracy of the depth milled surface and the development of freeform surface. Many studies have shown that there is a wide kind of process parameters in the AWJ process [4], [44], [57]. Thus it is difficult to control the amount of the removal material mass. Moreover, the process in itself also involves potentially with unpredicted variation of its characteristics, for example, an unstable value of water pressure due to the frequency of pressure pump or abrasive mass flow over the machining time. A small variation in the characteristic of the jet plume causes a fluctuation of eroded material mass along the trajectory of the jet plume. This raises a significant issue for controlled-depth milling in AWJ machining. For those reasons, controlling the jet footprint geometry plays the most important role in generating desirable surface geometries. Thus, a predictive geometrical surface profile model is very importance to fulfil these challenges and take more advantages from abrasive water jet technology.

Gaussian distributions have been considered as the energy distribution in the AWJ and could be identified experimentally [44], [80]. Besides, it was found that at high abrasive flow rates and high water pressures, the abrasive flow concentrates at the core region and is diverged towards walls of the focusing tube where lower energy of the jet [48]. At any cross-section of the jet plume (perpendicular to the jet axis), the velocity profile of water follows nearly Gaussian distribution [51]. Moving of the jet plume over a workpiece surface generates an elementary pass with bell shape as a result of Gaussian distribution.

It is also possible to consider an elementary pass profile [111], [114]–[116] to model it and calculate the shape of a pocket bottom profile by considering an offset between each pass [87], [116]. Besides, there are different approaches to predict the kerf geometry in AWJ machining technology. These approaches are based on statistical approaches [8], [44]–[46], [105], [106], [109], simulation approaches such as the finite element method [114] on an advanced computational method [113], on design of experiment [87], on analysis of the material removal mechanism [107]. However, the results from these studies above could not directly be adapted to AWJ machining due to the difference in fluid mechanics of the jet and variety of material properties.

Some reports [47], [100], [111] has shown that the desired 3D complex geometry milled by AWJ process can be achieved by governing different slopes which are equal to the local slope of that desired 3D geometry. This can be obtained by changing the jet impingement angle i.e. the angle between the jet axis and the target surface (Fig. 3-12a). D. Srinivasu et al. [47] has presented an analytical model for top width of jet footprint milled by AWJ machining at various jet impingement angles on SiC ceramic. He has confirmed that the proposed model can be applied to control both three-axis and five axis milling of complex-shaped parts by varying the traverse speed of the jet and impingement angle in continuously according to the shape to be machined. However, no more results are found in the literature of the application of this model for milling 3D complex shapes. Besides, M.C. Kong et al. [121] reported mathematical models for abrasive water jet footprints with arbitrarily moving jets. The proposed models discovered new foundation in geometrical modelling of AWJ machining under the real industrial conditions. With several variables to predict the footprints, for instance, various inclination angles (Fig. 3-12b), jet feed rates, and jet path directions, the models have shown a high degree of accuracy. But for application expansion of these models, in reality, it is too complicated due to requiring the definition of some factors in non-linear partial differential equations. Y.I. Oka et al. [110] presented a predictive model for estimating erosion damage caused by solid particle impact. This model can be utilized under any impact conditions and for any type of material and takes into account the particle hardness, the initial target hardness, and other influence conditions.

Papini et al. [122] observed the surface evolution of inclined masked micro-channels in glass and poly-methyl-methacrylate (PMMA) using abrasive jet micro-machining with a consideration of tilting angles and travelling straight. A ductile erosion response was observed, showing a maximum erosion rate at 45° . Similarly, the model is too complex and the work is conducted with one-phase flow (abrasive jet) process that cannot be compared with three-phase flow (abrasive water jet) process. M. Hashish [71] also investigated the influence of jet impingement angle in abrasive machining for several kinds of materials and noted that it is possible to obtain the maximum mass of the material removal rate corresponding to an optimal impingement angle.

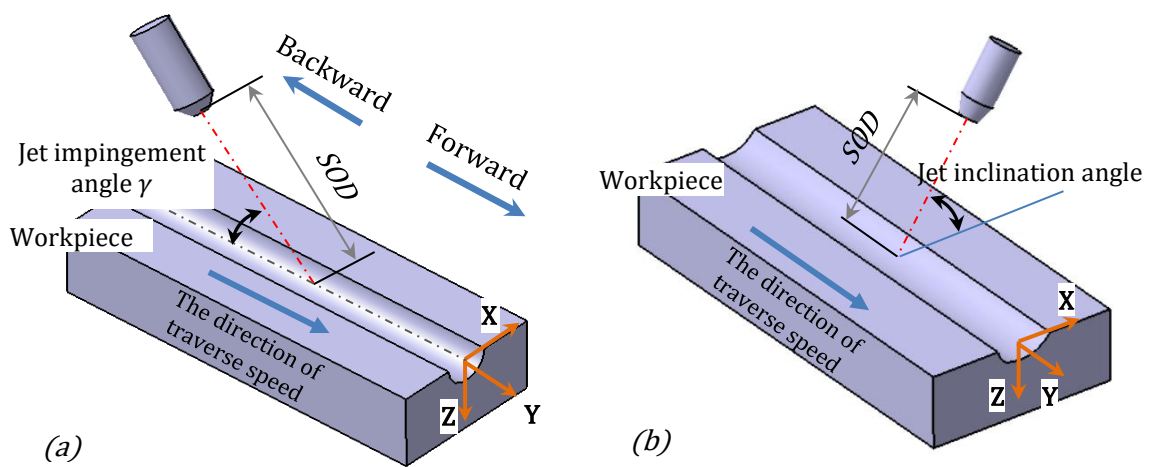


Fig. 3-12. Direction of the jet during machining

Consider the influence of the jet impingement angle on material removal mechanism during process [46], [71], [80] and the quality of milled surface [18], [70], [111], several studies demonstrated that reduction in the jet impingement angle results in a decrease of surface roughness and waviness. It can be seen that at higher impingement angles of the jet, the irregularity of surface machined is illustrated obviously and this irregularity reduce significantly at the lower impingement angles. It indicates that the relative contributions of wear modes (cutting-wear or deformation-wear) vary as the jet angle varies [71]. For metals such as Ti6Al4V, ductile erosive behaviour is revealed by either cutting wear occurring at low jet impingement angles and deformation wear occurring at higher jet impingement angles [96], [123]. In a study [80], K. MC Ojmertz reported that milling at 90° of the jet impingement angle, a mixed morphology of

craters due to deformation wear and scratch which are similar to grooves due to cutting wear. Recently, G. Fowler [18] showed that grooved morphologies occurs with milling at low impingement angles and an appearance of cratered morphology revealed with increasing in the impact angle. No evidence of grooving is presented when the jet impingement angle is higher than 75° . The evolution of surface milled depending on the jet inclination angles is explained by the effect of a secondary erosion phenomenon [111]. This phenomenon occurs due to a slurry including abrasive particle, metallic powder, and water flows beyond the primary footprint of the jet inclination angle especially for low traverse speed.

The present work develops an efficient geometrical milling model, with the benefit of simplicity, taking into account the inclination jet angle (α). As the study presented in [124], only the inclination angle variation is considered. Impingement angle and 5 axis combination will be studied in further works. It makes an effort to insight the kerf generation process with respect to a key kinematic process parameter (*Inclination angle* - α) as a basis to develop strategies for machining controllable pocket shape and further for complex geometries in abrasive water jet technology. To enable this, several works are conducted as follows:

- (i) Introduction of an extended model [124] of the kerf profile for the pocket machined taking into account the inclination angles of the jet (α).
- (ii) Experimentations with different inclination angles of the jet.
- (iii) Measurement of open pockets milled with their characteristics: depth, top width; and the slope of the pocket wall to demonstrate the efficiency of the proposed model.

In this work, the discussion is related to the importance of inclination angle (α) on the generation of geometry and dimensional characteristic the profile of open pockets milled by AWJ machining.

3.2.2 Proposed model with the inclination angle of the jet

The model of the kerf profile of the elementary pass and pocket milled by abrasive water jet process have been introduced [116], [124]. In addition, in order to narrow the influence of a complex operating parameters, a given configuration of the machine is

defined by dividing into two categories i.e. the setting parameters and controlled parameters. The setting parameters are not easily modifiable during milling: they are pressure (P), grade of abrasive particle, abrasive flow rate (ma), and standoff distance (SOD). The controlled parameters are those that can be modified by the NC program during machining. Considering an elementary pass, in this present study, the only controlled parameter is the traverse speed (Vf).

A modelling of kerf profile of elementary pass taking into account the influence of the jet inclination angle (Fig. 3-13) has been developed in the previous works (Eq. 3-7) [124]:

$$y(x) = Ke(\alpha).H(Vf).e^{-\left(\frac{x^2}{B(Vf)^2}\right)} + \cot(\alpha).x \quad \text{Eq. 3-7}$$

$Ke(\alpha)$ is the erosion factor which depends on the jet inclination angle and allows the governing the equation to be more suitable. $Ke(\alpha)$ is identified analytically to find the specific erosion rate on the target material. Once this factor is defined, it is possible to predict the kerf profile with a good accuracy for any cutting head traverse speed. For a considered traverse speed (Vf), the maximum depth $H(Vf)$ and the width factor $B(Vf)$ of the corresponding elementary pass generated at the jet inclination angle of 90° (Fig. 2-21) are computed by Eq. 3-8 and Eq. 3-9:

$$H(Vf) = Ho \times Vf^{Hv} \quad \text{Eq. 3-8}$$

$$B(Vf) = Bo \times Vf^{Bv} \quad \text{Eq. 3-9}$$

In these expressions Ho , Hv , Bo and Bv are coefficients that are determined experimentally [116].

The present model (Eq. 3-10) is being developed further to predict the open pocket on abrasive water jet milling. This model works with the open pocket generated at different focusing tube inclined angles corresponding to a specific machine configuration (Fig. 3-13).

$$Y(x) = \sum_{i=0}^n [Ke(\alpha).H(Vf).e^{-\left(\frac{x-i.Pitch.\sin(\alpha)}{B(Vf)}\right)^2}] + \cot(\alpha).x \quad \text{Eq. 3-10}$$

This modelling approach is adequate applicable and can effectively support the development of jet strategies to allow the controlled machining of complex geometries, for instance, freeform surface.

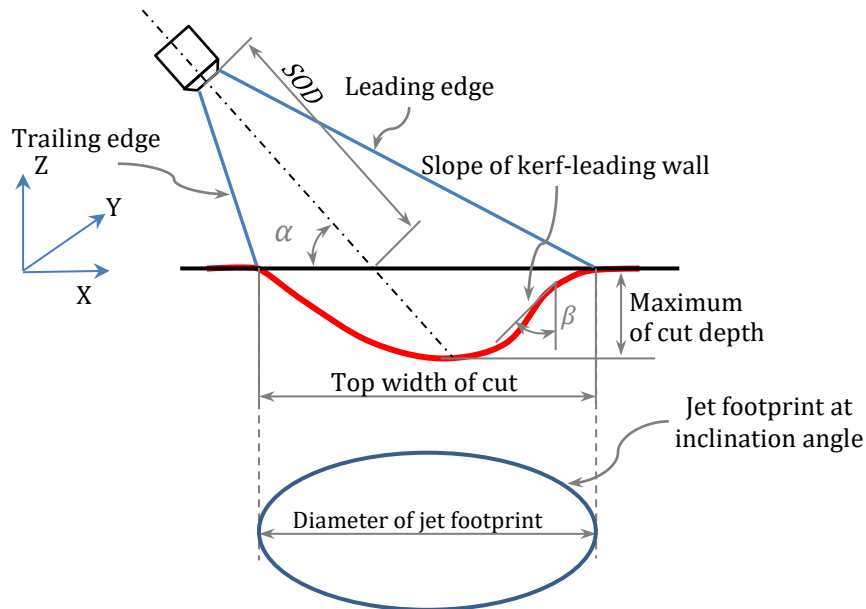


Fig. 3-13. Schematic of elementary pass profile corresponding to the jet inclination angle at α

3.2.3 Experimental set up

The experimental tests for model validation were conducted on a five-axis AWJ machining system (FLOW MACH4C). This machine equipped with a PASER4 cutting head with the diameter of 0.33 mm of a water orifice, a focusing tube diameter of 1.016 mm and 101.6 mm length. An Hyplex-Prime pump generates a maximum pressure of 370 MPa. The manufacturer gives a maximum acceleration on each axis at 0.5 m/s² while the jet feed rate can be varied in the range of 0-20000 mm/min. Two software packages, Flowpath and Flowcut, permit to manage the NC controller. The abrasive type is Opta Minerals 120# and an abrasive flow rate is set by an abrasive orifice with a diameter of 6 mm conditions the flow. The experimental setup for milling the elementary pass is described in Fig. 3-14a and for milling pocket with the trajectory of the jet is described in Fig. 3-14b.

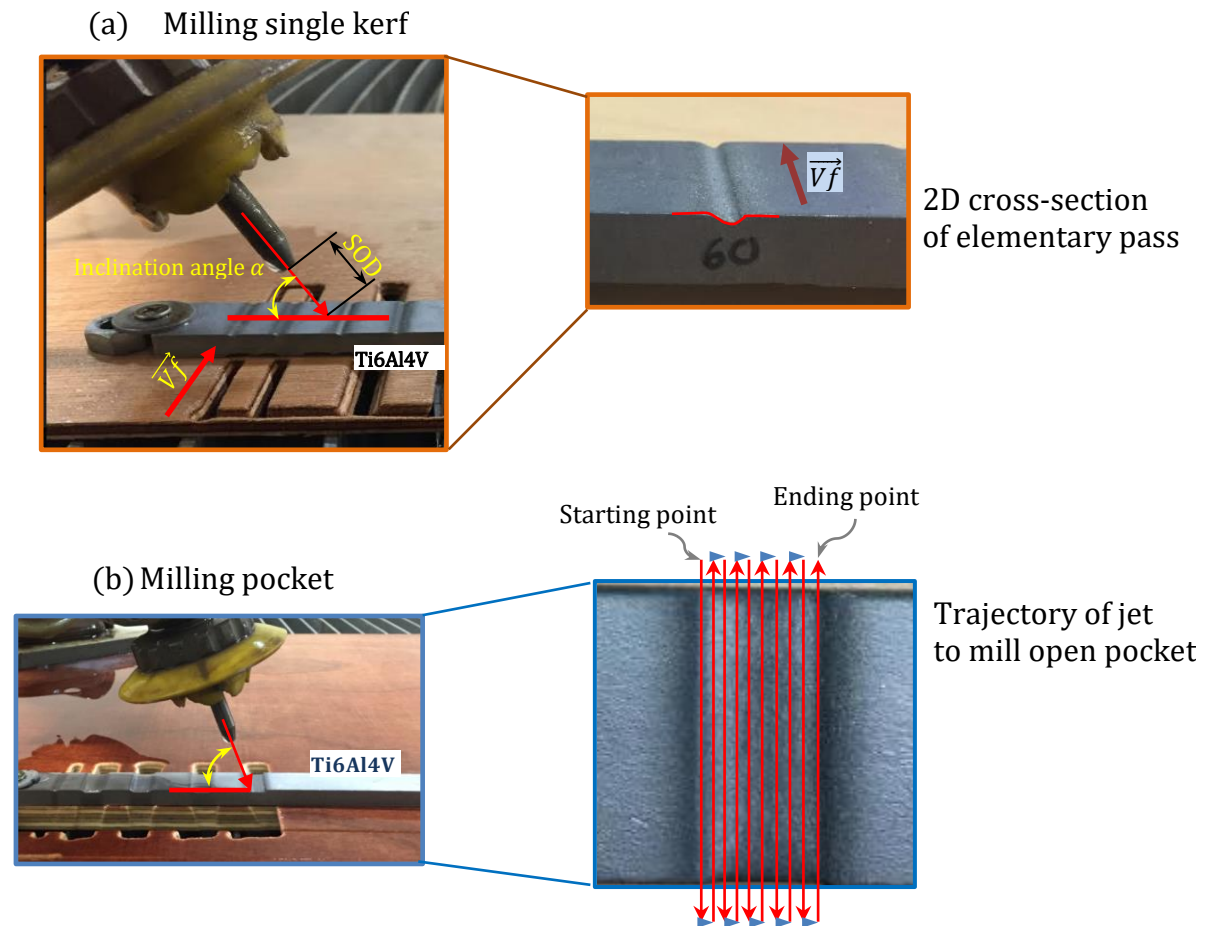


Fig. 3-14. Experimental setup employed for AWJ machining of Ti6Al4V

In this study, the type of abrasive particle employed is garnet (120 mesh size, average (\varnothing 180 – 350 μm – GMA Garnet) and Ti6Al4V specimens with dimensions 20x200x6 mm are used for all tests of the milling operation.

As mentioned above, the characteristic of the elementary pass is influenced by a vast of process parameters like pressure, abrasive flow rate, standoff distance, jet inclination angle, traverse speed of the jet. In order to gain a jet with a constant energy value, it is necessary to be careful in selecting the values of these process parameters in relation to the material to be machined (Ti6Al4V). To be more convenient, Table 3-3 presents the selected input parameters which play the role of the setting parameters in a given machine configuration. In addition, in case of controlled parameter, results from previous works [116], [124], [125] has demonstrated the efficiency of the model to predict the geometrical characteristics of the kerf profile of both the elementary pass and

pocket for various values of traverse speed. In such a manner, the present work only consider the influence of the jet inclination angle on the milling process, tests were implemented at a specific value of the traverse speed (V_f) with different jet inclination angles. This selection allows narrowing the number of the experiment but still assuring the reliability thanks to the inheritance of the previous studies.

Table 3-3. A given machine configuration.

Pressure (MPa)	100 (125)	Diameter of focusing nozzle (mm)	1.016
Washer diameter (mm)	6	Abrasive size (mesh)	120
Orifice diameter (mm)	0.3302	Standoff distance (mm)	20
Traverse speed (mm/min)	1000		

In order to demonstrate the efficiency of the model (Eq. 3-10) taking into account the jet inclination angle (α) on characteristics of the profile of the open pocket milled, the experimental procedure is implemented by the steps below:

- Validate the model of the elementary pass with different inclination angles. Experiments are conducted by varying the α in the range of 50° - 90° by steps of 10° using a given machine configuration (Table 3-3). These tests aim to demonstrate the effectiveness of the expression (Eq. 3-7) despite the setup has changed from the previous one presented in [124].
- Based on results from the elementary pass, investigation of the effect of the jet inclination angles in pocket generation is performed. Experiments are conducted by varying the α in the range of 50° - 90° by steps of 10° using a given machine configuration (Table 3-3) with two pitch values (0.7 mm and 1.1 mm).

To study the influence of jet inclination angle on the pocket milled surface, analysis is conducted in order to identify dimensional characteristics of the pocket such as the depth, the width, and the slope of the pocket trailing wall. To enable this analysis, the 2D cross-section of the profile of open pocket are extracted from the outcome of measuring on an ALICONA IF optical profilometer (Fig. 3-15). This apparatus is able to measure 1000

curves, distributed regularly over 2 mm, using an intersection between the measured surface and 1000 planes perpendicular to the direction of the traverse speed.

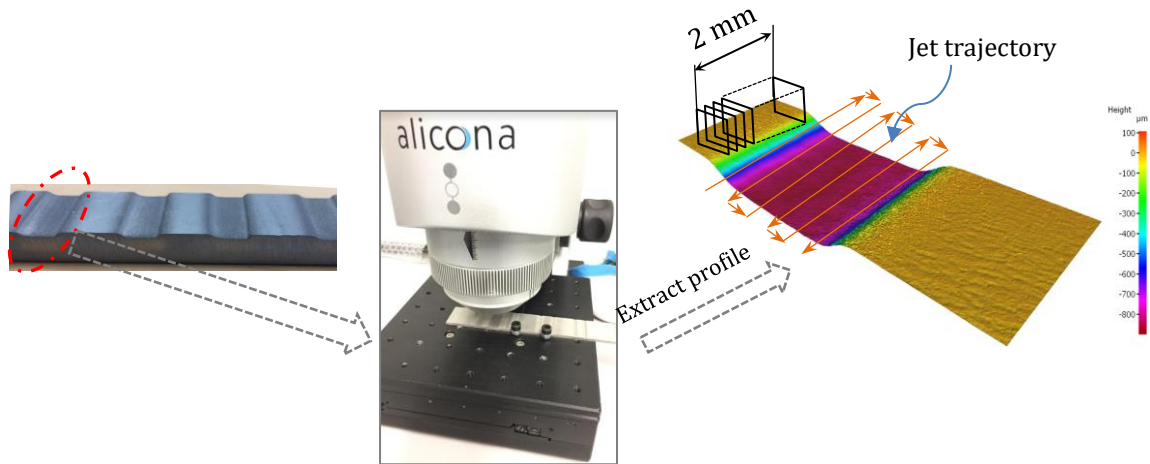


Fig. 3-15. Measurement on Alicona

3.2.4 Validation of the proposed model

In order to investigate the influence of the jet inclination for different angle values on the kerf profile of the elementary pass as well as milled pocket shape, analysing the 2D cross-section (Fig. 3-13) belonging in the plane of the focusing tube and z-axis is conducted. In following sections, the variation in 2D geometry of kerf profile of elementary pass and pocket are considered as caused the kinematic process parameter (α) evolution.

3.2.4.1 Assessment the proposed model for elementary pass

To assess the proposed models and provide compatible parameters which are the input parameters in this study, a global model corresponding to a given machine configuration is established [124]. Three elementary passes were machined at the perpendicular jet to workpiece surface corresponding to three levels of the traverse speed (800, 1000, and 1200 mm/min) other setting parameters were selected in Table 3-3. Base on Eq. 3-8 and Eq. 3-9 using the least squares method, coefficients $H_o = 336.074$, $H_v = -1.000$, $B_o = 1.224$, $B_v = -0.066$ were determined experimentally.

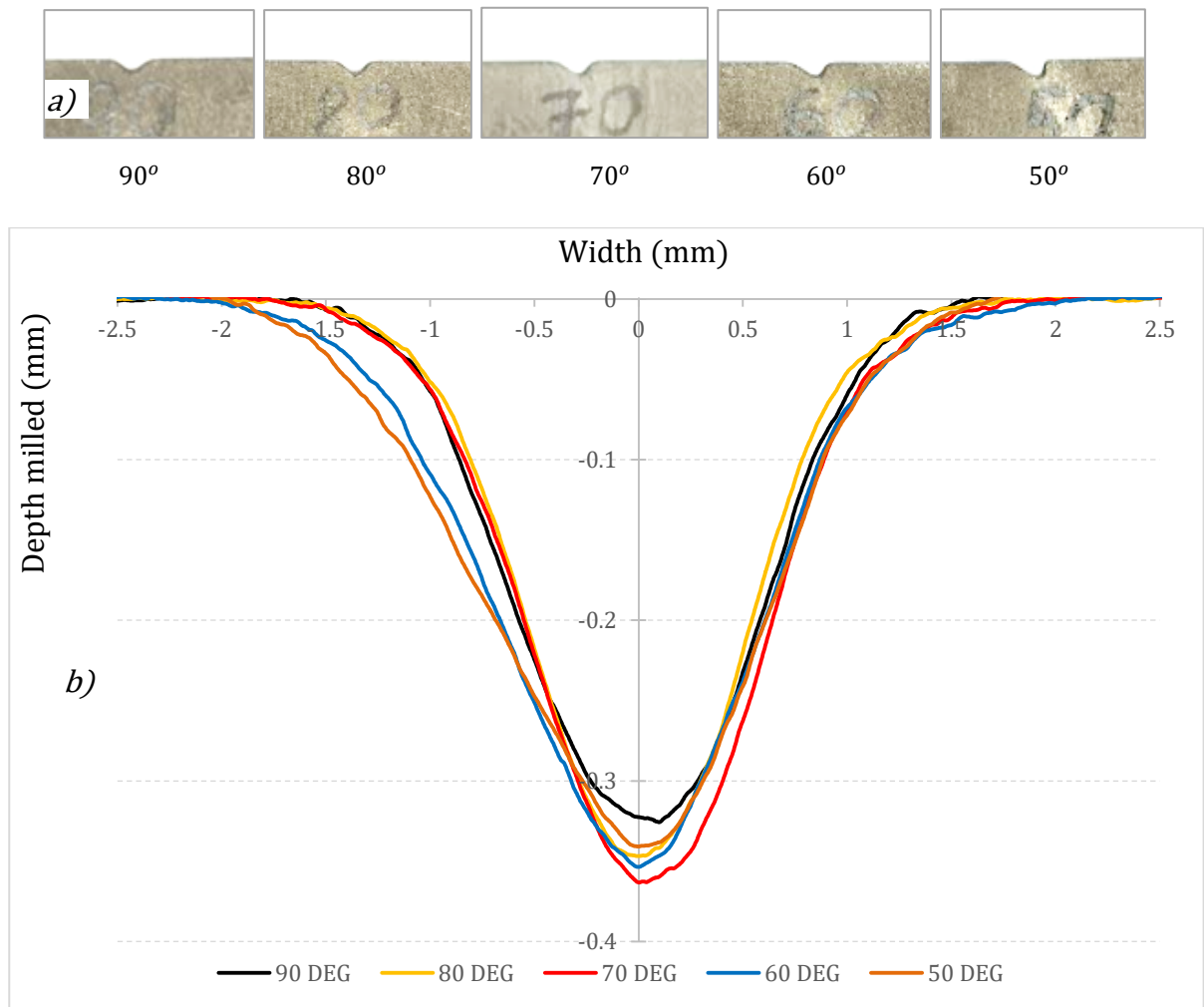


Fig. 3-16. The influence of the jet inclination angle on characteristics of the elementary pass. Images (a) and profiles (b) of elementary pass milled at different jet inclination

In order to verify the proposed model for the elementary pass, five elementary passes were milled at a given traverse speed of 1000 mm/min on varying of the inclination angle of the jet from 50° - 90° by step of 10°. Fig. 3-16a presents the geometry of elementary passes generated at different jet inclination angles. The observation confirms that at the normal jet ($\alpha = 90^\circ$), the kerf geometry is symmetric (Fig. 3-16b). It should be noted that the kerf profile of elementary pass milled is mainly governed by the jet energy across the material zone to be machined and local impact angles of abrasive particles attacking the material [44], [46], [71].

Gaussian distributions have been considered as the energy distribution in the jet (Fig. 3-17). At any cross-section of the jet plume (perpendicular to the jet axis), the velocity profile of water follows nearly Gaussian distribution [30] and the divergence radius of the jet plume is greater as the axial distance from the focusing tube increases. It

results in a decrease in axial velocity [46]. When the inclination angle of the jet equals to 90° , the velocity distribution in the radial direction of the jet footprint is symmetric and proportional to the erosion ability of abrasive particles. Consequently, the geometry of the elementary pass also follows a similar profile of the normal Gaussian distribution. The maximum depth of cut will be reached in the centre of the jet axis and then decreased gradually on both sides of the kerf profile. As observed in Fig. 3-17a, there are different local angles (γ_n) of jet impacting angle on the workpiece surface and these local angles reduce steadily on both sides of the jet axis. Hence, the local impact angle changes from 90° at centre of jet axis to a critical angle at which there is no material erosion was observed on both sides of the jet axis.

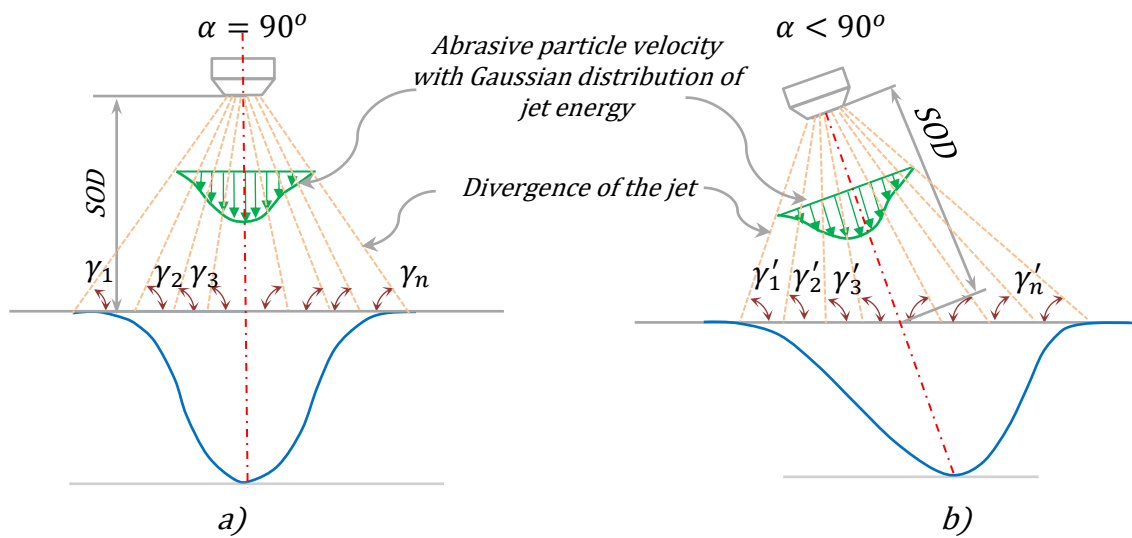


Fig. 3-17. The influence of the jet inclination angle on characteristics of the elementary pass

A decrease of the jet inclination angle influences the jet plume divergence as well as the local angle of abrasive particles impacting on the material (γ'_n), introducing changes in the velocities of water/abrasive particles (Fig. 3-17b). Thus it results in a variation of the kinetic energy across the jet footprint. It affects the capability of abrasive particles in removing material due to cutting erosion or plastic deformation mechanism [54]–[56]. Besides, as the jet inclination angle decreases, the kerf geometry becomes asymmetric. The top view of the kerf gradually transforms from circular (at 90°) to elliptical (at $0^\circ < \alpha < 90^\circ$). This leads to increase in the width of footprint in the plane which is perpendicular to the direction of the jet traverse speed. The maximum erosion depth was

observed along the jet axis where abrasive particles has the highest velocity. This phenomenon has been clearly explained in the study of Srinivasu et al. [46], [47].

A comparison between different cases of the jet inclination angles (50° - 90°) is presented in Fig. 3-18. Measurement results are shown that the maximum depth was found in the range of 60° - 80° (Fig. 3-18a) of the jet inclination angles while the maximum width occurs at 50° (Fig. 3-18b). This observation is similar to the results is found in [46] where the maximum depth of cut occurred at 70° of the jet impingement on milling silicon carbide (SiC) by abrasive water jet machining.

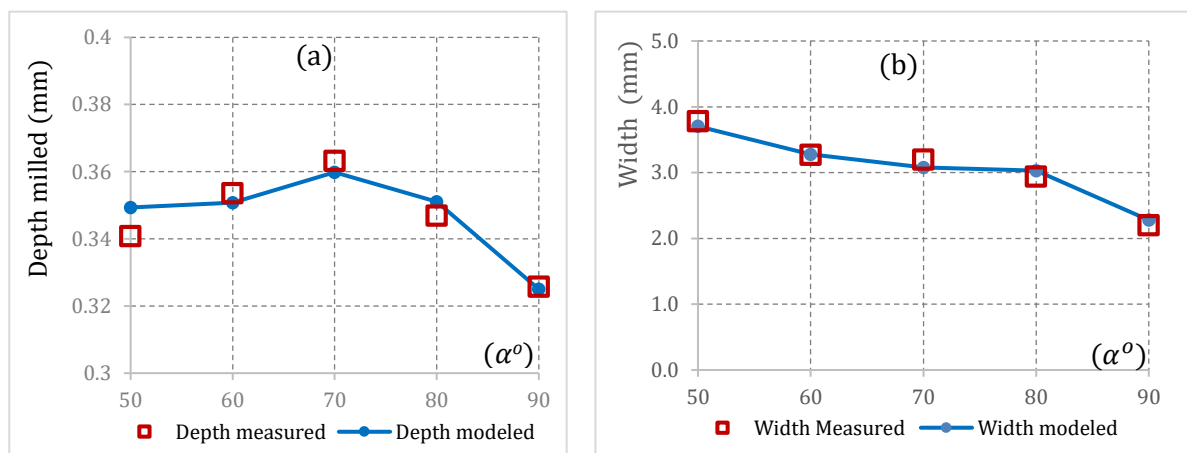


Fig. 3-18. The evolution of depth and width of elementary passes at various jet impingement angles

The material removal volume varies with inclination angle and the maximum erosion rate changes between different materials depending on the effective impact angle of abrasive particles (local impact angles) [110]. In fact, in each point the effective impact angle of abrasive particles cannot be 90° at the jet inclination angle of 90° . This effective impact angle of abrasive particles potentially reaches 90° at $\alpha < 90^\circ$. It lead to the maximum depth of cut occurs at an inclination angle less than 90° for the elementary pass (Fig. 3-18).

Moreover, different distances (Fig. 3-17b) between the tip of the focusing tube and the location on the workpiece are observed. The distances on the left side where the leading edge of the jet plume contacting the target surface is greater than that on the right side where the backward edge contacting the target surface. At a higher distance, the

kinetic energy of the jet becomes unstable, which leads to the evolution of the top width of the kerf profile is unsteady (Fig. 3-18b).

The cross-sectional profiles of the elementary pass were measured and compared with the model predictions. The result shows that the deviation in depth increases when the jet inclination angle decreases and the deviation in the width is smaller as comparing each case of the jet inclination angle. This deviation is attributed to the erosion mechanism which is different between the inclination angles of the jet. Therefore it is necessary to take into account the effect of erosion mechanism as a function of the inclination angle by the erosion factor $Ke(\alpha)$. This factor was determined by the experiments and given in Eq. 3-11

$$Ke(\alpha) = 1.79 - 0.009(\alpha) \quad \text{Eq. 3-11}$$

The correlation coefficient is $R^2 = 0.965$. It shows a good relationship between the inclination angle (α - deg) and erosion coefficient as can be seen in Fig. 3-19. The dot line represents the best fit to the data based on Eq. 3-7.

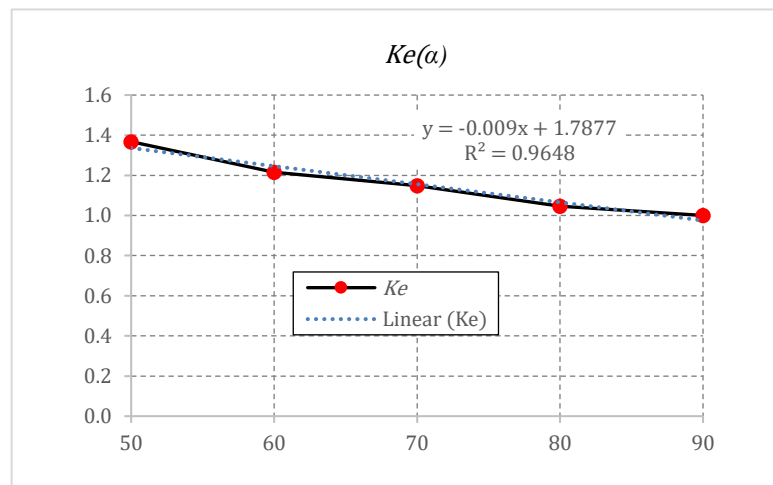


Fig. 3-19. Dependence of material removal mechanism on the jet inclination angle

Apply the erosion factor $Ke(\alpha)$ into the equation Eq. 3-7, Fig. 3-18a, b show the depth and width of elementary passes predicted by the proposed model and the experimentally achieved values at $V_f = 1000$ mm/min jet traverse speed. The predicted values are in close agreement with the experimental values with error less than 5% for the depth and 10% for the width. However, the error in the width predicted is

considerable as the jet inclination angle increases due to a significant divergence of the jet which results in unstable kinetic energy of the jet on both edge sides of the elementary pass. The result has confirmed the good model for prediction of the elementary pass milling by abrasive water jet at different jet inclination angle.

3.2.4.2 Assessment the proposed model for pocket

Owing to a good model for predicting dimensional characteristics of the elementary pass, the model proposed in Eq. 3-10 for prediction of geometry characteristics of the open pocket milled need to be assessed. Pockets are milled in the range $50^\circ - 90^\circ$ of jet inclination angles at a specific value 1000 mm/min of the traverse speed for two pitch values (0.7 mm and 1.1 mm), other parameters are selected in the following Table 3-3. It should be noted that in an attempt to understand the influence of the jet inclination angle on the material removal mechanism to produce pocket with flat bottom, the jet trajectory is described in Fig. 3-14b. This trajectory enables the jet moving from the left side to the right side of pocket with the zigzag tool path. It has the advantage of limiting the effect of secondary milling which takes place strongly in other tool paths of the jet [8], [57]. The profiles shown in (Fig. 3-20) and (Fig. 3-21) with experimentally achieved values and two models (Eq. 3-10) and (Eq. 3-12) considering the effect of erosion factor which dominate the difference of predicted pockets and measured pockets.

$$Y(x) = \sum_{i=0}^n [H_e(\alpha).Ke(\alpha).H(Vf).e^{-\left(\frac{x-i.Pitch.\sin(\alpha)}{B(Vf)}\right)^2}] + \cot(\alpha).x \quad \text{Eq. 3-12}$$

Where: $H_e(\alpha)$ factor consider the effect of a succession of elementary passes depending on the real inclination angle of the jet. The rapid calibration procedure described in article [116] was applied. In these experiments, the value of the width factor $B(Vf)$ is defined by Eq. 3-9 and equals to 0.78 mm. In order to obtain pockets with flat bottoms in case of the jet perpendicular to the workpiece surface [116], the pitch is selected in an interval of $[0.6 \times B(Vf) - 0.9 \times B(Vf)]$. So, when the pitch is 0.7 mm, the pocket bottom is flat one (Fig. 3-20) and for another value of pitch (1.1 mm), the waviness appears at the bottom obviously (Fig. 3-21).

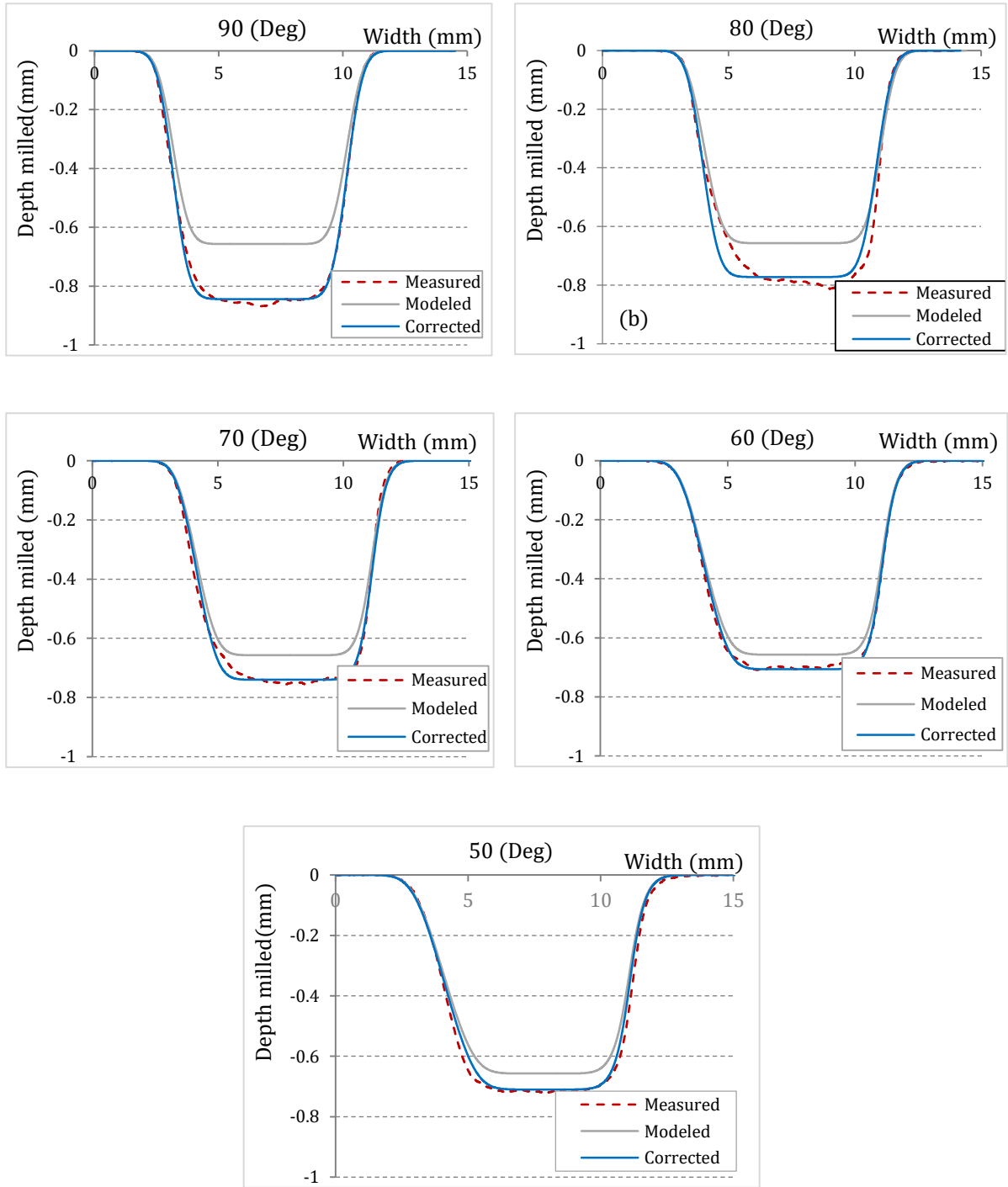


Fig. 3-20. Influence of the jet inclination angle on characteristics of pockets milled (SOD = 20 (mm); P = 1000 (MPa); Vf= 1000 (mm/min), Pitch = 0.7 (mm))

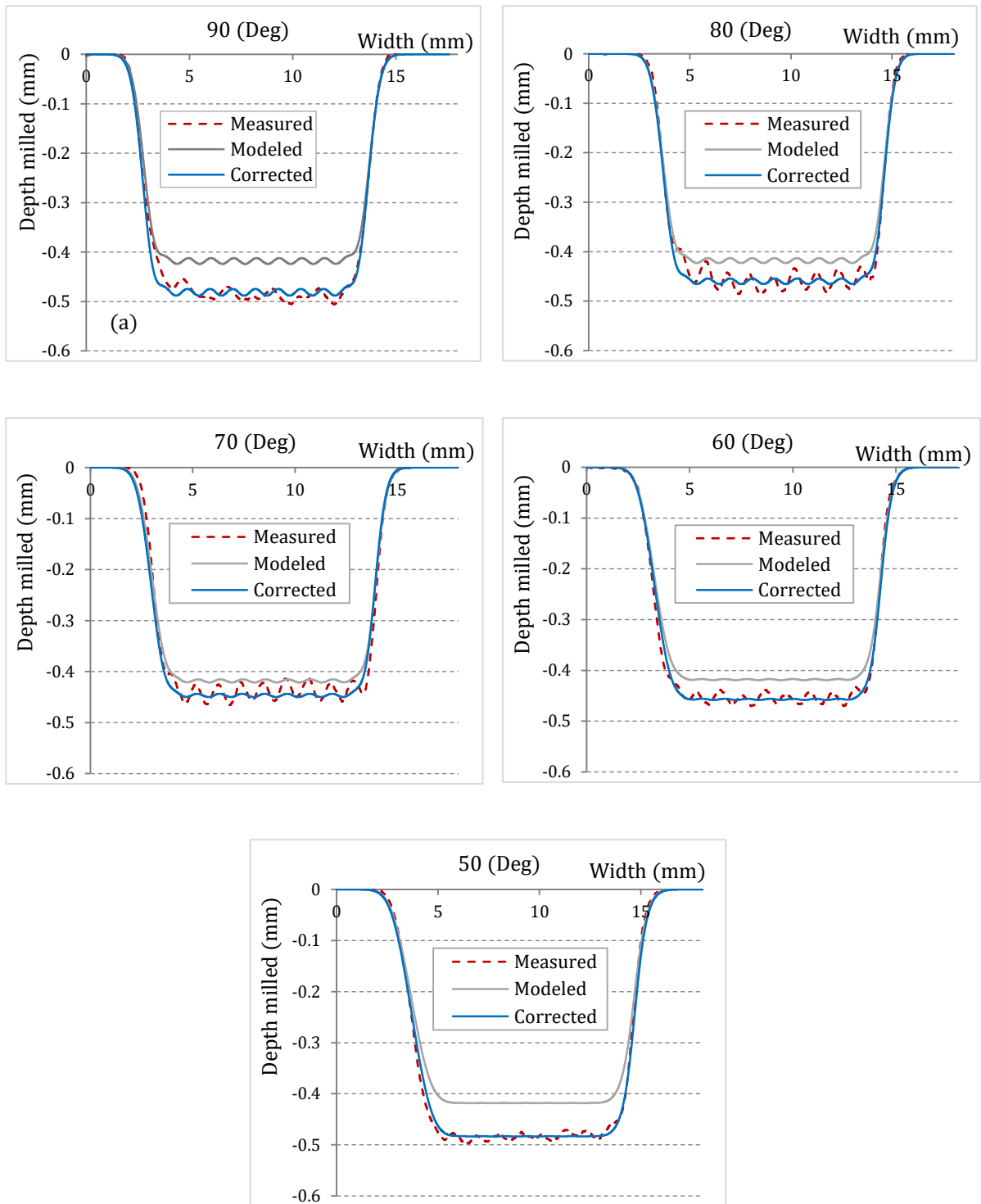


Fig. 3-21. Influence of the jet inclination angle on characteristics of pockets milled (SOD = 20 (mm); P = 1000 (MPa); Vf= 1000 (mm/min), Pitch = 1.1 (mm))

Fig. 3-22 shows the value of $H_e(\alpha)$ factor which defined by experiment at a given jet inclination angle for two values of the pitch steps. In both cases, the $H_e(\alpha)$ factor is a

function of the jet inclination angle and dependence of $H_e(\alpha)$ fully matches with the linear trendline (dot lines is the best fit line).

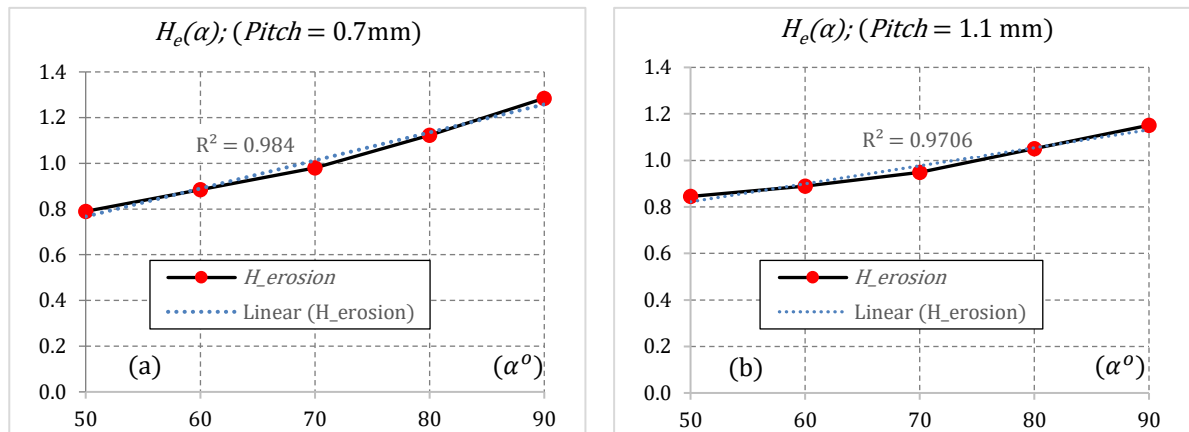


Fig. 3-22. $H_e(\alpha)$ factor defined experimentally as a function of jet inclination angle. The dot line represents the best fit line to the data based on Eq. 3-12: a) Pitch = 0.7 (mm); b) Pitch = 1.1 (mm)

Based on the good accordance between the experiment and prediction, in the following section, discussion is made in relation to the importance of controlling jet inclination angle (α). This parameter has a strong influence on the geometry and dimensional characteristics of the pocket milled by AWJ technology.

3.2.4.3 Influence of jet inclination angle on the geometrical characteristics of the milled pocket

3.2.4.3.1 Influence on the depth

In Fig. 3-20 and Fig. 3-21, it can be observed that the pocket reaches the highest value at 90° , and then reduces as the jet inclination decreases see in Fig. 3-24. This trend will stop at 60° with pitch = 0.7 mm and at 70° with pitch = 1.1 mm. For both values of the pitch, the magnitude of these depth values depend on the scanning step over (the *pitch*). This observation reveals a slight difference from the case of milling elementary pass at which the maximum depth achieved around $60^\circ - 70^\circ$.

A milling process on ductile material (Ti6Al4V) by abrasive water jet is considered as a process which is controlled by erosive wear at large particle impact angles. The material erosion mechanism will be varying when the jet inclination angle changes. In

order to mill a pocket by AWJ, it is necessary to use the method of superposition of several elementary passes. (Fig. 3-23) presents a schematic illustrating of the pocket generation at different jet inclination angles: $\alpha = 90^\circ$ (Fig. 3-23a) and $\alpha < 90^\circ$ (Fig. 3-23b) with three elementary passes over the workpiece surface.

At higher inclination angles of the jet, material is mainly removed by plastic deformation due to most of abrasive particles own the normal component of velocity vector greater than the tangential component. Oppositely, when the jet inclination angle decreases, material removal mechanism will be changed from plastic deformation to cutting erosion [55], [56]. The material erosion mechanism occurs at the first elementary pass has been mentioned above (§3.2.4.1). For the second elementary pass, impacting of abrasive particles on the target occurs totally difference with the previous one due to the presence of the wall slope (the leading edge of the pocket) see in Fig. 3-23b. Indeed, abrasive particles will attack the leading edge of the pocket (γ_n - on the left side of the jet axis) at lower inclination angles resulting in removing material by cutting erosion mode while the inclination α angles of abrasive particles attacking on the bottom of pocket (γ'_n - on the right side of the jet axis) is higher and results in removing material by plastic deformation mode. Depending on the effective impact angle of abrasive particles flow, either cutting wear mode or plastic deformation mode will dominate other.

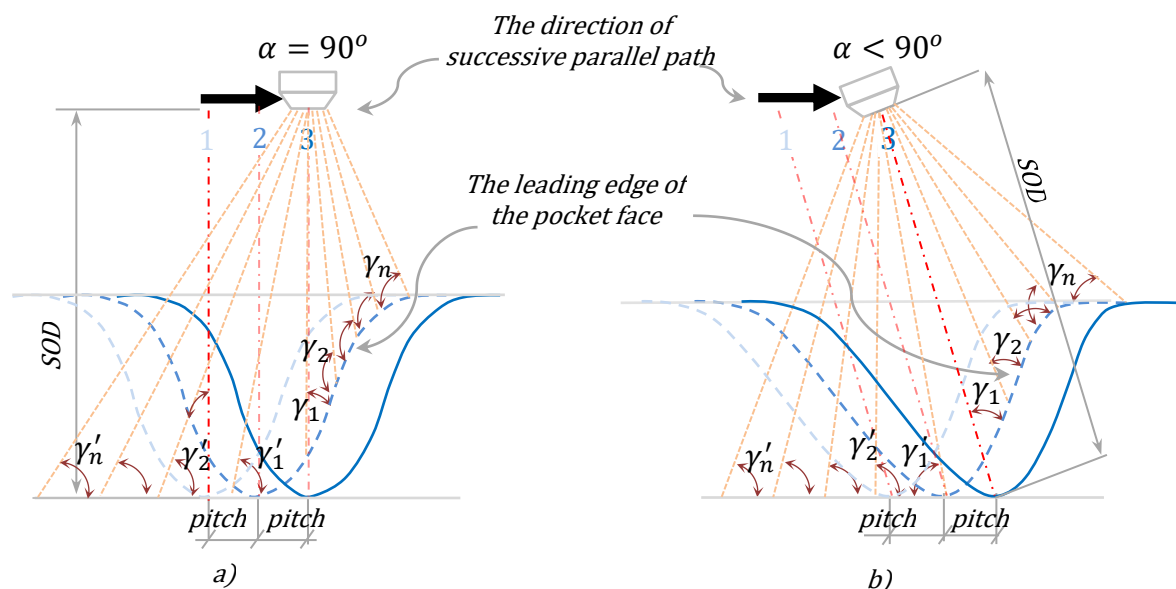


Fig. 3-23. Explanation of different erosion rate from inclination angle of the jet

Additionally, it can be seen that milling pocket by AWJ technology raises a problem of *secondary erosion* [4], [18], [111] which is created by the abrasive water flow beyond the primary footprint of the inclination jet. This problem becomes more important since the surface topography shifted after machining the first elementary pass. It leads to change the erosion mechanism in removing material of the jet. Indeed when the slope of the kerf-leading wall is changed after the first elementary pass, the local angle impacts of abrasive particles also varies strongly. As the jet varies the inclination angle (α), at lower values, the slope of the kerf-leading wall would be more vertical than that at higher angles (Fig. 3-16). From the second to the last elementary pass, the material removal rate has been changed significantly because of variation in the local impact angle of abrasive particles (Fig. 3-23). However, if the inclination angle of the jet further decreases, the divergence of the jet significantly increases. It leads that jet energy and cutting ability of particles are reduced obviously.

Thereby when the jet inclination angle changes, divergence of the jet also results in spreading directions of abrasive particles. The impacting particles forms more unpredictable erosion patterns. In these cases, the erosion capability of the abrasive particles is less and reduces the material removal mass. Overall, the erosion factor [116] which previously introduced in §2.1.2 when milling pocket at 90° is also changed.

It can be seen that without $H_e(\alpha)$ factor the proposed model is insufficient to predict geometrical characteristics of the pocket profile milled at different inclination angles (Fig. 3-24). Thus it is necessary to take into account the $H_e(\alpha)$ factor in the proposed model (Eq. 3-12). It is interesting to note that this $H_e(\alpha)$ factors in the two pitch cases are linearly proportional to the jet inclination angle (Fig. 3-22). It can be also observed that the magnitude of $H_e(\alpha)$ at higher inclination angles in case of a small pitch (0.7 mm) is greater than that at pitch = 1.1 mm (Fig. 3-22). This can be attributed by a more significant effect of secondary erosion mechanism at the small pitch.

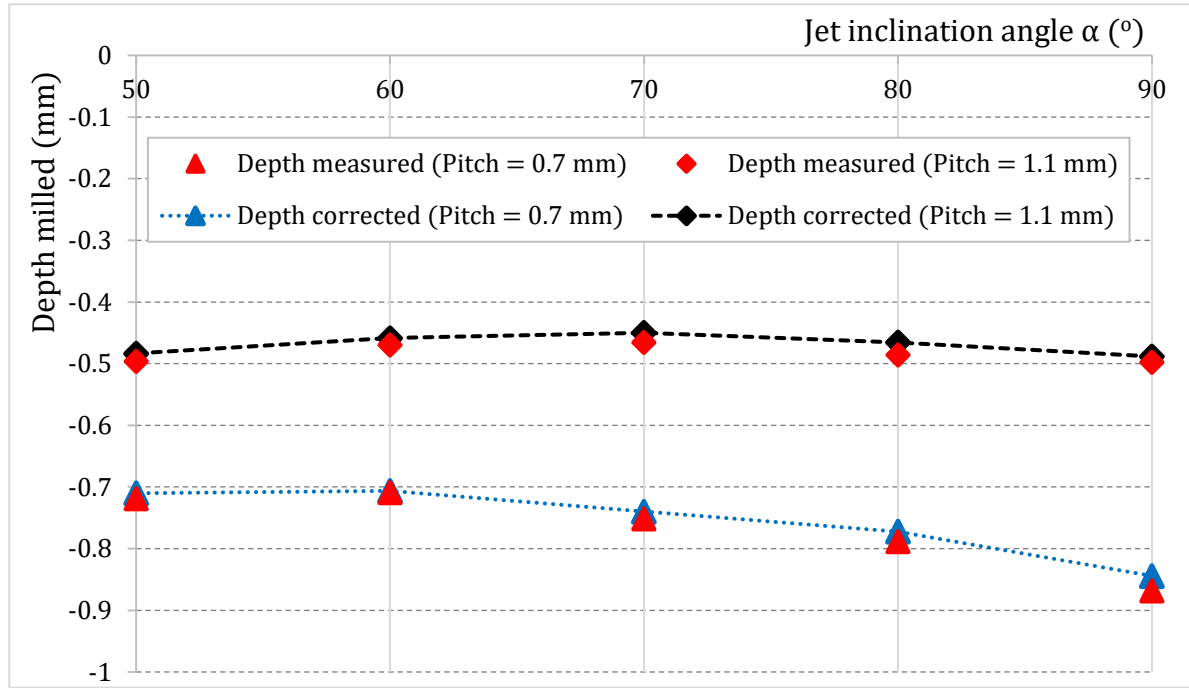


Fig. 3-24. Variation in the depth of pocket with two cases of the pitch

Once the erosion coefficient $H_e(\alpha)$ is taken into account in the model (Eq. 3-12), there is a good agreement (Fig. 3-24) between the model predictions and the measured profiles with an average error which is computed by Eq. 1-13.

$$Error = \frac{Depth_{Modeled} - Depth_{Measured}}{Depth_{Measured}} \quad \text{Eq. 3-13}$$

The average error is the relative deviation of the maximum value of the modelled depth compared to the measured depth on the milled pocket for each pitch case. As can be seen in Table 3-4 that: (i) these average errors are always negative values and all the absolute value of them is less than 5%; (ii) the maximum average value is observed at the inclination angles of 70° and 80° for both two cases of the pitch and these values in case of the pitch = 0.7 mm are bigger than that of the pitch = 1.1 mm. To explain this observation, it can be understood that there exist other material removal mechanisms that happened during the process and they are not taken into account in the proposed model. These negative values were only defined at local points where the depth was computed as the maximum value on the pocket bottom. Besides, as the jet is inclined the material removal mechanism is also gradually changed from the impacting to the eroding

phenomenon. In these cases, milling between a ranges of 70° to 80° of the jet inclination angle contains the critical point where this material removal mechanism is changing. Consequently, the average error in this interval is the biggest.

Table 3-4. Modeled and measured depth for milling pocket at different inclination angles.

α	Pitch = 0.7 mm			Pitch = 1.1 mm		
	Experiment (mm)	Model (mm)	Error (%)	Experiment (mm)	Model (mm)	Error (%)
90°	0.868	0.844	-1.63%	0.497	0.488	-1.84%
80°	0.789	0.772	-2.04%	0.485	0.466	-4.09%
70°	0.752	0.740	-1.56%	0.466	0.459	-3.35%
60°	0.709	0.706	-0.36%	0.470	0.453	-2.43%
50°	0.719	0.710	-1.23%	0.496	0.483	-2.57%

3.2.4.3.2 Influence on the width

Similarly, the width of the milled pocket is computed by all the points (Fig. 3-25) that have a depth greater than 0.12 mm that is the average size of abrasive particles [116], [124]. This calculation is to be sure that material removal action happened on these points.

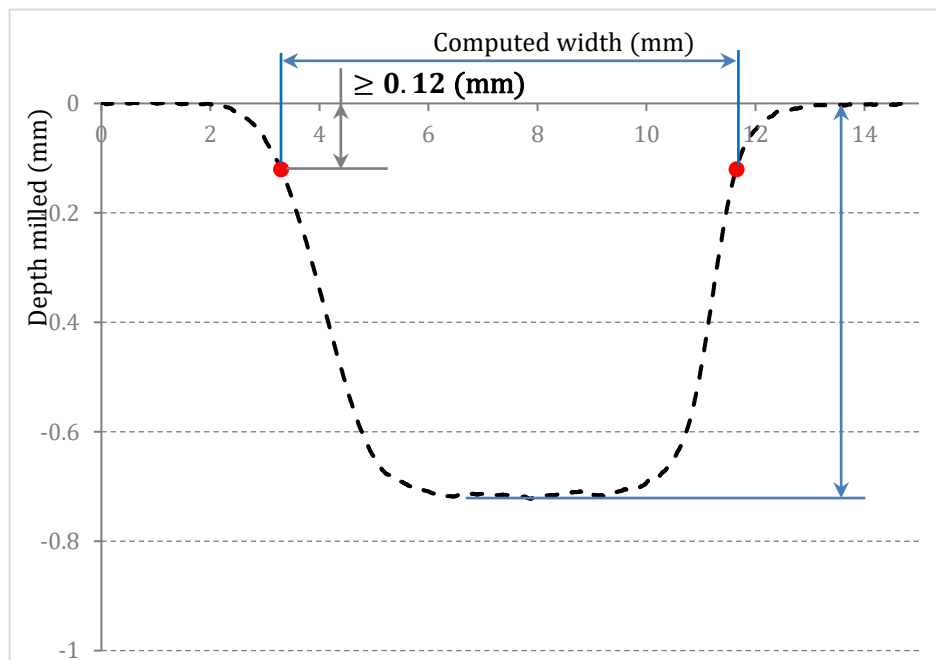


Fig. 3-25. Definition of the width of milled pocket

It can be observed from Fig. 3-20 and Fig. 3-21 that for a given machine configuration, the width of the cross-sectional geometry of pocket profile increases when the jet inclination angle decrease. This trend is similar to the trend observed for milling elementary passes by varying the jet inclination angles. This trend is also due to the divergence of the jet at lower inclination angles and leads to a greater diameter of the ellipse of jet footprint on machined surface [46], [47]. However, at a small value of jet inclination angle, the abrasive particles along the boundary of the jet have low erosion capability as interact with the material and do not enhance the erosion which results in a slight increase in kerf width Fig. 3-26.

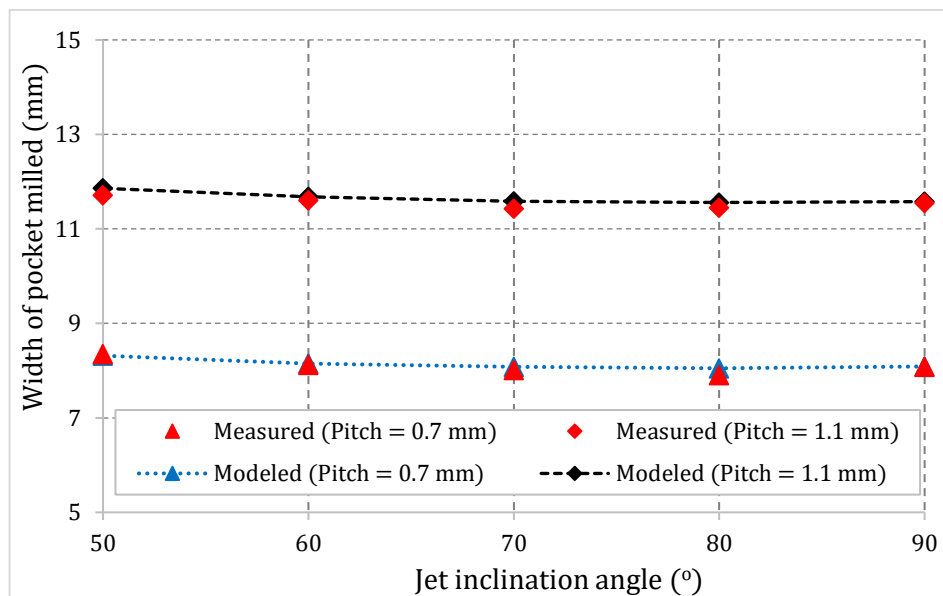


Fig. 3-26. Variation in the width of pocket with two pitch cases

Besides, consider the characteristic of the jet plume, it can be divided in two concentric zones where the kinetic energy of abrasive particles are different [51]. Hence, it could be noted that the erosive capability of the unstable outer part of the jet plume along its edges is less than at the inner part of the jet.

3.2.4.3.3 Influence on the slope of pocket walls

The pocket wall slope is characterized by a β angle and defined in Fig. 3-27 in which β is computed by the slope of a straight line through two points 1 and 2. The definition of points 1 and 2 is shown in Fig. 3-27. It should be noted that this slope is computed on the right side of the milled pocket related to the direction of successive parallel path (Fig. 3-23). Based on this definition, the slope angle of the pocket wall (Fig.

3-28) varies from 39° (pitch = 0.7 mm and $\alpha = 80^\circ$) to 22.5° (pitch = 1.1 mm and $\alpha = 90^\circ$). It is interesting to note that the maximum values of sidewall slope observed occurs at 80° of jet inclination angle.

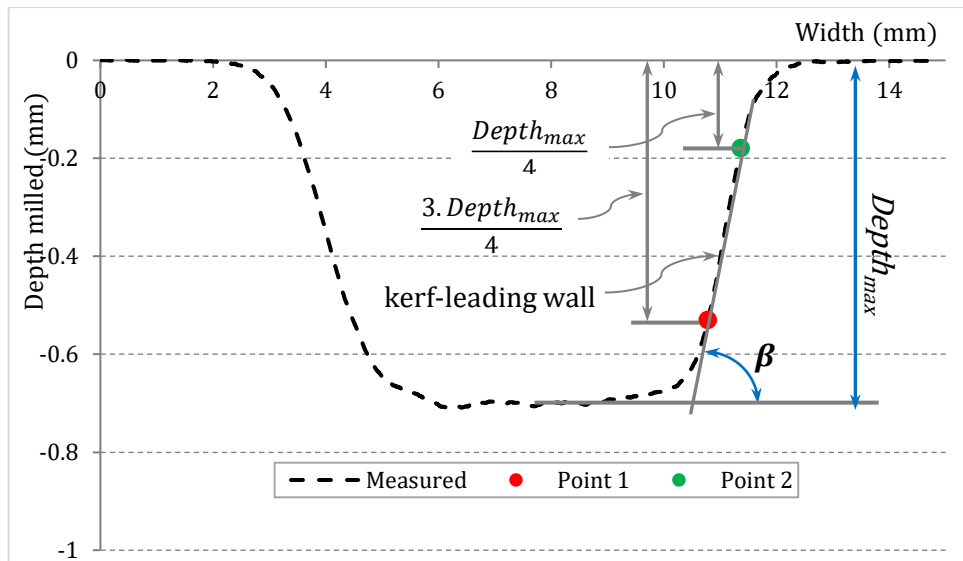


Fig. 3-27. Definition of the slope of pocket wall

The slope angle variation for small pitch is greater than that for large ones. These observations can be attributed to: (i) the effective impact angle of abrasive particles on the sidewall slope which depends on the jet inclination angle, the maximum value is observed in case of milling pocket corresponding to the maximum value which obtains for milling elementary pass (Fig. 3-28), and (ii) the effect of the overlapping gap between two adjacent elementary passes.

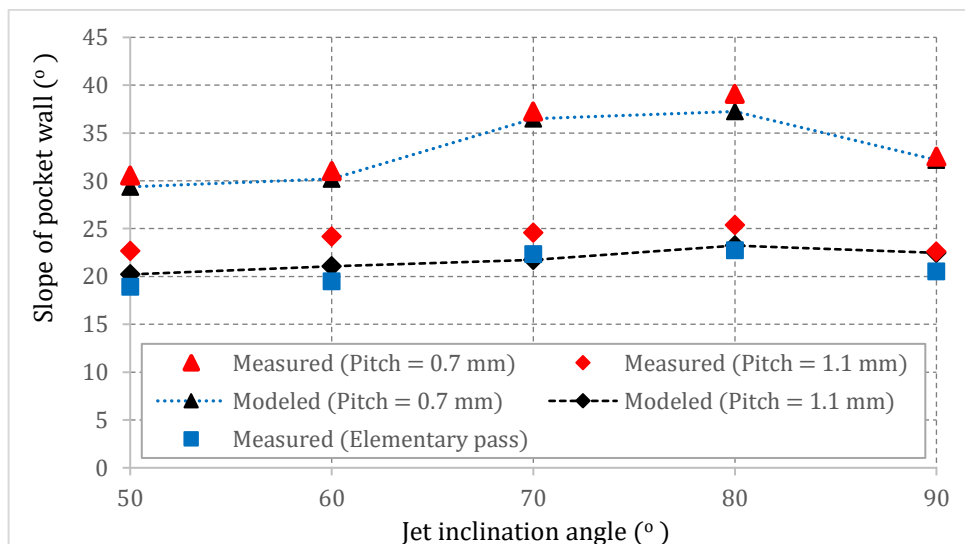


Fig. 3-28. Variation of slope of pocket wall depending on jet inclination angle

In order to master the complete pocket geometry, it is important to investigate whether this slope could be increased and controlled by the inclination angle of the jet. An initial experiment to mill steeper pocket sidewalls is performed using one orientation of the jet. In this case, pocket is machined with a jet inclination angle at 50° with a two times repeated trajectory (Fig. 3-14b) over the same pocket. The results illustrated in Fig. 3-29 indicate that the slope of the pocket sidewalls increases from 23° to 58° . Besides, the geometrical characteristics of this pocket were changed due to a significant increase of the milled depth while the width slightly increases less than 8%. It should be confirmed that using the proposed model is able to predict the milled pocket profile at the second time of the milling process (Fig. 3-29). Moreover, an attempt to predict the profile at the third time is presented in Fig. 3-29 (green line). It can be seen that repeating this milling process can increase the pocket sidewalls and for a given machine configuration, a given depth corresponding to a given slope angle of the pocket wall is defined. Once applying the method of the jet orientation, it's possible to obtain pocket milled by abrasive water jet technology with a more vertical angle of the sidewalls. Further works will be performed to have good predictions of these characteristics.

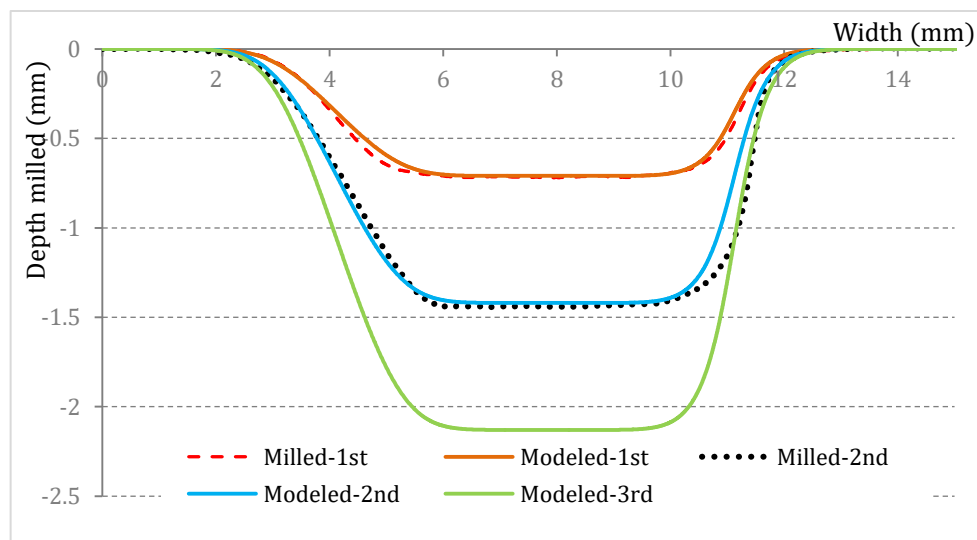


Fig. 3-29. Slope of pocket wall increased as repeating the trajectory over the same pocket milled at 50°

3.2.5 Conclusion

In this work, the generation of pocket milled at various jet inclination angles is investigated by considering the model for 2D cross-section profile milling by AWJ applications. The model has been assessed for milling open pockets using difficult-to-

machine titanium alloy (Ti6Al4V). The model can be used to control five-axis milling for parts with complex shape in which the milling process is controlled by the traverse speed of the jet and the jet inclination angles, other process parameters are chosen to establish a given machine configuration. The main contribution of this work can be summarized as follows.

The kerf profile of pocket machined is analysed to get control for the depth of the pocket by varying a jet inclination angles from 50° to 90° . It was found that the geometry of the kerf profile of the open pocket milled significantly depends on the jet inclination angle(α). The jet inclination angle contributes to local impact angles accounted across the jet footprint, which governs the formation of geometry characteristics as well as the surface quality of pocket milled.

The variation in the depth and width of pockets milled depends on the jet inclination angle. A decrease in the jet inclination angle influences the material removal capability of abrasive particles impacting, which leads a decrease in depth but results in a slightly increase in the width of pockets machined. The maximum depth was obtained at 90° while the maximum width was observed at 50° . Additionally, the variation in the impact angle induces a varying in the erosion mechanism behaviour along with the secondary erosion. On milling operation, the erosion mechanism switches between cutting wear and deformation wear according to the local impact angle of abrasive particles on the workpiece surface. A combination of varying in the erosion mechanism and the effect of the secondary erosion lead to the variation in the quality surface including *uniformity; roughness, waviness* at the bottom of the pocket, which will be studied in further works.

Assessment of the model predictions was done by experiments. By taking into account the effect of erosion factor $H_e(\alpha)$, the model has enabled for predicting the geometrical characteristics of kerf profile of the pocket milled. The results show a good agreement of measured and modelled values and erosion factor is demonstrated as a linear function of the jet inclination angles. This study reveals a good efficiency for modelling of open pocket milled by AWJ with considering different aspects during the process. However, to utilize the advantages of AWJ technology on the milling process, further studies like milling a closed pocket, controlling the slope of the sidewall of pocket are necessary.

GENERAL CONCLUSIONS AND

FUTURE WORK

4.1 General conclusions

Study of the bibliography indicates the use of metals with outstanding properties such as titanium alloy (a combination of resistance and lightness) is a prerequisite in the current aerospace manufacturing. The first chapter presents some problems involved with machining this alloy as using the conventional machining methods. It comes from a dramatic reduction of the tool life and deformation of parts due to high cutting forces and heat-affected zone during the process. Amongst non-conventional machining techniques like laser machining, abrasive water jet (AWJ) machining, and electrical discharge machining, AWJ revealed several advantages over other techniques of machining studied. This process is recognized for the cutting of all types of materials, but by controlling the operating parameters it has made machining at constant and variable depths. Thus, AWJ machining could be chosen for further inquiry with the intention of utilizing it for milling process of these metals especially in the case of large parts and small thicknesses. The following outlines the results of the bibliographical study:

- ✓ Some information is available on control depth milling by using AWJ machining, but it lacks a general methodology to obtain the desired depth. Indeed, for control the jet on milling Ti6Al4V, most of the outcomes are for controlling the depth of cut as milling single kerf.
- ✓ Milling by AWJ includes series process parameters and it is sensitive with changing of each parameter, which is an inherent problem and makes it more difficult to take advance of this technology.
- ✓ In the aspect of modelling for the milling process, some models are available but it is complex and difficult for applying broadly due to a vast of experiments need to be done for calibration of these models. Besides, no model mention to control the

jet by changing the jet inclination angle and take this kinetic parameter into account modelling.

Based on the effect of process parameters presented in Chapter 1, a categorization has been made between setting parameters and control parameters to establish a given machine configuration. This is a basic principle to narrow the effect of the complex input parameters during the process. On milling open pocket with a flat bottom, only traverse speed and scanning step (offset pitch) are considered as control parameters. The main objective is studied in two cases: abrasive water jet machining with a perpendicular attack angle of the jet to the workpiece surface and abrasive water jet machining with an inclination angle of the jet to the workpiece surface corresponding to the contents of Chapter 2 and Chapter 3.

The second chapter is dedicated to the first case of the perpendicular impact angle of the jet to the workpiece surface. Experimental analysis has been conducted to define a global model in relation to the Gaussian distribution. This model is to describe the single kerfs milled on Ti6Al4V according to controllable parameters (Vf). Then a new model has been developed by using successive elementary passes shifted by an offset pitch to compute the depth when milling pockets with open edges. Based on a given configuration including a given machine, a given abrasive, specific pressure with a constant value of the firing distance of the jet, a new rapid calibration is introduced. It allows a saving of setup time to establish a model to predict the depth milled on machining open pockets. This approach is validated experimentally with varying the pressure, standoff distance and type of abrasive particle, the accuracy obtained less than 5%.

Consider a process for the closed pocket machining, an idea to master this process is to control the change of the direction of the jet. Observation different trajectories of the jet as moving over the corner has been presented. Then, a proposed methodology is applied in milling the corner of pockets with an imposed corner radius. This new methodology permits to solve problems usually suffer in the course of machining pocket corners, especially the non-uniform in the depth due to the variation of the distributed energy on the surface according to a variation of kerf width. This method of generating the best strategy with a suitable traverse speed of the jet will be able to obtain a flat bottom on whole a pocket machined.

The third chapter is dedicated to observing the influence of the jet inclination angle on geometrical characteristics of both the elementary pass and pocket milled by AWJ. A new model is proposed and assessed by experiments. This chapter has been done by introducing two factors $Ke(\alpha)$ and $H_e(\alpha)$. $Ke(\alpha)$ is the erosion factor depending on the jet inclination angles in case of milling an elementary pass. $H_e(\alpha)$ is the erosion factor due to the effect of a succession of elementary passes depending on the inclination angle of the jet. The model has enabled for predicting the geometrical characteristics of the profile of the pocket milled effectively. Results show the presence of variation in geometrical characteristics of the milled pocket depending on the jet inclination angles. This has revealed that AWJ controlled depth milling of Ti6Al4V is possible and careful selection of machining parameters lead to acceptable surface parameters.

4.2 Future work

Researching on controlled-depth milling by AWJ can be further enhanced by using this study as a beginning point. For the perspectives, several points will be interesting to dig deeper. They are listed below:

1. Improve the simulation of the pockets taking into account the kinematic parameters of the real process. It is essential in order to get closer to the real process in AWJ machining.
2. Study on the experiment to realize the influence of the machining strategy on the generation of closed pocket machined. This is an important point to avoid issues of starting point and ending point of the jet and as the jet changing the direction during moving in a pocket milled.
3. Control the depth of the milled pocket with a given slope of the pocket sidewall.
4. Study the influence of jet impingement angle and 5 axis combination on the generation of the closed pocket machined. By this way, it will make it possible to propose machining solutions of pockets with arbitrary shape.
5. Conduct a study on the surface quality generated by AWJ milling in relation with the grit embedment phenomenon.

BIBLIOGRAPHY

- [1] N. C. Franz, "United States patent," *Geothermics*, vol. 14, no. 4, pp. 595–599, 1985.
- [2] M. Hashish, "Visualization of the abrasive-waterjet cutting process," *Exp. Mech.*, vol. 28, no. 2, pp. 159–169, 1988.
- [3] K. R. Momber A.W., "Principles of abrasif water jet machining," *Springer-Verlag*, 1998.
- [4] G. Fowler, "Abrasive Water-jet - Controlled Depth Milling Titanium Alloys," p. 209, 2003.
- [5] M. K. Kulekci, "Processes and apparatus developments in industrial waterjet applications," *Int. J. Mach. Tools Manuf.*, 2002.
- [6] N. Haghbin, F. Ahmadzadeh, J. K. Spelt, and M. Papini, "High pressure abrasive slurry jet micro-machining using slurry entrainment," *Int. J. Adv. Manuf. Technol.*, vol. 84, no. 5–8, pp. 1031–1043, 2016.
- [7] M. Hashish, "AWJ Milling of Gamma Titanium Aluminide," *J. Manuf. Sci. Eng.*, vol. 132, no. 4, p. 041005, 2010.
- [8] G. Fowler, P. H. Shipway, and I. R. Pashby, "Abrasive water-jet controlled depth milling of Ti6Al4V alloy - An investigation of the role of jet-workpiece traverse speed and abrasive grit size on the characteristics of the milled material," *J. Mater. Process. Technol.*, vol. 161, no. 3, pp. 407–414, 2005.
- [9] D. Arola and M. Ramulu, "Material removal in abrasive waterjet machining of metals a residual stress analysis," *Wear*, vol. 211, no. 2, pp. 302–310, 1997.
- [10] M. C. Kong, D. Axinte, and W. Voice, "Challenges in using waterjet machining of NiTi shape memory alloys: An analysis of controlled-depth milling," *J. Mater. Process. Technol.*, 2011.
- [11] J. Wang, T. Nguyen, and K. L. Pang, "Mechanisms of microhole formation on glasses by an abrasive slurry jet," *J. Appl. Phys.*, 2009.
- [12] H. Getu, A. Ghoheity, J. K. Spelt, and M. Papini, "Abrasive jet micromachining of polymethylmethacrylate," *Wear*, vol. 263, no. 7-12 SPEC. ISS., pp. 1008–1015, 2007.
- [13] D. A. Axinte, D. S. Srinivasu, M. C. Kong, and P. W. Butler-Smith, "Abrasive waterjet cutting of polycrystalline diamond: A preliminary investigation," *Int. J. Mach. Tools Manuf.*, 2009.
- [14] D. A. Axinte, D. S. Srinivasu, J. Billingham, and M. Cooper, "Geometrical modelling of abrasive waterjet footprints: A study for 90° jet impact angle," *CIRP Ann. - Manuf. Technol.*, 2010.
- [15] K. Gupta, *Advanced-Manufacturing-Technologies-Modern-Machining-Advanced-Joining-Sustainable-Manufacturing (2017).pdf*, 2017.
- [16] S. Paul, A. M. Hoogstrate, C. A. Van Luttervelt, and H. J. J. Kals, "Analytical and experimental modelling of the abrasive water jet cutting of ductile materials," *J. Mater. Process. Technol.*, vol. 73, no. 1–3, pp. 189–199, 1998.
- [17] J. J. Rozario Jegaraj and N. Ramesh Babu, "A soft computing approach for controlling

- the quality of cut with abrasive waterjet cutting system experiencing orifice and focusing tube wear," *J. Mater. Process. Technol.*, vol. 185, no. 1–3, pp. 217–227, 2007.
- [18] G. Fowler, P. H. Shipway, and I. R. Pashby, "A technical note on grit embedment following abrasive water-jet milling of a titanium alloy," *J. Mater. Process. Technol.*, vol. 159, no. 3, pp. 356–368, 2005.
- [19] B. H. Yan, F. C. Tsai, L. W. Sun, and R. T. Hsu, "Abrasive jet polishing on SKD61 mold steel using SiC coated with Wax," *J. Mater. Process. Technol.*, vol. 208, no. 1–3, pp. 318–329, 2008.
- [20] F. C. Tsai, B. H. Yan, C. Y. Kuan, and F. Y. Huang, "A Taguchi and experimental investigation into the optimal processing conditions for the abrasive jet polishing of SKD61 mold steel," *Int. J. Mach. Tools Manuf.*, vol. 48, no. 7–8, pp. 932–945, 2008.
- [21] R. Manu and N. R. Babu, "An erosion-based model for abrasive waterjet turning of ductile materials," *Wear*, 2009.
- [22] S. Paul, A. M. Hoogstrate, C. A. Van Luttervelt, and H. J. J. Kals, "Analytical modelling of the total depth of cut in the abrasive water jet machining of polycrystalline brittle material," *J. Mater. Process. Technol.*, vol. 73, no. 1–3, pp. 206–212, 1998.
- [23] J. Wang, "Predictive depth of jet penetration models for abrasive waterjet cutting of alumina ceramics," *Int. J. Mech. Sci.*, vol. 49, no. 3, pp. 306–316, 2007.
- [24] A. Ghobeity, H. Getu, M. Papini, and J. K. Spelt, "Surface evolution models for abrasive jet micromachining of holes in glass and polymethylmethacrylate (PMMA)," *J. Micromechanics Microengineering*, vol. 17, no. 11, pp. 2175–2185, 2007.
- [25] Z. W. Zhong and Z. Z. Han, "Turning of glass with abrasive waterjet," *Mater. Manuf. Process.*, vol. 17, no. 3, pp. 339–349, 2002.
- [26] D. A. Axinte, J. P. Stepanian, M. C. Kong, and J. McGourlay, "Abrasive waterjet turning-An efficient method to profile and dress grinding wheels," *Int. J. Mach. Tools Manuf.*, vol. 49, no. 3–4, pp. 351–356, 2009.
- [27] J. D. Fordham, R. Pilkington, and C. C. Tang, "The effect of different profiling techniques on the fatigue performance of metallic membranes of AISI 301 and Inconel 718," *Int. J. Fatigue*, 1997.
- [28] R. Teti, "Machining of Composite Materials," *CIRP Ann. - Manuf. Technol.*, vol. 51, no. 2, pp. 611–34, 2012.
- [29] A. Hejjaji, R. Zitoune, L. Crouzeix, S. Le Roux, and F. Collombet, "Surface and machining induced damage characterization of abrasive water jet milled carbon/epoxy composite specimens and their impact on tensile behavior," *Wear*, vol. 376–377, no. April 2017, pp. 1356–1364, 2017.
- [30] M. Haddad, R. Zitoune, H. Bougherara, F. Eyma, and B. Castanié, "Study of trimming damages of CFRP structures in function of the machining processes and their impact on the mechanical behavior," *Compos. Part B Eng.*, vol. 57, pp. 136–143, 2014.
- [31] M. Haddad, R. Zitoune, F. Eyma, and B. Castanie, "Study of the surface defects and dust generated during trimming of CFRP: Influence of tool geometry, machining

- parameters and cutting speed range," *Compos. Part A Appl. Sci. Manuf.*, vol. 66, pp. 142–154, 2014.
- [32] J. Wang, "Machinability study of polymer matrix composites using abrasive waterjet cutting technology," *J. Mater. Process. Technol.*, vol. 94, no. 1, pp. 30–35, 1999.
- [33] M. Ramulu and D. Arola, "The influence of abrasive waterjet cutting conditions on the surface quality of graphite/epoxy laminates," *Int. J. Mach. Tools Manuf.*, vol. 34, no. 3, pp. 295–313, 1994.
- [34] D. S. Srinivasu and D. A. Axinte, "Surface integrity analysis of plain waterjet milled advanced engineering composite materials," *Procedia CIRP*, vol. 13, pp. 371–376, 2014.
- [35] M. Ramulu and D. Arola, "Water jet and abrasive water jet cutting of unidirectional graphite/epoxy composite," *Composites*, vol. 24, no. 4, pp. 299–308, 1993.
- [36] D. K. Shanmugam, T. Nguyen, and J. Wang, "A study of delamination on graphite/epoxy composites in abrasive waterjet machining," *Compos. Part A Appl. Sci. Manuf.*, vol. 39, no. 6, pp. 923–929, 2008.
- [37] D. K. Shanmugam and S. H. Masood, "An investigation on kerf characteristics in abrasive waterjet cutting of layered composites," *J. Mater. Process. Technol.*, vol. 209, no. 8, pp. 3887–3893, 2009.
- [38] A. Hejjaji, R. Zitoune, L. Toubal, L. Crouzeix, and F. Collombet, "Influence of controlled depth abrasive water jet milling on the fatigue behavior of carbon/epoxy composites," *Compos. Part A Appl. Sci. Manuf.*, 2019.
- [39] A. Alberdi, T. Artaza, A. Suárez, A. Rivero, and F. Girot, "An experimental study on abrasive waterjet cutting of CFRP/Ti6Al4V stacks for drilling operations," *Int. J. Adv. Manuf. Technol.*, vol. 86, no. 1–4, pp. 691–704, 2016.
- [40] T. Sultan, "Usinage de metaux durs par Jet d'Eau Abrasif," p. 174, 2015.
- [41] S. Den Dunnen, G. Kraaij, C. Biskup, G. M. M. J. Kerkhoffs, and G. J. M. Tuijthof, "Pure waterjet drilling of articular bone: An in vitro feasibility study," *Stroj. Vestnik/Journal Mech. Eng.*, vol. 59, no. 7–8, pp. 425–432, 2013.
- [42] K. L. Pang, T. Nguyen, J. Fan, and J. Wang, "A study of micro-channeling on glasses using an abrasive slurry jet," *Mach. Sci. Technol.*, 2012.
- [43] D. S. Miller, "Micromachining with abrasive waterjets," in *Journal of Materials Processing Technology*, 2004.
- [44] A. Alberdi, A. Rivero, L. N. López de Lacalle, I. Etxeberria, and A. Suárez, "Effect of process parameter on the kerf geometry in abrasive water jet milling," *Int. J. Adv. Manuf. Technol.*, vol. 51, no. 5–8, pp. 467–480, Nov. 2010.
- [45] A. Alberdi, A. Rivero, and L. N. López de Lacalle, "Experimental Study of the Slot Overlapping and Tool Path Variation Effect in Abrasive Waterjet Milling," *J. Manuf. Sci. Eng.*, vol. 133, no. 3, p. 034502, 2011.
- [46] D. S. Srinivasu, D. A. Axinte, P. H. Shipway, and J. Folkes, "Influence of kinematic operating parameters on kerf geometry in abrasive waterjet machining of silicon carbide ceramics," *Int. J. Mach. Tools Manuf.*, vol. 49, no. 14, pp. 1077–1088, Nov. 2009.

- [47] D. S. Srinivasu and D. Axinte, "An analytical model for top width of jet footprint in abrasive waterjet milling: A case study on SiC ceramics," *Proc. Inst. Mech. Eng. Part B J. Eng. Manuf.*, vol. 225, no. 3, pp. 319–335, 2011.
- [48] K. Yanaida and A. Ohashi, "Flow characteristics of water jets in air," in *5th Int Symp Jet Cutt Technol*, 1980.
- [49] M. Hashish and M. P. du Plessis, "Prediction Equations Relating High Velocity Jet Cutting Performance to Stand Off Distance and Multipasses," *J. Eng. Ind.*, vol. 101, no. 3, p. 311, 2010.
- [50] M. Zaki, "Modélisation et simulation numérique du procédé de perçage non débouchant par jet d'eau abrasif," 2009.
- [51] T. Sultan, P. Gilles, G. Cohen, F. Cenac, and W. Rubio, "Modeling incision profile in AWJM of Titanium alloys Ti6Al4V," *Mech. Ind.*, vol. 17, no. 4, p. 403, 2016.
- [52] R. Balz, R. Mokso, C. Narayanan, D. A. Weiss, and K. C. Heiniger, "Ultra-fast X-ray particle velocimetry measurements within an abrasive water jet," *Exp. Fluids*, vol. 54, no. 3, 2013.
- [53] N. Zuckerman and N. Lior, "Jet impingement heat transfer: Physics, correlations, and numerical modeling," *Advances in Heat Transfer*, vol. 39, no. C, pp. 565–631, 2006.
- [54] I. Finnie, "Erosion of surfaces by solid particles," *Wear*, vol. 3, no. 2, pp. 87–103, 1960.
- [55] J. G. A. Bitter, "A study of erosion phenomena. Part I," *Test*, vol. 6, 1963.
- [56] J. G. A. Bitter, "A study of erosion phenomena. Part II," *Wear*, vol. 6, no. 3, pp. 169–190, 1963.
- [57] M. Hashish, "Milling With Abrasive-Waterjets: a Preliminary Investigation.," *Asme*, pp. 1–10, 1987.
- [58] G. L. Sheldon and I. Finnie, "The Mechanism of Material Removal in the Erosive Cutting of Brittle Materials," *J. Eng. Ind.*, 2011.
- [59] M. Buijs and J. M. M. Pasmans, "Erosion of glass by alumina particles: transitions and exponents," *Wear*, vol. 184, no. 1, pp. 61–65, 1995.
- [60] A. G. D. B. Marshall, B. R. Lawn and Evans, "Elastic/Plastic Indentation Damage in Ceramics: The Lateral Crack System," *J. Am. Ceram. Soc.*, vol. 65, no. 11, 1982.
- [61] P. J. Slikkerveer, "Erosion and damage by sharp particles," *Wear*217, pp. 273–250, 1998.
- [62] R. Haj Mohammad Jafar, J. K. Spelt, and M. Papini, "Surface roughness and erosion rate of abrasive jet micro-machined channels: Experiments and analytical model," *Wear*, vol. 303, no. 1–2, pp. 138–145, 2013.
- [63] M. Hashish, "A Modeling Study of Metal Cutting With Abrasive Waterjets," *J. Eng. Mater. Technol.*, vol. 106, no. 1, p. 88, 2009.
- [64] M. Hashish, "Waterjet Machining of Advanced Composites," *Mater. Manuf. Process.*, vol. 10, no. 6, pp. 1129–1152, 1995.
- [65] R. Kovacevic, "Surface texture in abrasive waterjet cutting," *J. Manuf. Syst.*, 1991.

- [66] J. Schwartzentruber, M. Papini, and J. K. Spelt, "Characterizing and modelling delamination of carbon-fiber epoxy laminates during abrasive waterjet cutting," *Compos. Part A Appl. Sci. Manuf.*, vol. 112, no. June, pp. 299–314, 2018.
- [67] J. Wang, "The Effects of the Jet Impact Angle on the Cutting Performance in AWJ Machining of Alumina Ceramics," *Key Eng. Mater.*, vol. 238–239, pp. 117–124, 2009.
- [68] J. Wang and W. C. K. Wong, "A study of abrasive waterjet cutting of metallic coated sheet steels," *Int. J. Mach. Tools Manuf.*, 1999.
- [69] D. Arola, M. Ramulu, and D. D. Arola, "Material removal in abrasive waterjet machining of metals surface integrity and texture," *Wear*, 1997.
- [70] P. H. Shipway, G. Fowler, and I. R. Pashby, "Characteristics of the surface of a titanium alloy following milling with abrasive waterjets," in *Wear*, 2005.
- [71] M. Hashish, "The Effect of Beam Angle in Abrasive-Waterjet Machining," *J. Eng. Ind.*, vol. 115, no. 1, p. 51, 2012.
- [72] F. Boud, L. F. Loo, and P. K. Kinnell, "The impact of plain waterjet machining on the surface integrity of aluminium 7475," in *Procedia CIRP*, 2014.
- [73] M. C. Kong, D. Axinte, and W. Voice, "Aspects of material removal mechanism in plain waterjet milling on gamma titanium aluminide," *J. Mater. Process. Technol.*, vol. 210, no. 3, pp. 573–584, 2010.
- [74] H. Getu, A. Ghoheity, J. K. Spelt, and M. Papini, "Abrasive jet micromachining of acrylic and polycarbonate polymers at oblique angles of attack," *Wear*, vol. 265, no. 5–6, pp. 888–901, 2008.
- [75] B. J. Griffiths, D. T. Gawne, and G. Dong, "A Definition of the Topography of Grit-Blasted Surfaces for Plasma Sprayed Alumina Coatings," *J. Manuf. Sci. Eng.*, vol. 121, no. 1, p. 49, 2008.
- [76] M. Hashish, "Controlled-Depth Milling of Isogrid Structures With AWJs," *J. Manuf. Sci. Eng.*, vol. 120, no. 1, p. 21, 2008.
- [77] A. W. Momber and R. Kovacevic, "Test parameter analysis in abrasive water jet cutting of rocklike materials," *Int. J. Rock Mech. Min. Sci.*, vol. 34, no. 1, pp. 17–25, 1997.
- [78] F. Cenac, "Etude de l'usinage non débouchant par jet d'eau abrasif des composites, Ph.D thesis," p. 188, 2011.
- [79] Z. Yong and R. Kovacevic, "Effects of water-mixture film on impact contact in abrasive waterjet machining," *Int. J. Mech. Sci.*, 2002.
- [80] K. M. C. Ojmertz, "Abrasive waterjet milling: An experimental investigation," 1997.
- [81] A. A. Abdel-Rahman and A. A. El-Domiatty, "Maximum depth of cut for ceramics using abrasive waterjet technique," *Wear*, 1998.
- [82] R. Kovacevic, "Monitoring the depth of abrasive waterjet penetration," *Int. J. Mach. Tools Manuf.*, 1992.
- [83] A. W. Momber and R. Kovacevic, *Principles of Abrasive Water Jet Machining*. 2011.
- [84] J. Wang and D. M. Guo, "A predictive depth of penetration model for abrasive waterjet cutting of polymer matrix composites," *J. Mater. Process. Technol.*, vol. 121,

- no. 2–3, pp. 390–394, 2002.
- [85] F. Tazibt, A., Abriak, N., Parsy, “Prediction of abrasive particle velocity in a high pressure water jet and effect of air on acceleration process,” *Eur. J. Mech. B/Fluids*, vol. 15, no. 4, pp. 527–543, 1996.
- [86] P. Vinod B., “Parametric analysis of Abrasives water jet machining of EN8 Material,” *Int. J. Eng. Res. Appl.*, vol. 2, no. 3, pp. 3029–3032, 2012.
- [87] M. Dittrich, M. Dix, M. Kuhl, B. Palumbo, and F. Tagliaferri, “Process analysis of water abrasive fine jet structuring of ceramic surfaces via design of experiment,” in *Procedia CIRP*, 2014, vol. 14, pp. 442–447.
- [88] M. A. Azmir, A. K. Ahsan, and A. Rahmah, “Effect of abrasive water jet machining parameters on aramid fibre reinforced plastics composite,” *Int. J. Mater. Form.*, vol. 2, no. 1, pp. 37–44, 2009.
- [89] A. H. AZIMI, “Experimental and Numerical Investigations of Sand-Water Slurry Jets in Water A thesis submitted to the Faculty of Graduate Studies and Research in partial,” 2012.
- [90] C. T. Crowe, “On models for turbulence modulation in fluid-particle flows,” *Int. J. Multiph. Flow*, 2000.
- [91] J. E. Goodwin, W. Sage, and G. P. Tilly, “Study of Erosion by Solid Particles,” *Proc. Inst. Mech. Eng.*, 1969.
- [92] G. Fowler, I. R. Pashby, and P. H. Shipway, “The effect of particle hardness and shape when abrasive water jet milling titanium alloy Ti6Al4V,” *Wear*, vol. 266, no. 7–8, pp. 613–620, 2009.
- [93] S. Ferrendier, “Influence de l’Evolution Granulométrique des Abrasifs sur l’Enlèvement de Matière lors de la découpe par JEA,” 2001.
- [94] K. Sugiyama, K. Harada, and S. Hattori, “Influence of impact angle of solid particles on erosion by slurry jet,” *Wear*, vol. 265, no. 5–6, pp. 713–720, 2008.
- [95] J. Wang, “Abrasive waterjet machining of polymer matrix composites - cutting performance, erosive process and predictive models,” *Int. J. Adv. Manuf. Technol.*, 1999.
- [96] S. Ally, J. K. Spelt, and M. Papini, “Prediction of machined surface evolution in the abrasive jet micro-machining of metals,” *Wear*, vol. 292–293, pp. 89–99, 2012.
- [97] H. Getu, J. K. Spelt, and M. Papini, “Thermal analysis of cryogenically assisted abrasive jet micromachining of PDMS,” *Int. J. Mach. Tools Manuf.*, vol. 51, no. 9, pp. 721–730, 2011.
- [98] B. Freist, H. Haferkamp, A. Laurinat, and H. Louis, “Abrasive jet machining of ceramic products,” *Proc 5th Am Water Jet Conf*, 1989.
- [99] G. M.-W. A. Laurinat, H. Louis, “A Model for Milling With Abrasive Water Jets,” in *Proceedings of the 7th American Water Jet Conference, Volume I*, 1993, pp. 119–140.
- [100] J. Billingham, C. B. Miron, D. A. Axinte, and M. C. Kong, “Mathematical modelling of abrasive waterjet footprints for arbitrarily moving jets: Part II - Overlapped single and multiple straight paths,” *Int. J. Mach. Tools Manuf.*, vol. 68, pp. 30–39, 2013.

- [101] R. Kovacevic, M. Hashish, R. Mohan, M. Ramulu, T. J. Kim, and E. S. Geskin, "State of the Art of Research and Development in Abrasive Waterjet Machining," *J. Manuf. Sci. Eng.*, vol. 119, no. 4B, p. 776, 2008.
- [102] M. C. Kong, D. Axinte, and W. Voice, "An innovative method to perform maskless plain waterjet milling for pocket generation: A case study in Ti-based superalloys," *Int. J. Mach. Tools Manuf.*, vol. 51, no. 7–8, pp. 642–648, 2011.
- [103] D. S. Srinivasu and D. A. Axinte, "Mask-Less Pocket Milling of Composites by Abrasive Waterjets: An Experimental Investigation," *J. Manuf. Sci. Eng.*, 2014.
- [104] K. M. C. Ojmertz and N. Amini, "Discrete approach to the abrasive waterjet milling process," 1997.
- [105] G. A. Escobar-Palafox, R. S. Gault, and K. Ridgway, "Characterisation of abrasive water-jet process for pocket milling in Inconel 718," *Procedia CIRP*, vol. 1, no. 1, pp. 404–408, 2012.
- [106] S. Paul, A. M. Hoogstrate, C. A. Van Luttervelt, and H. J. J. Kals, "An experimental investigation of rectangular pocket milling with abrasive water jet," *J. Mater. Process. Technol.*, 1998.
- [107] T. Nguyen, J. Wang, and W. Li, "Process models for controlled-depth abrasive waterjet milling of amorphous glasses," *Int. J. Adv. Manuf. Technol.*, 2015.
- [108] J. Folkes, "Waterjet-An innovative tool for manufacturing," *J. Mater. Process. Technol.*, 2009.
- [109] G. C. and M. K. U.Goutham, Basawaraj S.Hasu, "Experimental Investigation of Pocket Milling on Inconel 825 using Abrasive Water Jet Machining," *FME Trans.*, vol. 44, no. 2, pp. 133–138, 2016.
- [110] Y. I. Oka, K. Okamura, and T. Yoshida, "Practical estimation of erosion damage caused by solid particle impact: Part 1: Effects of impact parameters on a predictive equation," *Wear*, vol. 259, no. 1–6, pp. 95–101, 2005.
- [111] N. Tamannaee, J. K. Spelt, and M. Papini, "Abrasive slurry jet micro-machining of edges, planar areas and transitional slopes in a talc-filled co-polymer," *Precis. Eng.*, 2016.
- [112] K. Dadkhipour, T. Nguyen, and J. Wang, "Mechanisms of channel formation on glasses by abrasive waterjet milling," *Wear*, vol. 292–293, pp. 1–10, 2012.
- [113] A. Carrascal and A. Alberdi, "Evolutionary industrial physical model generation," *Lect. Notes Comput. Sci. (including Subser. Lect. Notes Artif. Intell. Lect. Notes Bioinformatics)*, vol. 6076 LNAI, no. PART 1, pp. 327–334, 2010.
- [114] S. Anwar, D. A. Axinte, and A. A. Becker, "Finite element modelling of overlapping abrasive waterjet milled footprints," *Wear*, vol. 303, no. 1–2, pp. 426–436, 2013.
- [115] K. Kowsari, H. Nouraei, B. Samareh, M. Papini, and J. K. Spelt, "CFD-aided prediction of the shape of abrasive slurry jet micro-machined channels in sintered ceramics," *Ceram. Int.*, vol. 42, no. 6, pp. 7030–7042, 2016.
- [116] V. H. Bui, P. Gilles, T. Sultan, G. Cohen, and W. Rubio, "A new cutting depth model with rapid calibration in abrasive water jet machining of titanium alloy," *Int. J. Adv. Manuf. Technol.*, vol. 93, no. 5–8, pp. 1499–1512, 2017.

- [117] L. G. Libor M. Hlaváč, Bohumír Strnadel, Jiří Kaličinský, “The model of product distortion in AWJ cutting,” *Int. J. Adv. Manuf. Technol.*, vol. 62, no. 1–4, pp. 157–166, 2012.
- [118] Y. W. Seo, M. Ramulu, and D. Kim, “Machinability of titanium alloy (Ti ± 6Al ± 4V) by abrasive waterjets,” no. December, 2003.
- [119] E. O. Ezugwu and Z. M. Wang, “Titanium alloys and their machinability—a review. J Mater Process Tech,” *J. Mater. Process. Technol.*, vol. 68, pp. 262–274, 1997.
- [120] A. W. Momber, “Energy transfer during the mixing of air and solid particles into a high-speed waterjet: An impact-force study,” *Exp. Therm. Fluid Sci.*, 2001.
- [121] M. C. Kong, S. Anwar, J. Billingham, and D. A. Axinte, “Mathematical modelling of abrasive waterjet footprints for arbitrarily moving jets: Part i - Single straight paths,” *Int. J. Mach. Tools Manuf.*, vol. 53, no. 1, pp. 58–68, 2012.
- [122] T. Burzynski and M. Papini, “A level set methodology for predicting the surface evolution of inclined masked micro-channels resulting from abrasive jet micro-machining at oblique incidence,” *Int. J. Mach. Tools Manuf.*, vol. 51, no. 7–8, pp. 628–641, 2011.
- [123] P. V. Rao, S. G. Young, and D. H. Buckley, “Morphology of an aluminum alloy eroded by a normally incident jet of angular erodent particles,” *Wear*, 1983.
- [124] V. H. Bui, P. Gilles, G. Cohen, and W. Rubio, “A modeling of elementary passes taking into account the firing angle in abrasive water jet machining of titanium alloy,” in *AIP Conference Proceedings*, 2018, vol. 1960.
- [125] V. H. Bui, P. Gilles, T. Sultan, G. Cohen, and W. Rubio, “Adaptive speed control for waterjet milling in pocket corners,” *Int. J. Adv. Manuf. Technol.*, 2019.

APPENDIX

Using Eq. 2-18 to Eq. 2-22, the variation between the outer toolpath and inter toolpath for the three areas 1, 2 and 3 can be evaluated (Fig. 2-24):

a. Area 1: distances in this area, $Pitch_{area1}$, are calculated considering the angle $\theta \in [\theta_1, 0]$ with θ_1 defined by:

$$\theta_1 = atan\left(\frac{-Pitch_{init}/2}{R - Pitch_{init}/2}\right) \quad \text{Eq. 2-30}$$

In this area, segments are always parallel to the X-axis and, from equations Eq. 2-18 and Eq. 2-22, the length of these segments is identified by:

$$Pitch_{area1} = R + Pitch_{init} - \sqrt{R^2 - y^2} \quad \text{Eq. 2-31}$$

Relation between y and θ is given by:

$$\tan(\theta) = \frac{-(Pitch_{init}/2 - y)}{R - Pitch_{init}/2} \quad \text{Eq. 2-32}$$

Replacing y from Eq. 2-32 in Eq. 2-31, $Pitch_{area1}$ is obtained by:

$$Pitch_{area1} = R + Pitch_{init} - \sqrt{R^2 - [(R - Pitch_{init}/2)\tan\theta + Pitch_{init}/2]^2} \quad \text{Eq. 2-33}$$

For $\theta = \theta_1$, $Pitch_{area1} = Pitch_{init}$ and for $\theta = 0$, Eq. 2-33 becomes:

$$Pitch_{area1} = R + Pitch_{init} - \sqrt{R^2 - [Pitch_{init}/2]^2} \quad \text{Eq. 2-34}$$

Considering $Pitch_{init} \ll R$, Eq. 2-34 can be written :

$$Pitch_{area1} \cong Pitch_{init} (1 + 1/(8R)) \cong Pitch_{init} \quad \text{Eq. 2-35}$$

b. Area 2: distances in this area, $Pitch_{area2}$, are calculated considering the angle $\theta \in [0, \theta_2]$ with θ_2 defined by:

$$\theta_2 = \text{atan}\left(\frac{Pitch_{init}/2}{R + Pitch_{init}/2}\right) \quad \text{Eq. 2-36}$$

This angular position θ is linked to $Pitch_{area2}$ by the length:

$$\cos\theta = \frac{R + Pitch_{init}/2}{O_{CmA} + AB} \quad \text{Eq. 2-37}$$

Considering the triangle $O_{C2}O_{CmA}$, it can be established:

$$O_{CmA}^2 - \sqrt{2}Pitch_{init}\cos\left(\frac{3\pi}{4} + \theta\right)O_{CmA} + \left(\frac{1}{2}Pitch_{init}^2 - R^2\right) = 0 \quad \text{Eq. 2-38}$$

Solving Eq.2-38 it is possible to calculate O_{CmA} :

$$O_{cm}A = \frac{-\sqrt{2}Pitch_{init}\cos\left(\frac{\pi}{4} - \theta\right) + \sqrt{4R^2 - 2Pitch_{init}^2\sin^2\left(\frac{\pi}{4} - \theta\right)}}{2} \quad \text{Eq. 2-39}$$

As $Pitch_{init} \ll R$, equation Eq.2-39 becomes:

$$O_{cm}A \cong \frac{-\sqrt{2}Pitch_{init}\cos\left(\frac{\pi}{4} - \theta\right) + 2R}{2} \quad \text{Eq. 2-40}$$

Substituting $O_{cm}A$ (Eq. 2-40) into equation Eq.2-37 it is possible to calculate the length:

$$Pitch_{area2} = AB \cong \frac{R(1 - \cos\theta) + \frac{Pitch_{init}}{2}[1 + \sqrt{2}\cos\theta\cos\left(\frac{\pi}{4} - \theta\right)]}{\cos\theta} \quad \text{Eq. 2-41}$$

As $Pitch_{init} \ll R$, the calculated angle θ is small and the length AB can be approximated:

$$Pitch_{area2} \cong \frac{Pitch_{init}}{2} \left(1 + \sqrt{2}\cos\left(\frac{\pi}{4} - \theta\right)\right) \quad \text{Eq. 2-42}$$

Area 3: distances in this area, $Pitch_{area3}$, are calculated considering the angle $\theta \in \left[\theta_2, \frac{\pi}{4}\right]$. From Fig. 2-24, the distances, $Pitch_{area3}$, are defined by:

$$Pitch_{area3} = EF = O_{cm}F - O_{cm}E \quad \text{Eq. 2-43}$$

Considering the triangle $O_{c1}O_{cm}F$ the expression can be established:

$$FO_{cm}^2 + O_{c1}O_{cm}^2 - 2O_{c1}O_{cm} \cdot FO_{cm} \cdot \cos\left(\frac{\pi}{4} - \theta\right) = FO_{c1}^2 \quad \text{Eq. 2-44}$$

Considering that $O_{c1}O_{cm} = \frac{\sqrt{2}Pitch_{init}}{2}$ and $FO_{c1} = R$, a new expression is established:

$$FO_{cm}^2 - \sqrt{2}Pitch_{init} \cdot \cos\left(\frac{\pi}{4} - \theta\right) \cdot FO_{cm} + \frac{1}{2}Pitch_{init}^2 - R^2 = 0 \quad \text{Eq. 2-45}$$

Similarly, considering triangle $O_{c2}O_{cm}E$, it can be written:

$$EO_{cm}^2 + \sqrt{2}Pitch_{init} \cdot \cos\left(\frac{\pi}{4} - \theta\right) \cdot EO_{cm} + \frac{1}{2}Pitch_{init}^2 - R^2 = 0 \quad \text{Eq. 2-46}$$

Subtracting Eq. 2-46 from Eq. 2-45, a simplified expression is established:

$$(FO_{cm}^2 - EO_{cm}^2) - \sqrt{2}Pitch_{init} \cdot \cos\left(\frac{\pi}{4} - \theta\right) \cdot (FO_{cm} + EO_{cm}) = 0 \quad \text{Eq. 2-47}$$

The distance $Pitch_{area3}$ can be calculated by:

$$Pitch_{area3} = EF = FO_{cm} - EO_{cm} = \sqrt{2}Pitch_{init} \cdot \cos\left(\frac{\pi}{4} - \theta\right) \quad \text{Eq. 2-48}$$